Synthesis and characterization of organic high-spin molecules

Dissertation

for the Degree of

Doctor of Natural Sciences (Dr. rer. nat.)

Ruhr-Universität Bochum

by

Patrik Neuhaus

from Nottuln

Bochum 2010

This work was carried out at the Ruhr-Universität Bochum from March 2006 to March 2010 under the supervision of Prof. Dr. W. Sander at the department of Organic Chemistry II, Ruhr-Universität Bochum, Germany.

I want to thank Prof. Dr. W. Sander for providing me with all necessary research facilities and the kind supervision of this thesis. Furthermore, I am very grateful to him for his guidance, the constant encouragement, and the innumerous stimulating discussions during all stages of this work.

First Referee:	Prof. Dr. W. Sander
Second Referee:	Prof. Dr. M. Feigel
Dissertation submitted:	August 2010
Disputation:	September 2010

List of Publications

1. Neuhaus, P.; Grote, D.; Sander, W. Matrix Isolation, Spectroscopic Characterization, and Photoisomerization of *m*-Xylylene. *J. Am. Chem. Soc.* **(2008)**, *130*, 2993.

2. Crabtree, K. N.; Hostetler, K. J.; Munsch, T. E.; Neuhaus, P.; Lahti, P. M.; Sander, W.; Poole, J. S. Comparative Study of the Photochemistry of the Azidopyridine 1-Oxides. *J. Org. Chem.* **(2008)**, *73*, 3441.

3. Quast, H.; Nudling, W.; Klemm, G.; Kirschfeld, A.; Neuhaus, P.; Sander, W.; Hrovat, D. A.; Borden, W. T. A Perimidine-Derived Non-Kekulé Triplet Diradical. *J. Org. Chem.* **(2008)**, *73*, 4956.

4. Bettinger, H. F.; Filthaus, M.; Neuhaus, P. Insertion into dihydrogen employing the nitrogen centre of a borylnitrene. *Chem. Comm.* **(2009)**, *16*, 2186.

5. Chapyshev, S. V.; Misochko, E. Ya.; Akimov, A. V.; Dorokhov, V. G.; Neuhaus, P.; Grote, D.; Sander, W. Molecular Structure and Magnetic Parameters of Septet 2,4,6-Trinitrenotoluene. *J. Org. Chem.* **(2009)**, *74*, 7238.

6. Zeng, X.; Beckers, H.; Willner, H.; Neuhaus, P.; Grote, D.; Sander, W. Difluorophosphoryl Nitrene $F_2P(O)N$: Matrix Isolation and Unexpected Rearrangement to F_2PNO. *Chemistry-- Eur. J.* **(2009)**, *15*, 13466.

7. Chapyshev, S. V.; Neuhaus, P.; Grote, D.; Sander, W. Matrix isolation and magnetic parameters of septet 3,5-dicyanopyridyl-2,4,6-trinitrene. *J. Phys. Org. Chem.* **(2010)**, *23*, 340.

8. Neuhaus, P.; Sander, W. Isolation and Characterization of the Triradical 1,3,5-Trimethylenebenzene. *Angew. Chem.* **(2010)**, in press.

9. Neuhaus, P.; Henkel, S.; Sander, W. Magnetic parameters of α,n-didehydrotoluenes. *Aust. J. Chem.* **(2010)**, in preparation.

Scientific Meetings

(P) Poster

International Symposium on Reactive Intermediates and Unusual Molecules (ISRIUM), Liblice, Czech Republic, July 5-10, 2009. (P)

7th International Conference on Low Temperature Chemistry (7th ICLTC), Helsinki, Finland, August 24-29, 2008. (P)

19th International Conference on Physical Organic Chemistry (ICPOC-19), Santiago de Compostela, Spain, July 13-18, 2008. (P)

International Conference on Reactive Intermediates and Unusual Molecules (ISRIUM), Ascona, Switzerland, August 19-24, 2007. (P)

To my parents and Y-am,
In remembrance of Sebastian, Ettje, and Karl.

Mit dem Wissen wächst der Zweifel.
Johann Wolfgang von Goethe

Man sollte eigentlich im Leben niemals die gleiche Dummheit zweimal machen, denn die Auswahl ist so groß.
Bertrand Russell

Index

1. Summary

m-Xylylene **1** and 1,3,5-trimethylenebenzene **2** are non-Kekulé hydrocarbons with open-shell high-spin ground states. Since both unpaired electrons are localized in nonbonding π orbitals in *m*-xylylene **1**, it can be classified as a π,π-diradical (Scheme 1). Similarly, 1,3,5-trimethylenebenzene **2** has three unpaired electrons in three π-NBMOs and therefore it belongs to the class of π,π,π-triradicals. Another type of system is represented by the α,2- and α,4-didehydrotoluenes **3** and **4**, respectively, which are σ,π-diradicals. An addition of a further methylene unit to these diradicals can lead to high-spin states as in 2-dehydro-*m*-xylylene **5** and 4-dehydro-*m*-xylylene **6**. Both systems can be described as σ,π,π-triradicals. A tetraradical with a *m*-xylylene core is found in the σ,π,π,π-tetraradical 3,5-*bis*-methylenephenylnitrene **7**.

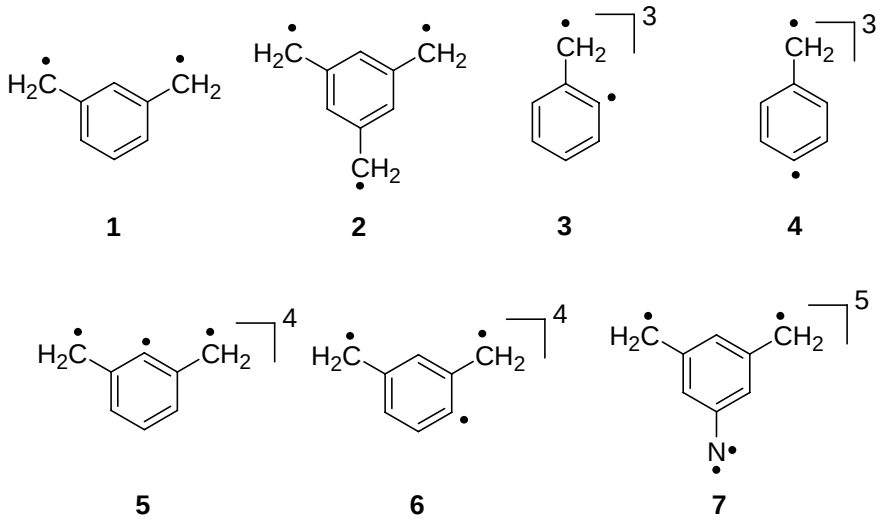

Scheme 1. Di-, tri-, and tetraradicals studied by matrix isolation spectroscopy.

1.1 High-spin EPR spectroscopy

308 nm irradiation of an argon matrix containing 2-iodo- and 4-iodobenzyl iodide **8** and **9**, respectively, results in appearance of EPR transitions indicative of triplet states. The spectra could be simulated for a triplet species with |D/hc| = 0.139 cm^{-1} and |E/hc| = 0.0081 cm^{-1} as well as |D/hc| = 0.212 cm^{-1} and |E/hc| = 0.0040 cm^{-1} and are assigned to α,2-didehydrotoluene **3** and α,4-didehydrotoluene **4**, respectively (Scheme 2). The obtained D values are indicative of diradicals having carbenic resonance structures. 3-Iodobenzyl iodide **10** on the contrary does not give any high-spin signals under identical photolytic

conditions, as the expected α,3-didehydrotoluene **11** is supposed to be a singlet ground state molecule.

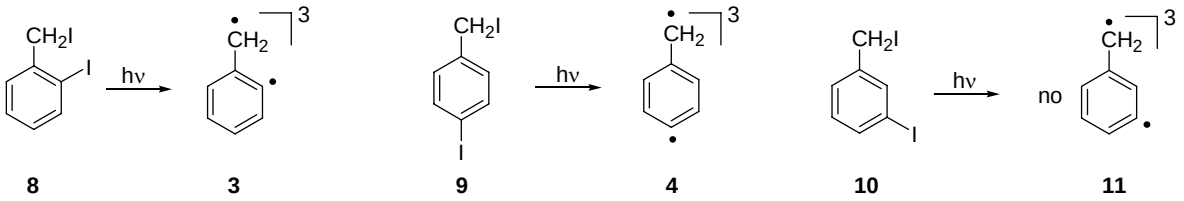

8 **3** **9** **4** **10** **11**

Scheme 2. Photolysis of 2-iodobenzyl iodide **8** and 4-iodobenzyl iodide **9** results in formation of α,2- and α,4-didehydrotoluenes **3** and **4**, respectively. No triplet signals are detected upon photolysis of 3-iodobenzyl iodide **10**.

Similarly, photolysis of 2,6-*bis*-(iodomethyl)iodobenzene **12** and 2,4-*bis*-(iodomethyl)iodobenzene **13** results in quartet EPR spectra which could be assigned to 2-dehydro-*m*-xylylene **5** and 4-dehydro-*m*-xylylene **6**, respectively. The corresponding zero field splitting parameters are |D/hc| = 0.0920 cm^{-1} and |E/hc| = 0.0032 cm^{-1} for **5** and |D/hc| = 0.0935 cm^{-1} and |E/hc| = 0.0008 cm^{-1} for **6**, respectively (Scheme 3). However, irradiation of 3,5-*bis*-(iodomethyl)iodobenzene **14** does not result in any attributable high-spin transitions – 5-dehydro-*m*-xylylene **15** is predicted to have a doublet ground state.

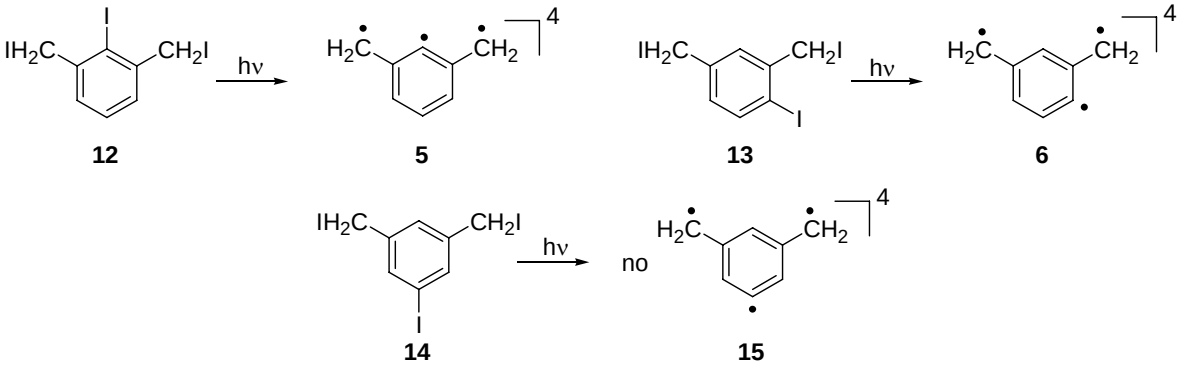

12 **5** **13** **6**

14 **15**

Scheme 3. Irradiation of 2,6-*bis*-(iodomethyl)iodobenzene **13** and 2,4-*bis*-(iodomethyl)iodobenzene **14** results in EPR transitions of quartet 2-dehydro-*m*-xylylene **5** and quartet 4-dehydro-*m*-xylylene **6**, respectively. Irradiation of 3,5-*bis*-(iodomethyl)iodobenzene **14** results in no high-spin EPR transitions.

Finally, photolysis of 3,5-*bis*-(iodomethyl)azidobenzene **16** with λ = 308 nm produces signals of a quintet species. The zfs parameters which can be extracted from the EPR spectrum are |D/hc| = 0.167 cm^{-1} and |E/hc| = 0.0034 cm^{-1} and might be due to quintet 3,5-*bis*-methylenephenylnitrene **7** (Scheme 4).

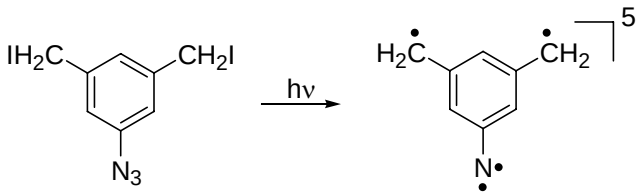

16 **7**

Scheme 4. A quintet species assigned to tetraradical 3,5-*bis*-methylenephenylnitrene **7** is detected by EPR spectroscopy upon photolysis of 3,5-*bis*-(iodomethyl)azidobenzene **16**.

1.2 *m*-Xylylene

The ground state of *m*-xylylene **1** is the triplet state with both unpaired electrons delocalized over the molecular skeleton. Since all known routes to *m*-xylylene **1** are photochemical in nature, a thermal source of this biradical was needed to obtain high yields, prerequisite for a reliable characterization of this elusive molecule by IR spectroscopy. 1,3-*Bis*-(iodomethyl)benzene **17** was found to be an excellent precursor, decomposing into iodine atoms and **1** upon flash vacuum pyrolysis at moderate temperatures. Selective photobleaching of an argon matrix containing *m*-xylylene **1** with linearly polarized light was used to determine its C_{2v} structure. Furthermore, it was found that the diradical is photolabile and can be converted into three different C_8H_8-isomers **18**, **19**, and **20** by appropriate choice of the irradiation wavelength, no rearrangement to **21** was observed under these conditions (Scheme 5).

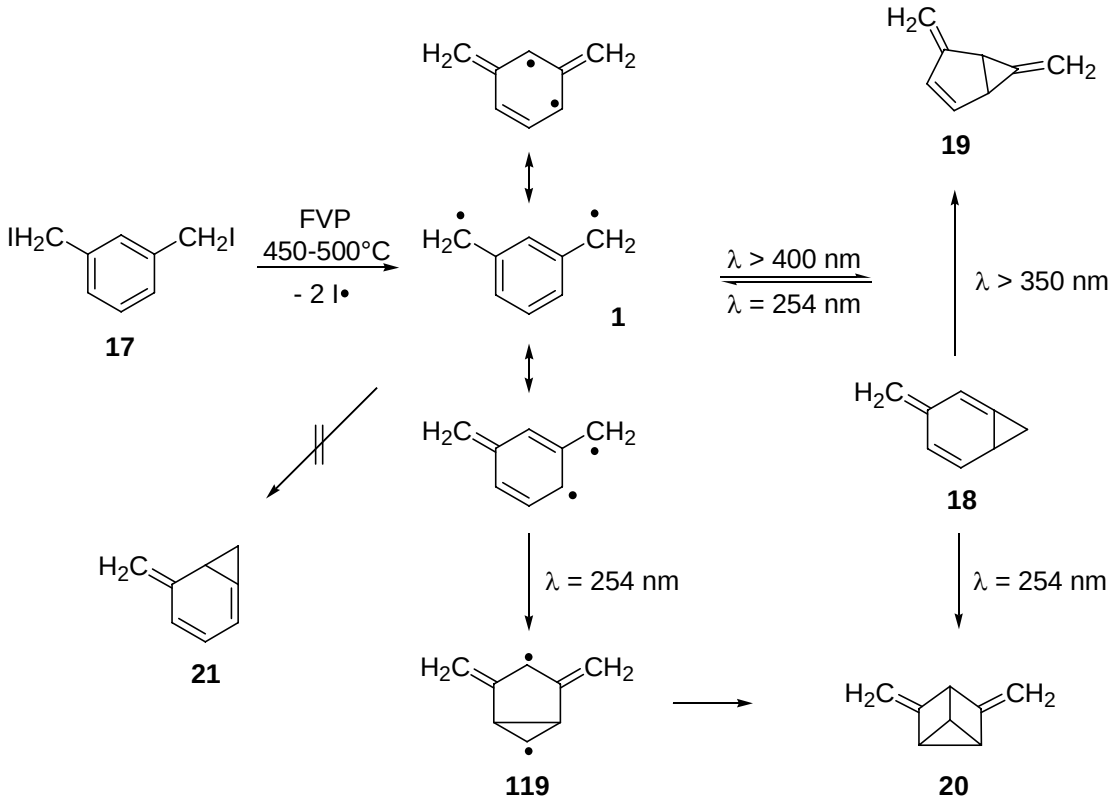

Scheme 5. Thermal synthesis of *m*-xylylene **1** from 1,3-*bis*-(iodomethyl)benzene **17** at moderate temperature and observed photochemical conversion of **1** into **18**, **19**, and **20**.

A photoequilibrium between all three C_8H_8-isomers is obtained. All assignments were verified by deuteration of the exocylic methylene units – also showing that no deuterium scrambling is taking place in the experiments. Several transitions in the UV/Vis spectrum of triplet *m*-xylylene **1** were known from photolytic studies, while the yield of *m*-xylylene **1** was low in these experiments due to the photolability of the parent compound. Additional bands in the UV/Vis spectrum of **1** could be assigned. The triplet ground state of *m*-xylylene **1** was established by EPR spectroscopy with detection of a half-field signal characteristic of triplet molecules.

1.3 Trapping of *m*-xylylene with oxygen

Since FVP of 1,3-*bis*-(iodomethyl)benzene **17** was found to be effective to produce the signals of *m*-xylylene **1** in its triplet ground state, the reactivity of this species towards molecular oxygen was investigated. Triplet diradicals are known to add molecular oxygen to produce a peroxy biradical, which itself has not been detected so far, as it easily forms a second bond to produce a closed-shell peroxide molecule. The IR spectra obtained after FVP of 1,3-*bis*-(iodomethyl)benzene **17** and subsequent trapping of the products in an

oxygen doped argon matrix are in good accordance with an open-shell peroxy biradical species **22**. Fused peroxide structures like **23**, **24**, and **25**, or *bis*oxygen addition products were not found (Scheme 6).

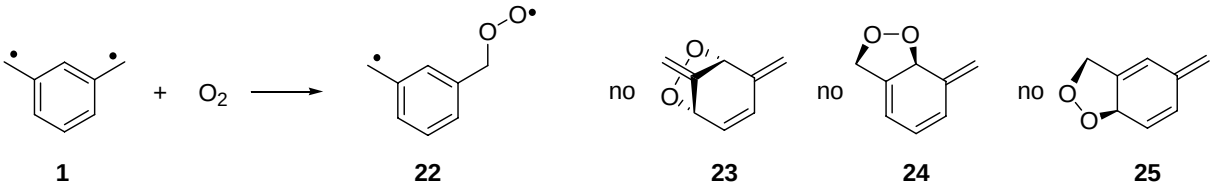

Scheme 6. Trapping of *m*-xylylene **1** with oxygen leads to peroxy biradical **22**, no indication of fused peroxides **23**, **24**, and **25** is obtained.

Upon long wavelength irradiation of matrix isolated **22**, a complexed *m*-xylylene molecule **1**-O_2 is obtained (Scheme 7). As both electrons in peroxy biradical **22** are confined in different regions of the molecule, the singlet-triplet gap is expected to be small. DFT calculations place the broken-symmetry singlet slightly below the triplet. No signals indicative of any triplet molecule were observed in the EPR measurements, while the UV/Vis spectrum does not give direct information on the ground state of peroxy biradical **22**.

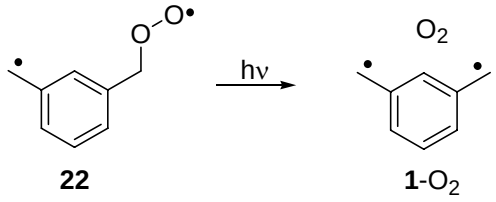

Scheme 7. Irradiation of peroxy biradical **22** gives signals, which could be assigned to a complex between *m*-xylylene **1** and O_2.

1.4 1,3,5-Trimethylenebenzene

1,3,5-Trimethylenebenzene **2** is a highly symmetric triradical in which all three unpaired electrons are coupled in a ferromagnetic way to give a quartet ground state. Indeed, the EPR spectrum obtained after FVP of 1,3,5-*tris*-(iodomethyl)benzene **26** is characteristic of a quartet triradical with a relative low D value and a threefold axis of symmetry. A completely analogous EPR spectrum was obtained after 308 nm photolysis of matrix isolated 1,3,5-*tris*-(iodomethyl)benzene **26**. The D value could be determined to be $|D/hc| = 0.0128\ cm^{-1}$. The quartet signals were found to be in accordance with a high-spin ground state due to a linear Curie-Weiss plot. The IR spectrum after FVP of **26** showed

several signals assigned to quartet 1,3,5-trimethylenebenzene **2** and several other products. Hydrogen addition to the exocyclic methylene units was found to be responsible for some of the signals. In order to verify this, 5-methyl-*m*-xylylene **27** and 3,5-*bis*-methylbenzyl radical **28** were characterized through independent FVP of the corresponding iodides **29** and **30**, respectively (Scheme 8).

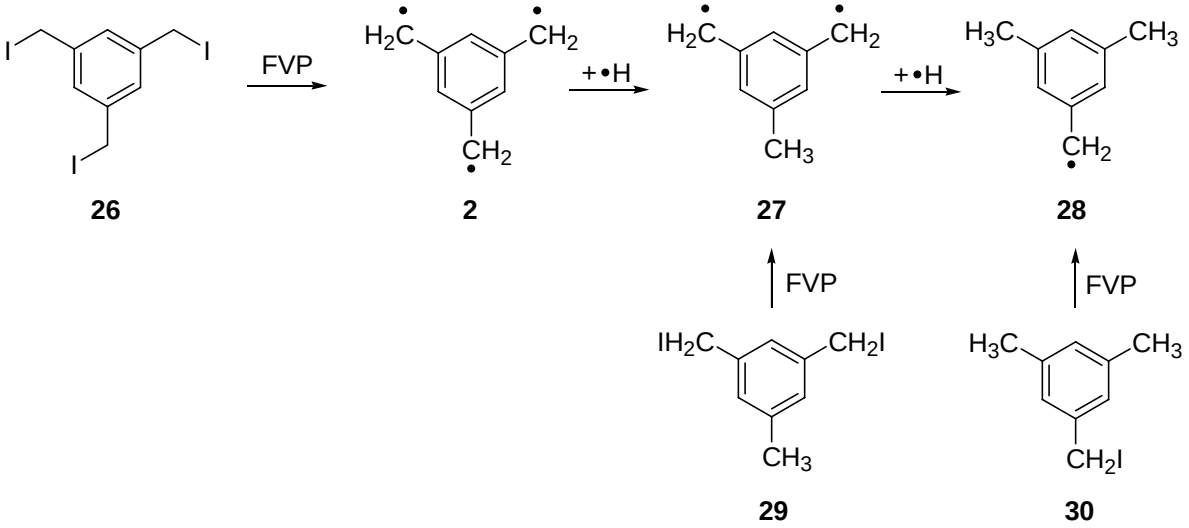

Scheme 8. FVP of 1,3,5-*tris*-(iodomethyl)benzene **26** yields quartet triradical **2**, triplet diradical **27**, and doublet radical **28**. The latter two substances were independently obtained through FVP of the corresponding iodides **29** and **30**, respectively.

Triplet **27** and doublet **28** were characterized by EPR and UV/Vis spectroscopy. Both radicals were observed after FVP of 1,3,5-*tris*-(iodomethyl)benzene **26** in IR, UV/Vis and EPR spectroscopic measurements. Their independent isolation allowed the distinction of signals from **27** and **28** with signals assigned to triradical **2**.

It is not clear if the UV/Vis spectrum obtained after FVP of **26** shows absorptions of triradical **2**, as absorptions due to impurities can not be excluded. The amount of **2** in the matrix does not allow a characterization of the photoproducts of **2**, as all resulting signals are weak and broad.

1.5 2-Dehydrophenylnitrene

Dehydrophenylnitrenes are triradicals with two electrons located in σ orbitals and one in a π orbital. Depending on the topology of the molecule, the ground state can be a quartet or doublet state. Unsubstituted dehydrophenylnitrenes have not been reported in

literature, so far, and 2-dehydrophenylnitrene **31** is found to give a quartet EPR spectrum in close similarity to the 3,4,5,6-tetrafluoroderivative (Scheme 9).[1]

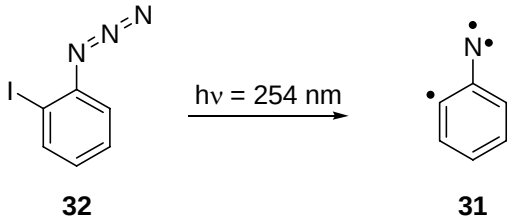

Scheme 9. The EPR spectrum recorded after UV irradiation of 2-iodophenyl azide **32** gives rise to quartet signals, which can be assigned to 2-dehydrophenylnitrene **31**.

Upon short wavelength photolysis of 2-iodophenyl azide **32** with λ = 254 nm peaks belonging to triplet 2-iodophenylnitrene **33** are appearing in the IR spectrum. This triplet nitrene was interconverted into two isomeric ketenimines **34** and **35**, with **34** formed in higher yield (Scheme 10).

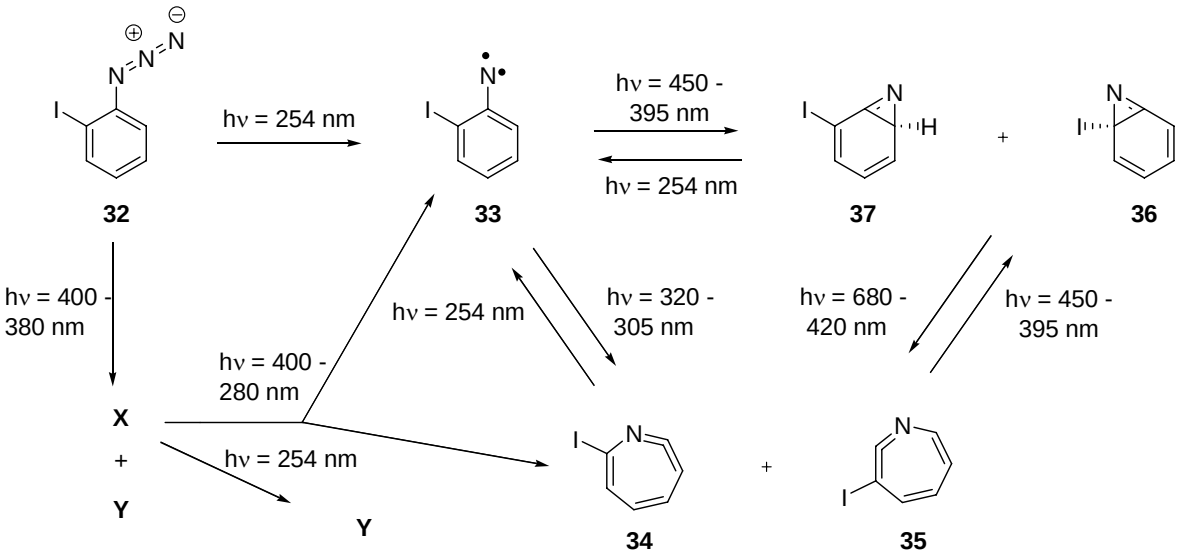

Scheme 10. Photochemistry of 2-iodophenyl azide **32** yields triplet 2-iodophenylnitrene **33**, ketenimines **34** and **35**, benzazirines **36** and **37** as well as some unidentified photoproducts **X** and **Y**. No indication of 2-dehydrophenylnitrene **31** is obtained in the IR spectra.

The corresponding benzazirines **36** and **37**, which are formed through ring-closure of the nitrenes are as well observed under the photolytic conditions. Upon long wavelength irradiation with 400 – 380 nm some new signals are appearing, which nevertheless could not be assigned to any of the supposed ring-opening isomers of 2-iodophenylnitrene **33**.

1.6 Triazatrimethylenemethanes

Triaza derivatives of trimethylenemethane (TMM) were studied by EPR spectroscopy. Upon short wavelength photolysis of tetrazoline **38**, triplet signals attributable to triplet triazaTMM **39** were detected. The Curie-Weiss analysis in combination with *ab initio* calculations led to the conclusion of a triplet ground state for **39** (Scheme 11).

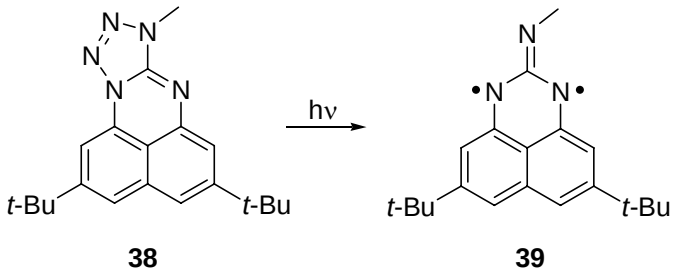

38 **39**

Scheme 11. Photochemistry of tetrazoline **38** results in formation of triplet triazaTMM **39**.

Less constrained triazaTMM derivatives like **40** and **41** were obtained from short wavelength photolysis of the corresponding tetrazoles **42** and **43** isolated in rare-gas matrices (Scheme 12).

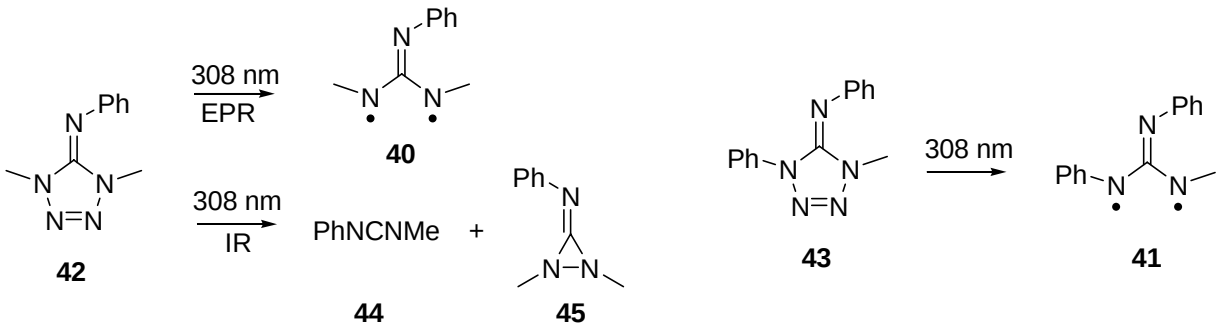

42 **40** **44** **45** **43** **41**

Scheme 12. Unconstrained tetrazoles **42** and **43** give the corresponding triplet triazaTMM derivatives **40** and **41** on irradiation with 308 nm light of a XeCl excimer laser. However, IR experiments on **42** allow only the identification of closed-shell molecules **44** and **45**.

In addition to signals assignable to triazaTMM **40** and **41**, some new EPR transitions were obtained, which might belong to a delocalized diradical. Nevertheless, IR experiments with **42** do not give conclusive evidence for any delocalized diradical, indicating the difference in sensitivity between EPR and IR spectroscopy. Instead, some closed-shell molecules like **44** and **45** with characteristic IR absorptions could be detected after photolysis.

2. Introduction

In general, there are two complementary experimental spectroscopic approaches to study reactive intermediates. In matrix isolation spectroscopy, the reactive intermediate - or a precursor thereof – is trapped in a rare gas matrix at low temperature on a cold spectroscopic window. Laser flash photolysis (LFP) and the step-scan technique, on the contrary, are solution phase spectroscopic techniques. While in matrix isolation spectroscopy, the isolation and interconversion of reactive species under "single molecule" conditions is of interest, the latter techniques are appropriate to study the kinetics of short-lived molecules as well as solvent effects on the kinetics.[2, 3]

The first stabilized radical which was observed in solution is the trityl radical **46** (Scheme 13). Gomberg reported in 1900 that the reduction of triphenylchloromethane **47** with zinc results in a yellow coloration of the benzene solution, which is caused by formation of the trityl radical **46**.[4]

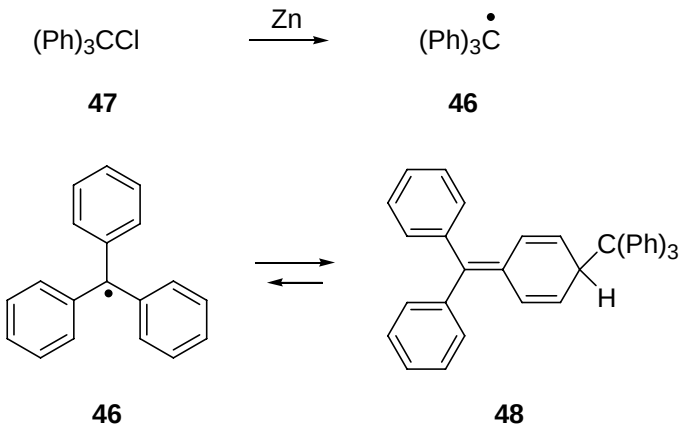

Scheme 13. Gombergs experiment from 1900 to produce trityl radical **46** from chloride **47** (above).[4] Trityl radical dimer **48** is in equilibrium with radical **46**.

The structure of the trityl radical dimer **48**, a quinoide species, was conclusively established more than half a century later.[5, 6] As shown in the example in Scheme 13, radicals are open-shell species and therefore they can achieve a closed-shell singlet electron configuration through dimerization. In nearly all known instances the dimerization has no barrier and only demands the encounter of two such radical species in solution.

15 years after Gomberg's experiments, Schlenk and Brauns prepared the first stabilized organic diradical based on *m*-xylylene **1**, and in 1937 Leo prepared a triradical which has a 1,3,5-trimethylenebenzene unit **2** as basic entity.[7, 8]

A special characteristic of a diradical – which makes it very different from a monoradical - is its possibility to form a singlet configuration through bond formation between its radical centers (“dots”), located within *one* molecule. Formation of an open-shell singlet state in which both electrons are unpaired and have antiparallel spin or a triplet state with both unpaired electrons coupled ferromagnetically are two further possible electronic configurations for a diradical.

The same is true for all molecules which have an even number of unpaired electrons such as triplets, quintets, septets, etc. (Scheme 14). All molecules with an odd number of electrons and thus an even multiplicity, i.e. doublets, quartets, sextets, etc. always have at least one unpaired electron in their electronic ground state, but of course they might also have more than one unpaired electron ferromagnetically coupled (Scheme 14).

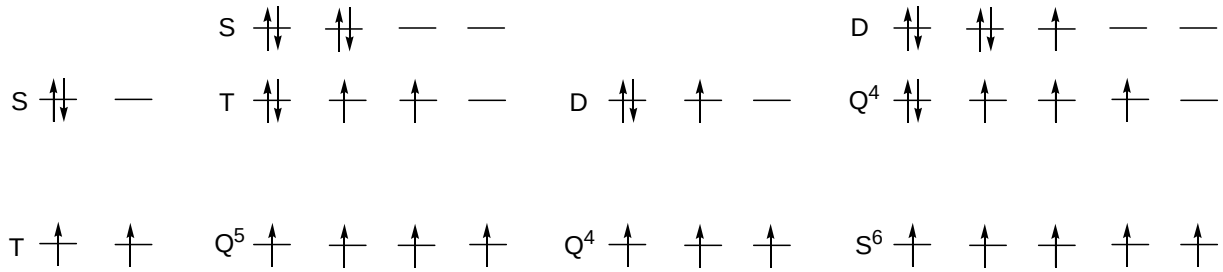

Scheme 14. Different electronic configurations of triplet, quintet, quartet, and sextet ground state species. For reasons of simplification only one electronic configuration is shown for each low-spin state.

There are for example 70 ways to arrange four electrons in four orbitals. This will give rise to 36 states: 20 singlets, 15 triplets and one quintet.[9] In Scheme 14 all molecular orbital (MO) energies are of the same energy, i.e. they are degenerate. In general, degeneracy will only result due to symmetry reasons. In molecules bigger than a few atoms, the only irreducible representations that are degenerate are of *E* type, that means doubly degenerate (for example in D_{3h} symmetry). A symmetry-induced degeneracy is often not necessary to couple two or more electrons in a ferromagnetic fashion, but the energy gap between the MOs holding the unpaired electrons should not be too large.[9] If the energy gap between two orbitals gets larger than the energy needed to antiferromagnetically couple two electrons in the lower energy orbital, the ground state will be a low-spin state. The orbitals, in which the electrons are located, are of nonbonding

nature, as they do not contribute (or contribute insignificantly) to the bonding energy of the molecule and are therefore nonbonding MOs (NBMOs).

Two of the above mentioned molecules, namely *m*-xylylene **1** and 1,3,5-trimethylenebenzene **2**, belong to the class of non-Kekulé molecules. Another prominent member of this class of molecules is trimethylenemethane (TMM) **49**. A non-Kekulé molecule is defined by IUPAC as a molecule, that is fully conjugated, but in which each Kekulé structure contains at least two atoms that are not π bonded (Scheme 15).[10]

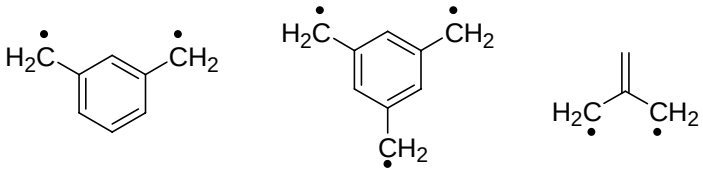

1 **2** **49**

Scheme 15. Non-Kekulé molecules *m*-xylylene **1**, 1,3,5-trimethylenebenzene **2**, and trimethylenemethane **49**.

In general, a Kekulé structure represents the (aromatic) molecule with fixed alternating single and double bonds. Clearly, there will be more than one Kekulé structure for each of the non-Kekulé molecules, but none of these will have all its π electrons paired.

2.1 Ground state predictions

The simplest model for the prediction of a molecule's ground state is the two-electron two-orbital approach. Dougherty as well as Rajca used this model to clarify why molecules should at all have electrons coupled in a ferromagnetical way. The most important factors are found to be the overlap integral S and the exchange integral K between the interacting orbitals. While the first should be minimized to the largest extent, the second should be large for ferromagnetic coupling between the electrons.[9, 11] In the usual MO approach, two MOs of the same irreducible representation can mix and form a bonding, lower energy orbital, and an antibonding, higher energy orbital. This is shown in Scheme 16 for two hydrogen atoms forming a hydrogen molecule.

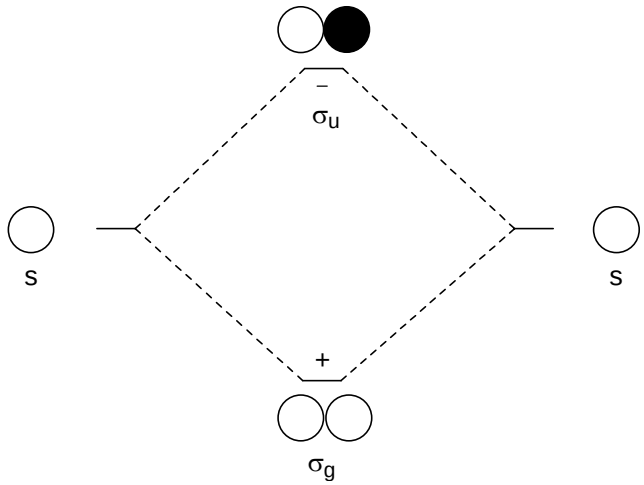

Scheme 16. Mixing of two 1s hydrogen atomic orbitals to an in-phase and an out-of-phase MO.

In general, the overlapping of the orbitals will result in an energy gap between the in-phase and out-of-phase combination of the orbitals, leading to an antiferromagnetical coupling between the electrons – that means a bond is formed. As the singlet is the ground state even at very high bond distances where no gain in energy can be expected, it was concluded that *nature favours antiferromagnetical coupling of two weakly interacting electrons*.[9]

In which cases ferromagnetic coupling is favoured can be seen in the carbon atom, where two perpendicular p-orbitals are singly occupied. The overlap integral S amounts to zero, as positive and negative contributions cancel each other, while the exchange integral K is substantial. It is very important to consider that there is a *formal* overlap between the orbitals (if only the orbitals without signs are considered), as only in this case the exchange integral K will be effective (Scheme 17).[9]

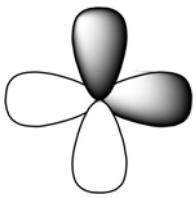

Scheme 17. Two perpendicular p-orbitals having an overlap integral S of zero, while the exchange integral K is quite substantial.

Since the exchange integral K considers the exchange interaction between electrons of the same spin, it will reduce the energy of the high-spin state while the low-spin state is not affected.

2.2 Predictions for non-Kekulé molecules

In 1950 Longuet-Higgins already concluded, that for non-Kekulé molecules, which contain no odd membered rings, the number of NBMOs is the same as the number of deficient carbons in any principle resonance structure.[12] In the ground state there will be just one electron in each of such NBMO, with their spins coupled ferromagnetically. The results are applicable to all alternant hydrocarbon systems. The distinction between alternant and non-alternant hydrocarbons can simply be made by a counting procedure. One carbon atom is chosen as a starred one with all its neighbours unstarred having starred neighbours and so forth. If this motif of starring is followed over the whole molecule and no two starred or unstarred carbons are nearest neighbours, the hydrocarbon belongs to the alternant class. Otherwise it is stated as a non-alternant hydrocarbon. This simple procedure describes the topology of the molecule, i.e. its connectivity. A typical example is given by the isomeric quinodimethanes **50**, **51**, and **1** (Scheme 18).

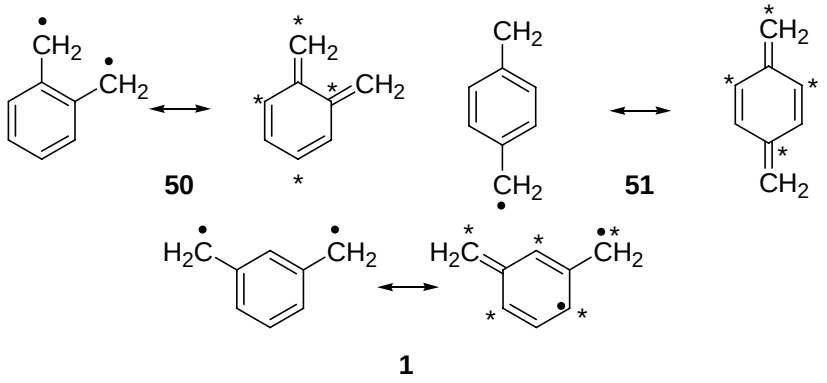

Scheme 18. *Ortho*- **50** and *para*-quinodimethane **51** have resonance structures with all spins paired. No such resonance structure is possible for *m*-xylylene **1**.

The *ortho* **50** and *para* **51** isomers are Kekulé molecules in which a resonance structure exists which has all electrons paired (X = 0, N = 8, T = 4, see below). In contrast, *m*-xylylene (*meta*-quinodimethane) **1** has two unpaired electrons in two NBMOs, as all resonance structures will have at least two electron deficient carbon atoms (X = 2, N = 8, T = 3, see below). An equation describing the finding is as follows:

$$X = N - 2T$$

X denotes the number of corresponding NBMOs, while N resembles the number of π carbons and T the maximum number of double bonded carbon atoms in any principle

resonance structure. As discussed by Itoh et al. the given multiplicity of an alternant hydrocarbon might even be higher than the value derived by the Longuet-Higgins procedure.[13] It should be mentioned that the above procedure is applicable exclusively for the resonance of π systems. For instance, any n-orbitals, as in carbenes, are also nonbonding in a first approximation and therefore might be singly-occupied.[13] For example, a quintet state is found to be the ground state for *meta*-phenylene-*bis*-phenylene **52**, while the Longuet-Higgins procedure predicts a triplet ground state (X = 2, N = 20, T = 9), correspondingly the NBMOs are doubled due to the nearly degenerate n-orbitals (Scheme 19).[13]

52

Scheme 19. The Longuet-Higgins procedure predicts the NBMOs of the π system, the actual multiplicity of a molecule might be higher. **52** is predicted to be a triplet ground state molecule, but was found to be a quintet ground state molecule.[13]

A similar reasoning might be applied for other systems in which the additional electrons are perpendicular to the π system.

2.3 Valence-bond approach

Ovchinnikov developed a valence bond model for the ground state prediction in alternant molecules.[14] It was explicitly stated that the model is equally applicable to hydrocarbons as to molecules with heteroatoms within the boundaries of the theoretical model. The ground state spin is simply given by the following equation:

$$S = |N_A - N_A^+|/2$$

A and A^+ resemble different atoms in the molecule which are simply found by restricting the neighbours of A^+ to be A and vice versa. In principle, the separation of A and A^+ follows the typical spin polarization within the molecule, where positive and negative spin density occur alternant. From the above mentioned discussion it becomes evident that counting of starred and unstarred carbons and A and A^+ carbons is the same. To apply the VB approach of Ovchinnikov it was a precondition that the molecule is alternant, therefore each A^+ will always have only A neighbours and each A only A^+.

2.4 Disjoint and non-disjoint approach

A perturbative MO approach was described by Borden and Davidson to shed light on the ground state of hydrocarbons, which are formed by the union of two odd alternant hydrocarbon units. In order to find the ground state of a hydrocarbon, the NBMOs have to be known. For alternant hydrocarbons the NBMOs can be found by the zero-sum rule. Two important cases have to be differentiated. In the disjoint case, the NBMOs have no atoms in common, while in the non-disjoint case the NBMOs have atoms in common. If the NBMOs have atoms in common, the exchange interaction will result in a high-spin ground state. Since only in the high-spin state the electrons are correlated to stay apart from each other because of the antisymmetry of the wave function, the high-spin state lies below the low-spin state, in which the electrons can come close to each other resulting in high coulomb repulsion and corresponding energy enhancement. If the electrons can stay apart as the NBMOs are located in different parts of the molecule, the low-spin and high-spin states are degenerate in a first appoximation. Due to second-order effects the low-spin state is stabilized to a greater extent than the high-spin state and thus becomes the ground state. In order to decide if the NBMOs are disjoint or non-disjoint, care must be taken and only the symmetry-adapted linear combination of the MOs is useful. Moreover, if the NBMOs span common atoms it is found that the low-spin and high-spin wavefunctions use different sets of MOs.

2.5 The spin-rules

Radhakrishnan subsums some of the above mentioned models and developed some very simple spin rules.[15] In general, his ideas are based on the finding that ferromagnetic coupling is favoured for systems that have an odd chain length for their coupling unit. The three rules are as follows:[15]

1) Find the maximum number of double bonds with radical centers remaining, if any, separated by the least number of π electrons.

2) If the number of radical sites is 2, S = 0 if the shortest path between the electrons has an even number of π electrons and S = 1 if the number is odd.

3) If the number of radical sites is higher than 2, start at any radical site with S_0 and use rule 2 to find the coupling to S_1 then modify $S = S_0$ +/- S_1. Afterwards move from this electron to the next unpaired electron and update S as before.

The model can be used for alternant and non-alternant molecules as well as for hydrocarbons and heteroatomic systems.

2.6 Fusion of odd alternant hydrocarbons

A further approach which could be used to predict the ground state multiplicity of alternant hydrocarbons uses units, which consist of an odd number of carbon atoms. The position of fusion is determined to predict the ground state of the molecule. Odd alternant systems are for example a single carbon atom **53**, the allyl radical **54**, the benzyl radical **55**, and so forth (Scheme 8). Dewar already used this kind of designation of active and inactive carbon atoms. Active is meant to represent a carbon atom having non zero spin density, while inactive carbon atoms will have zero spin density in first approximation. It is found that the fusion of two odd units at active carbons will lead to strong antiferromagnetic coupling and a singlet ground state. Similarly, the fusion of two inactive sites will lead to nearly degenerate low-spin and high-spin states, with singlet being the ground state. Itoh et al. used this approach in their weak interaction model.[13] In contrast, the third possible kind of fusion at an active and an inactive carbon should favour a high-spin ground state. Examples of all kinds of fusions are given in Scheme 20.

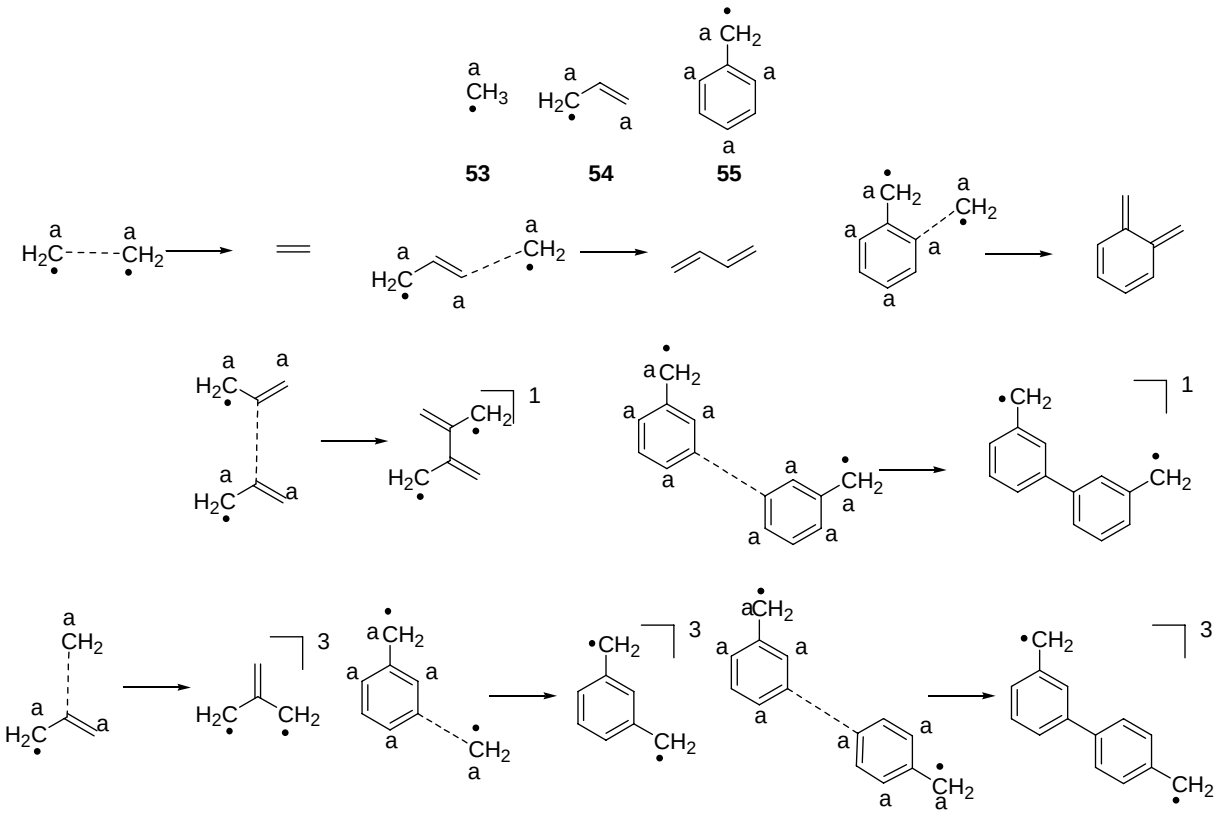

Scheme 20. Three different modes of fusion of odd alternant hydrocarbon systems are possible. Fusion can take place at active and inactive carbon atoms. Active carbons are marked with an a, while inactive carbons have no label.

As can be seen from the chosen examples, fusion of two active carbons will lead to closed-shell systems with all electrons paired, while fusion at two inactive carbons or an inactive and an active can lead to open-shell systems. Another point to be highlighted is that for the active-inactive combination the active carbons are identical to the starred carbons (or unstarred, but belong to the same class), while for the inactive-inactive combination the starred carbons do not coincide with the active carbons.

A very similar approach which is often used is based on the spin alignment of two fragments which are combined. In this context, the matching of the spins, i.e. alternation of *alpha* (α,$\uparrow$) and *beta* (β,$\downarrow$) spins throughout the product molecule results in high-spin ground states, while a spin mismatch most often gives rise to a low-spin ground state (Scheme 21).[16]

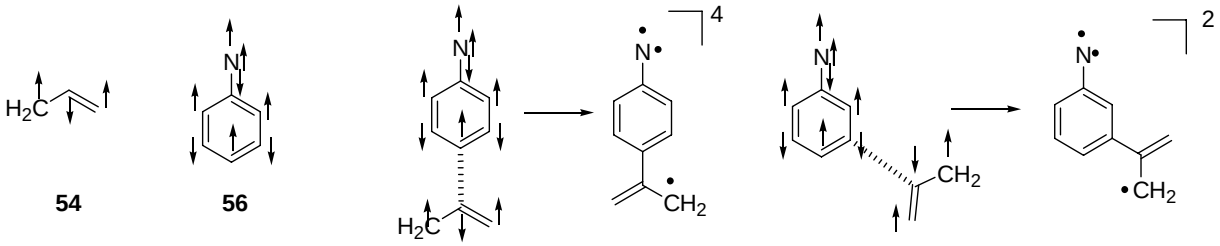

Scheme 21. Spin fragment analysis. Spin polarization pattern for allyl radical **54** and phenylnitrene **56**. Two different modes of fusion between allyl radical **54** and phenylnitrene **56** lead to different ground states.

3. Electron paramagnetic resonance

Electron paramagnetic resonance spectroscopy (EPR) is a very valuable method to study molecules with unpaired electrons. The vast majority of stable organic molecules has all its spins paired resulting in no external electron spin S (S = 0) and therefore giving no EPR transitions. All molecules with at least one unpaired electron (S > 0) interact with an external magnetic field. A free electron at zero magnetic field has two possible orientations of its electron spin relative to a specified direction *z*. If the electron precesses around the positive axis, the spin is said to be up (or *alpha*) with a spin angular momentum of S = + ½. For precession around the negative axis, the spin is said to be down (or *beta*) with a spin angular momentum of S = - ½. If no magnetic field is applied, no energy difference for the precession around any axis is expected for a free electron, and therefore the energy levels are of the same energy: they are degenerate (Scheme 22). The application of an external magnetic field lifts the degeneracy and the corresponding energy level splitting is found to be proportional to the magnetic field strength and is referred to as *Zeeman* splitting.

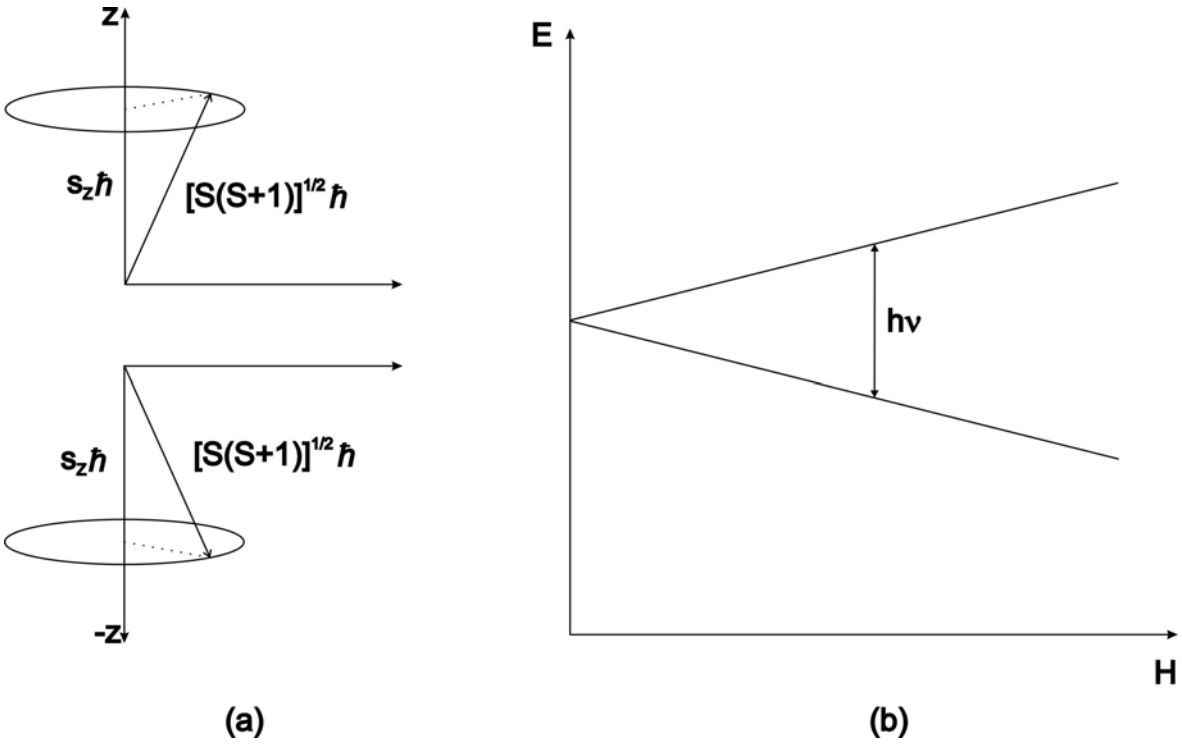

Scheme 22. (a) In an external magnetic field, the electron spin can have two orientations. (b) The free electron energy levels are degenerate at zero magnetic field and are splitted in energy if H > 0. Resonance can occur, if hν equals ΔE.

In the commonly used experimental EPR setups the magnetic field strength is varied, while the microwave frequency is fixed. If the energy difference between the two electronic levels reaches the value of the microwave energy, the resonance condition is met and energy exchange is possible. The magnetic field at which resonance occurs is recorded and interpreted. The energy of an electron as well as the resonance condition are given by

$$E = m_s * \mu_B * g_e * H$$

$$\Delta E = m_s(\alpha) * \mu_B * g_e * H - m_s(\beta) * \mu_B * g_e * H = \mu_B * g_e * H = h\nu$$

m_s denotes the projection of the spin angular momentum on the magnetic field axis, μ_B is a constant known as the Bohr magneton, g_e is the Landé factor of the free electron which can change for different radicals and H is the magnetic field strength.

If there are two energy levels, only one transition is possible and therefore only one signal is expected for the free electron (Scheme 22b).

In addition to the Zeeman splitting due to the interaction of the electron with the magnetic spin, a similar nuclear Zeeman splitting results from the interaction of a nuclear spin with the applied magnetic field. The nuclear Zeeman term in general has the same form as the electron Zeeman term ($H = \mu_I * \mathbf{H} * \mathbf{g_I} * \mathbf{I}$) and will add a constant value to the energy of the state. Since the selection rules in EPR spectroscopy are given by:

$$\Delta m_s = +/- 1; \Delta m_I = 0$$

the transitions will not be affected by this term, as the constant energy value is also added to the energy of the final state to which the transition leads.

The important interaction which makes EPR spectroscopy such a powerful tool for radicals is given by the interaction of the electron spin with nuclear spins and is known as hyperfine coupling. This interaction also occurs if no external magnetic field is applied. The Hamiltonian describing this phenomena is given by:

$$H = \mathbf{S} * \mathbf{A} * \mathbf{I}$$

S and **I** are the electron and nuclear spin operators, respectively, while **A** is a tensor, which can be diagonalized. Three different values of **A**, namely A_{xx}, A_{yy}, and A_{zz} are

therefore found in molecules lacking a threefold symmetry axis. If such a symmetry is present, only two specific **A** values are expected, $A_{||}$ and A_{+}. For molecules with spherical symmetry, the **A** tensor is expected to be isotropic. As can be seen in the Hamiltonian, the hyperfine interaction is not dependent on the applied external magnetic field, which is true only in the high magnetic field limit.

For a nuclear spin with nuclear spin quantum number I = ½ (for example a hydrogen atom), each electronic level is splitted into two parallel levels (Scheme 23). As the only field dependent term is the electron Zeeman term, the slope of the two levels is the same so that they run parallel. As $\Delta m_I = 0$, the transition occurs between energy levels having their nuclei proceeding in the same direction. In contrast to the nuclear Zeeman term this interaction adds a term to the energy of the molecule as is seen if the nuclear spin quantum numbers of the different levels are added to the scheme (Scheme 23). The preferential orientation of a nuclear spin in the external magnetic field next to an electron with α spin is different from the one of β spin. The resultant state, where a nucleus with $m_I = -½$ is next to an electron with $m_s = +½$ is lower in energy than the state where $m_I = +½$. On the contrary, for an electron with $m_s = -½$, the state with $m_I = +½$ of the nuclear spin is lower in energy than the state with $m_I = -½$. The orientation of the nuclear spin in the external magnetic field is controlled by its magnetic moment, but it will always be opposite to each other in the lower and higher electronic energy levels.

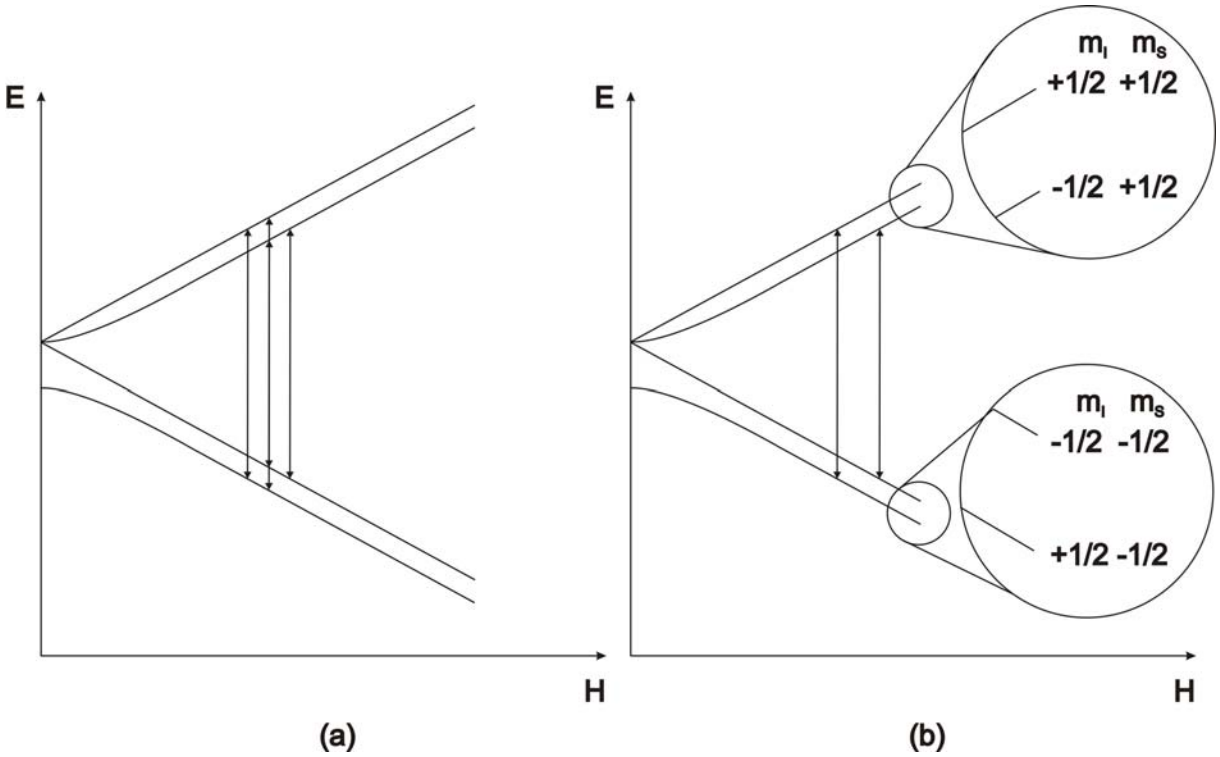

Scheme 23. (a) In principle, four transitions could be imagined between four energy levels. (b) The EPR selection rules only allow change of the electron spin, thus two EPR transitions are observed.

Regarding the nuclear spin states, transitions will occur between the outer and the inner energy levels as the nuclear spin state is not allowed to change during an EPR transition. There are two allowed transitions in this case, separated by the hyperfine splitting. A nucleus with a nuclear spin of 1 like a deuterium atom accordingly splits each spin transition into three lines with equal intensity. In general, the number of splittings produced by a nucleus with nuclear spin of I is given by (2I+1). If there are several equivalent nuclei, their spin nuclear quantum numbers can be added to an effective nuclear spin.

$$I_{eff} = I_1 + I_2 + I_3 + ...$$

In these cases, the intensity pattern is given by the Pascal triangle.

3.1 Introduction to triplet and high-spin EPR spectroscopy

The distinction of S = ½ EPR spectroscopy and S > ½ EPR spectroscopy stems from the very different EPR spectra obtained for radicals in contrast to triplet diradicals, quartet triradicals, etc.. If only organic radicals are considered, in most cases the **g** value is

quite near to 2.0023, the free electron value. As **g** indicates the position where the resonance lines are found, most organic monoradicals are observed near 3400 G in X-band EPR spectroscopy. EPR spectra of triplet and higher multiplicity molecules instead can be spread over the whole available magnetic field strength under special conditions, or even beyond. In matrix EPR we primarily focus on powder spectra, in which the molecules are rigidly held but randomly oriented in the rare gas matrix. In contrast to this, in single crystal EPR the molecules are aligned in a prefered direction.

The reason for the difference of high-spin EPR spectroscopy is seen in the perturbation of the first electron due to the magnetic field of the second unpaired electron. This interaction is described by an additional spin Hamiltonian, which has to be added to the before mentioned Hamiltonian as follows:

$$H_S = \mathbf{S} * \mathbf{D} * \mathbf{S}$$

In comparison to the hyperfine interaction which has a similar form, this term is normally much larger than the latter and it is therefore labelled fine structure term. **D** again is a tensor which can be diagonalized (sometimes collinear with the principle directions of **g**, sometimes with different principle directions). In order to have an idea of the energy relations between the different terms in EPR spectra, the following table gives the values reported by Hutchison (Table 1):[17, 18]

Table 1. General energetic magnitudes of the different terms in EPR spectra.

Term	Photoexcited triplet molecules [MHz]	Substituted methylenes [MHz]
$\mathbf{S} * \mathbf{D} * \mathbf{S}$	3000	12000
$\mu_B * \mathbf{S} * \mathbf{g_e} * \mathbf{H}$	6000 – 12000	3000 – 22000
$\mu_I * g_I * \mathbf{H} * \mathbf{I}$	8 – 16	4 – 35
$\mathbf{S} * \mathbf{A} * \mathbf{I}$	0 – 20	0 - 8

It is obvious from Table 1, that the interaction between the two unpaired electrons can be quite substantial. The conversion of MHz to cm^{-1} is given by

$$1\ cm^{-1} = 29979\ MHz$$

Since the fine structure term does not contain the magnetic field, it also acts at zero magnetic field and lead to the well known zero field splitting (zfs) of the triplet sublevels.

D is a traceless tensor and therefore there are only two independent parameters, D and E, describing its effect. These are called zero field parameters and are commonly given in units of cm^{-1}. If D and E are used to describe a high-spin system, the Hamiltonian is given as:

$$H = [DS_z^2 - 1/3S(S+1)] + E[S_x^2 - S_y^2]$$

In order to obtain a unique definition, there are two conditions which have to be met:

1. $|D| > |3E|$
2. the signs of D and E have to be opposite to each other.

If D and E are assumed to be only of dipole-dipole nature, it can be described by the following formula:

$$D \sim < ¾\ g_e^2 * \mu_B^2 * [3z^2 - r^2]/r^5 >$$

$$E \sim < ¾\ g_e^2 * \mu_B^2 * [y^2 - x^2]/r^5 >$$

For molecules with a C_3 symmetry axis, E is 0 and the zfs is given solely by D. The D value related to the average distance between the unpaired electrons, while the E value depends on the symmetry of the molecule. A schematic visualization of the zfs parameters D and E on the energy level scheme is given in Scheme 24 for H || z.

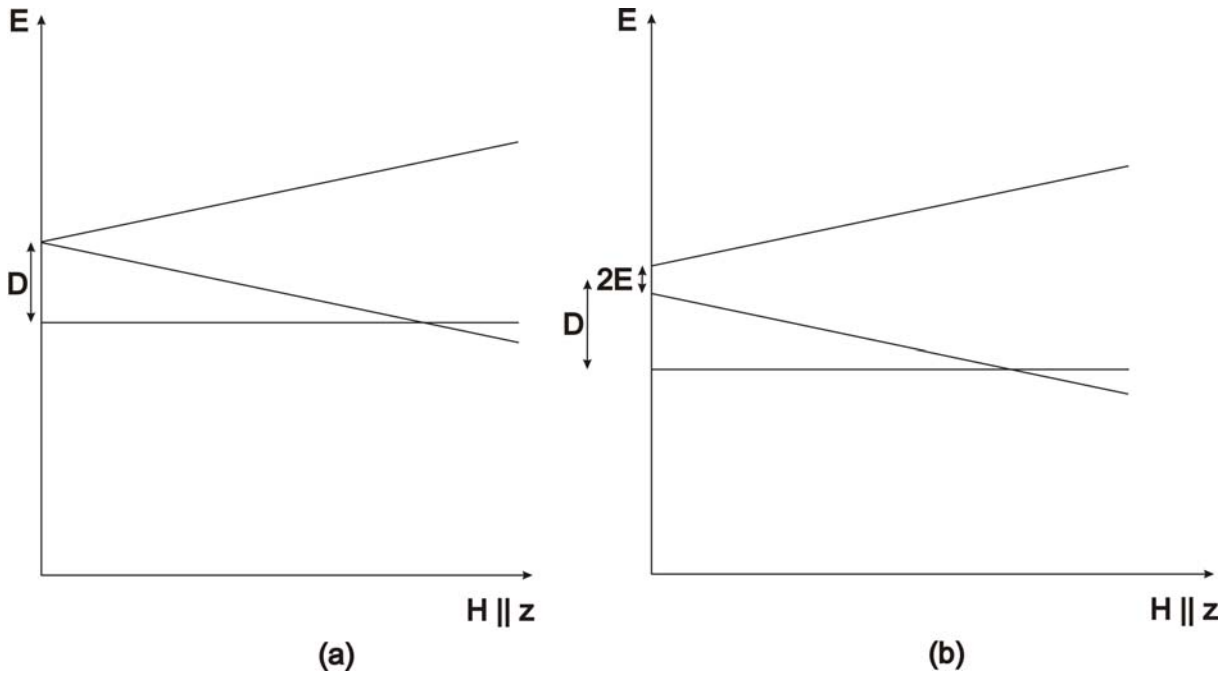

Scheme 24. (a) For molecules with a threefold or higher axis of symmetry E = 0 and D is the only zfs parameter obtained from an EPR spectrum. (b) The general definition of the zfs parameters D and E for a triplet molecule with H || z.

The zfs parameters are affecting the energy splitting of the states at zero magnetic field, while the electron Zeeman term is affecting the further splitting in an applied external magnetic field.

Single crystal studies on dilute organic molecules in host crystals have shown that the resonance field at which the molecule absorbs is highly dependent on the orientation of the molecule in the EPR spectrometer. As the molecule is rotated in one plane, the resonance field changes. Positions where the resonance fields are highest and lowest belong to orientations where the magnetic axis of the corresponding molecule are parallel or perpendicular with the externally applied magnetic field. These orientations are called canonical orientations. It can be shown that in powder spectra of triplet molecules only the canonical orientations give rise to signals, while all other orientations contribute to the background noise, as in the usual setup, the first derivative of the absorbance spectrum is recorded (Scheme 25).

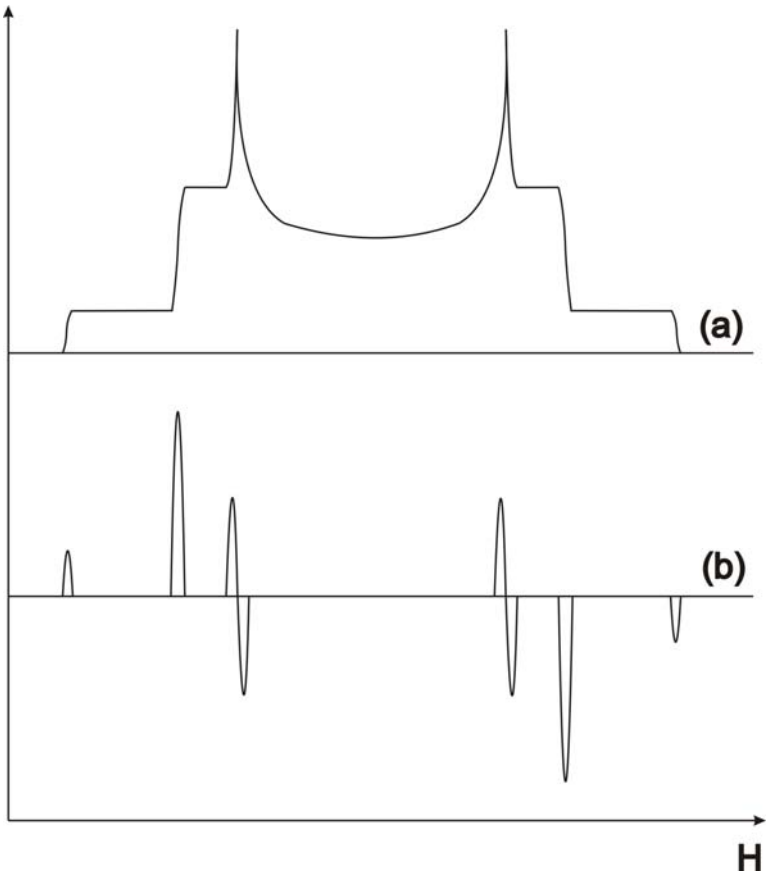

Scheme 25. (a) Absorbance of microwave irradiation by a triplet molecule, which is rigidly held but randomly oriented. (b) Corresponding EPR spectrum with signals appearing at the canonical orientations.

Since the number of molecules in the x and y direction is much higher than in the z direction, the x and y transitions are significantly higher in intensity in the observed EPR spectrum. Generally, the intensity of the transitions is proportional to the sinus of the angle (γ) between the magnetic axis and the microwave field as well as to the instantaneous change of magnetic field with orientation.

$$\text{Int} \sim \sin\gamma \; ; \; dH/d\theta$$

The spin eigenfunctions of a triplet state are given below:

$$|1\rangle = |\alpha\alpha\rangle$$

$$|0\rangle = 1/\sqrt{2}|\alpha\beta - \beta\alpha\rangle$$

$$|-1\rangle = |\beta\beta\rangle$$

An equivalent description is found for linear combinations of these eigenfunctions which are often denoted T_{+1}, T_0, and T_{-1}. Since there is always one spin eigenfunction which has no magnetic moment in one canonical orientation, it is not affected by the application of a magnetic field. The other two triplet spin states conversely have a magnetic moment in field direction and therefore split in energy. Correspondingly, one state decreases in energy, while the other state increases. Since there are three canonical orientations and three energy levels, which means there are two Δms = +/- 1 transitions possible for each orientation, there are six transitions in the Δms = +/- 1 region of the spectrum for E > 0 (Scheme 26).

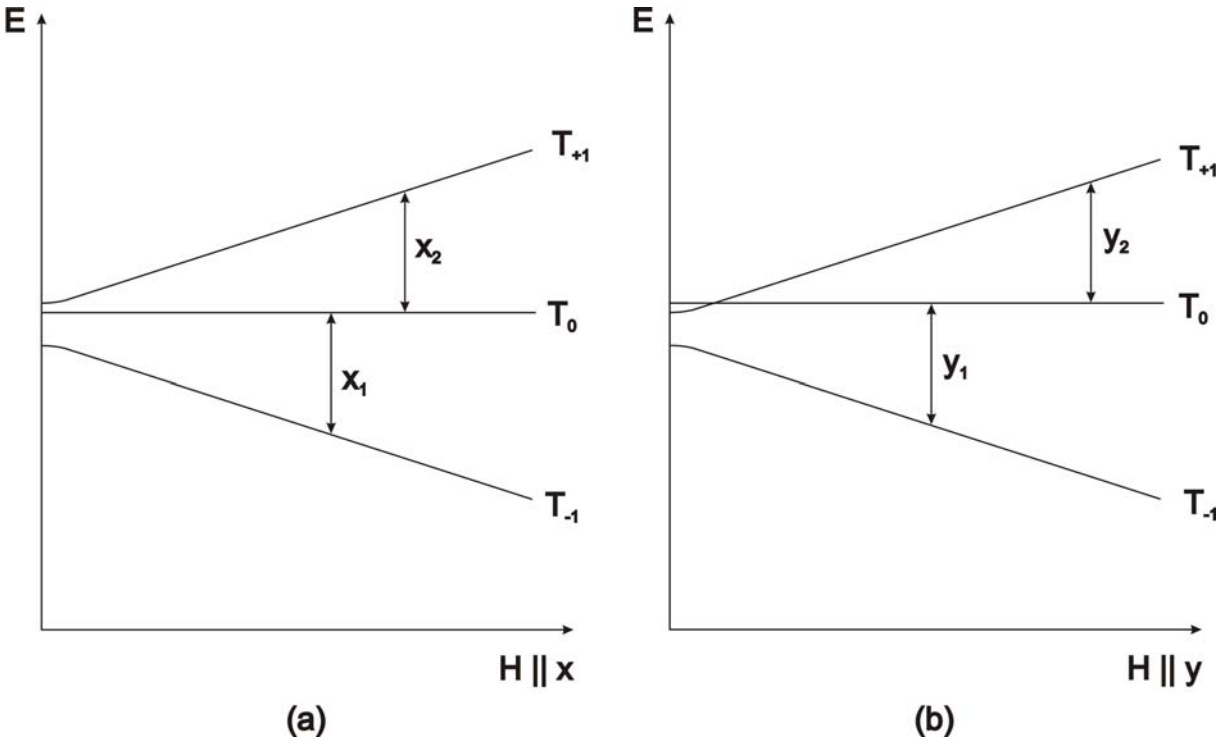

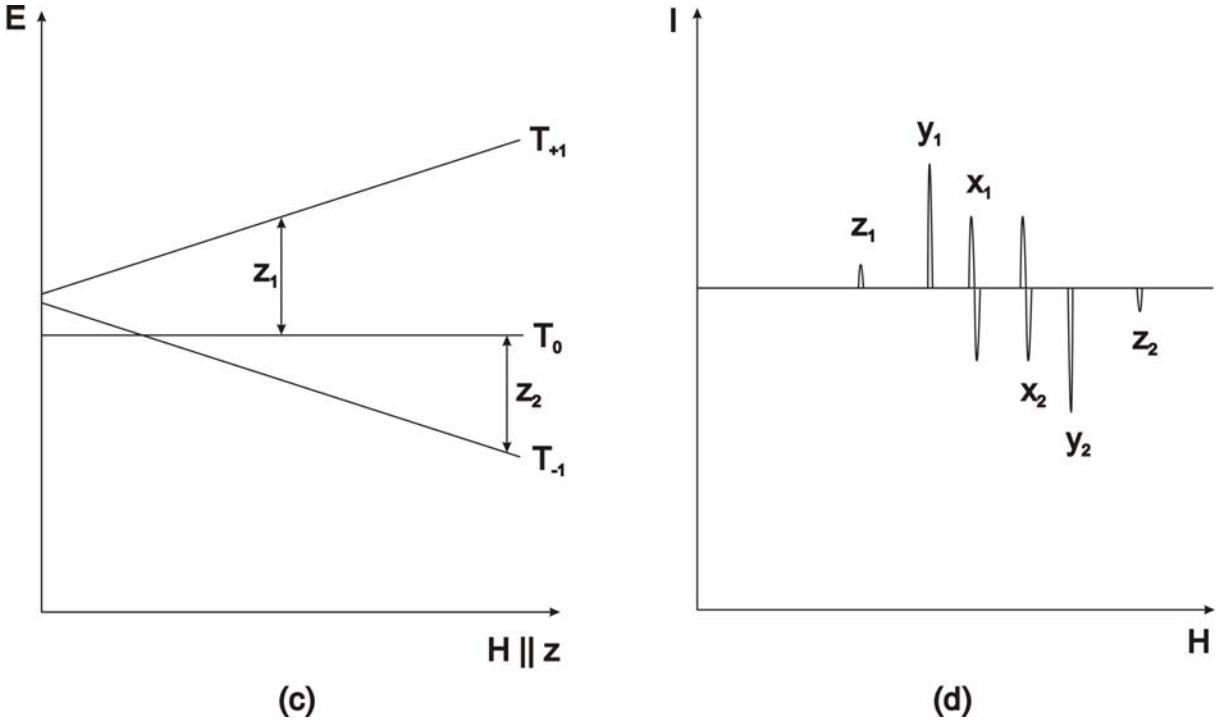

Scheme 26. Splitting of the triplet energy levels for canonical orientations: (a) H || x. (b) H || y. (c) H || z. (d) Expected EPR spectrum in the Δms = +/- 1 region. The signals are labelled according to their appearance.

This analysis is only valid as long as the D value is relatively small. If the zfs is very large, the distance between the energy levels is already quite large, even if no magnetic field is applied. The application of a magnetic field further increases the splitting between the outer levels and if the splitting is larger than the constant microwave frequency, no transition ever occurs between these levels. This is schematically depicted in Scheme 27 a and b for the energy levels of a triplet molecule with $D > h\nu$ and $E = 0\ cm^{-1}$.

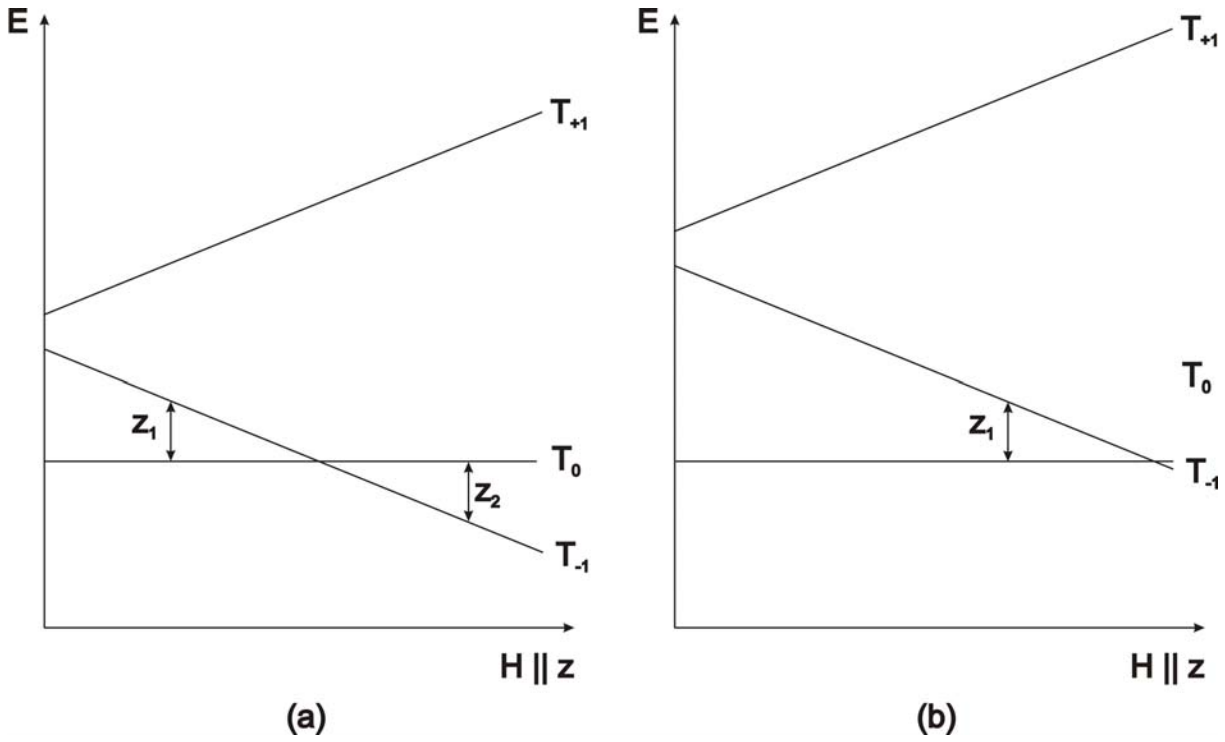

Scheme 27. (a) If the D value of a triplet molecule is larger than the microwave frequency, no transition to the T_{+1} level is possible. Instead two transitions occuring between the same energy levels are found. (b) A still larger D value results in the observation of only one z transition, which disappears at very high D value.

Two further kinds of transitions are possible between the energy levels of a triplet state. The first one is a double-quantum transition and involves two quanta of photon energy, the first one to reach an intermediate state and the second one to reach the final state from this intermediate state. The energy difference between the inital and the final state is therefore 2hν. It is important to consider that the intermediate state does not need to be at exactly half energy between the inital and the final state, because otherwise the transition would be a simple Δm_s = +/- 1 transition.

The second possible transition is most often referred to as the Δm_s = +/- 2 transition, the forbidden transition. It actually represents a transition between the outer energy levels which have to be separated by hν to satisfy the resonance condition. Compared to Δm_s = +/- 1 this transition is often stated to be much less anisotropic, clarifying that its resonance fields for the canonical orientations are far less separated in this case. It can be shown that the most intense transition is not due to any canonical orientation. It is actually shifted to lower fields than the canonical Δm_s = +/- 2 transitions. For small D values, it is found around the g = 4 region. The intensity of this transition is proportional to the square of the D value and inversely proportional to the square of the

resonance field. Even if this transition is often found to be quite small, it can be the largest observed transition in the EPR spectrum in special cases. For small D values, the forbidden transition is very often taken as a characteristic transition indicating that a triplet state is observed. The allowed transitions are centered around g = 2 in this case and cannot be properly distinguished from impurity radicals, which also absorb in this region. In contrast, the forbidden transition is clearly separated from the radical region.

The **D** tensor is not only a function of the spin-spin interaction but also has contributions from spin-orbit coupling. In fact, **D** is proportional to the square of the spin-orbit coupling constant ζ and directly proportional to the spin-orbit matrix element. In general, **D** is then written as the sum of the spin-spin interaction $\mathbf{D}_{SS}$ and the spin-orbit part $\mathbf{D}_{SO}$:

$$\mathbf{D} = \mathbf{D}_{SS} + \mathbf{D}_{SO}$$

The spin-orbit interaction can mix in near-lying states of any multiplicity and not only states of the same multiplicity. It was found that the spin-orbit interaction in the photoexcited state of naphtalene is negligible, as it is a thousand times smaller than the spin-spin interaction. However, in triplet imidogen NH, $\mathbf{D}_{SS}$ is found to be responsible for 85 % of **D**, and 15 % are due to $\mathbf{D}_{SO}$.[19] A completely different EPR spectrum results, if the spin-orbit contribution is not properly accounted for. At the same time, as **D** is the sum of two contributions, there is no experimental way to differentiate the contributions from measurement of the zfs parameters.

In order to get an idea of the zfs parameters for triplet molecules, some representative examples are shown in Table 2.

Table 2. Zfs parameters of different molecules in their triplet state.

Molecule	|D/hc|	|E/hc|	Conditions	Reference
N-H **57**	1.8394	-	gas	[19]
N-Ph **56**	0.9896	-	Ar	[20]
m-$(NH)_2C_6F_3H$ **58**	0.019 +/- 0.0003	0	2MTHF / 77 K	[21]
H-C-H **59**	0.601	0.0069	Ne	[22]

H-C-Ph **60**	0.5150	0.0251	In *p*-dichlorobenzene / 77 K	[23]
m-$(CH_2)_2C_6H_4$ **1**	0.011	0.001	Ar	[24]
Ph-C-Ph **61**	0.40505	0.01918	Single Crystal Benzophenone host	[25]
H-C-CCH **62**	0.630	0 +/- 0.001	PCTFE	[26]
CCO **63**	0.7395	-	Ne	[19]
CNN **64**	1.159	-	Ne	[19, 27]
NCN **65**	1.544	-	Hexafluorobenzene / 4 K	[27]
p-N-C_6H_4-N **66**	0.169	0.004	2MTHF / 77 K	[28, 29]
TMM **49**	0.025	0	2MTHF	[30]
DCMP **67**	0.0204	0.0028	2MTHF / 4 -140 K	[31]
1,8-CH_2-Naph **68**	0.0218	0.0021	C_6F_6 / 77 K	[32]
m-CH_2-C_6H_4-O **69**	0.027	0.008	2MTHF / 11 K	[33, 34]
α,2-DHT-CH_3CN **70**	0.1069 +/- 0.0005	0.0058 +/- 0.0003	Pentane-Isopentane glass / 77 K	[35]
C_6H_6 **71**	0.1580	- 0.0064	In C_6D_6 host / 1.95 K	[36]
$C_{10}H_8$ **72**	0.1003	- 0.0140	In durene host / 77 K	[37, 38]

TMM: Trimethylenemethane; DCMP: 2,4-dimethylene-1,3-cyclobutanediyl; 1,8-CH_2-Naph: 1,8-dimethylenenaphthaline; (CH_3)(CN)-α,2-DHT: α-methyl,α-cyano-2-didehydrotoluene

The theory deduced for triplet state EPR spectroscopy in this chapter is equally applicable to higher spin states, as well. If there are three unpaired electrons in three degenerate or nearly degenerate orbitals, this can give rise to quartet states, which could also be described by two zfs parameters, D and E. The same is true for quintet and higher

spin multiplicity. It was shown by Weltner that for S > 3/2, second order terms have to be taken into account to properly describe the zfs of these molecules. Next to D and E, there are B and H terms (with H not having the meaning of the magnetic field), which are needed for a correct description of the zfs in these molecules. Nevertheless, higher order terms are often negligible in organic molecules, as was shown by Weltner and can thus be introduced as a correction to the zfs parameters.[19]

For higher spin states the number of observed lines can easily be higher than the predicted number of the canonical orientations. This is ascribed to the well known phenomena of off-axis transitions. While canonical orientations were defined as being due to the collinearity of the intrinsic magnetic axis in the molecule and the external magnetic axis, the off-axis transitions have no such peculiarity. Instead, they can be found at any angle of the external field and the magnetic axis, when the angular dependance of the energy level has a zero slope as exemplified in Scheme 28.

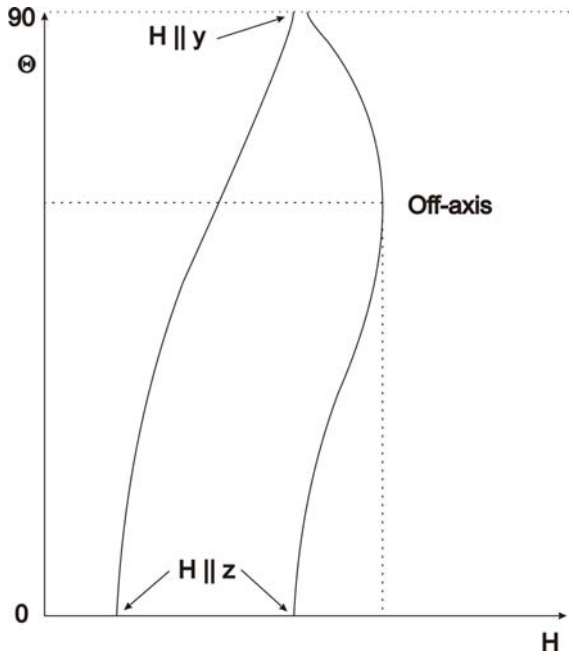

Scheme 28. Schematic variation of the angular dependance of the Δm_s = +/- 1 transitions in the zy-plane. For the energy level variation on the left, only canonical orientations will lead to transitions in the EPR spectrum, the right energy level variation has a strong signal due to an off-axis transiton at $\Theta = 70°$ next to the canonical transitions.

The higher the spin state, the more energy levels are available, the more avoided crossings between the energy levels and the more off-axis transitions are expected. Off-axis transitions are therefore most often found in molecules with S > 3/2. Besides this,

higher spin multiplicites will also allow the observation of transitions between Δm_s = +/- 3, +/- 4..., which are not possible for triplet states.

4. High-spin EPR

4.1 Triplet α,n-didehydrotoluenes and quartet dehydro-*m*-xylylenes

It is known that the photolysis of molecules containing carbon halogen bonds at low temperatures can result in the formation of the corresponding radicals. Platz et al. synthesized high-spin molecules in their triplet state via successive cleavage of two C-Cl or C-Br bonds.[39-41] Scission of carbon iodine bonds has as well been found to produce diradicals.[24] Most of these studies focused on the abstraction of a halogen atom from a benzylic position to give the corresponding stabilized radicals and diradicals. Photolytic cleavage of C-I bonds which are directly attached to an aromatic ring was used to produce the phenyl radical **73**.[42, 43] Similarly, it was shown that small amounts of *para*-benzyne **74** and *meta*-benzyne **75** were obtained by photolysis of the corresponding diiodides.[44, 45] Recently, it was reported that quartet 2- and 4-dehydrophenylnitrene **76** and **77** were obtained from the fluorinated *ortho*- and *para*-iodophenyl azides **78** and **79**, respectively.[46] However, dehydro-*m*-xylylenes formally accessible by cleavage of three C-I bonds, have not been studied experimentally, so far. Likewise, the "simpler" α,n-didehydrotoluenes were studied by mass spectrometry, while several derivatives of α,2-didehydrotoluene **81** were observed by Closs et al. via EPR spectroscopy by photolysis of 3H-indazoles **80** in glassy media (Scheme 29).[35]

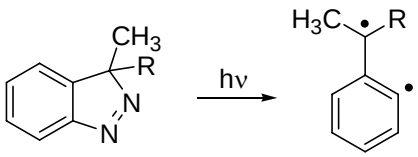

80 **81**

R = CN (**a**)
COOCH3 (**b**)
OCH3 (**c**)

Scheme 29. Synthesis of α,2-didehydrotoluene derivatives **81** from 3H-indazoles **80**.

The zfs parameters obtained by Closs et al. are summarized in Table 3.

Table 3. EPR spectroscopic data obtained by Closs et al. for triplet **81a-c**.

Structure	D [a]	E [a]	Media	T [c]	Ref.
81a	0.1069 +/- 0.0005	0.0058 +/- 0.0003	PIP glass [b]	77	10
81b	0.1110 +/- 0.0005	0.0069 +/- 0.0003	PIP glass [b]	77	10
81c	0.1217 +/- 0.0008	0.0066 +/- 0.0003	PIP glass [b]	77	10

[a] in cm^{-1}. [b] PIP = pentane – isopentane. [c] in K.

In previous experiments it was found that photolysis of 1,3-*bis*-(iodomethyl)benzene **17** leads to the same triplet EPR spectrum as flash vacuum pyrolysis (FVP) at 450°C – with minor differences due to different impurities obtained during photolysis and pyrolysis. The problem of high-spin coupled radical pairs obtained by photocleavage of C-I bonds in the rigid low-temperature matrix, which are close in distance to each other, could thus be excluded in these experiments (Scheme 30).

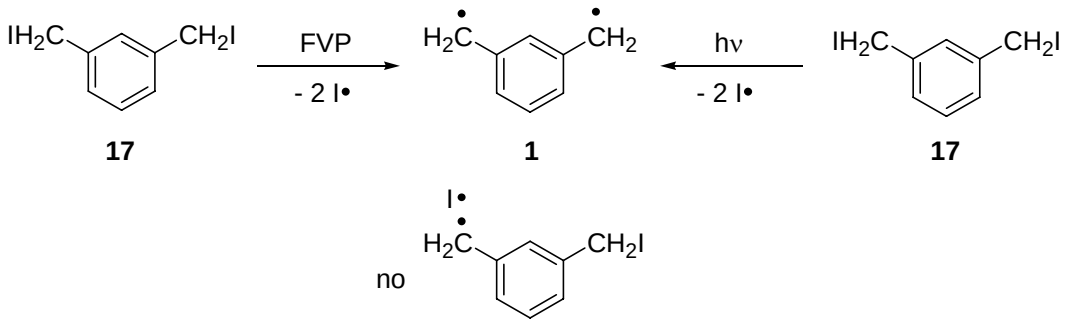

Scheme 30. Thermal and photochemical routes to *m*-xylylene **1** using 1,3-*bis*-(iodomethyl)benzene **17** as precursor.

2-Iodobenzyl iodide **8** and 4-iodobenzyl iodide **9** were synthesized to obtain the zfs parameters of the triplet states of α,2-didehydrotoluene **3** and α,4-didehydrotoluene **4**, respectively (Scheme 31). Deposition of the precursors in an argon matrix and subsequent irradiation with 308 nm light of a XeCl-excimer laser leads to rapid formation of a radical signal centered at 3480 G and several signals belonging to triplet species. One set of signals attributed to triplet α,2-didehydrotoluene **3** were fitted to the zfs parameters |D/hc| = 0.139 cm^{-1} and |E/hc| = 0.0081 cm^{-1} (Figure 1). Similarly, the set of signals attributed to triplet α,4-didehydrotoluene **4** were simulated with the zfs parameters |D/hc| = 0.212 cm^{-1} and |E/hc| = 0.0040 cm^{-1} (Figure 2).

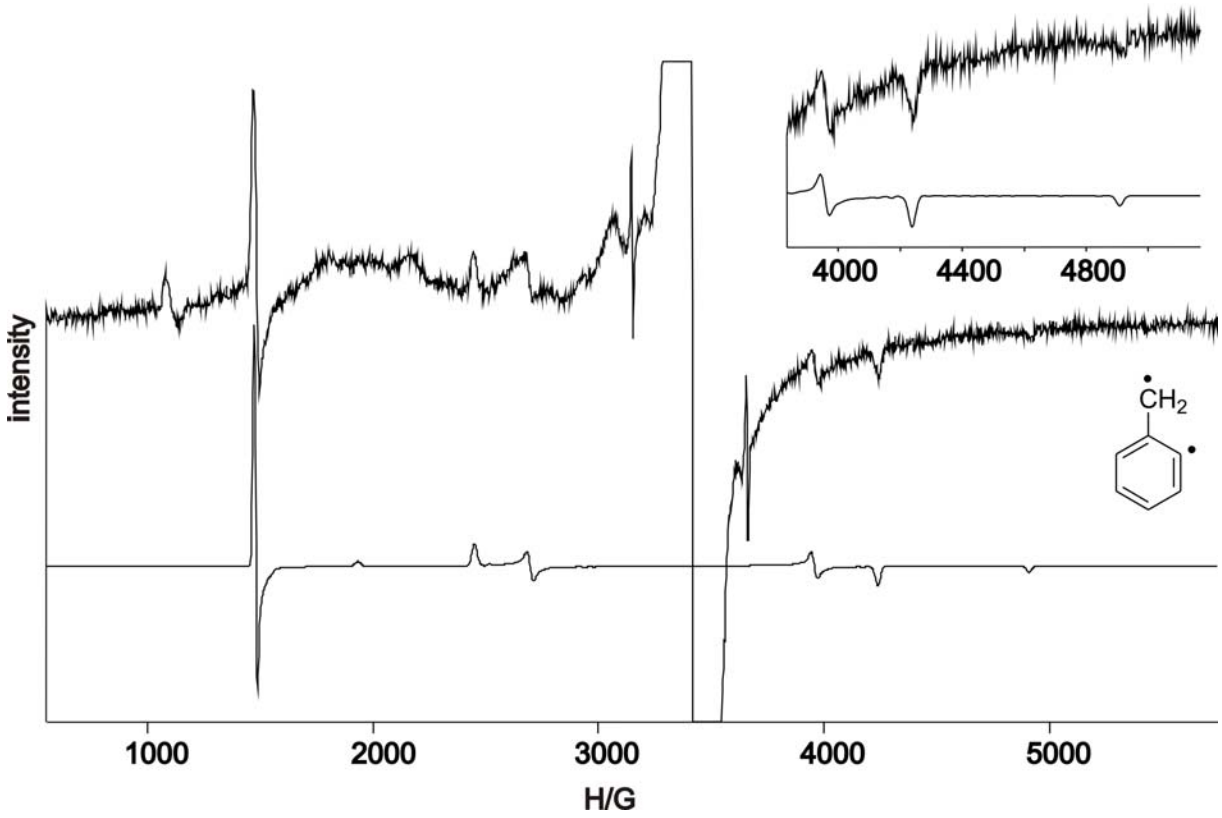

Figure 1. EPR spectrum obtained after irradiation of matrix isolated **8** with λ = 308 nm. a) Simulated triplet EPR spectrum using |D/hc| = 0.139 cm^{-1}; |E/hc| = 0.0081 cm^{-1}; g = 2.0023; μ = 9.60067 GHz. Inset: expansion of the high field region.

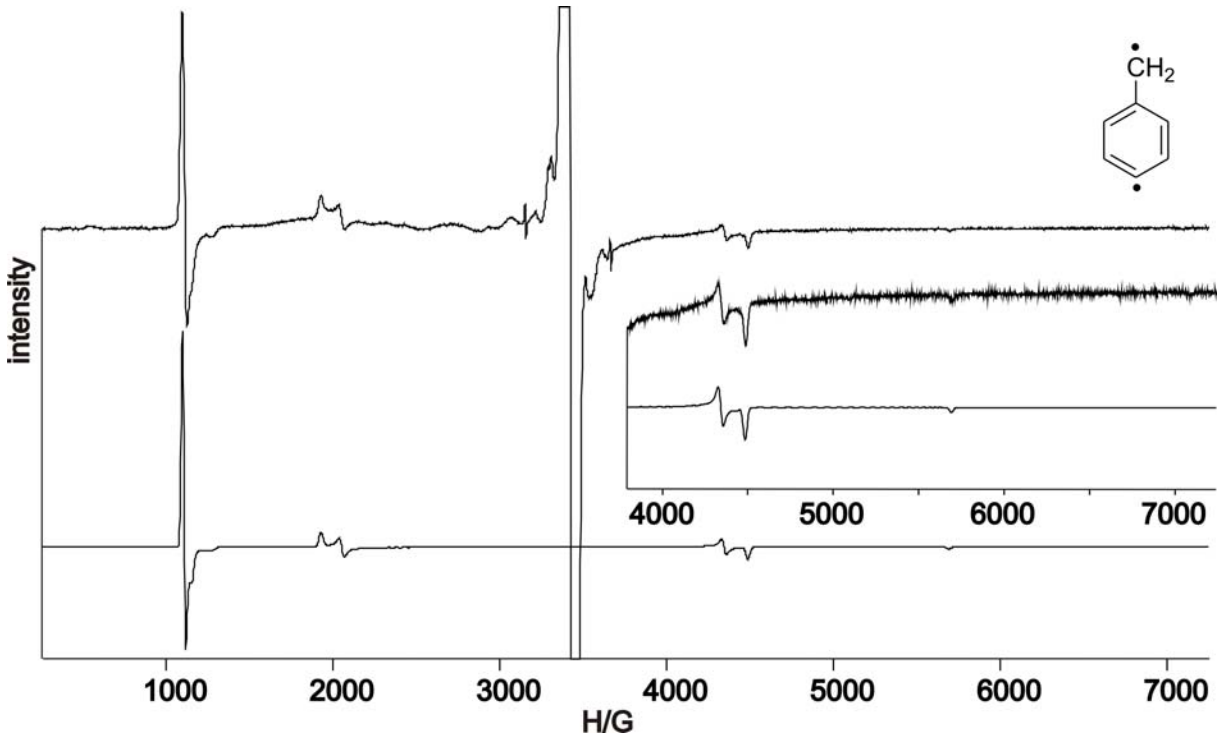

Figure 2. EPR spectrum obtained after irradiation of matrix isolated **9** with λ = 308 nm. a) Simulated triplet EPR spectrum using |D/hc| = 0.212 cm^{-1}; |E/hc| = 0.0040 cm^{-1}; g = 2.0023; μ = 9.60067 GHz. Inset: expansion of the high field region.

In addition to radical signals, strong transitions due to triplet diradicals **3** and **4** are experimentally observed (Scheme 31).

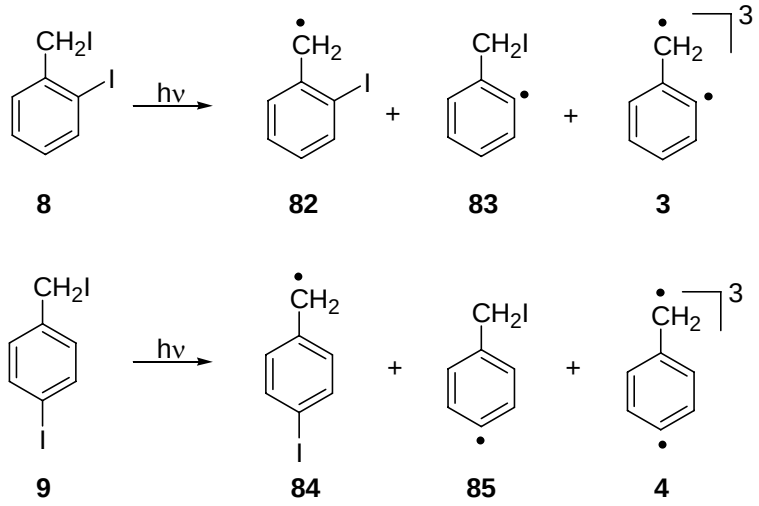

Scheme 31. 308 nm photolysis of 2-iodobenzyl iodide **8** and 4-iodobenzyl iodide **9** leads to various radicals as well as triplet α,2-didehydrotoluene **3** and triplet α,4-didehydrotoluene **4**, respectively.

FVP of 4-iodobenzyl iodide **9** at 560°C produces an EPR spectrum that is very similar to the one obtained by photolysis (Figure 3). All EPR transitions assigned to triplet α,4-dehydrotoluene **4** are clearly visible.

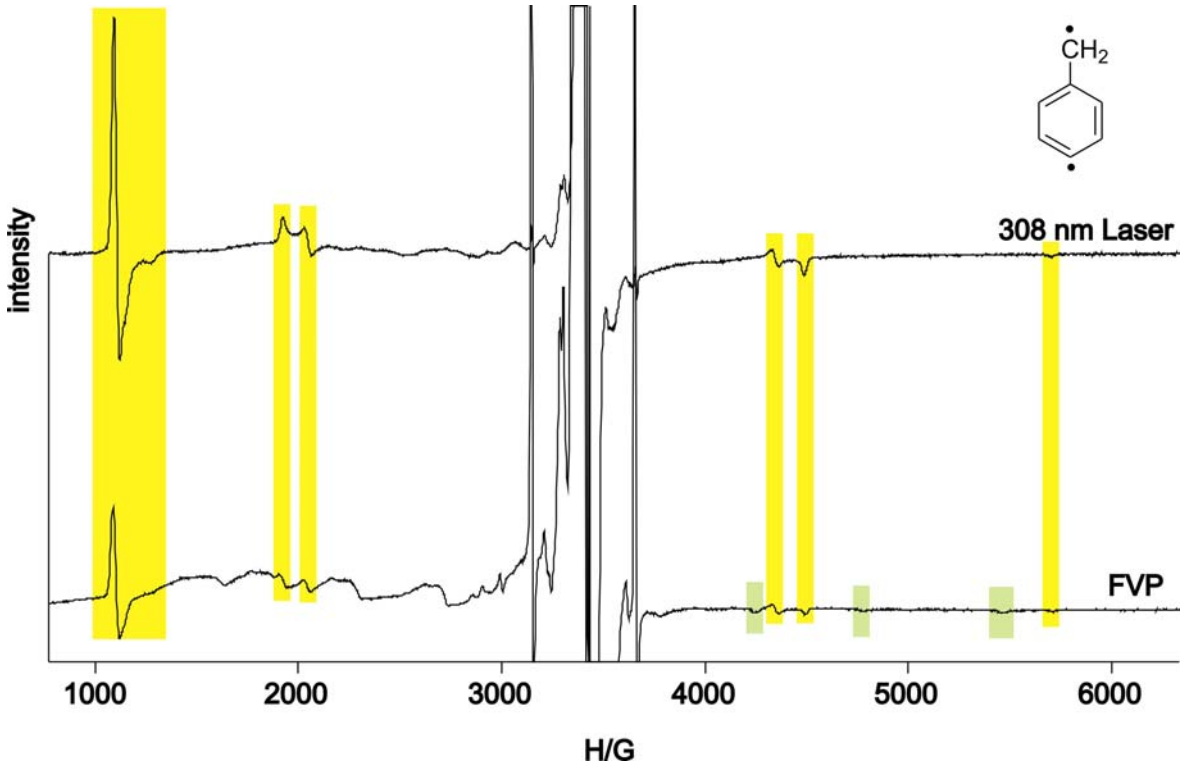

Figure 3. EPR spectra obtained after FVP and 308 nm photolysis of 4-iodobenzyl iodide **9**. Transitions assigned to triplet α,4-didehydrotoluene **4** are marked with yellow bars. Signals obtained through thermal decomposition of **9** are marked with green bars.

Nevertheless, additional transitions due to some unknown high-spin species are also observed (Figure 3, green). The thermal production of triplet α,4-didehydrotoluene **4** allows to perform a Curie analysis of the spin system (Figure 4).

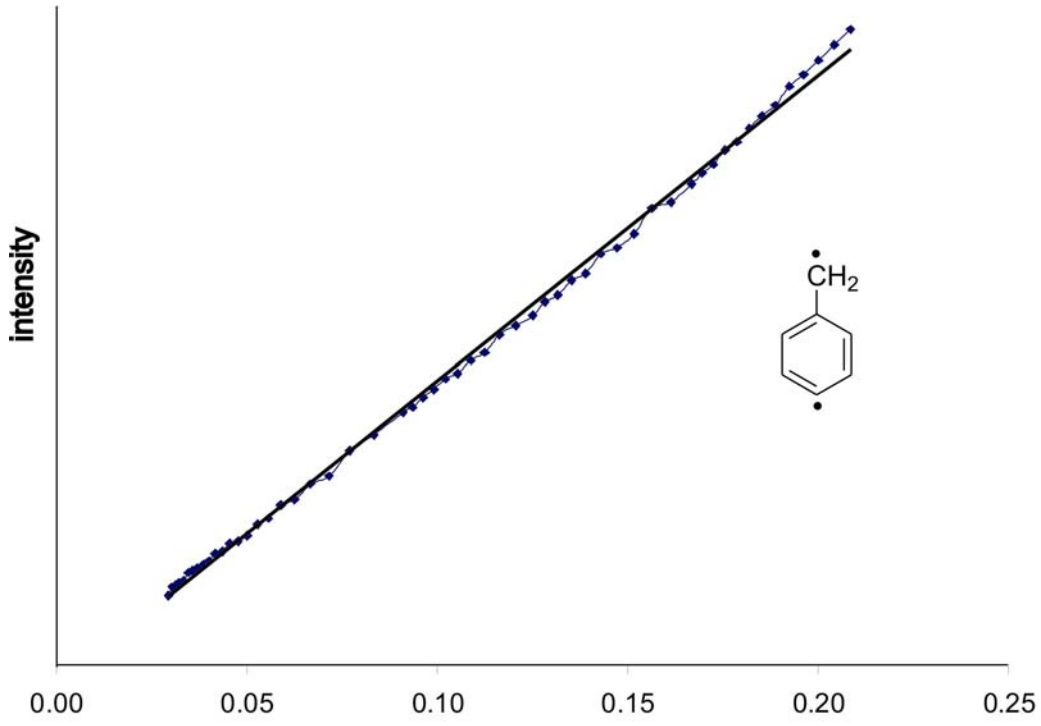

Figure 4. Curie-Plot for the strongest EPR transition of α,4-didehydrotoluene **4**.

The signal intensity is found to linearly decrease with increasing temperature, thus confirming that the species is in its ground state. Near-degeneracy of the singlet and triplet state can not be excluded, but it seems unreasonable as the triplet state is predicted by high-level CASSCF calculations to be 8.1 kcal/mol lower in energy than the open-shell singlet state.[47] The signal intensity was found to be reversibly formed back after annealing the matrix to 26 K and cooling down to 4 K, while at 32 K the signal slowly diminished irreversibly with no additional signals obtained in the EPR spectrum. Since the calculated singlet-triplet gap is 8.1 kcal/mol, thermal activation of the excited singlet state with subsequent reaction from this state (kT is very small at 30 K) seems improbable. The softening of the argon matrix at this temperature allows diffusion of trapped radical species like hydrogen atoms which can react with **4** and thereby diminish the EPR signal intensity.

FVP of 2-iodobenzyl iodide **8** does not give an EPR spectra which is similar to the one obtained after 308 nm photolysis (Figure 5). A very weak transition can be seen around 1500 gauss, while no further transitions are detected. Ring-closure of the thermally produced diradical **3** probably leads rapidly to benzocyclopropane, thus prohibiting the detection of larger amounts of **3**.

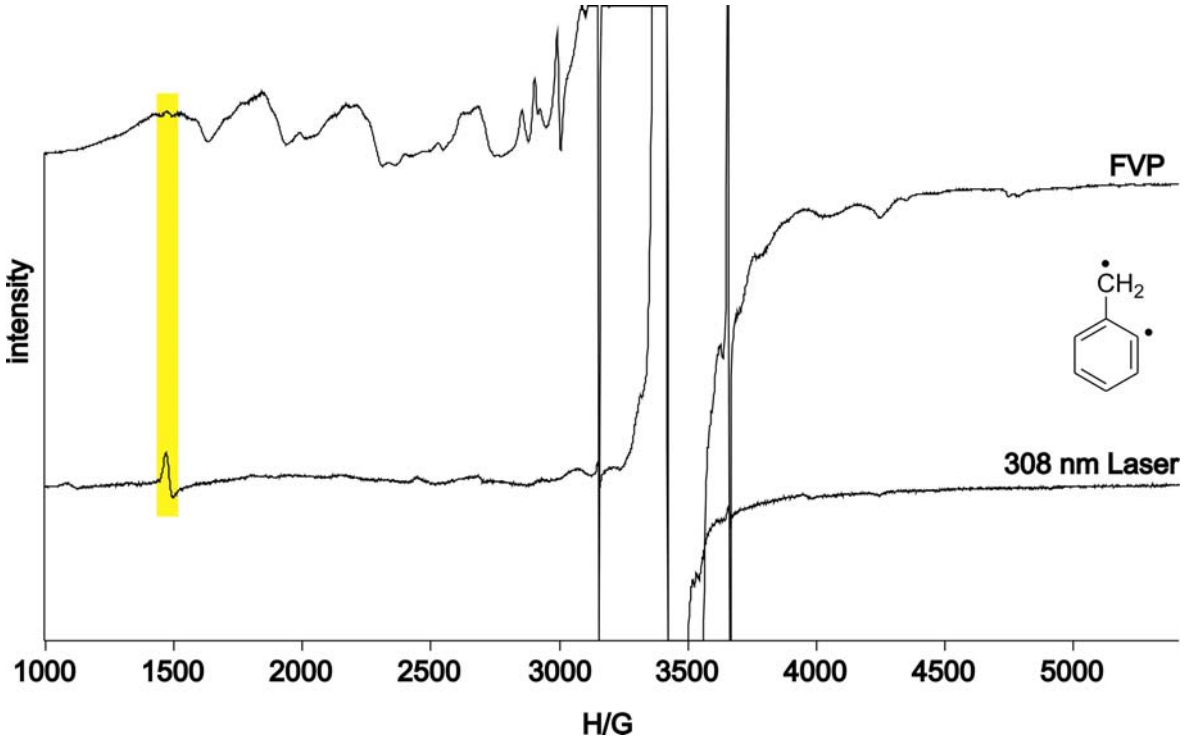

Figure 5. EPR spectra obtained after FVP and 308 nm photolysis of 2-iodobenzyl iodide **8**.

Experiments with 2,4-*bis*-(iodomethyl)iodobenzene **13** and 2,6-*bis*-(iodomethyl)iodobenzene **12** yielded the EPR spectra shown in Figure 6 and 7, respectively.

Upon λ = 308 nm photolysis of an argon matrix containing **13**, a radical signal as well as several high-spin signals probably belonging to triplet and quartet species are evolving. The quartet signals were fitted to |D/hc| = 0.0935 cm^{-1} and |E/hc| = 0.0008 cm^{-1} and are assigned to 4-dehydro-*m*-xylylene **6** (Scheme 32).

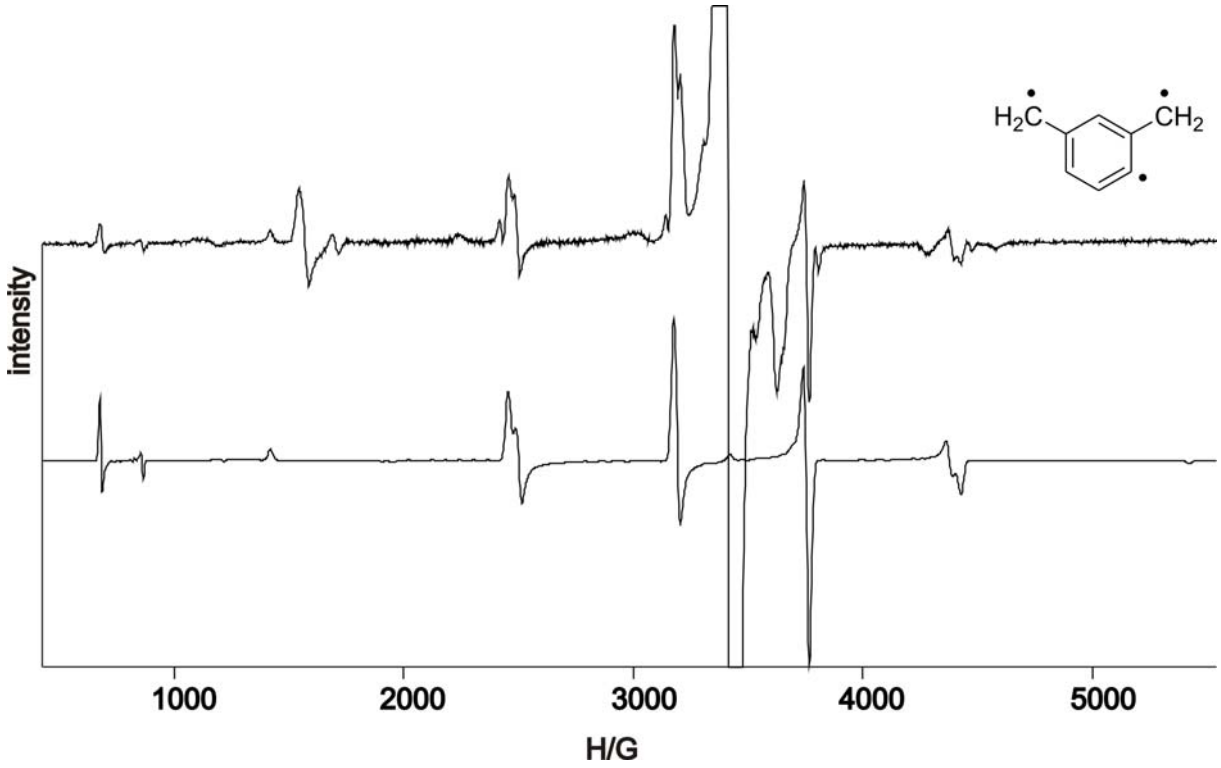

Figure 6. EPR spectrum obtained after irradiation of matrix isolated **13** with λ = 308 nm. a) Simulated quartet EPR spectrum using |D/hc| = 0.0935 cm^{-1}; |E/hc| = 0.0008 cm^{-1}; g = 2.0023; μ = 9.60067 GHz.

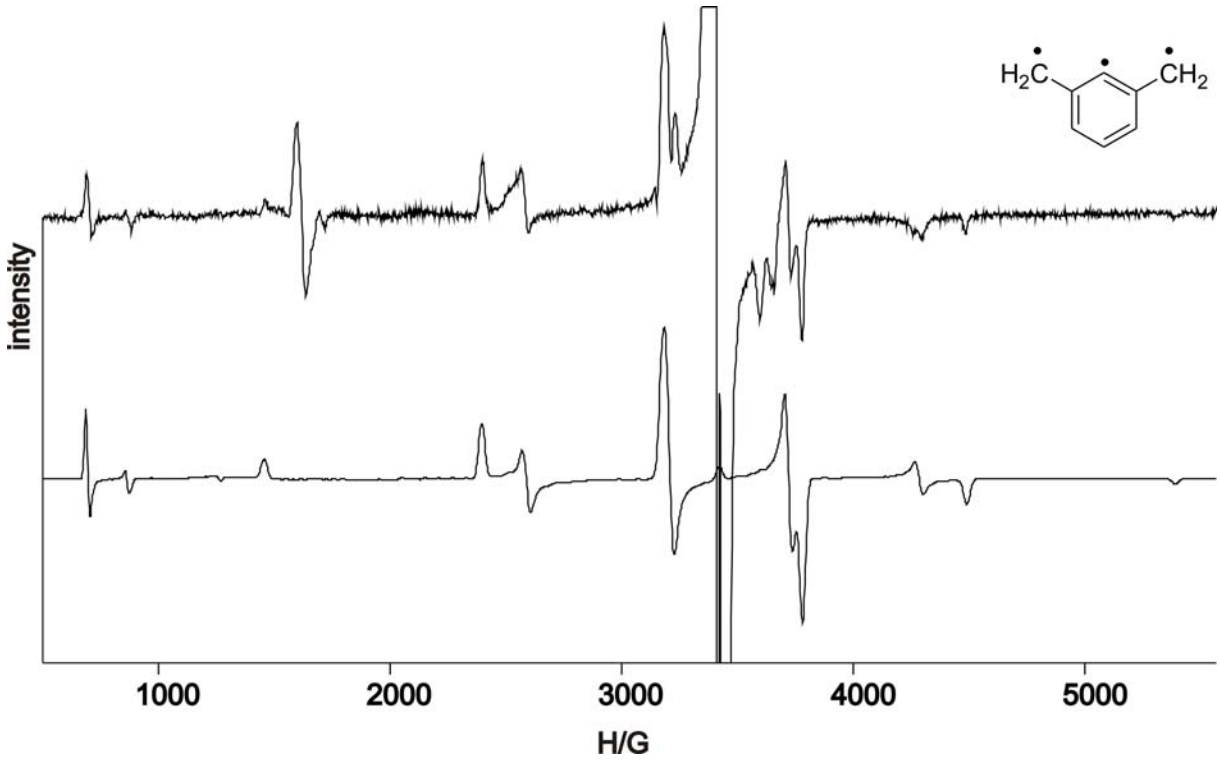

Figure 7. EPR spectrum obtained after irradiation of matrix isolated **12** with λ = 308 nm. a) Simulated quartet EPR spectrum using |D/hc| = 0.0920cm^{-1}; |E/hc| = 0.0032 cm^{-1}; g = 2.0023; μ = 9.60067 GHz.

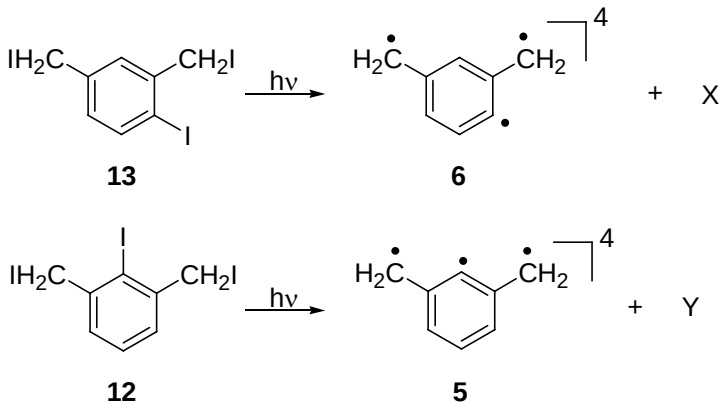

Scheme 32. 308 nm photolysis of 2,4-*bis*-(iodomethyl)iodobenzene **13** and 2,6-*bis*-(iodomethyl)iodobenzene **12** can lead to different EPR active species (symbolized as X and Y) next to the quartet states of 4-dehydro-*m*-xylylene **6** and 2-dehydro-*m*-xylylene **5**, respectively.

Although the dehydro-*m*-xylylenes **5** and **6** are the most probable carriers of the quartet signals, rearrangements under the photolysis conditions can not be excluded. It is possible that the signals are due to carbene-radicals like **86**, for which no experimental EPR spectra are available (Scheme 33). Nevertheless, the corresponding quartet nitrene **87** was reported with zfs parameters of $|D/hc| = 0.26\ cm^{-1}$ and $|E/hc| = 0.015\ cm^{-1}$ in a MTHF matrix.[48]

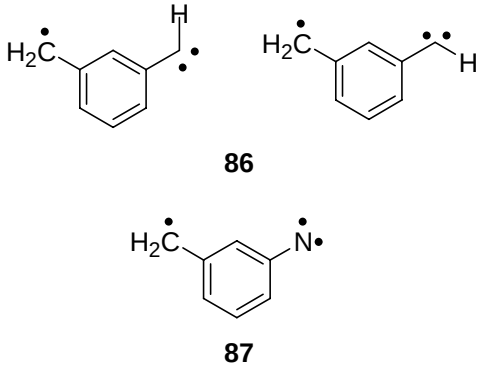

Scheme 33. Possible carbene-radicals like **86** might be formed through photolysis of **12** and **13**. **87** is known and was found to have zfs parameters of $|D/hc| = 0.26\ cm^{-1}$ and $|E/hc| = 0.015\ cm^{-1}$.[48]

All obtained EPR spectra are summarized in Figure 8 for the sake of comparison.

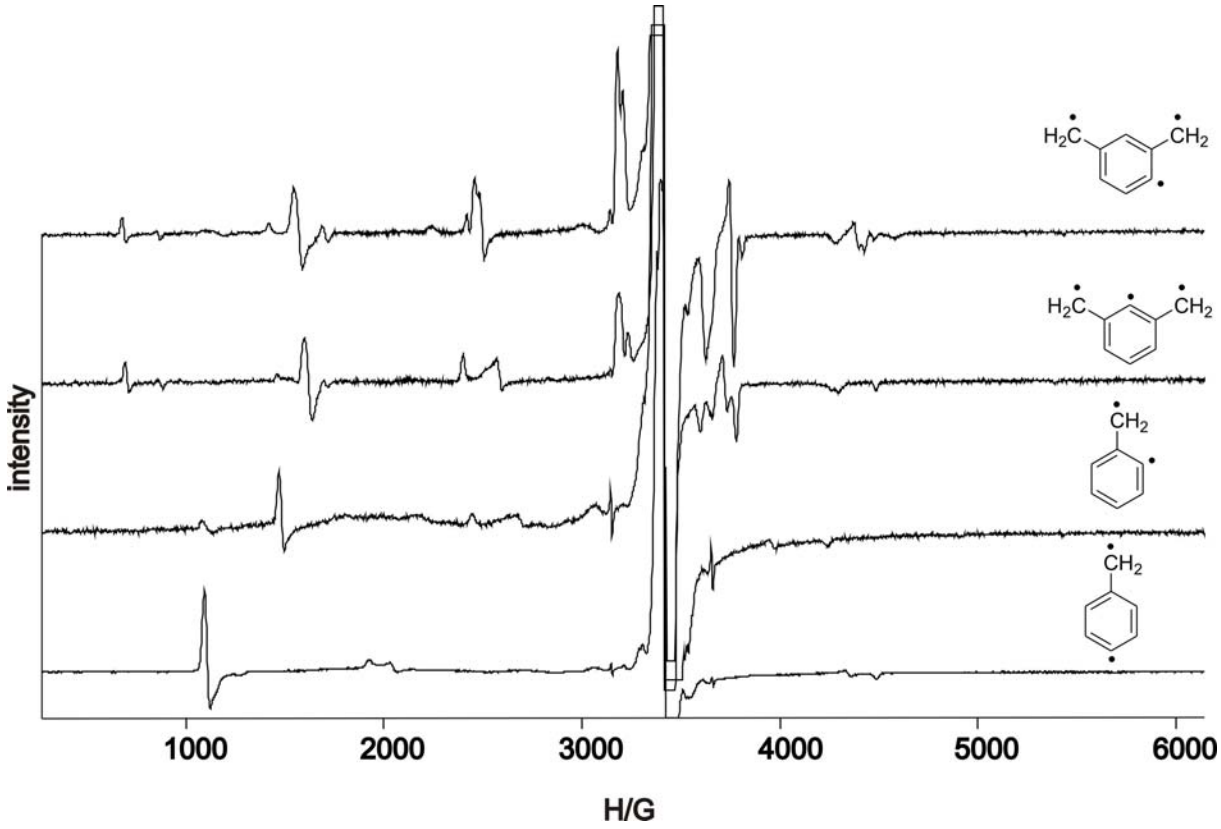

Figure 8. EPR spectra obtained after irradiation of matrix isolated **9**, **8**, **5**, and **6** with λ = 308 nm (from bottom up).

Photolysis of 3-iodobenzyl iodide **10** and 3,5-*bis*-(iodomethyl)iodobenzene **14** results in no high-spin signals attributable to triplet and quartet species, respectively (Scheme 34).

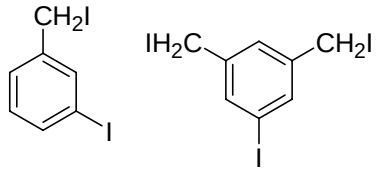

10 **14**

Scheme 34. EPR spectra recorded after 308 nm photolysis of 3-iodobenzyl iodide **10** and 3,5-*bis*-(iodomethyl)iodobenzene **14** results in no signals due to a triplet or a quartet species, respectively.

The zfs parameters are given in Table 4.

Table 4. ZFS parameters for triplets **81a-c**, **3**, and **4** and quartets **5**, **6,** and **87**.

Structure	D [a]	E [a]	Media	T [d]	Ref.
81a	0.1069 +/-	0.0058 +/-	PIP glass [b]	77	10

	0.0005	0.0003			
81b	0.1110 +/- 0.0005	0.0069 +/- 0.0003	PIP glass [b]	77	10
81c	0.1217 +/- 0.0008	0.0066 +/- 0.0003	PIP glass [b]	77	10
3	0.139	0.0081	argon	5	-
4	0.212	0.004	argon	5	-
5	0.0935	0.0008	argon	5	-
6	0.0920	0.0032	argon	5	-
87	0.26	0.015	MTHF [c]	18 +/- 2	11
87	0.3340	0.0014	argon	5	-

[a] in cm^{-1}. [b] PIP = pentane – isopentane. [c] 2-Methyltetrahydrofuran. [d] in K.

Usually, if a radical center is formed photolytically, the two resulting radicals are separated by some rare gas atoms in the rigid matrix. In most cases, annealing of the matrix gives the starting material back as the barrier to recombination is quite low or absent. A possibility to establish a small energy gap between the lowest and the first excited state in an EPR experiment is the Curie analysis. However, in EPR experiments in which the high-spin species is photolytically formed, the signal intensity often changes irreversible by annealing, since the radicals recombine. In contrast to this, the generation of high-spin molecules by FVP allows to trap the reactive species with an excess of rare gas. A single molecule is distant from another molecule and thus a Curie analysis can be performed, as was shown in the case of α,4-didehydrotoluene **4**.

Wenthold et al. have determined triplet ground states for α,2-didehydrotoluene **3** and α,4-didehydrotoluene **4**, while α,3-didehydrotoluene **11** was found to be a singlet ground state molecule. In this study, the collision induced dissociation threshold energies of different halocarbanions were determined. Significant variations in the heats of formation obtained with different halides used for the production of diradicals **3** and **4** was interpreted as indication for the triplet ground state of **3** and **4**, since the dissociation to form triplet products is a spin-forbidden reaction.[47] The absence of this variation in the measurements of the heat of formation of diradical **11** indicates a singlet ground state – a spin-allowed reaction to a singlet ground state molecule.[47, 49, 50] CASSCF(8/8)/6-31G* calculations as well as SDCI-DV/pVDZ calculations on **3** place the first excited open-shell

singlet state 6.86 and 4.11 kcal/mol higher in energy than the triplet ground state, respectively (CASSCF(8/8)/pVDZ calculation predicts ΔE_{ST} = 7.4 kcal/mol). Using the same methods, a singlet-triplet gap of 6.76 and 3.10 kcal/mol, respectively, is found for α,4-didehydrotoluene **4** (CASSCF(8/8)/pVDZ predicts ΔE_{ST} = 8.1 kcal/mol).[47] Difference-dedicated configuration interaction (DDCI2) calculations using a 6-31G* basis set similary predict triplet ground states for **3** and **4**, with singlet-triplet energy gaps in the order of the CASSCF results of Wenthold et al.[51] The singlet open-shell ground state of α,3-didehydrotoluene **11** was calculated at the CASSCF(8/8)/6-31G* level of theory to be 2.52 kcal/mol lower in energy than the triplet state.[47] CASSCF(8/8)/pVDZ slightly increase the energy difference between both electronic states to 3.02 kcal/mol in favour of the singlet state.[47] The CASSCF(8/8)/pVDZ calculations predict the singlet state of α,3-didehydrotoluene **11** to be the most stable α,n-didehydrotoluene isomer, while α,4-didehydrotoluene **4** is calculated to be the least stable isomer. The energy separation between S-**11** and T-**3** as well as S-**11** and T-**4** is calculated to amount to 0.14 kcal/mol and 0.26 kcal/mol, respectively.

Regarding the dehydro-*m*-xylylene isomers, calculations of Krylov et al. using the EOM-SF-CCSD/6-31G* level of theory predict a $^4B_2$ ground state, with a vertical energy gap to the next higher doublet state of 10.61 kcal/mol for 2-dehydro-*m*-xylylene **5**.[52] The same calculations for 5-dehydro-*m*-xylylene **15** place the quartet state 4.20 kcal/mol higher in energy than the $^2B_2$ ground state.[52] Spin-flip CCSD/6-311G** calculations on the manifold of triradical states possible for 5-dehydro-*m*-xylylene **15** predict an energy gap between the doublet and the quartet state of 3.69 kcal/mol in favour of the doublet state.[53] No such calculations were reported for the third isomer, 4-dehydro-*m*-xylylene **6** – with a reduced symmetry of C_s compared to the other isomers. It was found that the spin polarization mechanism gives qualitatively correct answers for the ground state of didehydrotoluenes as well as 2- and 4-dehydro-*m*-xylylene, so that it seems to be reasonable to apply it to the unexplored 4-dehydro-*m*-xylylene **6**. In this manner, σ-π exchange interactions lead to a high-spin quartet ground state for **6**.

4.2 Quintet 5-Nitreno-*m*-xylylene

No experimental data is available on systems composed of a *m*-xylylene core coupled with a nitrene center. It is well known that *m*-xylylene **1** and phenylnitrene **56** are ground state triplet molecules. The combination of these motifs in a ferromagnetic

coupling fashion results in a quintet ground state and is expected to occur in 3,5-*bis*-methylenephenylnitrene **7**. Since iodomethylenes were shown to be useful precursors of radical centers, breaking the C-I bond by photolysis with 308 nm of a XeCl-excimer laser, the anticipated stable target molecule is 3,5-*bis*-(iodomethyl)azidobenzene **16**. Matrix isolation of **16** in an argon matrix at 5 K and subsequent irradiation of this matrix with 308 nm light results in the appearance of EPR transitions which are attributed to a quintet species (Figure 9).

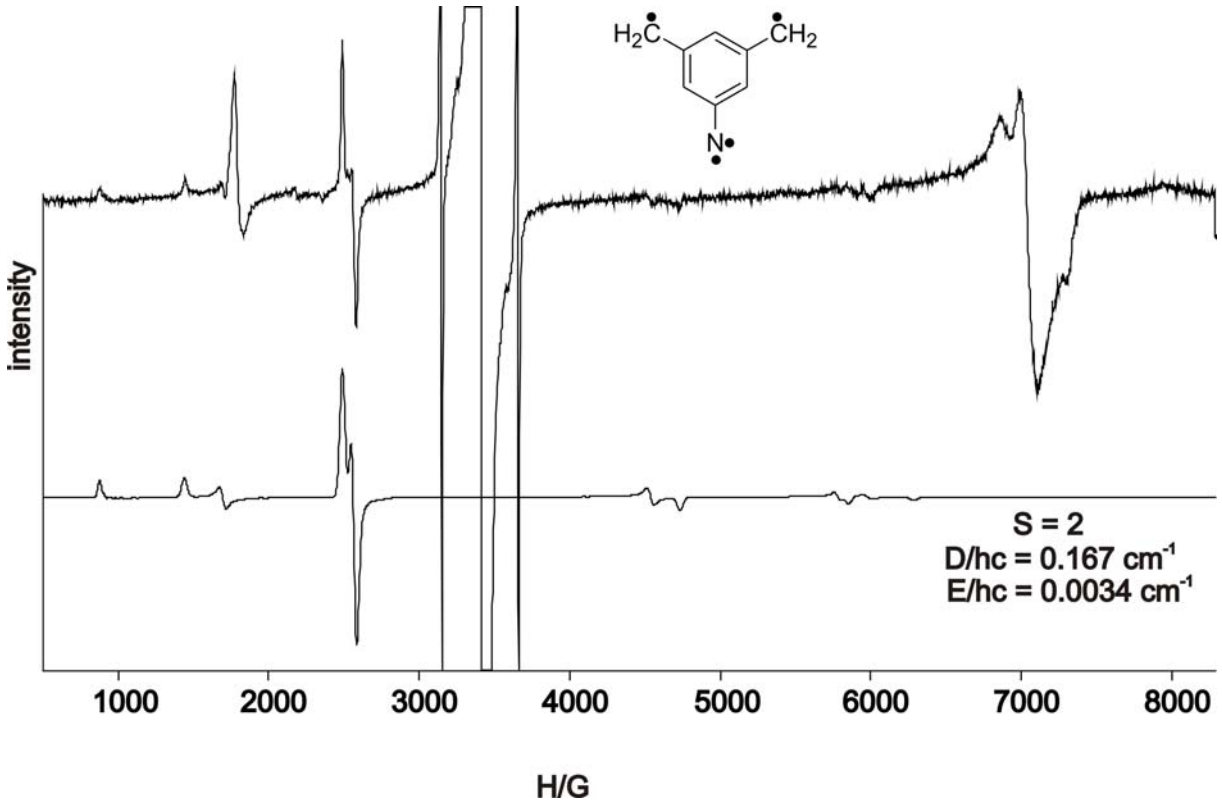

Figure 9. Calculated EPR spectrum of a quintet species with zfs parameters |D/hc| = 0.167 cm^{-1} and |E/hc| = 0.0034 cm^{-1} (below). Experimental EPR spectrum obtained after photolysis of an argon matrix containing 3,5-*bis*-(iodomethyl)phenyl azide **16** at 5 K with 308 nm light.

A broad and strong xy_2 transition of the 3,5-*bis*-(iodomethyl)phenylnitrene system is as well observed. Good resemblance of the experimental quintet spectrum is obtained with a simulation using the zfs parameters |D/hc| = 0.167 cm^{-1} and |E/hc| = 0.0034 cm^{-1} (g = 2.003). It seems to be reasonable to assign the quintet signals to 3,5-*bis*-methylenephenylnitrene **7** (Scheme 35).

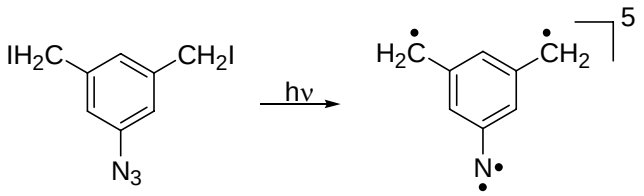

16 **7**

Scheme 35. The quintet tetraradical **7** is obtained after photolysis of 3,5-*bis*-(iodomethyl)azidobenzene **16** isolated in an argon matrix at 5 K.

Tukada obtained a similar quintet EPR spectrum for tetraradical **88** which is composed from a triplet azatrimethylene ferromagnetic coupling unit and a nitrene center. Both high-spin elements were coupled through a benzene core in a *meta* topology as shown in Scheme 36.[54]

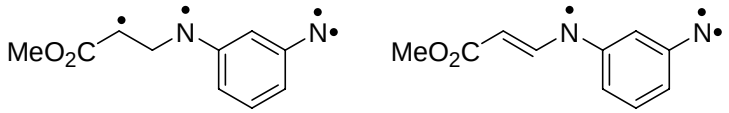

88 **89**

Scheme 36. Quintet tetraradical **88** and quartet hydrogen abstraction product **89** studied by Tukada via EPR spectroscopy in MTHF glass.

The zfs parameters published by Tukada are very close to the zfs parameters obtained for the parent tetraradical **7**. Quintet **88** is reported to have a D value of 0.170 cm^{-1} and an E value of 0.004 cm^{-1}. The corresponding quartet state of the hydrogen abstraction product **89** shows the zfs parameters |D/hc| = 0.345 cm^{-1} and |E/hc| = 0.0003 cm^{-1}.[54] These measurements performed by Tukada were carried out in MTHF similar to his study on quartet 3-nitrenobenzyl radical **87**, for which a D value of 0.26 cm^{-1} was reported.[48, 54] The basic structural unit of both triradicals **87** and **89** are a 3-nitrenobenzyl radical and the 3-nitrenoazabenzyl radical unit, respectively, with the radical center in **89** being stronger delocalized. The average distance between the radical centers in **89** is expected to be larger than the one in **87**, however, the zfs parameters indicate a different trend. In order to unravel the origin of this discrepancy, 3-azidobenzyl iodide **90** was synthesized independently and investigated in an argon matrix. A quartet EPR spectrum is observed after 308 nm photolysis of 3-azidobenzyl iodide **90** (Figure 10).

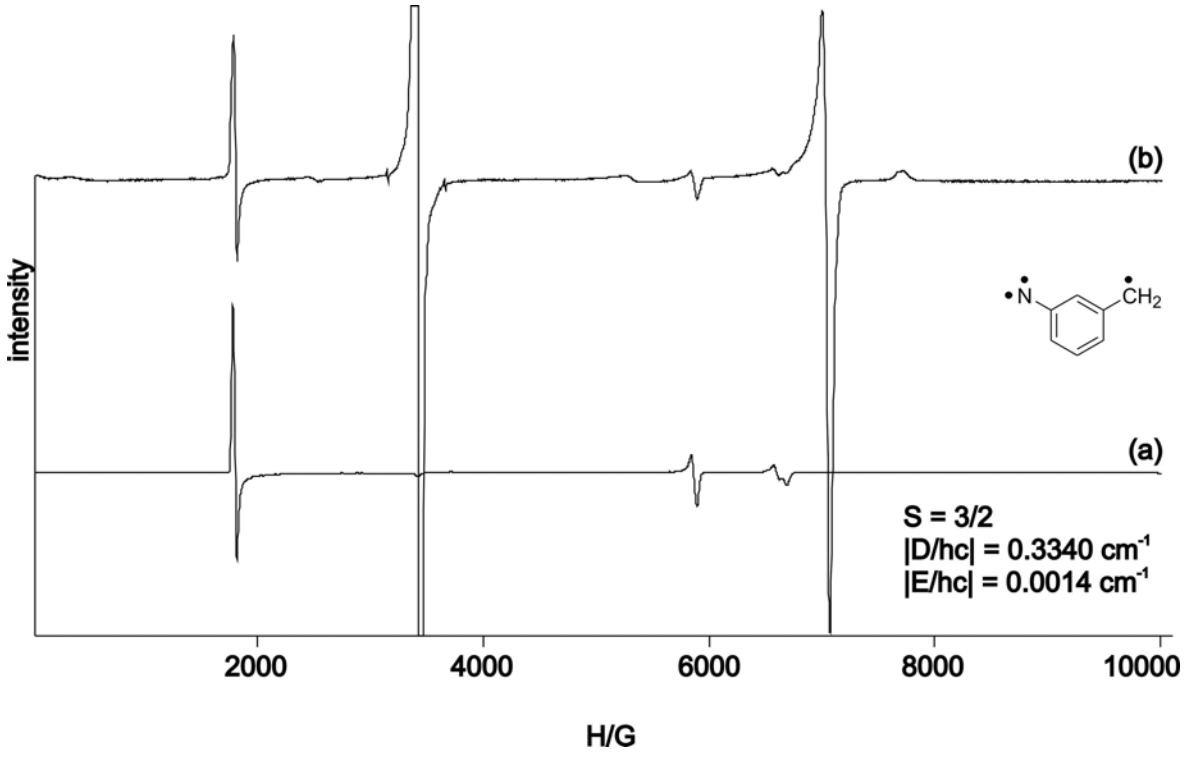

Figure 10. (a) Calculated EPR spectrum of a quartet molecule with zfs parameters of $|D/hc| = 0.3340\ cm^{-1}$, $|E/hc| = 0.0014\ cm^{-1}$. (b) EPR spectrum obtained after 308 nm photolysis of matrix isolated 3-azidobenzyl iodide **90** assigned to quartet 3-nitrenobenzyl radical **87**, Ar, 4 K.

The EPR spectrum obtained for quartet 3-nitrenobenzyl radical **87** in an argon matrix can be simulated with $|D/hc| = 0.3340\ cm^{-1}$ and $|E/hc| = 0.0014\ cm^{-1}$. The zfs parameters reported by Tukada for the same molecule in a MTHF glass are probably inaccurate, as they used the strongest transition at 1690 gauss to estimate the zfs parameters for the quartet state. It is found that for quartet molecules with large D values, this transition is very insensitive to changes in the D value, thus other transitions have to be used. In an argon matrix this transition is observed at 1800 gauss. Tukada reported a value of 1690 gauss for this characteristic and strong transition. The microwave frequency in these experiments was much lower than the one used for the parent experiment. Nevertheless, a completely different EPR spectrum was obtained when the estimated zfs parameters of Tukada were used for the simulation, showing neither resemblance to the experimental EPR spectrum, nor to the published EPR spectrum of Tukada. The matrix effect on the zfs parameters is usually in the order of 10 to a maximum of 20 %. However, using the same parameters for the simulation of a quartet triradical as the one applied in the MTHF experiments gives a strong EPR transition at 1690 gauss for D values greater than $0.32\ cm^{-1}$. In conclusion, it is assumed that the spectrum described by Tukada is indeed 3-

nitrenobenzyl radical **87** –in good accordance with the experimental EPR spectrum in an argon matrix - while his estimated zfs parameters are inaccurate.

The comparison of the EPR spectrum of **7** with the EPR spectrum obtained for **87** in an argon matrix is shown in Figure 11. The strong transition around 1800 gauss in the EPR spectrum of **7** is assigned to quartet monoiodide **91** (Scheme 37), since the zfs parameters of **91** are expected to be close to the parameters of **87**.

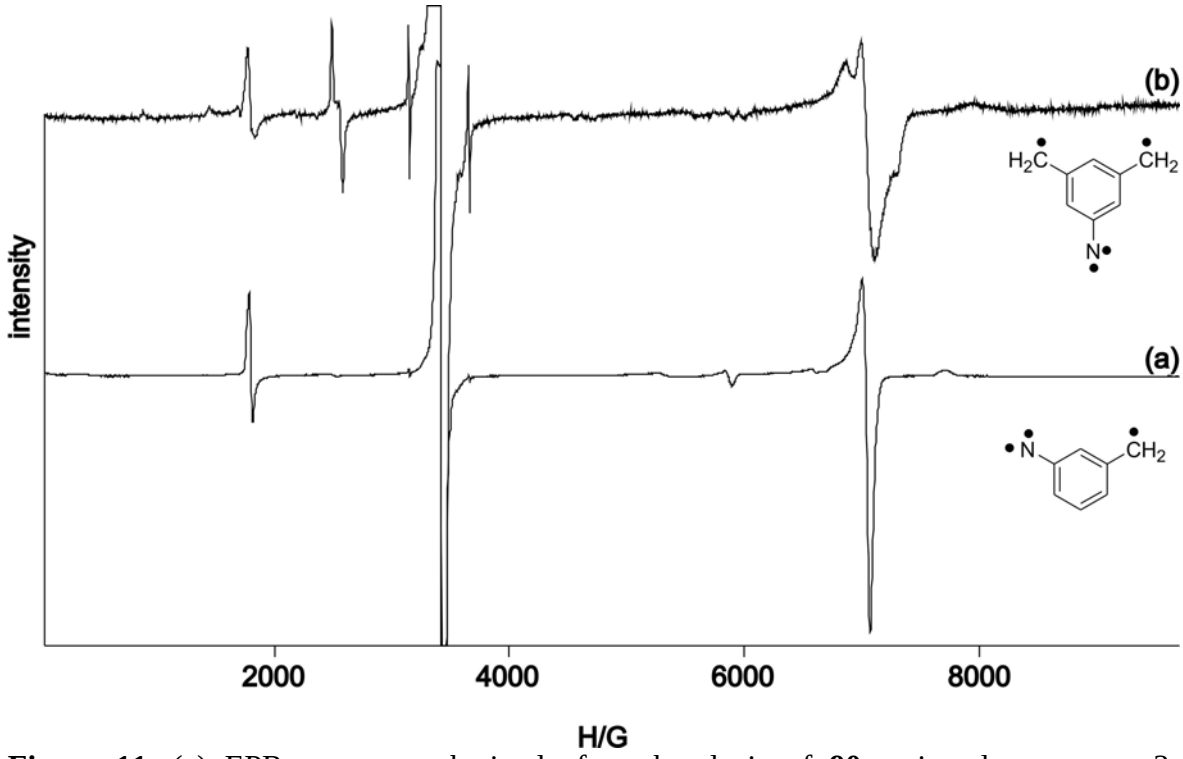

Figure 11. (a) EPR spectrum obtained after photolysis of **90** assigned to quartet 3-nitrenobenzyl radical **87**. A large nitrene signal is also observed. (b) EPR spectrum obtained after photolysis of **16**. Signals due to quintet **7**, quartet **91**, and triplet nitrene **92** are observed.

In summary, photolysis of 3-azidobenzyl iodide **90** in an argon matrix gives rise to EPR signals due to triplet nitrene **93** and quartet 3-nitrenobenzyl radical **87**. The EPR spectrum obtained after photolysis of *bis*iodide **16** gives rise to signals which are assigned to triplet nitrene **92**, quartet monoiodide **91**, and quintet tetraradical 3,5-*bis*-methylenephenylnitrene **7**. The EPR spectrum assigned to **87** is found to be close to the EPR spectrum of quartet monoiodide **91** (scheme 37).

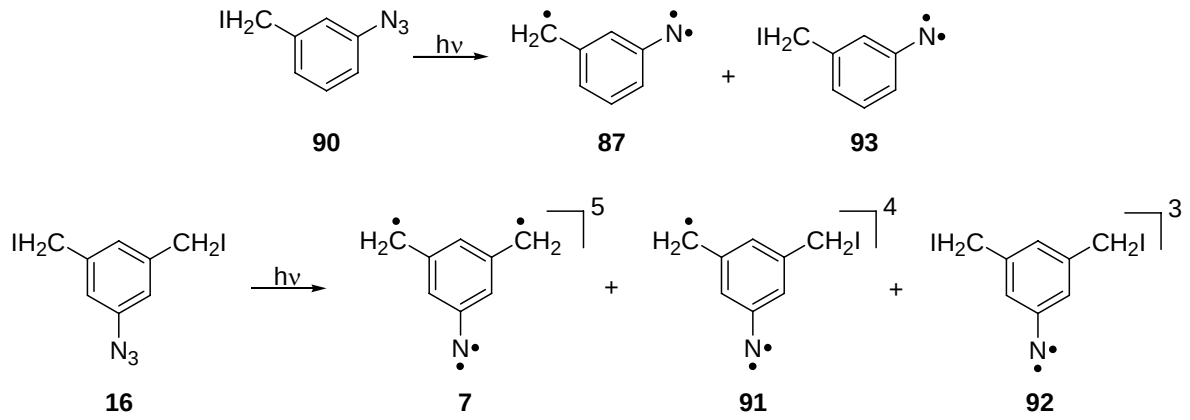

Scheme 37. Transitions of different high-spin molecules are observed after photolysis of **90** and **16** with 308 nm. Quartet triradical **87** and triplet diradical **93** are observed after photolysis of **90**. Quintet tetraradical **7**, quartet triradical **91**, and triplet diradical **92** are the most probable carriers of the EPR transitions after photolysis of **16**.

The zfs parameters of tetraradical **7** are between the experimental zfs parameters of *meta*-phenylene-*bis*-nitrene **94** and 3-nitrenophenylcarbene **95**, for which zfs parameters of |D/hc| = 0.205 cm^{-1} and |E/hc| = 0.041 cm^{-1} and |D/hc| = 0.124 cm^{-1} and |E/hc| = 0.002 cm^{-1}, respectively, were determined in MTHF.[55-57] The EPR spectrum of quintet *meta*-phenylene-*bis*-carbene **96** was recorded by Wasserman et al. and was determined to be |D/hc| = 0.0844 cm^{-1} and |E/hc| = 0.0233 cm^{-1} in MTHF (Scheme 38).[57]

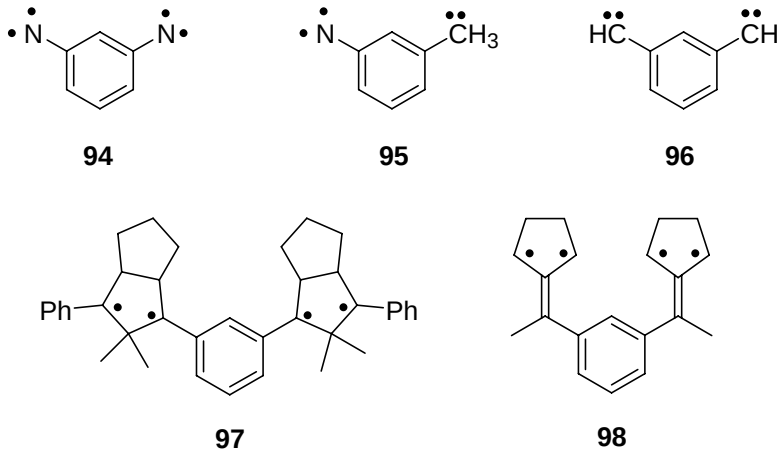

Scheme 38. Different tetraradicals which were studied by EPR spectroscopy.

4.3 Discussion of the zfs parameters

Adam et al. studied system **97** via EPR spectroscopy, a tetraradical solely composed of π radical centers. **97** is best described with the zfs parameters of |D/hc| =

0.00955 cm^{-1} and |E/hc| = 0.0029 cm^{-1}.[58] Dougherty et al. found |D/hc| = 0.0076 cm^{-1} and |E/hc| = 0.0003 cm^{-1} for tetraradical **98**. [59] The observed zfs parameters of these species are nearly one order of magnitude smaller than the values obtained for the quintet species with carbene or nitrene units.

It seems reasonable that the zfs parameters of tetraradical **7** composed of one nitrene unit and two conjugated π radical centers has zfs parameters that are intermediate between *bis*nitrene **94** and carbene-nitrene **95**. In *bis*nitrene **94** the small average distance between the electrons on the nitrogen atoms gives rise to large one-center terms to the zfs parameters and thus large zfs parameters. The unpaired electron of carbenes is placed in a larger p orbital and thus it has a larger average distance to the σ electron. In general, zfs parameters of carbenes are remarkably smaller than the zfs parameters of nitrenes. The decrease of the D value with decrease in average distance between the unpaired electrons is also seen for carbene-nitrene **95** and *bis*carbene **96**, since **95** and **96** show a remarkably decrease in zfs parameters compared to **94**. Tetraradical **7** lacks a second nitrene or carbene unit and thus only one large one-center term contributes to the zfs parameters. Nevertheless, **7** has three π electrons delocalized through 9 non-hydrogen atoms while **95** has two π electrons delocalized through 8 non-hydrogen atoms. It can be assumed that the average distance of the unpaired π electrons in **7** is therefore smaller than the average distance of the unpaired π electrons in **95**.

The D value of quartet triradical **87** is found only slightly lower than the D value of 2-dehydro-3,4,5,6-tetrafluorophenylnitrene **76** (D = 0.357 cm^{-1}) and higher than the D value of 4-dehydro-2,3,5,6-tetrafluorophenylnitrene **77** (D = 0.285 cm^{-1}).[1, 60] **76** and **77** are σ,σ,π triradicals and have a strong σ,π one-center interaction between the unpaired electrons of the nitrene unit and a noticeable contribution of a carbenic resonance form. **87** as well has a strong σ,π nitrene interaction and a third electron in a delocalized π orbital. Compared to **76** and **77** where the unpaired π electron is delocalized on 7 non-hydrogen atoms, there are two π electrons in **87** which are delocalized on 8 non-hydrogen atoms. Similar to the observed effect on the D value of quintet **7**, the D value of **87** is relatively large, since the ferromagnetically coupled electrons come close to each other.

5. *m*-Xylylene

5.1 Introduction

The unusual electronic structure of small organic high-spin coupled diradicals as well as their elusive nature has attracted attention of theoreticians and experimentalists for decades. Potential application of these molecules as organic magnetic materials was envisaged in the recent past. While trimethylenemethane (TMM) **49** with a triplet ground state is perhaps the best studied diradical, *m*-xylylene **1** (also named *m*-benzoquinodimethane) has found much more application as ferromagnetic coupling unit (Scheme 39).[61]

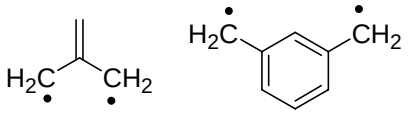

49 **1**

Scheme 39. Triplet trimethylenemethane **49** (TMM) and triplet *m*-xylylene **1** are robust ferromagnetic coupling units.

m-Xylylene **1** is the parent molecule of all high-spin coupled polyradical systems with *meta*-phenylene coupling units used to design organic magnetic materials. It can be classified as π,π-diradical with both unpaired electrons each in different π-NBMOs. A triplet ground state is consistently predicted by Ovchinnikov's analysis, Longuet-Higgins´ methodology and Borden and Davidson's NBMO comparison (Figure 12). High coulombic repulsion between the singlet coupled electrons at the exocylic methylene positions disfavour this state in comparison to the triplet state in which the Pauli principle circumvent these ionic terms in the wavefunction.

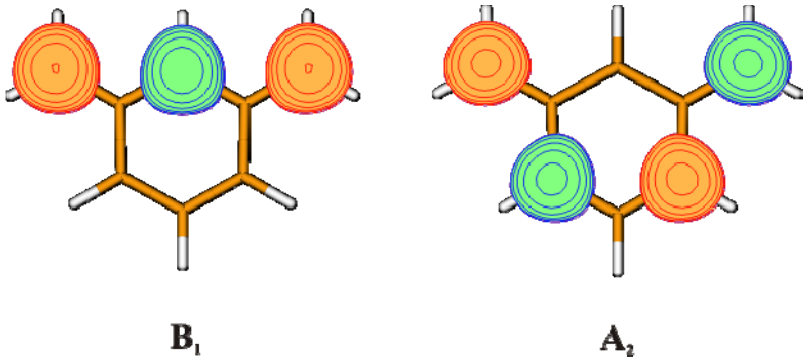

Figure 12. The non-disjoint NBMOs of triplet *m*-xylylene **1** calculated at the UB3LYP/6-311G** level of theory.

In 1915, Schlenk and Brauns prepared the first stabilized derivative of *m*-xylylene **98**.[7] The first reaction step of molecular silver with dichloride **97** was found to be fast and easy while the second halogen removal had to be performed under reflux to obtain tetraphenyl-substituted diradical **98**, known as Schlenk's hydrocarbon (Scheme 40).

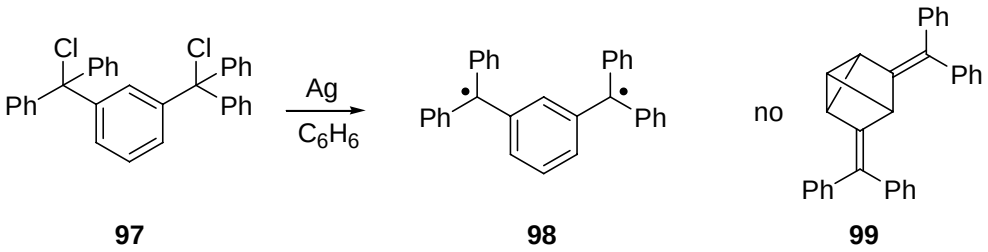

Scheme 40. Schlenk and Brauns´ synthesis of tetraphenyl-substituted *m*-xylylene **98** from 1915.[7]

Fast bleaching of the solution upon exposure to oxygen let the authors discriminate the *bis*-trimethylphenyl radical **98** from a *meta*-quinoide structure like **99**.

Kothe at al. verified these early experiments in 1970, as they were able to measure the EPR spectrum of a triplet species after electrochemical reduction of the perchlorate dication derivative of *m*-xylylene.[62] The difference in the half-wave potential for the first and second reduction step of the dication was found to be much smaller in **98** than in the corresponding *para* derivative **100**. This was explained by the smaller electrostatic repulsion of the unpaired electrons in the triplet ground state of tetraphenyl-substituted *m*-xylylene **98** as compared to the singlet ground state of tetraphenyl-substituted *para*-benzoquinodimethane **100** – in accordance with theory.

The parent *m*-xylylene **1** was generated first by UV irradiation of *m*-xylene **101** in organic glasses, however, in very low yield with the corresponding monoradical **102** as major radical species formed. Diradical **1** could be identified by the sensitive fluorescence spectroscopy in these experiments.[63]

Later it was found that in the comparable system of 5-methyl-*m*-xylylene **27**, the corresponding monoradical **28** is not the photoprecursor of the triplet state of **27**. Instead, diradical **27** is formed by a mechanism in which the nascent hydrogen, formed through initial scission of a benzylic C-H bond, partitions between reacting with the surrounding matrix and reaction with the 3,5-*bis*-methylbenzyl radical **28** in a dark reaction (Scheme 41).[40] Monoradical **28** is generated by a two-photon process through an excited triplet state of mesitylene T_n-**103**, which is populated through absorption of a second photon of the first excited triplet state of mesitylene T_1-**103** within its lifetime.[40]

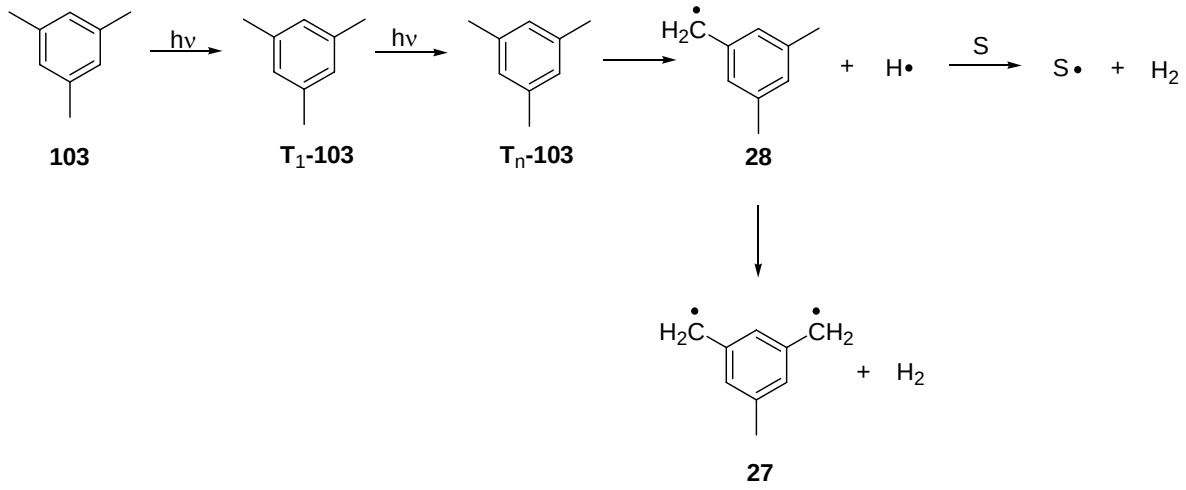

Scheme 41. Formation of *m*-xylylene derivative **27** from mesitylene **103** was found to proceed through secondary photolysis of the first excited triplet state followed by a dark reaction with the nascent hydrogen atom. S resembles a solvent molecule. [40]

The yield of *m*-xylylene **1** can be increased by using either 1,3-*bis*-chloromethylbenzene **104** or *bis*-diazo compound **105** as photochemical precursors in ethanol glasses at 77 K.[41, 64] *Bis*-carbene **96** in its quintet ground state readily abstracts hydrogen atoms at elevated temperatures from organic glasses and showed no thermal reactivity if non-hydrogen donating glasses like hexafluorobenzene were used. Platz et al. thus were able to record the EPR spectrum of **1** in organic glasses by this route. It was concluded that **1** has a triplet ground state or that this state is within a few calories per mole of the ground state as a linear Curie plot of the EPR signal intensity was obtained.[64] An

alternative synthesis was proposed by Berson et al., who used the Norrish-II photoreaction of aceton derivative **106** to produce the highly strained hydrocarbon **19** which rapidly rearranges to **1** (Scheme 42).[34]

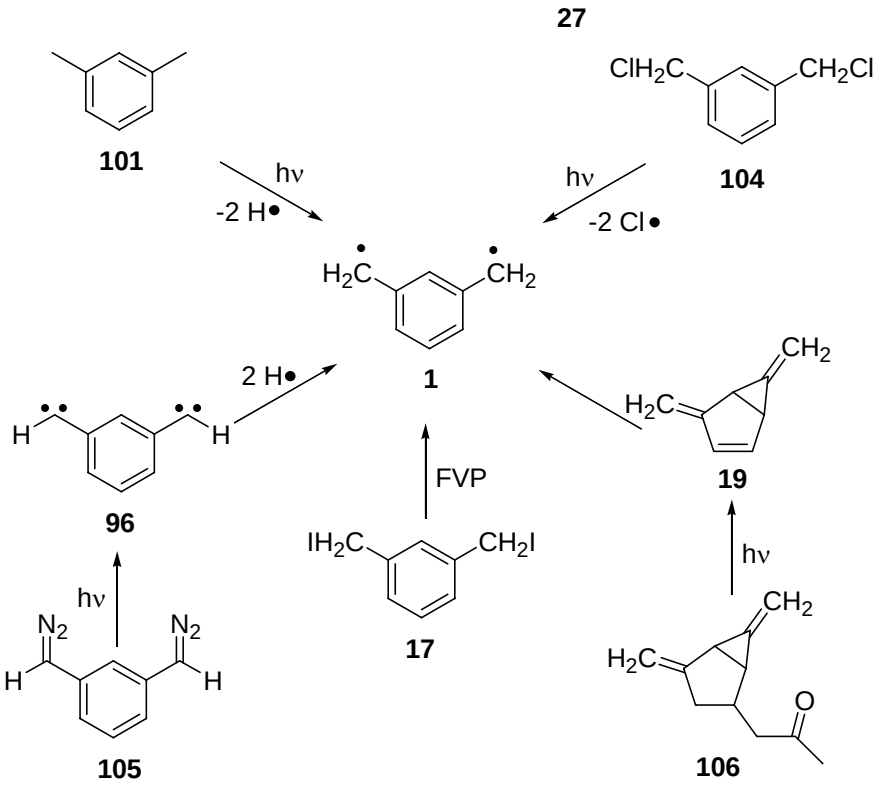

Scheme 42. Synthesis of *m*-xylylene **1**.

The singlet-triplet gap of diradical **1** was determined by Wenthold et al. using photoelectron spectroscopy to be 9.6 +/- 0.2 kcal/mol.[65] The authors produced the negative anion of *m*-xylylene **1**$^-$ in its Jahn-Teller distorted $^2B_1$ ground state through reaction of *m*-xylene **101** with the oxygen radical anion (Scheme 43).[65, 66]

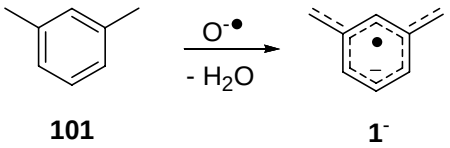

Scheme 43. Precursor used by Wenthold et al. to generate the radical anion of *m*-xylylene **1**$^-$.[66]

Electron detachment from **1**$^-$ actually produced a photoelectron spectrum in which three electronic states of *m*-xylylene **1** were observed. Next to a band due to the $^3B_2$ ground state of **1** at lowest electron binding energy of 0.919 +/- 0.008 eV (corresponding to the electron affinity of *m*-xylylene **1**), the first excited singlet $^1A_1$ state which is 9.6 +/- 0.2

kcal/mol higher in energy was also observed. It was found by careful analysis of the photoelectron angular distribution to be generated by electron detachment from a different orbital than the $^3B_2$ ground state.[65] Vibrational structures were visible for both states in the photoelectron spectrum, while the second excited singlet state, namely the $^1B_2$ state, showed no resolvable peaks and lies less than 21.5 kcal/mol above the ground state.[65]

Some years later, measurements of the acidity of the 3-methylbenzyl radical **102** were conducted, by which it was possible to determine the enthalpy of formation of *m*-xylylene **1**.[66] Deuterium labelling of precursor **17** and reactivity studies of radical anion **1**$^-$ ruled out other possible isomeric molecules, like the radical anion of α,n-didehydrotoluenes or a carbene intermediate as the reactive species in this gas-phase approach. An independent determination of this quantity by measurement of the collision induced dissociation threshold energy of the 3-(chloromethyl)benzyl ion **107**$^-$ was reported as well.[66] The heat of formation was measured by these gas-phase ion chemistry approach to be 80.8 +/- 2.4 kcal/mol, ca. 33 kcal/mol higher than the quinoid *ortho*- and *para*-xylylene **50** and **51**, respectively. This enthalpy of formation could be used to get the second C-H bond dissociation energy (BDE) of *m*-xylene **101** and was determined to be 90.7 +/- 2.9 kcal/mol, only slightly higher than the first bond dissociation energy of 90.1 +/- 1.7 kcal/mol. The similarity between the first and second BDEs was interpreted to show negligible interaction between the two unpaired electrons in the triplet state of diradical **1**.[66] The slightly higher second BDE of *m*-xylene **101** can also indicate a small destabilizing interaction between the radical centers and was shown to be highly path dependent for non-Kekulé molecules like *m*-xylylene **1** (Scheme 44).[67] Only diradicals which can be formed from only one hydrocarbon (all σ,σ diradicals) have a unique bond dissociation energy difference.

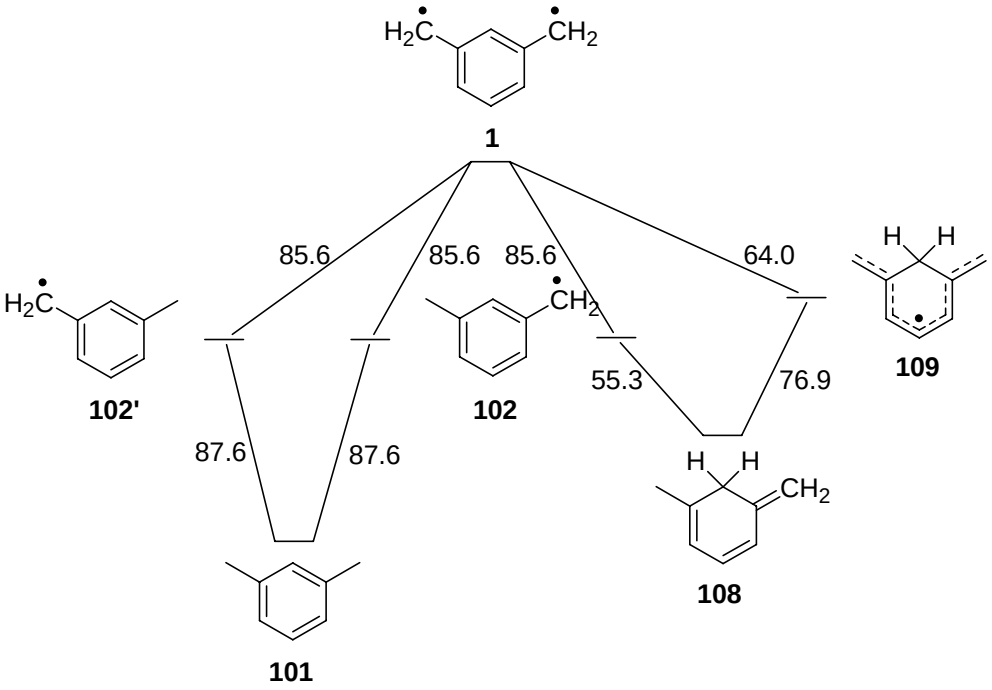

Scheme 44. Borden et al. showed the path dependance of the first and second bond dissociation energy for non-Kekulé molecules like *m*-xylylene **1** [kcal/mol]. Values taken from JOC, 2002, 67, 3989.[67]

Borden et al. furthermore showed that for the parent molecule *m*-xylylene **1**, the difference between the first and second bond dissociation energy is calculated to -2.0 kcal/mol for formation of triplet **1** starting from *m*-xylene **101** (left way in Scheme 44) while the same quantity is calulated to be 8.7 kcal/mol if triene **108** is taken as starting compound and the heptatrienyl radical **109** as intermediate monoradical (right way in Scheme 44). The former case would be interpreted as support for a stabilizing interaction between the radical centers, while the latter value could be interpreted as a destabilizing interaction for the secondly introduced radical center due to the first radical center.[67]

Berson et al. tested the reactivity of *m*-xylylene **1** towards dienes (Scheme 45).[34] The EPR spectrum which they obtained after irradiation of an organic glass containing **106** was in accordance with the g = 2 region of the triplet EPR spectrum recorded before, while no half-field transition could be detected.

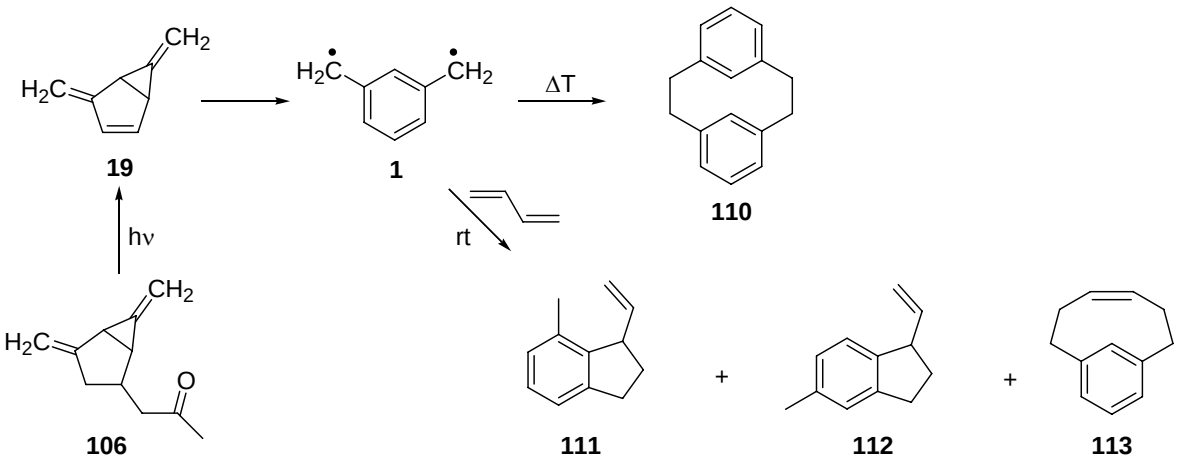

Scheme 45. Berson et al. studied the reactivity of *m*-xylylene **1** towards dienes.[68]

Upon annealing of the organic glass, it was possible to isolate the *meta*-cyclophane **110**. Reaction of *m*-xylylene **1** with dienes in *n*-pentane at room temperature leads to the trapping of only one type of intermediate and results in the isolation of two different indanes **111** and **112** as well as cyclophane **113**. The product distribution obtained from this intermediate was shown to be consistent with a two-step cycloaddition mechanism through a long-lived adduct biradical. Deuterium labelling studies conclusively demonstrated that the intermediate has static or time-averaged bilateral symmetry while no evidence was obtained regarding the spin-state.[68]

Early semiempirical π electron configuration interaction calculations predicted a triplet ground state for **1**.[69] The same prediction was obtained by Borden et al. in 1983 using a STO-3G basis set and the UHF method for the $^3B_2$ ground state and a two configurational SCF (TCSCF) for the first excited $^1A_1$ state.[70] The singlet-triplet energy difference was calculated to ca. 10 kcal/mol in favour of the triplet state. The NBMOs of the two lowest singlet states were shown to be more localized than those of the triplet ground state in order to minimize the coulombic repulsion. This also has consequences on the bonding situation in the singlet states, as the $^1A_1$ state preserves aromaticity of the benzene unit and localizes its electrons mainly on the exocyclic methylene units, the bonding in the $^1B_2$ state is best described as an allyl radical and an “independent” pentadienyl radical moiety (Scheme 46).[71]

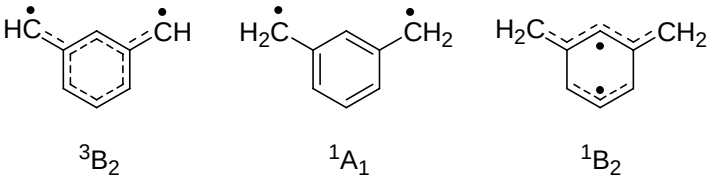

Scheme 46. Bonding situation in the lowest electronic states of *m*-xylylene **1**.[70, 71]

(8/8) CASSCF calculations with the 6-31G* basis set predict the $^3B_2$ to be 12.9 kcal/mol below the $^1A_1$ state and 24.4 kcal/mol below the $^1B_2$ state.[72]

Twisting both exocyclic methylene units out of conjugation, does not only diminish the singlet-triplet energy difference but results in a reversal of the ground state multiplicity, as was shown by Borden et al..[73] In effect *m*-xylylene **1** has a very robust triplet ground state but can become an antiferromagnetic coupling unit if it is highly twisted (Scheme 47).

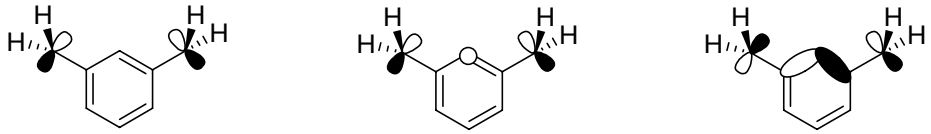

Scheme 47. Twisting of *m*-xylylene **1** results in an energetic splitting of the singly occupied orbitals and a singlet ground state. S-**1'** and a-**1'** denote the symmetric and antisymmetric linear combination of the SOMOs with the benzene σ orbitals, respectively.

An explanation for this reversal was found in the increased energetic splitting of the two NBMOs (SOMOs) through mixing with the benzene σ orbitals. The antisymmetric combination (**a-1'**) is destabilized through this mixing to a greater extent than the symmetric combination (**s-1'**).

Zhang et al. performed a density functional study on the singlet-triplet energy difference of *m*-xylylene derivatives.[74, 75] It was found that substitution in 4 and 6 position or at the exocyclic positions, generally leads to a triplet ground state, although the singlet-triplet gap becomes smaller. Twisting the substituents out of conjugation by only some degree (up to 30°) has only a very little effect on ΔE_{ST}. If only one substituent is twisted out of conjugation, while the aromatic conjugation remains intact for the second substituent, the NBMOs can become disjoint and therefore ΔE_{ST} is calculated to be small or even negative. Nevertheless, the topological features of the SOMOs were found to be the most important factor for predictions on the ground state multiplicity. Overlap between the two NBMOs is most important for a robust triplet. Furthermore, it was depicted that a

high energy difference between both SOMOs will result in a singlet ground state. An energy difference of 0.02 hartree (12.5 kcal/mol) of both SOMOs is predicted to result in an antiferromagnetically coupled singlet ground state.

Some push-pull diradicals, like the tetracyanodiamino-*m*-xylylene **114** or the tetraaminodinitro-*m*-xylylene **115** were calculated to have an energy splitting of the SOMOs of 0.026 and 0.022 hartree, respectively, and thus are predicted to be singlet ground state molecules with ΔE_{ST} = - 8.44 and ΔE_{ST} = -19.42 kcal/mol, respectively (Scheme 48).[74]

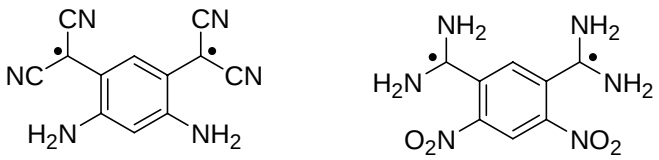

114 **115**

Scheme 48. *m*-Xylylene derivatives **114** and **115** are predicted to have singlet ground states.

The effect of substituents in 2 position of *m*-xylylene **1** on ΔE_{ST} was calculated by Krylov et al. using the SF-EOM-CCSD method.[76] Only little changes in ΔE_{ST} were observed for electron-donating and electron-withdrawing substituents in this position while charged species like the pyridinium cation derivative reverses the spin preference into a singlet ground state. The best way to explain this is given by resonance theory (Scheme 49).

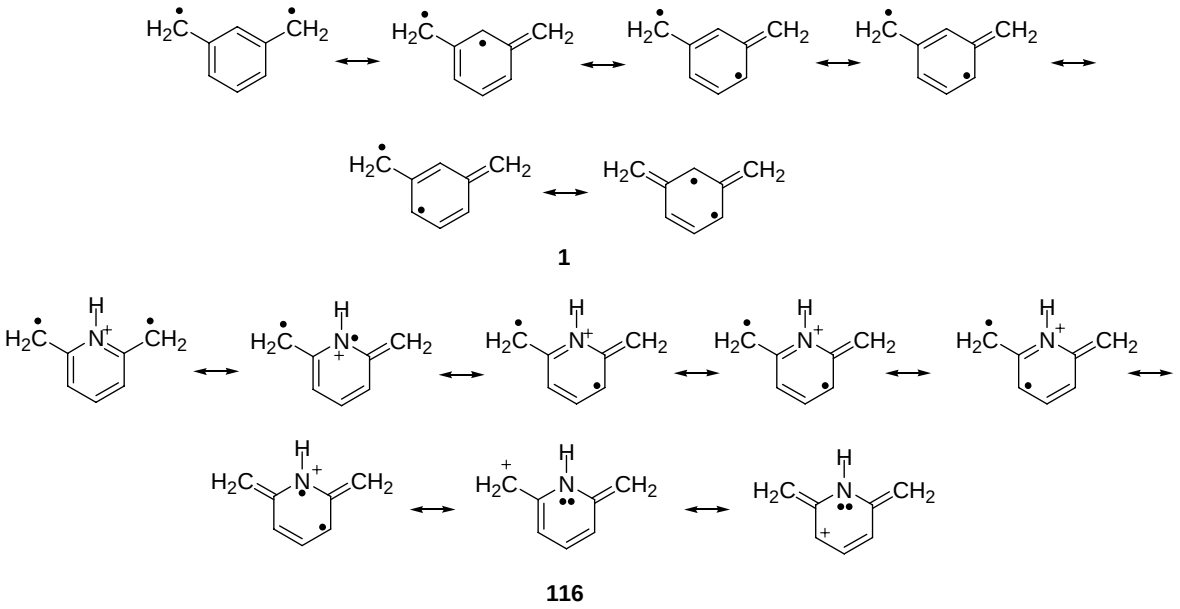

Scheme 49. Possible resonance structures for *m*-xylylene **1** and pyridinium cation **116**.

The additional resonance structures possible for **116** in comparison to **1** have all spins paired and are thus applicable only for the singlet state. This leads to preferential stabilization of the singlet state of **106** and makes it the ground state of this charged molecule.[76]

5.2 Infrared experiments

All known routes to *m*-xylylene **1** are photochemical in nature and were used to isolate only small amounts of the reactive diradical to study **1** with sensitive techniques like fluorescence and electron paramagnetic resonance spectroscopy.[34, 40, 41, 63, 64, 68] In order to find a thermal precursor of diradical **1** and to be able to increase the yield for IR measurements, cyclophanedione **117** was synthesized and studied by IR spectroscopy (Scheme 50).

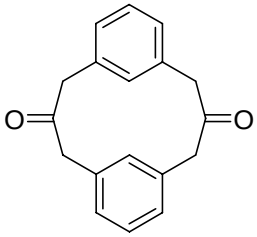

117

Scheme 50. Possible precursor of *m*-xylylene.

It was known that the strained C-C single bond of cyclophandiones can be cleaved under release of CO to give the corresponding diradicals.[77, 78] Platz et al. have used dichloro-*m*-xylene **104** and 1,8-*bis*-bromomethyl-naphthalene **118** as photochemical precursor to study the corresponding diradicals by EPR spectroscopy.[41, 64] It is well-known that the C-I bond due to its low electronegativity difference is much weaker than the similar C-Cl or C-Br bonds. Furthermore, a relatively low temperature in a thermal synthesis of a reactive intermediate has the advantage to reduce secondary thermal rearrangements as well as ring-opening products, at least if these pathways are high energy pathways. Another precursor which was tested on this grounds was 1,3-*bis*-(iodomethyl)benzene **17**, which was further used as it proves to be easily sublimable and further showed abstraction of the corresponding iodine atoms at relatively moderate temperatures.

In all flash vacuum pyrolysis (FVP) experiments small amounts of unreacted starting compound 1,3-*bis*-(iodomethyl)benzene **17** remain visible in the IR spectrum while only the three most intense signals could be observed. Figure 13 shows the IR spectrum after deposition of 1,3-*bis*-(iodomethyl)benzene **17** in an argon matrix at 30 K, together with the calculated IR spectrum (B3LYP; 6-311G(d,p)). As can be seen from the

Figure, no decomposition is taking place during the deposition of the substance – a fact that can also be infered by comparison with an IR spectrum taken at rt as KBr pellet.

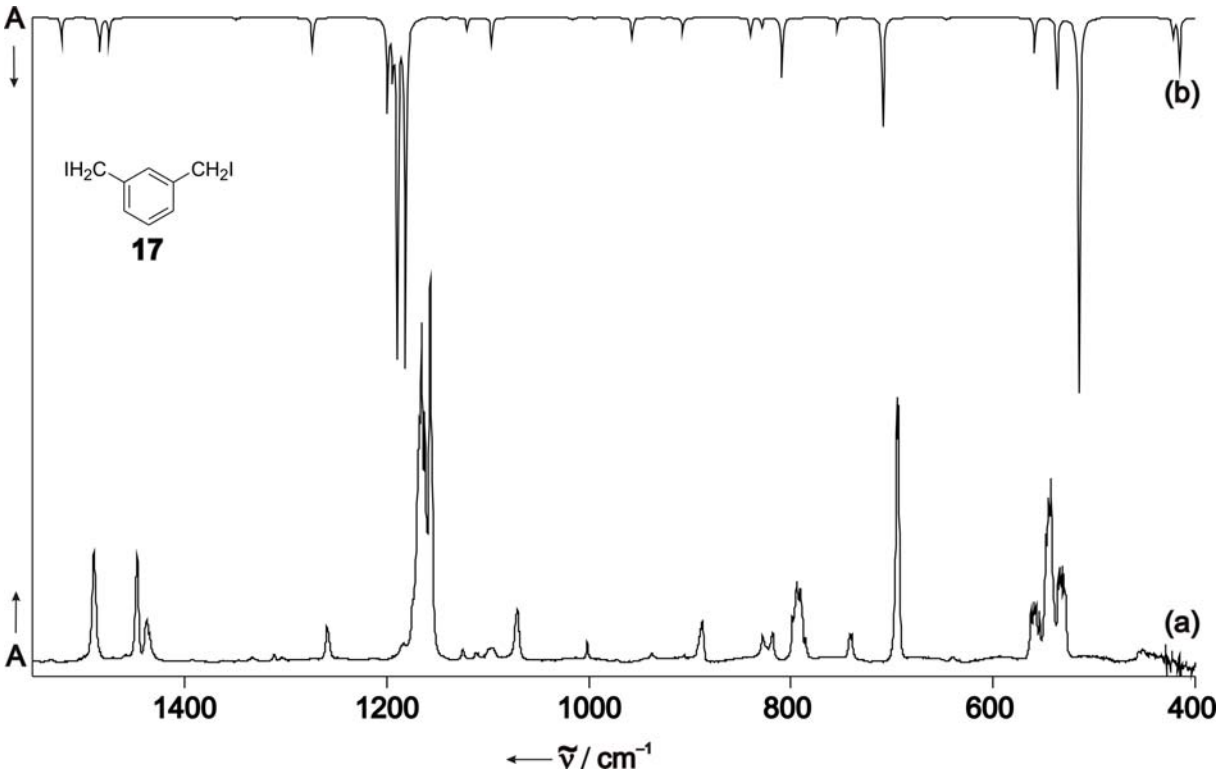

Figure 13. IR spectra of 1,3-*bis*-(iodomethyl)benzene **17**. (a) IR spectrum after 90 min deposition of 1,3-*bis*-(iodomethyl)benzene **17** in argon at 30 K. (b) IR spectrum of 1,3-*bis*-(iodomethyl)benzene **17** calculated at the B3LYP level of theory (6-311G(d,p)).

The flash-vacuum pyrolysis conditions were tested in the temperature range of 350°C up to 650°C. At 350°C 1,3-*bis*-(iodomethyl)benzene **17** is the main species trapped in the matrix, while some new signals are already appearing. In contrast to this, it was found that ring opening takes place at high temperatures between 550 - 650°C, resulting in absorptions which are known from the literature to belong to HI, acetylene HCCH, and diacetylene.

Flash-vaccum pyrolysis (FVP) of 1,3-*bis*-(iodomethyl)benzene **17** at 400°C and subsequent trapping of the products in argon at 10 K results in a marked decrease of precursor **17** and formation of a new product. The newly formed product shows strong IR absorptions at 1434, 835, 766, 724 and 641 cm^{-1} (Figure 14, Figure 15, Table 5). The highest yield of the newly formed product is obtained at 450 °C, whereas above 500°C further products are formed and the amount of the inital thermal product decreases.

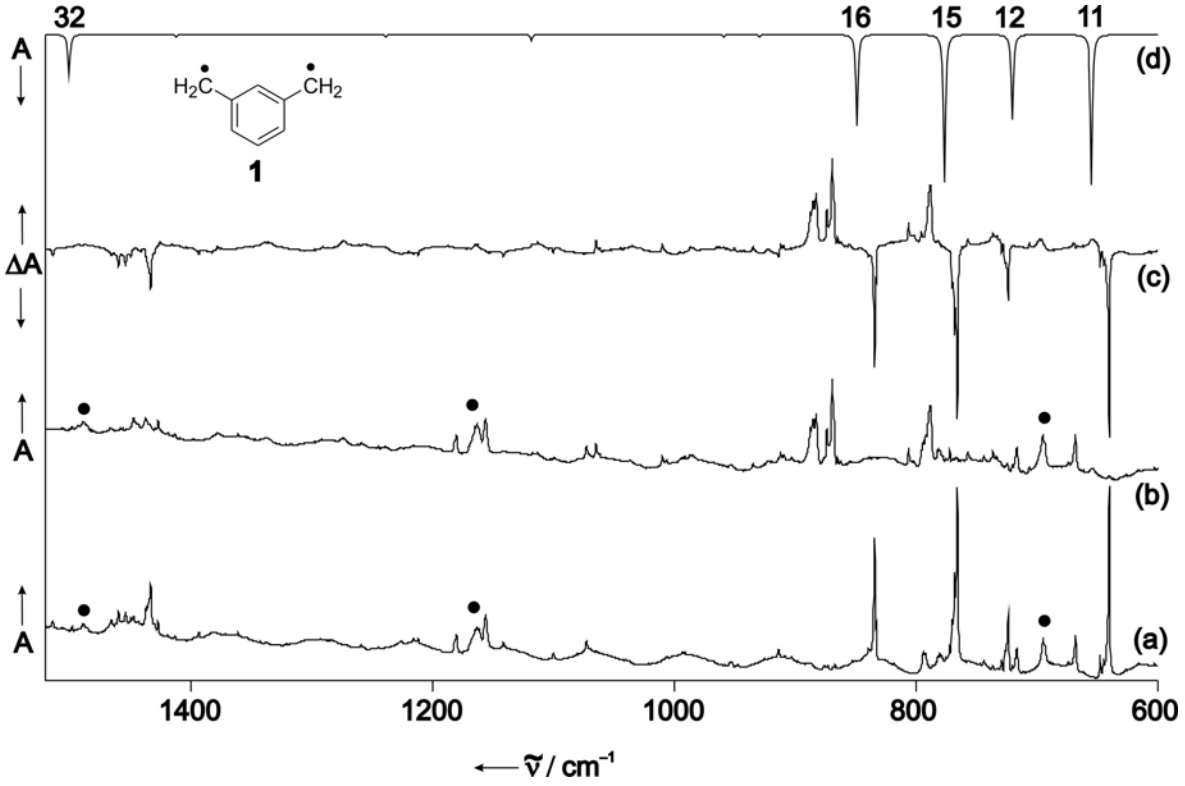

Figure 14. IR specta showing the synthesis and the photochemistry of *m*-xylylene **1** in argon at 10 K. (a) FVP of 1,3-*bis*-(iodomethyl)benzene **17** at 450°C and trapping the products in an argon matrix at 10 K. Black dots indicate remaining **17**. (b) Same matrix after $\lambda > 400$ nm irradiation. (c) Difference IR spectrum (b) – (a). (d) IR spectrum of **1** calculated at the UB3LYP/6-311G(d,p) level of theory.

By comparison of the experimental IR spectrum obtained after FVP of **17** with DFT calculations at the UB3LYP level of theory using the 6-311G(d,p) basis-set, the newly formed species was assigned to *m*-xylylene **1** in its triplet state. Traces of **1** were also formed on direct UV irradiation with 308 nm light of a XeCl excimer laser of matrix-isolated 1,3-*bis*-(iodomethyl)benzene **17** (Figure 16). However, due to the photolability of **1** the photochemical generation is a highly inefficent process and upon prolonged irradiation, all IR signals assigned to **1** decrease in intensity. Apparently, the signals assigned to *m*-xylylene **1** do not belong to the main product formed under these conditions. All assigned vibrations of **1** in its triplet state are given in Table 5.

Table 5. IR spectroscopic data of *m*-xylylene **1** and d_4-**1**.

Mode #	Sym.	Argon [b]	B3LYP [a]	Argon [b] **d_4**	B3LYP [a] **d_4**	Assignment	Pol.

11	B_1	640.5 (100)	655.5 (99)	645.6 (45)	661.3 (46)	$C_{1,3}$-H out-of-plane deformation	-
12	B_1	723.9 (45)	721.1 (57)	581.0 (100)	576.5 (100)	C_5-H_2 out-of-plane wagging	-
15	B_1	766.4 (90)	777.2 (96)	759.1 (65)	772.6 (70)	$C_{1,3,4}$-H out-of-plane deformation	-
16	B_1	834.9 (60)	849.5 (61)	831.4 (50)	847.3 (51)	C_1-H out-of-plane deformation	-
32	B_2	1433.9 (25)	1502.4 (28)	1459.8 (15)	1488.5 (18)	C_5-H_2 rocking; C=C aromatic stretching; $C_{1,3,4}$-H in-plane deformation	+
35	A_1	c	3144.6 (4)	2214.4 (15)	2283.6 (4)	symmetric C_5-H_2 stretching	n.a.
36	B_2	3034.4 (23)	3145.1 (25)	2214.4 (15)	2283.9 (14)	symmetric C_5-H_2 stretching	n.a.
41	B_2	3110.6 (8)	3240.9 (8)	2347.3 (15)	2415.7 (7)	asymmetric C_5-H_2 stretching	n.a.
42	A_1	3114.2 (27)	3241.1 (29)	2347.3 (15)	2416.0 (18)	asymmetric C_5-H_2 stretching	n.a.

[a] UB3LYP/6-311G(d,p). [b] Argon, 10K. [c] not assigned due to the broad peaks in this region.

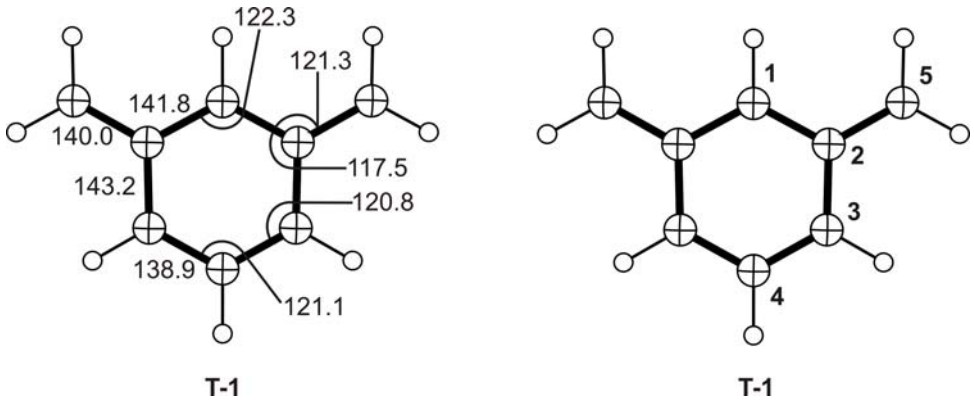

Figure 15. UB3LYP optimized geometry of T-**1**. Bond lengths are given in pm, and bond angles in degree. Numbering used in the table to describe the vibrations are also given.

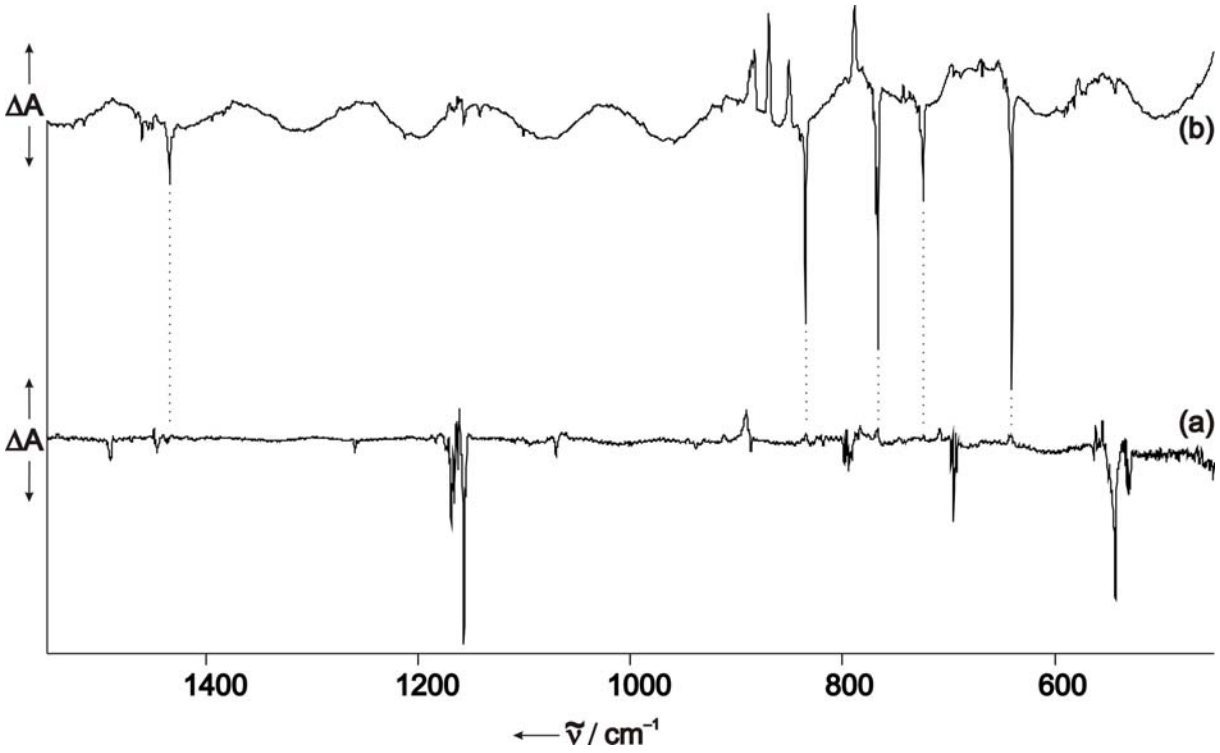

Figure 16. Photochemical generation of triplet *m*-xylylene **1** from 1,3-*bis*-(iodomethyl)benzene **17**. (a) IR difference spectrum of an argon matrix containing 1,3-*bis*-(iodomethyl)benzene **17** after irradiation with 308 nm light of a XeCl excimer laser (5 Hz, 6 min). (b) IR difference spectrum of an argon matrix containing the FVP products of 1,3-*bis*-(iodomethyl)benzene **17** after irradiation with 450 – 400 nm. Peaks pointing downwards in spectrum (b) are due to *m*-xylylene **1** and are correlated with some appearing signals of IR spectrum (a).

The four strong vibrations of triplet **1** between 835 and 641 cm^{-1} are assigned to B_1 symmetrical out-of-plane C-H deformation vibrations and the absorption at 1434 cm^{-1} to a B_2 symmetrical combination of C-C stretching and in-plane C-H deformation vibration (Figure 17). For the B_2 symmetrical mode a frequency of 1500 +/- 40 cm^{-1} was previously determined from photoelectron spectroscopy in the gas phase.[65, 66]

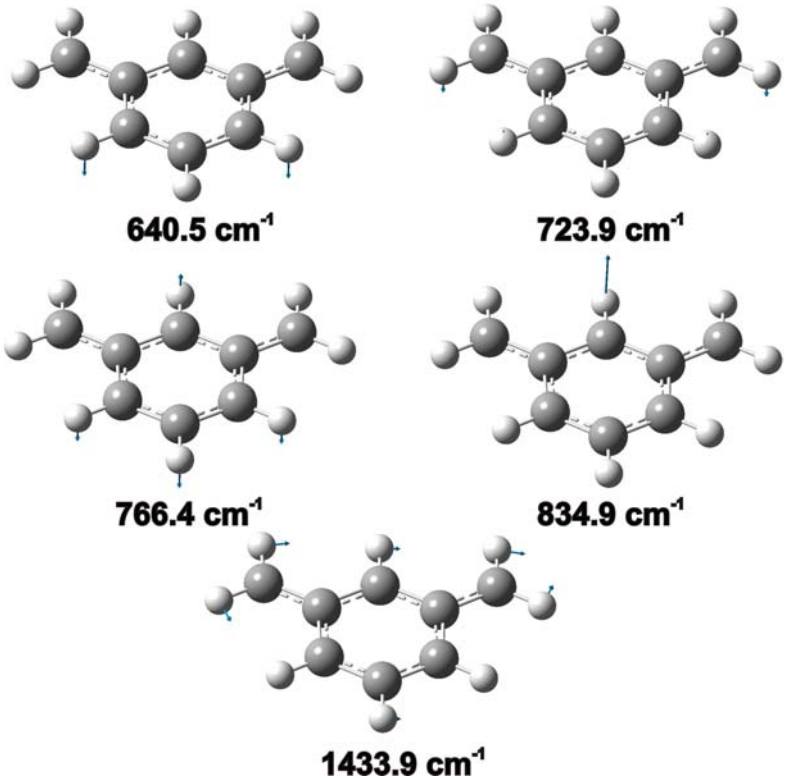

Figure 17. Calculated normal coordinates of the strongest IR vibrations of triplet *m*-xylylene **1** (UB3LYP/6-311G(d,p)).

Deuteration of the benzylic positions in d_4-**1** leads to characteristic isotopic shifts, again in excellent agreement with the calculated values (Figure 18, Table 5). The largest red-shift of 143.2 cm^{-1} (calculated 144.6 cm^{-1}) is found for the vibration at 724 cm^{-1}, indicating a large contribution of the exocyclic H atoms. The other three B_1 vibrations are characterized as benzene C-H out-of-plane (oop) deformation vibrations and consequently show only small isotopic shifts (3-8 cm^{-1}) in d_4-**1**. For the C-H stretching vibrations involving the benzylic hydrogen atoms also large isotopic shifts are predicted; however, these vibrations are overlapping with bands of the precursor, secondary products, and contaminations and are thus difficult to assign.

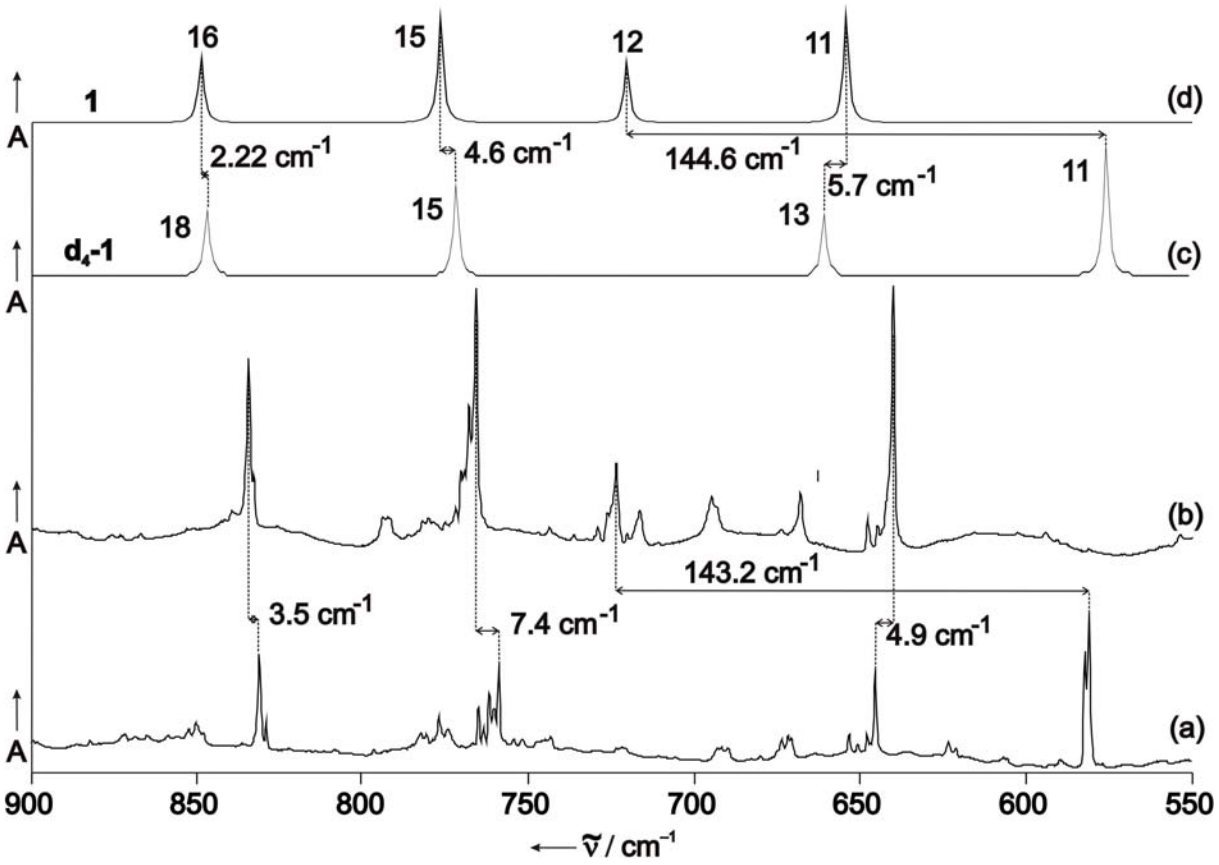

Figure 18. IR spectra in the range 550 – 900 cm^{-1} of *m*-xylylene **1** and its tetradeuterated isotopomer d_4-**1** showing isotopic shifts of the out-of-plane deformation modes. (a) d_4-**1** in argon at 10 K. (b) **1** in argon at 10 K. (c) UB3LYP/6-311G(d,p) calculated IR spectrum of d_4-**1**. (d) UB3LYP/6-311G(d,p) calculated IR spectrum of **1**.

5.3 IR dichroism

The symmetry of the strongest IR bands of **1** was determined by measuring the IR dichroism of partially oriented matrices. This method depends on the partial bleaching of a matrix-isolated compound with linear polarized light.[79, 80] Diradical **1** is photolabile towards 400 nm irradiation (see Photochemistry part) and linear polarized light of this wavelength was used for the photoselection experiments. The molecules of **1** are initially randomly oriented in the matrix. Molecules with their electronic transition moments oriented parallel to the E-vector of the polarized light will show a more efficient photochemistry than those with a perpendicular orientation. The result is a photoselection of both **1** and the photoproducts with respect to E. Since the symmetry of **1** is C_{2v}, the transition moment of the electronic excitation as well as the vibrational transition moment have to be parallel to the principal axes x, y, or z of the molecule. Since the orientation is uniaxial, only two distinct polarization orientations are possible (parallel or perpendicular to this axis, the two perpendicular axes are undistinguishable in these experiments). This is found in the experiment (Figure 19): the out-of-plane deformation vibrations of B_1 symmetry are polarized perpendicular to the B_2 symmetrical in-plane deformation vibration.

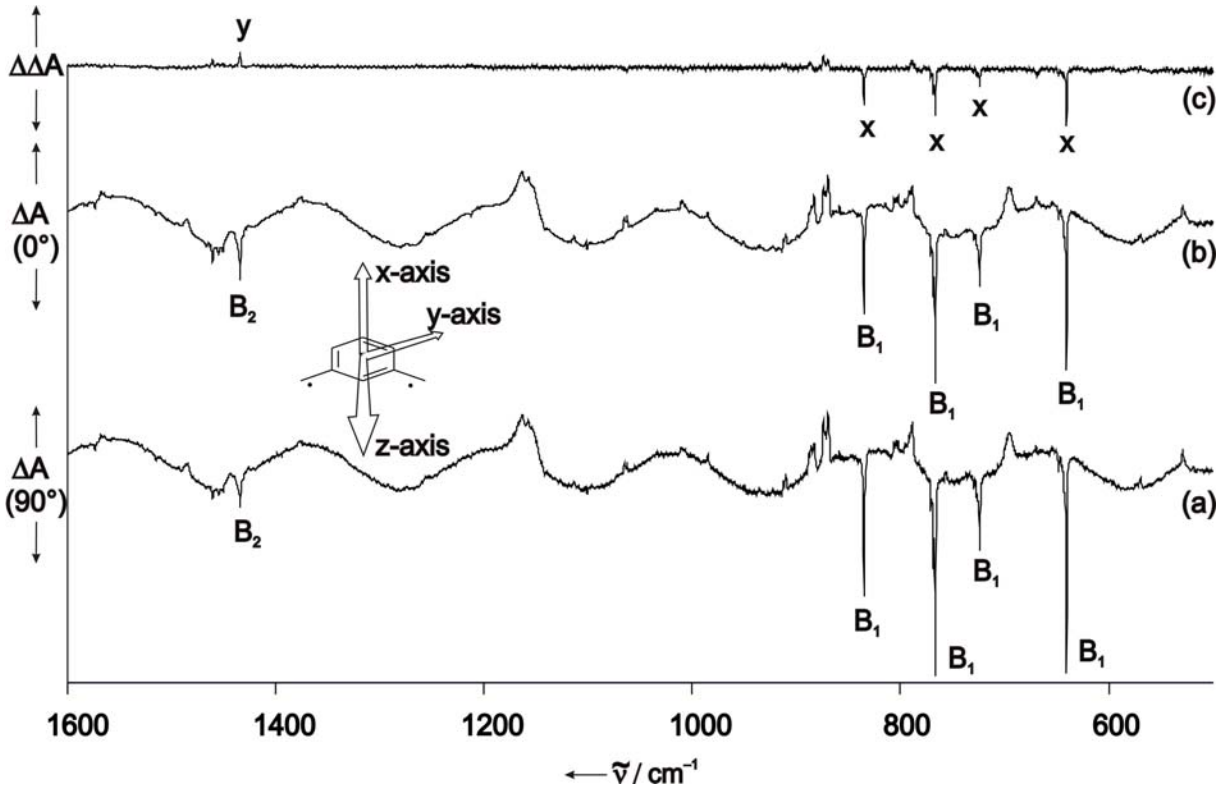

Figure 19. IR dichroism of **1** in argon at 10 K after partial photolysis of **1** using linearly polarized visible light (400 – 450 nm). The IR bands assigned to **1** are marked with their symmetry label. (a) Difference IR spectrum with the IR polarization filter perpendicular to the polarization direction of the photolysis (90° between IR and vis light polarization). Peaks pointing downward decrease and peaks pointing upward increase during irradiation. (b) Difference IR spectrum with the IR polarization filter parallel to the polarization direction of the photolysis (0° between IR and vis light polarization). Peaks pointing downwards decrease upon irradiation, and peaks pointing upwards increase during irradiation. B_1 and B_2 indicate the symmetry of the vibrations. (c) Difference spectrum between (a) and (b) showing differences in the polarization directions of IR bands. Since this effect is small, only strong absorptions can be observed.

The transition moments of the B_1 vibrations are oriented parallel to the z axis, whereas that of B_2 is parallel to x. This clearly demonstrates the C_{2v} symmetry of **1** and confirms the assignment of the five strongest IR bands of **1**. Since the photoselection of **1** is low and the effect is very small, the polarization direction of the weaker bands could not be determined.

5.4 UV/Vis spectroscopy

The UV/Vis spectrum of matrix isolated **1** shows a strong and broad transition at 231 nm, a strong and sharp transition at 287 nm presumably with a vibrational progression at 279 nm (weak) and a very weak electronic transition at 433 nm (Figure 20). The 279 and 287 nm absorptions are similar to the transitions observed by Migirdicyan and Baudet in their fluorescence excitation spectrum of *m*-xylylene **1** in a shpolskii matrix at 295 and 287 nm.[63] An additional transition at 312 nm described in this paper could not be verified, while a very weak transition at 315 nm is observed which, nevertheless, does not show photochemistry upon irradiation with $\lambda > 400$ nm.[63] Platz et al. also observed the 295 nm transition in 3-methylpentane as well as an electronic transition at 323 nm, the former was assigned to *m*-xylylene **1** and the latter to the corresponding monoradical **102**.[40, 41] The very weak transition at 433 nm is in accordance with the observation of fluorescence on excitation of **1** at 439 nm by LeJeune et al..[81] The strong and broad absorption with a maximum at 231 nm has not been described in literature, thus far.

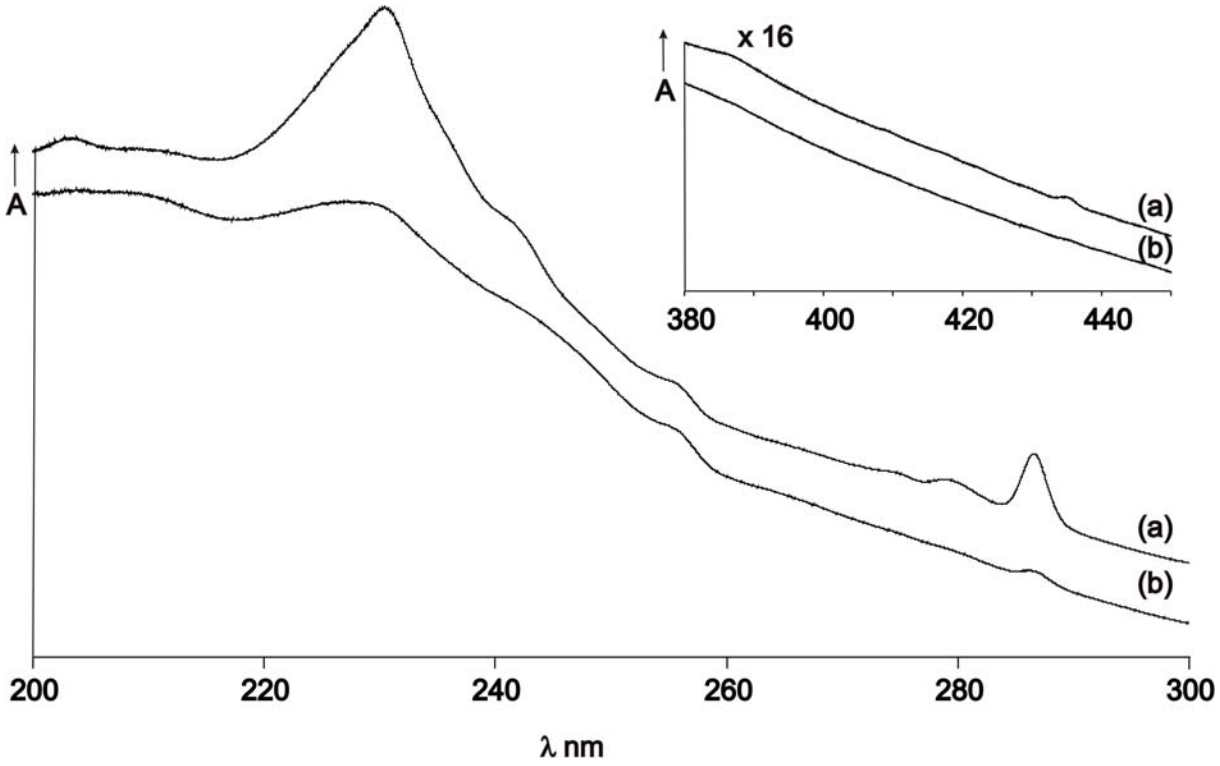

Figure 20. UV/Vis spectrum of an argon matrix containing the FVP products of 1,3-*bis*-(iodomethyl)benzene **17**. (b) UV/Vis spectrum of the same matrix after irradiation with λ = 400 - 450 nm. Inset shows the 380 – 350 nm region.

All electronic transitions assigned to *m*-xylylene **1** decrease in intensity upon irradiation with λ > 400 nm and subsequently gain in intensity if the matrix is irradiated with UV light (λ = 254 nm).

TD-DFT calculations do not predict the electronic transition at 433 nm, while the higher energy transitions between 300 and 200 nm are correctly calculated with the oscillator strength in the right order of magnitude by this level of theory.

5.5 Electron paramagnetic resonance

The EPR spectrum of **1**, matrix isolated in argon at 4 K by trapping of the FVP products of 1,3-*bis*-(iodomethyl)benzene **17** at 450°C, showed a centrosymmetric four line spectrum together with a radical impurity on the center. The very intense triplet signal could best be simulated with zero field splitting parameters |D/hc| = 0.011 cm^{-1} and |E/hc| = 0.001 cm^{-1}, in excellent agreement with the published values by Platz et al..[41, 64] The small E value results in no additional splitting of the xy transitions but leads to some broadening of the signal. The magnitude of the zfs parameter D is in the dimension of what could be expected for a weakly coupled triplet ground state π,π-diradical. In addition, a low-intensity half-field signal, characteristic of triplet EPR spectra, was found at 1708 G. This was the first observation of this "forbidden" transition for this molecule and clearly demonstrates that indeed a triplet state is observed (Figure 21).

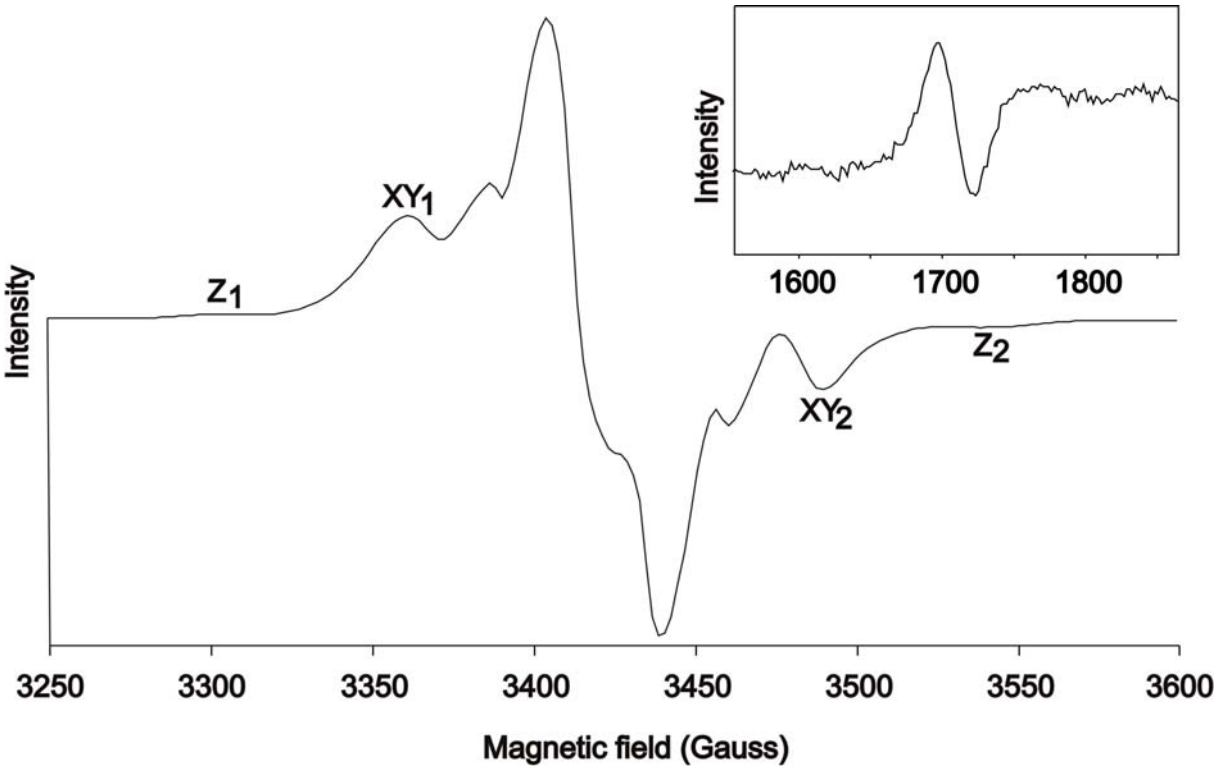

Figure 21. EPR spectrum obtained after FVP of 1,3-*bis*-(iodomethyl)benzene **17** at 450°C and subsequent trapping of the products in argon at 4 K. Inset: half-field region of the spectrum.

The EPR signal corresponding to the triplet state diminish in intensity upon irradiation with λ > 400 nm of a mercury high-pressure lamp which is in agreement with the IR and UV/Vis experiments.

In the IR studies it was found that *m*-xylylene **1** is also formed in small amounts upon 308 nm laser irradiation. Since EPR spectroscopy is a very sensitive technique, it can be expected that the triplet diradical will also show up in the EPR spectrum upon irradiation of 1,3-*bis*-(iodomethyl)benzene **17**, as indeed is found experimentally. Figure 22 shows a comparison of *m*-xylylene **1** produced by photolytic scission of the weak C-I bond of *bis*iodide **17** and the thermal route through FVP of **17** (Figure 22).

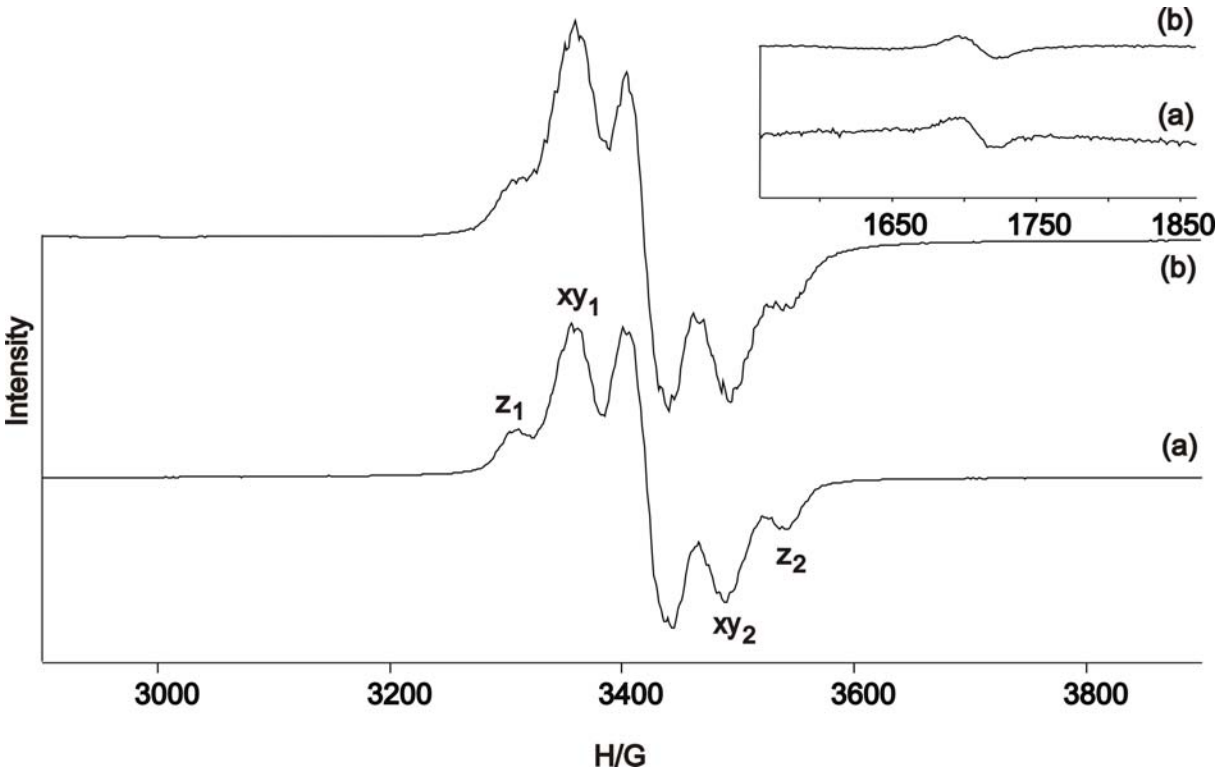

Figure 22. (a) EPR spectrum of *m*-xylylene **1** obtained after irradiation of an argon matrix containing 1,3-*bis*-(iodomethyl)benzene **17** with 308 nm of a XeCl excimer laser. (b) EPR spectrum of **1** obtained after FVP of 1,3-*bis*-(iodomethyl)benzene **17** at 450°C and subsequent trapping of the products in an argon matrix at 4 K. Inset shows the half-field region.

The obtained spectra are superimposable in respect to the triplet radical signals, while they show differences in the monoradical impurity region. As the abstracted iodine radicals are formed in the same matrix cage, this result shows that the respective triplet EPR signal is not disturbt by the close proximity of iodine atoms or molecular iodine.

5.6 Photoisomerization of *m*-xylylene

Irradiation of matrix isolated **1** with visible light (λ > 400 nm) results in a decrease of all IR, UV/Vis, and EPR bands assigned to **1** and formation of the two new C_8H_8-isomers 4,6-dimethylene-bicyclo[3.1.0]hex-2-ene **19** and 3-methylene-bicyclo[4.1.0]hepta-1,4-diene **18** (Scheme 51). Irradiation at a slightly shorter wavelength (λ > 350 nm) results in the rearrangement of **18** to **19** (Figure 23) while short wavelength UV irradiation (λ = 254 nm) leads partially back to diradical **1** and partially to the formation of a further isomer, 3,5-dimethylene-tricyclo[2.2.0.0*2,6*]hexane **20**. The reversible photochemistry (Figures 18 - 20) demonstrates that **19**, **18**, and **20** are C_8H_8-isomers of **1** formed in photostationary equilibria.

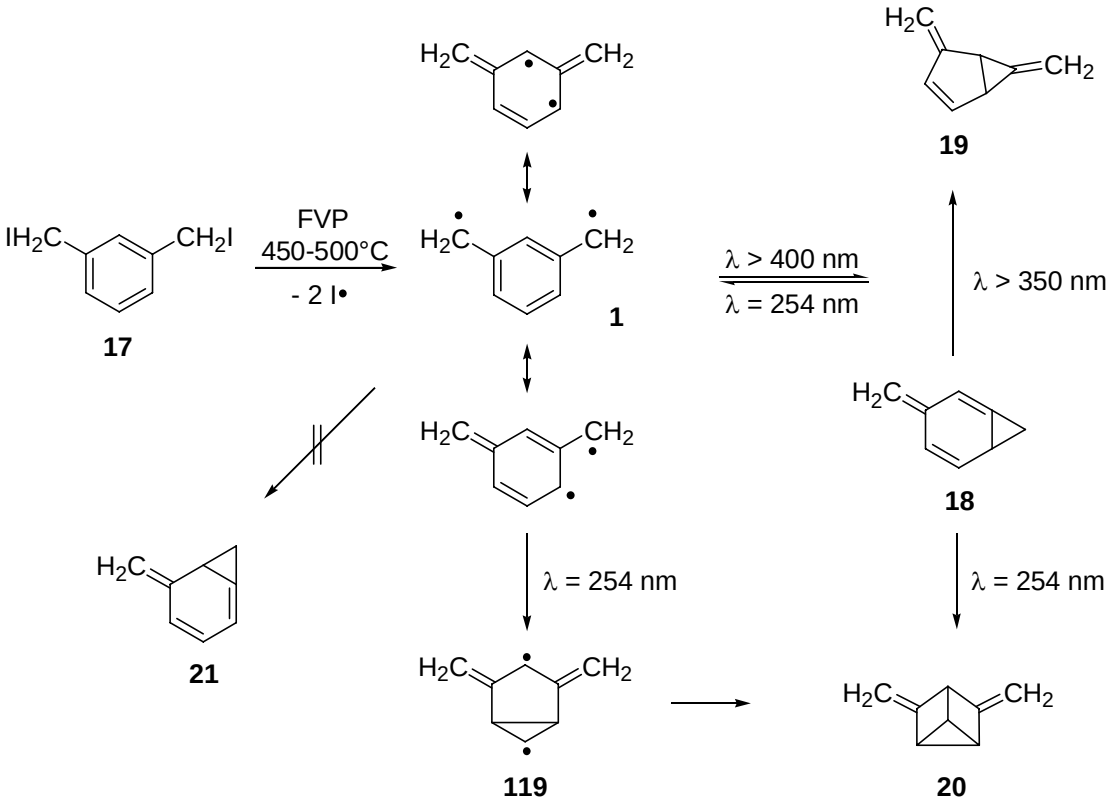

Scheme 51. Photochemistry of *m*-xylylene **1**.

Since the equilibrium between these species depends on the irradiation conditions, sets of IR bands can be assigned to each isomer and the comparison with the results of DFT calculations allows the identification of the different compounds.

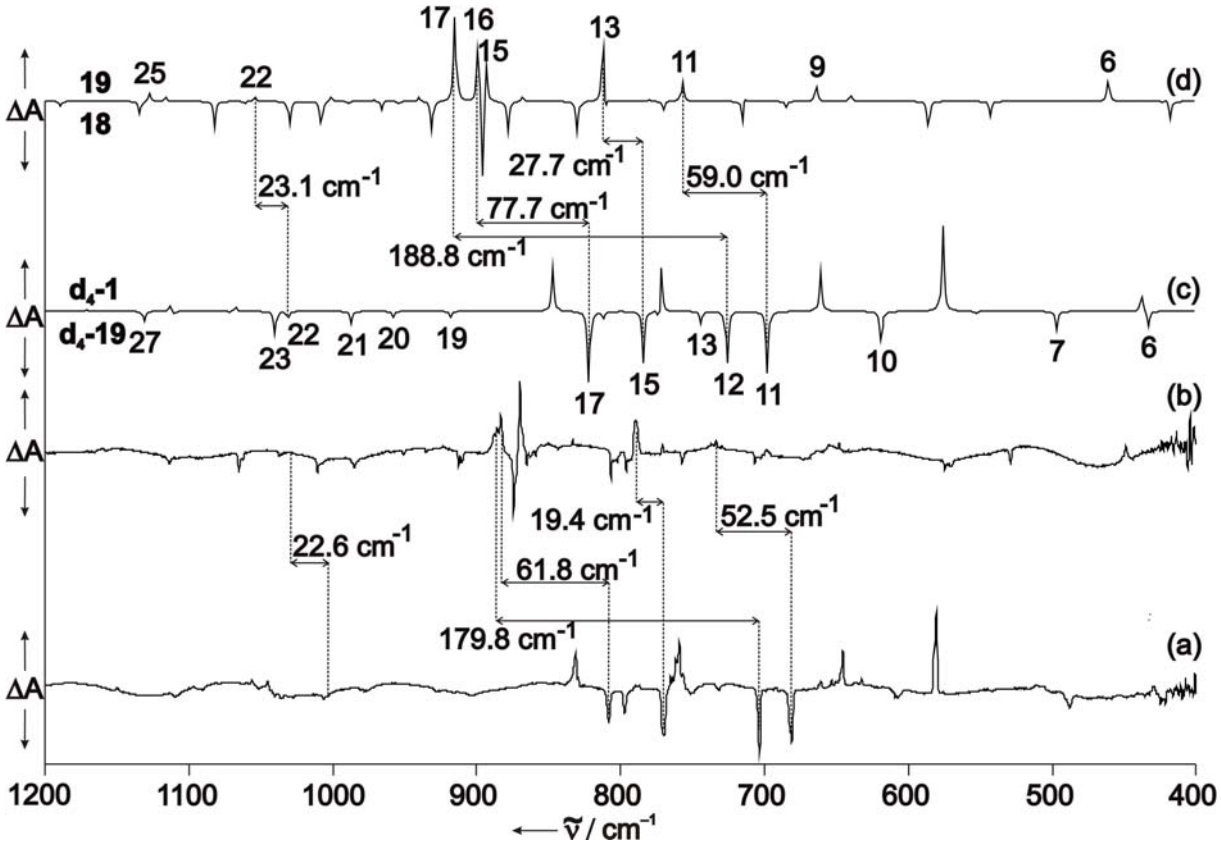

Figure 23. Difference IR spectra showing the photochemical interconversion of **1**, **19**, and **18** in argon at 10 K. The experimental difference spectra are compared to simulated difference spectra based on calculations at the B3LYP/6-311G(d,p) level of theory. (a) λ = 254 nm irradiation converts *d*$_4$-**19** (disappearing, peaks pointing downward) into *d*$_4$-**1** (appearing, peaks pointing upward). (b) λ >350 nm irradiation converts **18** (disappering, peaks pointing downward) into **19** (appearing, peaks pointing upward). (c) Simulated difference spectrum *d*$_4$-**1** – *d*$_4$-**19** corresponding to (a). (d) Simulated difference spectrum **19** – **18** corresponding to (b). The isotopic shifts of the *exo*-methylene groups of **19** are shown in the spectra.

All characteristic vibrations of hydrocarbon **19** and its deuterated isotopomer are collected in Table 6.

Table 6. IR spectroscopic data of **19** and *d*$_4$-**19**.

Mode #	Argon, 10 K	B3LYP[a]	Argon, 10 K **d$_4$**	B3LYP[a] **d$_4$**	Assignment
6	448.8 (25)	461.8 (23)	424.8 (20)	433.1 (21)	C_1-C_3-C_8 deformation
7	n.a.	605.4 (0)	487.7 (20)	497.4 (22)	$C_{7,8}$-H_2 twisting; in-plane ring deformation

8	628.0 (5)	640.3 (7)	607.5 (25)	619.5 (36)	skeletal vibration
11	733.6 (20)	757.8 (23)	681.1 (75)	698.8 (74)	asymmetric H-C_1-C_2-H bending; out-of-plane ring deformation
12	n.a.	780.4 (2)	731.7 (15)	744.9 (15)	asymmetric H-C_1-C_2-H bending; in-plane ring deformation
13	789.7 (80)	812.5 (84)	770.3 (65)	784.7 (62)	H-C_4=C_5-H out-of-plane deformation; C_8-H_2 twisting
14	855.5 (2)	868.7 (5)	n.a.	851.9 (3)	asymmetric H-C_1-C_2-H bending
15	869.9 (110)	893.2 (51)	797.1 (25)	813.0 (9)	C_8-H_2 twisting; C_7-H_2 out-of-plane wagging
16	869.9 (sh)	899.9 (69)	808.1 (45)	822.2 (84)	C_8-H_2 twisting; C_7-H_2 out-of-plane wagging
17	883.2 (100)	915.3 (100)	703.4 (60)	726.5 (62)	C_8-H_2 out-of-plane wagging
18	923.3 (5)	941.0 (5)	797.1 (25)	813.0 (9)	C_7-H_2 in-plane rocking
22	1029.1 (5)	1054.2 (5)	1006.5 (5)	1031.1 (9)	$C_{1,2}$-H bending
24	n.a.	1117.0 (5)	1036.0 (10)	1040.8 (27)	asymmetric H-C_4=C_5-H in plane deformation; C_7-H_2 rocking
25	1099.6 (10)	1127.3 (10)	1109.5 (10)	1131.4 (11)	asymmetric H-C_4=C_5-H in plane deformation; C_7-H_2 rocking
29	1336.2 (10)	1358.8 (15)	1341.2 (20)	1364.5 (20)	symmetric H-C_4=C_5-H in plane deformation; C_7-H_2 bending
32	1565.3 (5)	1620.7 (7)	1573.0 (10)	1615.2 (17)	C_4=C_5 stretching
33	1640.6 (80)	1696.4 (76)	1614.4 (70)	1658.8 (100)	C_6=C_7 stretching

34	1745.3 (40)	1817.1 (41)	1726.4 (50)	1783.7 (69)	C_3=C_8 stretching

[a]B3LYP/6-311G(d,p).

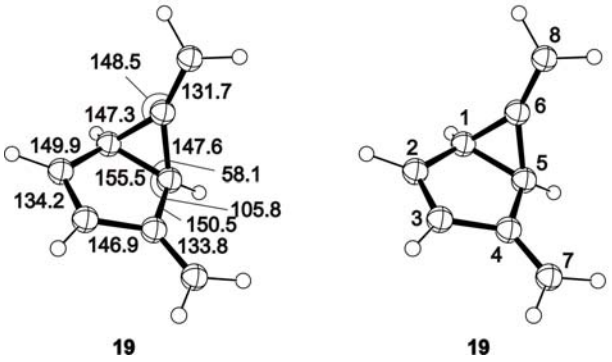

Figure 24. B3LYP optimized geometry of hydrocarbon **19**. Bond lengths are given in pm, and bond angles in degree. Numbering used in the table to describe the vibrations is also given.

Hydrocarbon **19** shows characteristic C=C stretching vibrations of the two *exo*-methylene groups at 1745.3 cm^{-1} (C(6)=C(8)) and 1640.6 cm^{-1} (C(4)=C(7)) with deuterium shifts of 18.9 and 26.2 cm^{-1}, respectively, in d_4-**19** (Figure 23, Figure 24, Table 6). The high frequency of the former vibration is characteristic of methylenecyclopropanes, and the isotopic shifts demonstrate that both *exo*-methylene groups are deuterated in d_4-**19**; no scrambling of deuterium is observed. Other intense IR absorptions are found in the fingerprint region of the spectrum. The most intense band at 883.2 cm^{-1} shows a very large isotopic shift of 179.8 cm^{-1} and is assigned to the C(8)-H_2 out-of-plane wagging deformation. The band positions, relative intensities, and isotopic shifts are nicely reproduced by DFT calculations, as can be seen by the very similar patterns of the simulated (from DFT calculations) and experimental IR spectra (Figure 23).

The strongest IR absorption of hydrocarbon **18** is (like in **19**) the C(8)-H_2 out-of-plane wagging vibration of the *exo*-methylene group at 874.2 cm^{-1}, in good agreement with the calculation (Figure 25, Figure 26, Table 7).

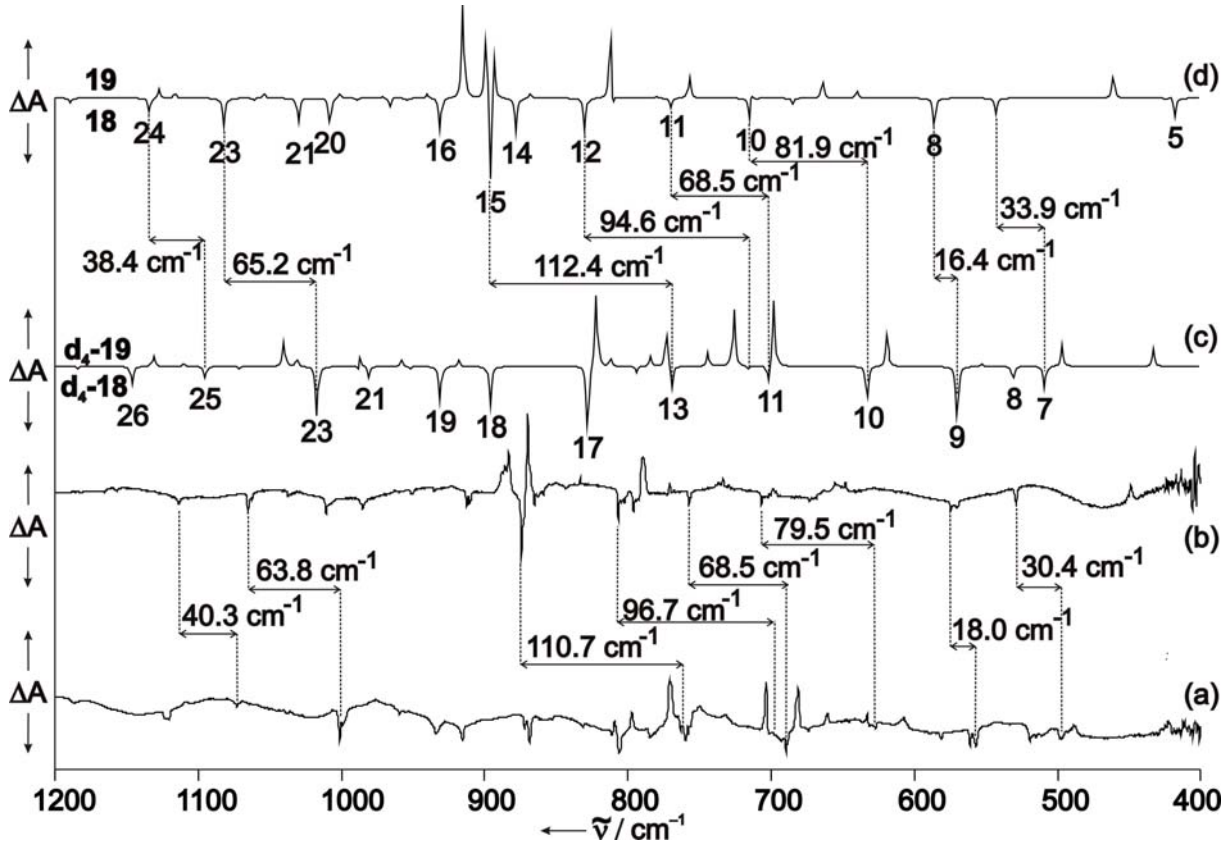

Figure 25. Difference IR spectra showing the photochemical conversion of **19** and **18** in argon at 10 K. The experimental difference spectra are compared to simulated difference spectra based on calculations at the B3LYP/6-311G(d,p) level of theory. (a) λ > 350 nm irradiation converts d_4-**18** (disappearing, peaks pointing downward) into d_4-**19** (appearing, peaks pointing upward). (b) λ > 350 nm irradiation converts **18** (disappearing, peaks pointing downward) into **19** (appearing, peaks pointing upward). (c) Simulated difference spectrum d_4-**19** – d_4-**18** correspond to (a). (d) Simulated difference spectrum **19** – **18** corresponding to (b). The isotopic shifts of the *exo*-methylene groups of **19** are shown in the spectra.

As expected, in d_4-**18** this band shows a very large isotopic shift (110.7 cm^{-1}). Another band with a large isotopic shift is the C(7)-H_2 twisting vibration at the cyclopropane ring at 796.0 cm^{-1} (96.7 cm^{-1} isotopic shift in d_4-**18**).

Table 7. IR spectroscopic data of **18** and d_4-**18**.

Mode #	Argon, 10 K	B3LYP[a]	Argon, 10 K **d_4**	B3LYP[a] **d_4**	Assignment
7	528.9 (20)	543.6 (19)	498.5 (30)	509.7 (23)	in-plane ring deformation; C_3-H_2 twisting
8	575.0 (30)	586.7 (30)	557.0 (75)	570.3 (54)	skeletal vibration

10	706.6 (25)	715.8 (32)	627.1 (25)	633.9 (34)	C_3-H_2 twisting; ring deformation
11	757.4 (15)	770.8 (12)	689.7 (30)	702.3 (21)	C_7-H bending,C_8-H_2 twisting; in-plane ring deformation
12	796.0 (30)	811.1 (44)	699.3 (1)	716.5 (6)	symmetric H-C_6=C_7-H out-of-plane deformation; C_3-H_2 twisting
13	806.6 (35)	830.2 (37)	n.a.	769.3 (27)	C_4-H bending, C_3-H_2 rocking; C_8-H_2 twisting
15	874.2 (100)	896.6 (100)	763.5 (100)	784.2 (51)	C_8-H_2 out-of-plane wagging
14	-	878.9 (37)	806.1 (80)	828.6 (66)	C_3-H_2 twisting; C_1-C_2-C_7 deformation
16	912.6 (30)	931.2 (37)	868.5 (75)	896.4 (43)	$C_{2,4}$-H bending, C_3-H_2 twisting, C_5-C_6-C_7 deformation
20	985.1 (30)	1009.0 (28)	n.a.	988.7 (10)	C_3-H_2 wagging, C_4-C_1-C_3 deformation
23	1065.2 (35)	1082.7 (32)	1001.4 (80)	1017.5 (53)	C_3-H_2 rocking; C_2-H bending
24	1113.4 (10)	1134.4 (18)	1073.1 (15)	1095.9 (14)	C_2-H bending; asymmetric H-C_6-C_7-H in-plane deformation
25	1157.1 (5)	1189.0 (6)	n.a.	1184.6 (5)	asymmetric H-C_6-C_7-H in-plane deformation, C_2-H bending
26	1256.4	1281.9 (3)	n.a.	1271.7 (1)	$C_{2,4}$-H bending
29	1378.0 (10)	1399.6 (17)	1378.9 (25)	1402.0 (14)	H-C_6-C_7-H in-plane deformation
32	1567.2 (10)	1622.2 (15)	1541.2 (35)	1595.3 (35)	C_6=C_7 stretching; C_5=C_8 stretching
33	1612.9 (15)	1671.2 (40)	1599.6 (25)	1650.0 (19)	C_5=C_8 stretching; C_6=C_7 stretching

34	1753.6 (20)	1768.7 (11)	n.a.	1765.0 (17)	C_1=C_4 stretching
36	n.a.	3096.5 (81)	2211.1 (15)	2247.1 (40)	symmetric C_3-H_2 stretching
41	n.a.	3180.1 (40)	2313.7 (25)	2369.8 (29)	asymmetric C_3-H_2 stretching
42	n.a.	3220.5 (31)	2330.7 (25)	2399.4 (19)	asymmetric C_8-H_2 stretching

[a]B3LYP/6-311G(d,p).

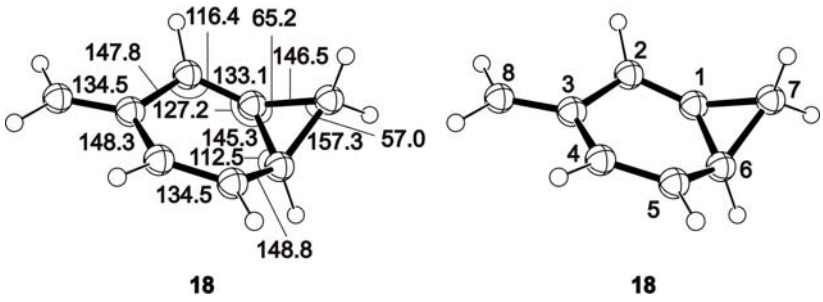

Figure 26. B3LYP optimized geometry of hydrocarbon **18**. Bond lengths are given in pm, and bond angles in degree. Numbering used in the table to describe the vibrations is also given.

The strongly distorted bridgehead double bond C(1)=C(2) is part of a methylenecyclopropane unit. Consequently, the C(1)=C(2) stretching vibration is found at very high frequency (1753.6 cm^{-1}). Since no deuterium atoms are directly attached to this double bond in d_4-**18** the isotopic shift is small.

The third isomer formed during the photolysis of **1** is the tricyclic hydrocarbon **20**. Due to its higher symmetry, the IR spectrum of **20** is simpler than that of **19** and **18** (Figure 27, Figure 28, Table 8). The strongest absorptions are the antisymmetrical and symmetrical combinations of the two *exo*-methylene C=C stretching vibrations at 1678.6 (16.0 cm^{-1} isotopic shift) and 1683.8 cm^{-1} (14.6 cm^{-1} isotopic shift), respectively.

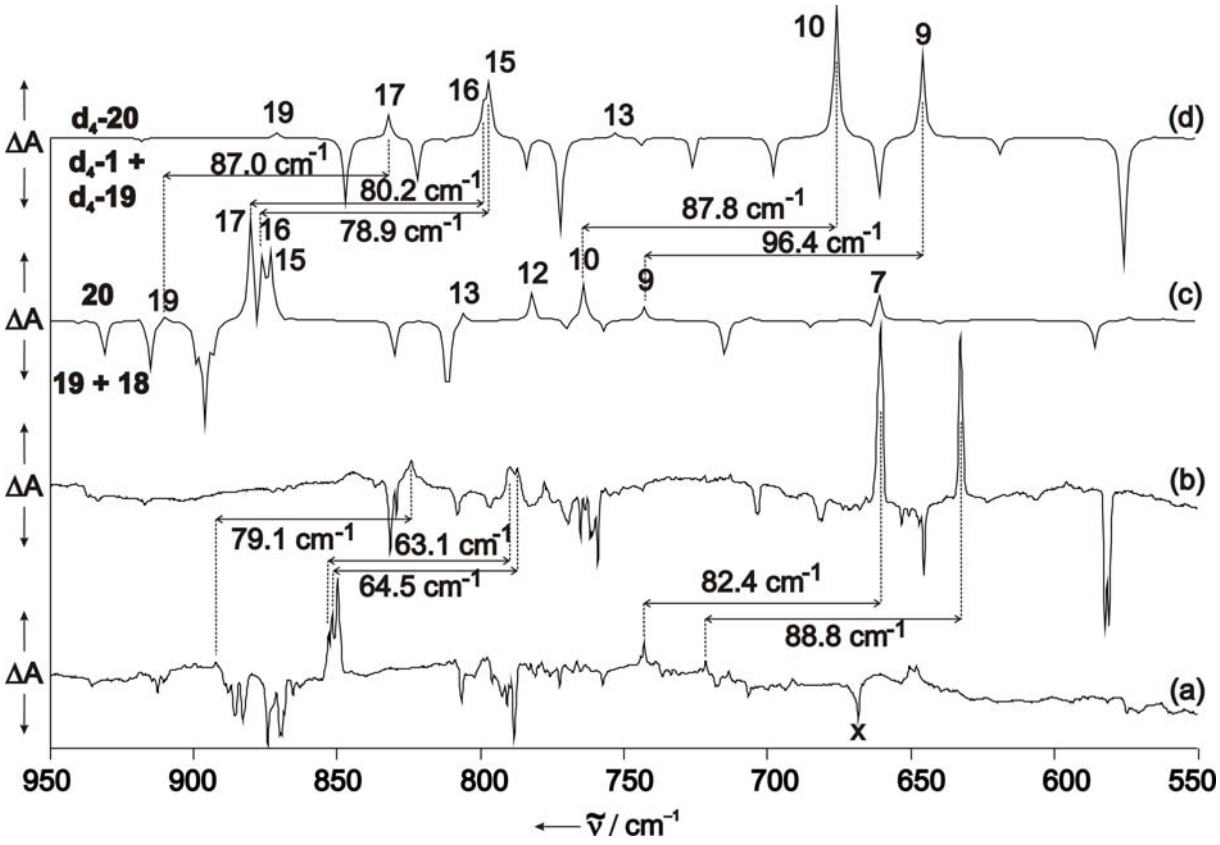

Figure 27. Difference IR spectra showing the photochemical interconversion of **1**, **19**, **18**, and **20** in argon at 10 K. The experimental difference spectra are compared to simulated difference spectra based on calculations at the (U)B3LYP/6-311G(d,p) level of theory. (a) λ > 320 nm irradiation converts a mixture of **19** and **18** (disappearing, peaks pointing downward) into **20** (appearing, peaks pointing upward). (b) λ > 260 nm irrradiation converts a mixture of d_4-**1** and d_4-**19** (disappearing, peaks pointing downward) into d_4-**20** (appearing, peaks pointing upward). (c) Simulated difference spectrum **20** – (**19** + **18**) corresponding to (a). (d) Simulated difference spectrum d_4-**20** – (d_4-**1** + d_4-**19**) corresponding to (b). The isotopic shifts of the *exo*-methylene groups of **20** are shown in the spectra.

The antisymmetrical and symmetrical combinations of the wagging vibrations of the *exo*-methylene groups are found at 851.7 (64.5 cm^{-1} isotopic shift) and 852.9 cm^{-1} (63.1 cm^{-1} isotopic shift), respectively.

Table 8. IR spectroscopic data of **20** and d_4-**20**.

Mode. #	Sym	Argon [b]	B3LYP [a]	Argon [b] **d_4**	B3LYP [a] **d_4**	Assignment
9	A"	721.6 (5)	743.0 (7)	632.8 (40)	646.6 (33)	C_5-H_2 twisting
10	A'	742.9	764.2 (20)	660.5 (60)	676.4 (53)	C_5-C_1-C_2 out-of-plane

		(30)				deformation ;C_2-H bending
12	A"	763.8 (25)	782.4 (15)	n.a.	771.8 (4)	$C_{3,4}$-H bending
13	A'	784.5 (1)	806.6 (7)	n.a.	753.5 (3)	C_4-H bending
16	A"	851.7 (60)	876.4 (31)	787.2 (15)	797.5 (20)	C_5-H_2 wagging
17	A'	852.9 (40)	880.1 (55)	789.8 (15)	799.9 (12)	C_5-H_2 wagging
18	A"	899.7 (1)	910.8 (5)	867.1 (1)	871.0 (3)	C_5-H_2 rocking; C_2-H bending
19	A'	903.2 (1)	919.5 (3)	824.1 (10)	832.5 (11)	C_5-H_2 rocking;
20	A"	n.a.	994.7 (4)	940.9 (10)	957.5 (9)	$C_{3,4}$-H deformation; C_5-H_2 twisting
24	A'	1092.2 (1)	1117.8 (7)	1069.0 (1)	1085.2 (2)	$C_{2,3}$-H bending
28	A'	1237.4 (1)	1259.3 (7)	1211.7 (10)	1229.7 (8)	$C_{3,4}$-H bending, C_5-H_2 rocking
33	A"	1678.6 (60)	1747.1 (99)	1662.6 (60)	1709.7 (100)	C_1=C_5 stretching
34	A'	1683.8 (100)	1758.7 (69)	1669.2 (100)	1719.9 (71)	C_1=C_5 stretching

[a] B3LYP/6-311G(d,p). [b] 10 K.

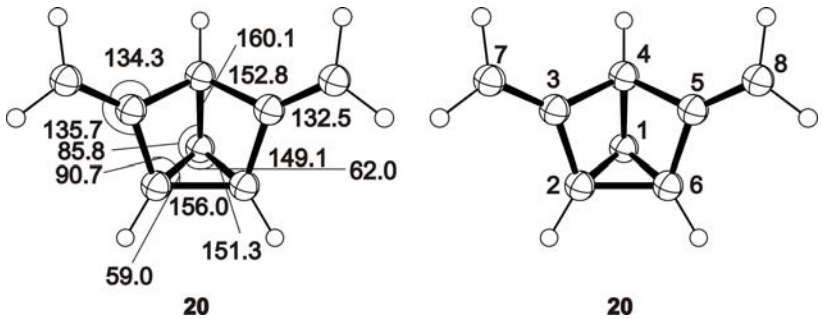

Figure 28. B3LYP optimized geometry of hydrocarbon **20**. Bond lengths are given in pm, and bond angles in degree. Numbering used in the table to describe the vibrations is also given.

As with **19** and **18** the IR spectrum of **20** is very nicely reproduced by DFT calculations. There is no evidence for the formation of further isomeric hydrocarbons such as **21** (Figure 23, Figure 25, Figure 27 , Scheme 51).

5.7 The C_8H_8-hypersurface

All three isomers **19**, **18**, and **20** contain a fused three-membered ring resulting in high strain energy which pushes their energy well above that of T-**1** and even S-**1**. The most stable of the three isomers is **19** which at the B3LYP/6-311G(d,p) level of theory is calculated to be 19.2 kcal/mol above T-**1** and 13 kcal/mol above S-**1** (Table 9).

Table 9. Calculated energies of the C_8H_8-isomers **1**, **18**, **19**, **20**, and **21**.

Molecule	*(E + ZPC)* hartrees	E_{rel}, kcal/mol
T-**2** [a]	-309.534386	0
S-**2** [a]	-309.524472	6.22
19 [b]	-309.503791	19.20
18 [b]	-309.493361	25.74
20 [b]	-309.456873	48.64
21 [b]	-309.491230	27.08

[a] UB3LYP/6-311G(d,p). [b] B3LYP/6-311G(d,p).

Bond length and angles for the optimized geometry of **21** are shown in Figure 29 below.

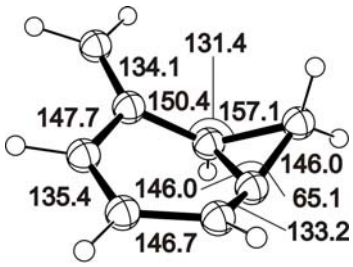

21

Figure 29. B3LYP optimized geometries of hydrocarbon **21**. Bond lengths are given in pm, and bond angles in degree.

The hydrocarbon **19** with an *anti*-Bredt bridgehead double bond is with 25.7 kcal/mol relative to T-**1** even less stable (Table 9, Scheme 53). In **20** the three membered ring is fused to two four-membered rings resulting in a relative energy of 48.6 kcal/mol. Thus, even from S-**1** the ring-closure to give **19**, **18**, or **20** is highly endothermic and thus

requires photochemical excitation in addition to populate the singlet state from the triplet ground state.

The hydrocarbons **19**, **18**, and **20** show the same CH- and CC- connectivity as diradical **1**. Formally, the rearrangement of **1** to **19** requires the formation of one new bond between C(2) and C(6) in diradical **1**, and that of **1** into **18** requires the formation of one new bond between C(2) and C(7). In **1** these carbon atoms bear high spin density as can be deduced from the corresponding resonance structures (Scheme 49, Scheme 52).

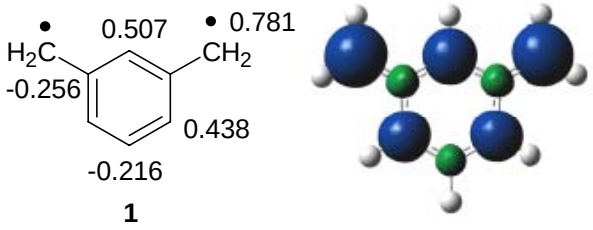

1

Scheme 52. Spin density distribution of triplet *m*-xylylene **1**. Blue colour indicates an excess of α-spin at the atom (positive spin density), and green colour shows an excess of β–spin-density at the atom (negative spin density).

The formation of **21** requires the formation of two new bonds: one between C(2) and C(5) and the other one between C(4) and C(6). A diradical such as **119** could be an intermediate; however, there is no evidence for this in our experiments.

In order to get an idea of the barriers connecting the different C_8H_8-isomers, the transition states on the singlet hypersurface connecting **1** with **19**, **18**, **20**, and **21** were calculated on the B3LYP level of theory using Poples 6-311G(d,p) basis set.

The C_8H_8-isomers **18** and **21** are of comparable energy with **18** 1.34 kcal/mol lower in energy than **21**. The energy difference calculated for the transition states from singlet **1** to **18** and **21**, respectively, are as well very near to each other, differing by only 1.78 kcal/mol (36.26 kcal/mol from T-**1** to **18**, 38.04 kcal/mol from T-**1** to **21**). The transition state connecting T-**1** with **19** is calculated to be 37.96 kcal/mol above T-**1**. Interestingly, all three transition states from T-**1** to isomeric products **19**, **18**, and **21** are within 2 kcal/mol, thus other factors than simple energetics determine the photochemistry (Table 10). It seems rather unlikely that the reaction converting T-**1** to the photoisomers are hot ground state reactions (Scheme 53).

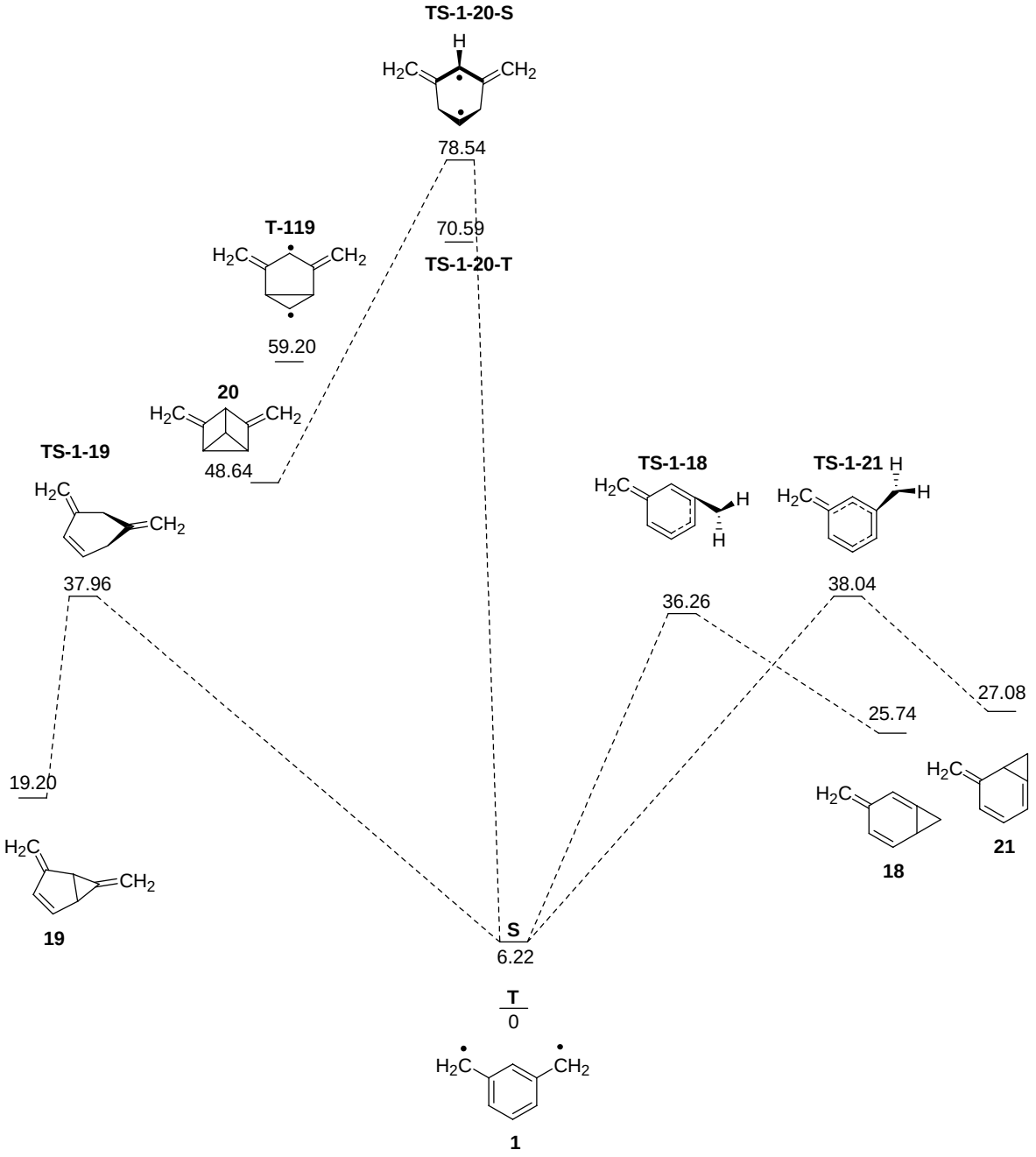

Scheme 53. Calculated energy minima and transition states at the UB3LYP/6-311G** level of theory for the conversion of *m*-xylylene **1** into its photoisomers. Values are given in kcal/mol.

The transition state for interconversion of *m*-xylylene **1** to **20** is 78.54 kcal/mol higher than the triplet ground state and therefore more than two times higher than all other transition states.

Table 10. Calculated energies of the C_8H_8-isomers **1**, **19**,**18**, **20**, and **21**.

Molecule [c]	*E + ZPC* hartrees	E_{rel}, kcal/mol	IMAG [d]
T-**1** [a]	-309.534386	0	-
S-**1** [a]	-309.524472	6.22	-
19 [b]	-309.503791	19.20	-
18 [b]	-309.493361	25.74	-
20 [b]	-309.456873	48.64	-
21 [b]	-309.491230	27.08	-
T-**119** [a]	-309.440050	59.20	-
S-**119** [b]	-309.396657	86.42	-
BS-**119** [a]	-309.441222	58.46	(1.0349)
TS-**1**-**21** [b]	-309.473762	38.04	-225.9
TS-**1**-**18** [b]	-309.476594	36.26	-255.5
TS-**1**-**19** [b]	-309.473898	37.96	-144.4
TS-**1**-**20**-S [b]	-309.409224	78.54	-491.04
TS-**1**-**20**-T [a]	-309.421886	70.59	-901.5
BS-**1**-**21** [a]	-309.475391	37.02	-784.8 (0.1464)
BS-**1**-**18** [a]	-309.477943	35.42	-766.0 (0.1368)
BS-**1**-**19** [a]	-309.476304	36.45	-657.5 (0.1837)
BS-**1**-**20** [a]	-309.409224	78.54	-491.0 (0.0000)

[a] UB3LYP/6-311G(d,p). [b] B3LYP/6-311G(d,p). [c] TS = Transition state, BS = Broken Symmetry, S = Singlet, T = Triplet [d] IMAG = Imaginary Frequency (<S**2> =)

6. Trapping of *m*-xylylene with oxygen

6.1 Introduction

The bulk of organic chemistry deals with molecules which have a closed shell electronic structure with all of their electrons paired in molecular orbitals and a wide energy gap between the HOMO and LUMO. Radicals and di- as well as polyradicals instead belong to the subclass of organic molecules which usually have an open-shell electronic structure. The intrinsic instability of this subclass of molecules makes most of them highly reactive and short-lived, and thus difficult to study by conventional spectroscopic means. The high reactivity of open-shell molecules towards other open-shell molecules most often gives a closed-shell molecule. Characterization of the stable reaction product of two radical moieties was used quite extensively to prove the intermediary of reactive molecules (Scheme 54).

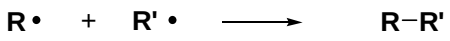

Scheme 54. Reaction of two radicals to form a stable closed-shell product.

A similar approach is often used with so called spin-traps, in which the radical reacts with a closed-shell precursor, forming a persistent radical adduct. For example, the detection of nitroxide radicals by EPR spectroscopy with determination of hfs constants is frequently used to study intermediate radicals. 5,5-dimethyl-1-pyrroline N-oxide (DMPO) **120** and some derivatives thereof are probably the most often used spin-traps (Scheme 55). [82, 83]

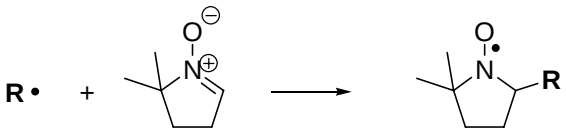

120 **121**

Scheme 55. DMPO **120** is frequently used as spin trap for reactive radicals **R**˙.

The reaction of oxygen in its triplet ground state with radicals is also a well established reaction and was studied extensively due to its importance in combustion processes, atmospheric chemistry and solution oxidation reactions. In a first step, the oxygen molecule most often adds to the radical center and forms a peroxy radical. There

are a lot of different peroxy radicals which were identified and characterized through addition of oxygen to the free radical. The simplest member of a peroxy radical is the hydroperoxy radical **122**[84-87] while methylperoxy radical **123**[88-90] and ethylperoxy radical **124**[91, 92] are the simplest carbon containing radicals (Scheme 56).

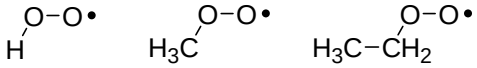

122 **123** **124**

Scheme 56. Some relatively simple and well studied peroxy radicals.

Different electronic structures are found for the vinylperoxy radical **125**[93-95] and the phenyl peroxy radical **126**[42, 96, 97] which are formed from reaction of vinyl radical **127** and phenyl radical **73** with oxygen, respectively (Scheme 57). Since the reacting radicals are sp^2 radicals - having their unpaired electron in the sp^2 orbital perpendicular to the π system - the π system is slightly affected by additon of oxygen and both oxygen atoms lie in the plane of the molecule. In principle, two different conformers **125a** and **125s** are possible minima on the PES of **125** while only the *trans* form **125a** is found experimentally, in good accordance with a calculated barrier of 5.8 kcal/mol for interconversion of **125a** to **125s**. The *trans* form is predicted to lie 1.2 kcal/mol lower in energy than the *syn* form (UB3LYP/6-311++G(d,p)).[95]

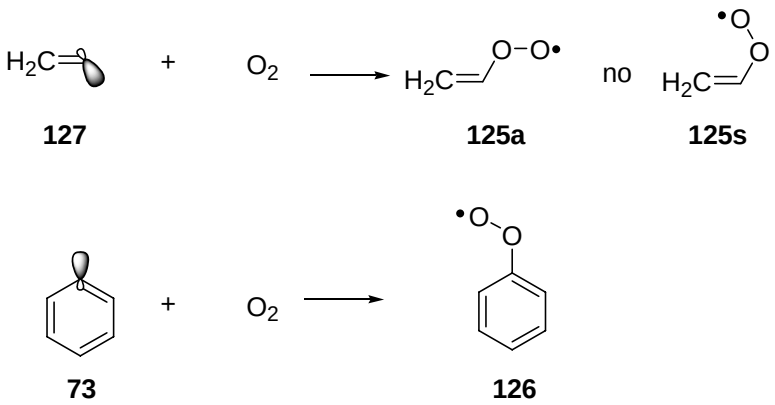

Scheme 57. Vinylperoxy **125** and phenyl peroxy radical **126** have its π system perpendicular to the peroxy group.

Only theoretical data is available for the ethynylperoxy radical **128** in which the peroxy group is found to be in the same plane as one π system from the triple bond.[98-100] MP2 calculations[100] predict a linear HCCO structure while MCSCF calculations[99] find a slightly bent structure to be the minimum (Scheme 58).

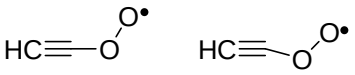

128

Scheme 58. Possible minimum structures predicted by theory for ethynylperoxy radical **128**.

Another kind of peroxy radicals are formed from conjugated radicals like the allyl radical **54** or the benzyl radical **55**. In both cases, the unpaired electron is delocalized throughout the π system. In general, different regiochemical attack is possible for the oxygen molecule in these cases. Due to its symmetry there is only one possible product in the case of the allyl radical **54** - allylperoxy radical **129** -, while the benzyl radical **55** could in principle react on different spin sites, resulting in benzyl peroxy radical **130** or one of its constitutional isomers (Scheme 59).

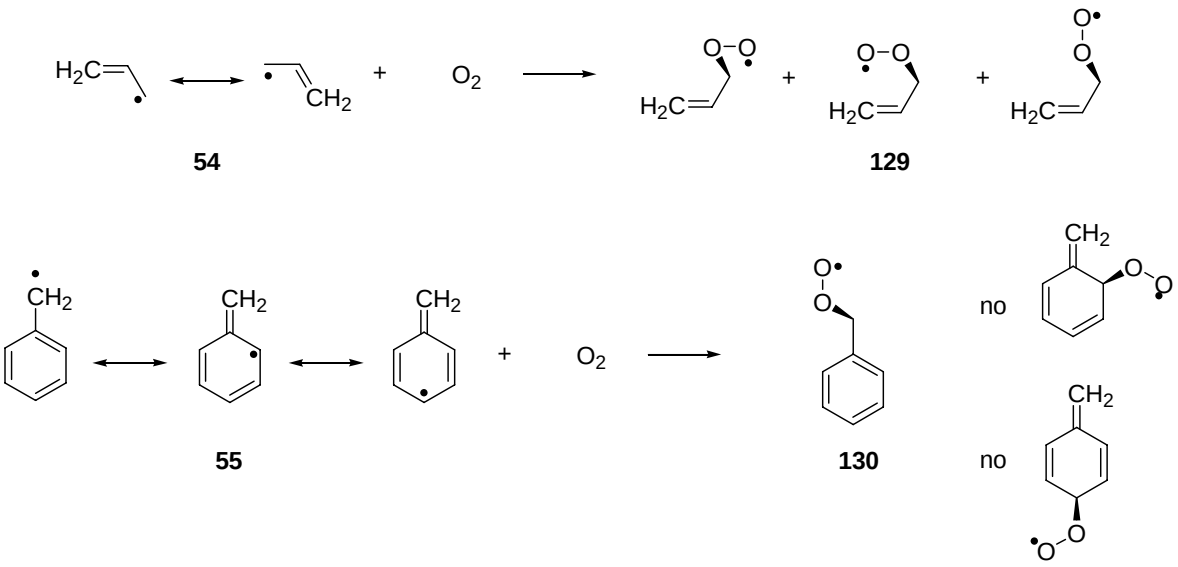

54 **129**

55 **130**

Scheme 59. The conjugated nature of the stabilized radicals can lead to different isomers like in the case of benzyl peroxy radical **130**. Allyl peroxy radical **129** can be formed in different conformers.

It is known that the autoxidation of organic unsaturated compounds gives allylperoxy radicals which were shown to isomerize by a [2,3] rearrangement (Scheme 60).[101, 102]

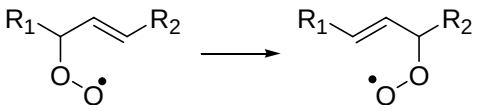

Scheme 60. [2,3] rearrangement of allylperoxy radicals.

Different allylperoxy radical rotational conformers were obtained theoretically for **129**, with the energy difference being only a few tenth of a kcal/mol thus showing that the PES is probably quite flat (Scheme 59).[103, 104] Baskir et al. isolated the allylperoxy radical **129** in an argon matrix at 12 K and studied its photochemistry.[105]

The benzyl peroxy radical **130** was characterized experimentally by its UV/Vis spectrum in an LFP study as well as by its IR spectrum in a recent matrix isolation study.[106, 107] In this study only one rotational isomer and no other regioisomers of **130** were found (Scheme 59).

This is in good accord with a computational study by Chepelev at al. in which it was shown that the carbon atom carrying the highest unpaired spin-density is usually the thermodynamically preferred site of addition of molecular oxygen.[108] Furthermore, it was shown in different experimental and theoretical studies that carbon centered radicals show a diminished reactivity towards molecular oxygen, if they have favourable

i) benzylic resonance stabilization,

ii) unpaired spin delocalization onto oxygen or other heteroatoms,

iii) stereoelectronic effects,

iv) electron withdrawing effects,

v) steric effects.

The cooperative interaction of several of these effects can lead to quite persistent radicals which do not add oxygen at all.[108-110]

The addition of oxygen to diradicals is much less studied than the addition of molecular oxygen to radicals. In general there are three different possibilities for the diradical: it can react with one equivalent of oxygen and form a peroxy diradical, it can react with one equivalent of oxygen and form a ring system (thereby yielding a peroxide compound), or it can react with two equivalents of oxygen to form a highly reactive diperoxy radical. Rajca et al. studied solutions of different Schlenk`s hydrocarbon derivatives such as **98** which were treated with molecular oxygen (Scheme 61).[111]

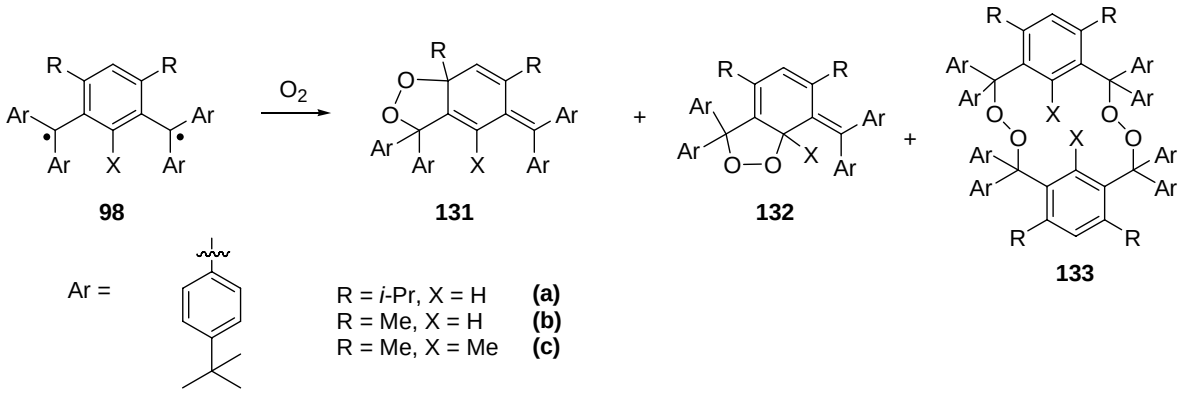

Scheme 61. Oxygen trapping products of Schlenk`s hydrocarbon derivatives **98.**[111]

The main products obtained in this study were cylic peroxides **131** and **132**. Evidence for small amounts of diperoxide dimer **133** have also been obtained. The high reactivity of possible peroxy radical intermediates allows their detection only under special circumstances, as are given under matrix isolation or time-resolved spectroscopy.

It is known that the spin of a molecule can play a crucial role in its reaction rate with other molecules. If two triplet molecules collide with one another, it is assumed that they form a collision complex whose spin state is governed by a spin statistical factor. Only 1/9 of the collision complexes will be in the singlet state, whereas 3/9 will be in the triplet state and 5/9 in the quintet state – if it is assumed that intersystem crossing (ISC) of the collisional complex among the spin states is much slower than any spin allowed process of the complex (Scheme 62).[112]

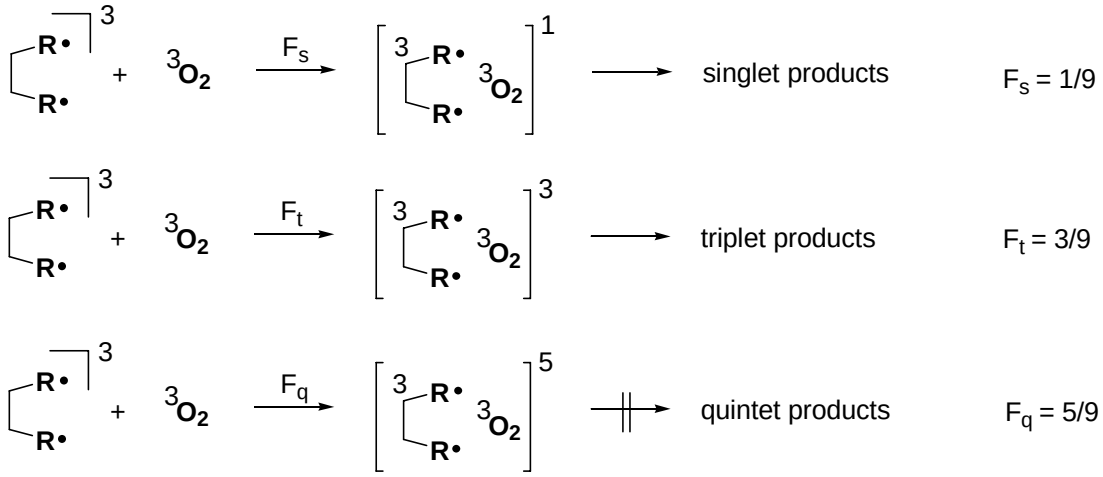

Scheme 62. Spin statistical factors determine the spin state of the collision complex.

The quintet collisional complex is expected to give no reaction but form back the starting molecules. However, the rate of reaction of the molecules will be lower than the diffusional limit due to the spin statistical factors.

Abe et al. studied the thermal conversion of triplet diradical **134** produced photochemically from diazene **135** into the peroxide **136** through reaction with oxygen (Scheme 63).[113] In this study, it was found that exclusively the fused peroxide **136** was formed, while no *endo* peroxide **137** could be detected.

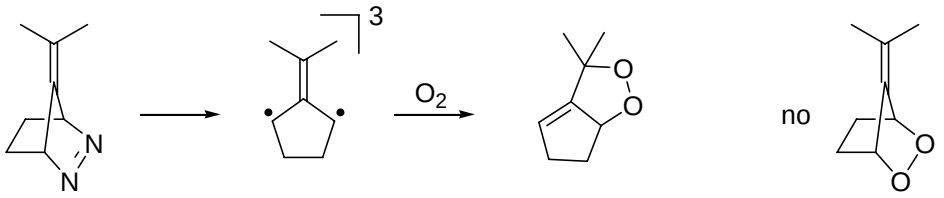

135 **134** **136** **137**

Scheme 63. Fused peroxide **136** is thermally formed from triplet diradical **134** at 38 K in an Ar matrix through reaction with oxygen.[113]

The thermal conversion of **134** into **136** in a 0.5 % oxygen doped argon matrix at 40 K could not be detected directly, and was only detected after deposition of excess oxygen during annealing to 38 K.

There is no experimental study in which signals from a peroxy diradical were observed. Wirz et al. speculated that the hydroperoxide **138**, can be formed through an intermediate peroxy biradical **139**, if the collision complex formed from oxygen with 1,4-perinaphthadiyl **140** in its triplet ground is in the singlet state (Scheme 64).[114]

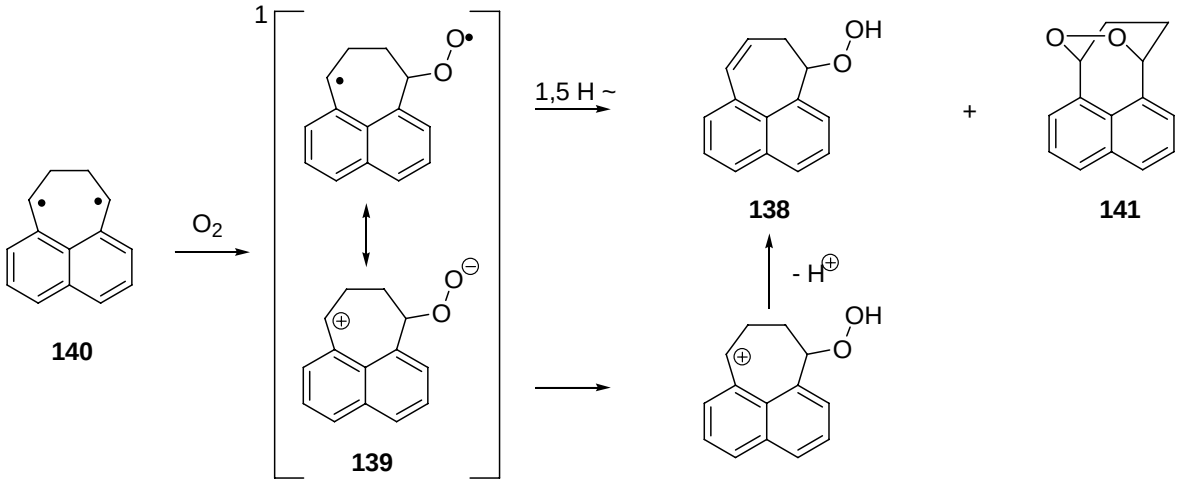

Scheme 64. Reaction of triplet 1,4-perinaphtadiyl **140** with oxygen yields hydroperoxide **138** which could be formed from singlet peroxy diradical **139**. Peroxide **141** is a further product.[114]

The rate constant for the reaction of oxygen with diradical **140** was found to be close to one ninth of the oxygen diffusion rate and is in good accord with expectations from spin statistics, if all triplet and quintet encounter complexes are unreactive.

The high quenching rate of 1,4-cycloalkadiyls[115] with oxygen was explained by the assumption that the triplet encounter complex might irreversibly lead to peroxy biradicals.[114]

Most studies on peroxy diradicals are evolved from studies on the Diels-Alder reaction of singlet oxygen with dienes. Bobrowski et al. found that the singlet oxygen addition to butadiene **142** preferentially occurs through a singlet peroxy diradical intermediate **143** with a barrier of 7.4 kcal/mol (MCQDPT2/6-31G(d)//CASSCF(10/8)/6-31G(d)) to ring-closure to *endo* peroxide **144** (Scheme 65).[116]

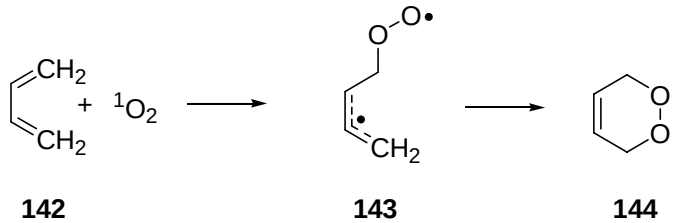

Scheme 65. Diels–Alder reaction of singlet oxygen with butadiene **142** is predicted to be stepwise and to form peroxy diradical **143** in an inital step.

A related study by Maranzana et al. also found the diradical pathway to be the lowest energy pathway by calculations at the CASPT2/6-31G(d)//CASSCF/6-31G(d) or

UB3LYP/6-31G(d) and UB3LYP/6-311+G(2d,2p)/UB3LYP/6-31G(d) level of theory.[117] The barrier to ring-closure to form dioxetane **145** is predicted to be 11 - 12 kcal/mol (Scheme 66).

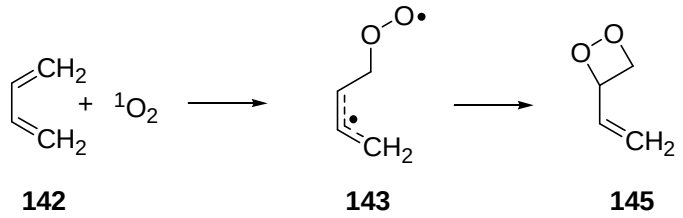

142 **143** **145**

Scheme 66. Ring-closure of singlet peroxy diradical **143** to dioxetane **145**.

In a comparative study Leach et al. concluded that the Diels-Alder reaction between singlet oxygen and simple open chain or cyclic dienes is calculated to proceed *via a stepwise path involving a polarised diradical intermediate – the extreme case of an asynchronous mechanism. The magnitude of the second barrier [to ring-closure] is still in doubt, and is most likely negligible in some cases. The reaction with aromatic dienes are predicted to have higher barriers and to proceed through concerted mechanisms.*[118]

The same authors also found that the ene reaction of nitroso compounds are stepwise reactions that proceed through polarised diradical intermediates.[118, 119] It is remarkable, that the UB3LYP method correctly predicts the mechanism of these reactions which was verified by higher-level CCSD(T) and CASPT2 single-point calculations.[119]

6.2 IR characterization of the trapping products

Usage of an oxygen doped argon matrix to trap the FVP products of 1,3-*bis*-(iodomethyl)benzene **17** gives an IR spectrum remarkably different from the one obtained in pure argon. Since it was found that 1,3-*bis*-(iodomethyl)benzene **17** is a quite efficient precursor for the production of *m*-xylylene **1** in its triplet ground state, this process is indispensable paired with the production of iodine atoms and/or molecular iodine. It is known that halogen atoms can add oxygen and form superoxide molecules (Scheme 67). The smaller halogen superoxide molecules are known and characterized by IR spectroscopy and recently Maier et al. described a pyrolytic synthesis of iodine superoxide IOO **146**. It was found to be impossible to obtain an IR spectrum of this species, while upon irradiation with 254 nm the superoxide rearranges to iodine dioxide OIO **147**. The authors assume that the interconversion of these species takes place through iodine

monooxide IO **148** as intermediate, as formation of ozone **149** was observed in this study (Scheme 67).

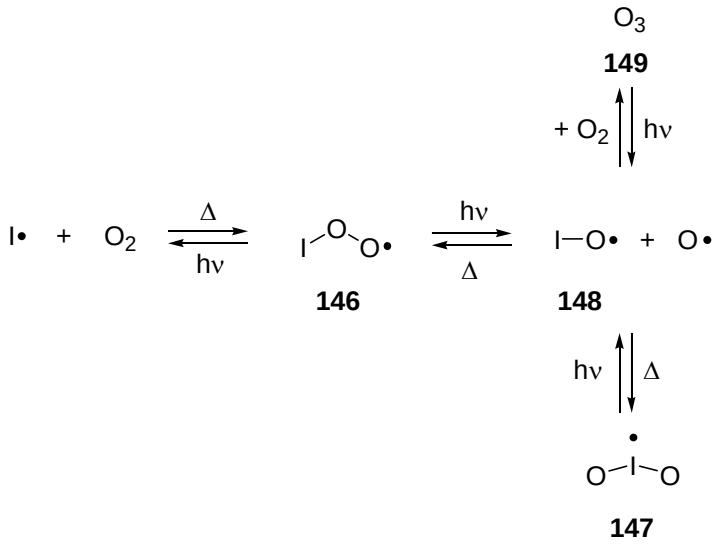

Scheme 67. Proposed mechanistic Scheme by Maier et al. for interconversion of iodine superoxide IOO **146**, iodine dioxide OIO **147**, iodine monoxide IO **148**, and ozone **149** in an argon matrix.

Upon visible light photolysis with λ = 680 – 475 nm of an oxygen doped argon matrix containing the FVP (450°C) products of 1,3-*bis*-(iodomethyl)benzene **17**, some signals are disappearing which do not belong to any of the *m*-xylylene isomers **1**, **18**, **19**, and **20**. Moreover, under these photolytic conditions, none of the *m*-xylylene isomers should show any photochemical conversion. However, peroxides are known to be photolabile species which are relatively easily accessible through reaction of radical centers with molecular triplet oxygen. Only relatively small amounts of the trapped species are formed, when the argon matrix is doped with 1 % oxygen, clearly obvious from Figure 30. Large amounts of triplet *m*-xylylene **1** are also formed in addition to signals assigned to the precursor 1,3-*bis*-(iodomethyl)benzene **17** at this oxygen concentration.

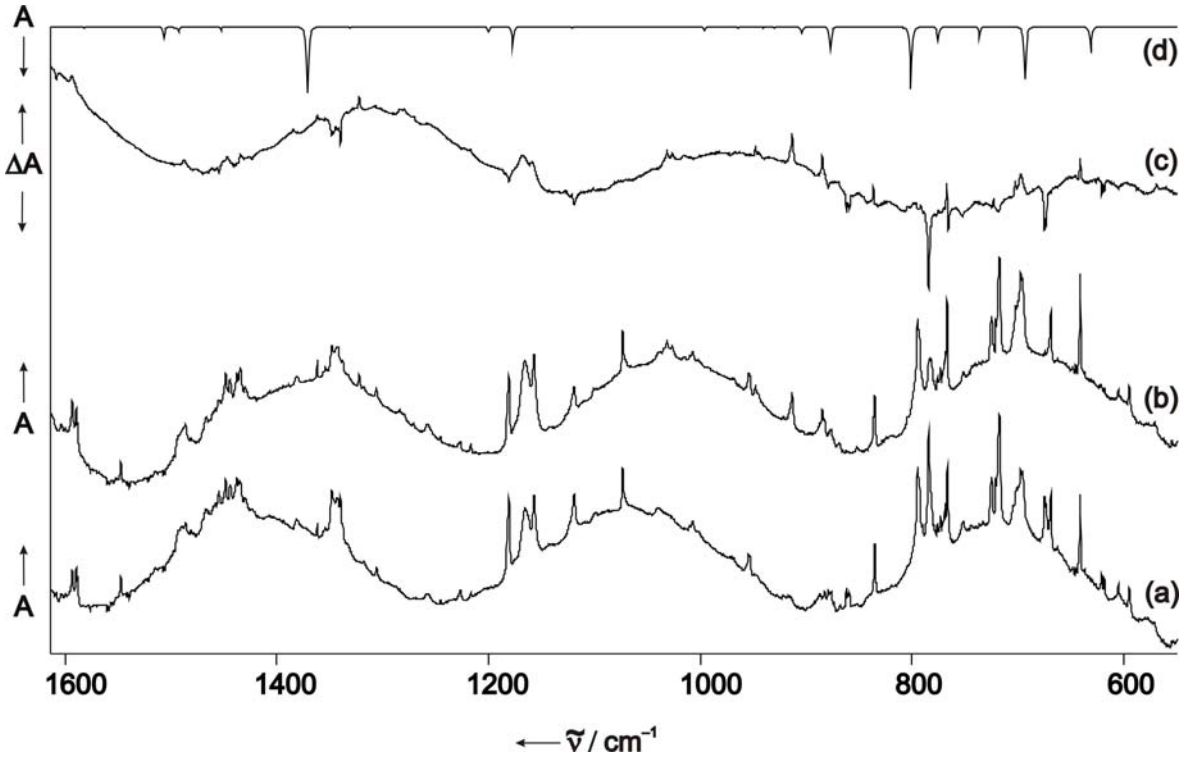

Figure 30. (a) IR spectrum of the trapping products after FVP of 1,3-*bis*-(iodomethyl)benzene **17** in an 1 % oxygen doped matrix. (b) IR spectrum of the same matrix after irradiation with λ = 680 – 475 nm. (c) Difference IR spectrum (b) – (a). Peaks pointing downwards are decreasing in intensity, peaks pointing upwards are increasing in intensity upon irradiation. (d) UB3LYP/cc-pVTZ calculated IR spectrum of triplet peroxy biradical **22** (scaled with 0.98).

Prolonged irradiation conditions (two hours) are necessary for full conversion of the proposed oxygen adduct. All solution phase studies as well as matrix isolation studies have observed closed-shell oxygen adducts, from reaction of triplet species with molecular oxygen. Nevertheless, several annelated peroxide structures were calculated at the B3LYP/cc-pVTZ level of theory and comparison with the observed photolabile species did not give any useful correlation. Instead, the oxygen adduct biradical **22** is found to be in good accordance with the observed matrix isolated species (Scheme 68).

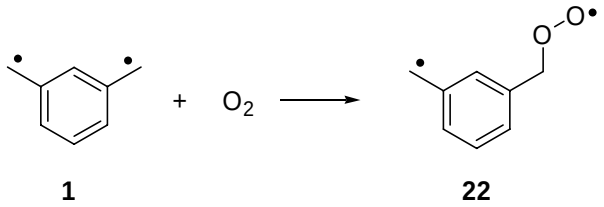

1 **22**

Scheme 68. Doping of an argon matrix with oxygen and trapping of the FVP products of 1,3-*bis*-(iodomethyl)benzene **17** leads to formation of peroxy biradical **22**.

The experimental difference spectrum after irradiation of a matrix containing the FVP products of 1,3-*bis*-(iodomethyl)benzene **17** in an oxygen doped matrix is shown in Figure 31. It can be seen from this spectrum, that one species which is formed during the irradiation is triplet *m*-xylylene **1** for which the assignment is shown by dotted lines.

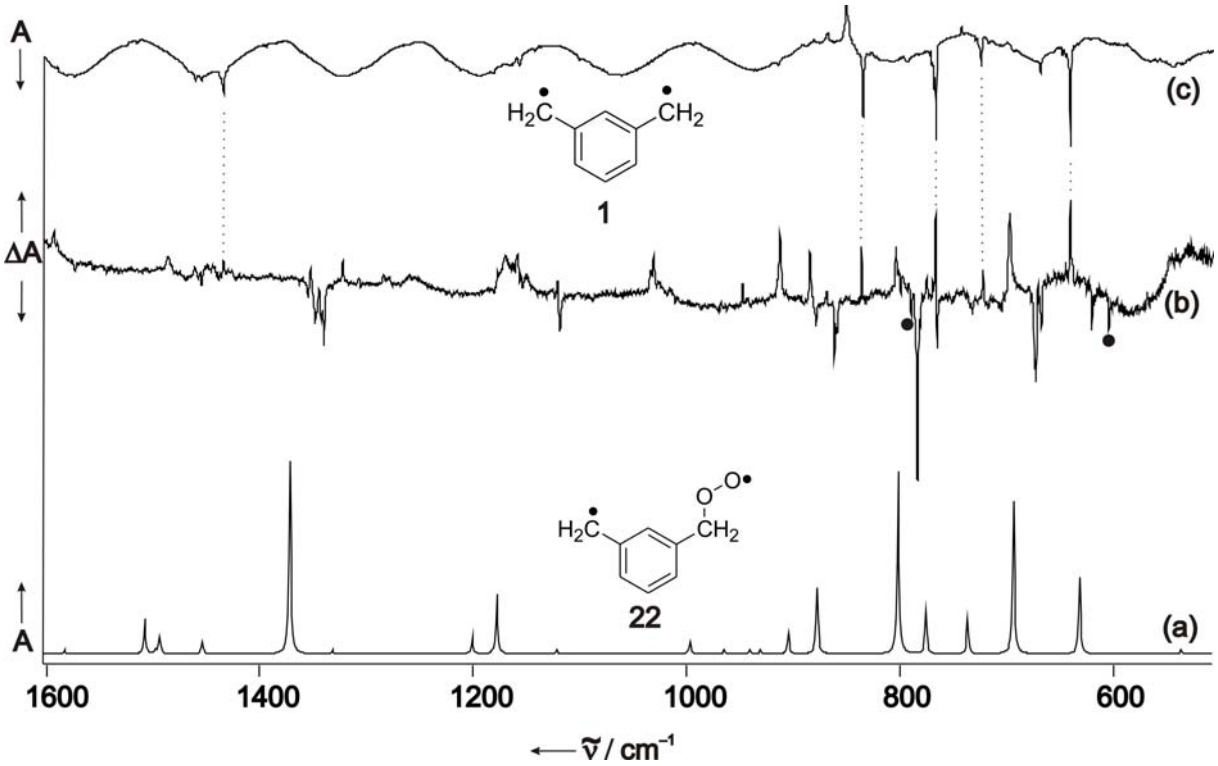

Figure 31. (a) UB3LYP calculated IR spectrum of triplet peroxy biradical **22**. (b) Difference spectrum obtained after photolysis of an oxygen doped argon matrix containing the FVP products of 1,3-*bis*-(iodomethyl)benzene **17**. Peaks showing downwards are decreasing in intensity, peaks showing upwards are increasing in intensity upon irradiation. (c) Difference spectrum showing the photochemistry of triplet *m*-xylylene **1**, which is decreasing in intensity. Dotted lines give the correlation between **1** and the observed photoproduct of peroxy biradical **22**. Points might denote the *bis*-oxygen adduct **140**.

Other isomers formed by reaction of *m*-xylylene **1** and one molecule of oxygen followed by ring-closure or from reaction of *m*-xylylene **1** and two molecules of oxygen did not result in a better agreement with the observed photolabile species, as is shown in Figure 32.

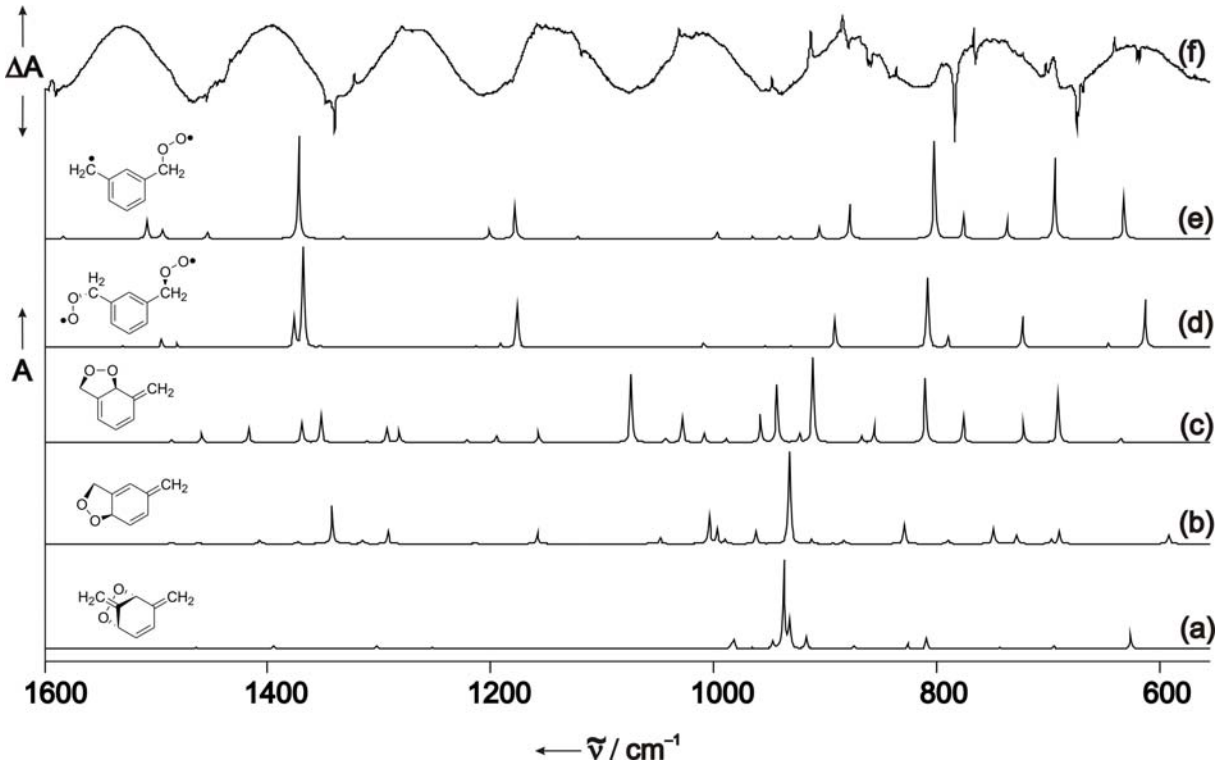

Figure 32. (a) – (e) UB3LYP/cc-pVTZ calculated IR spectra of different oxygen adducts of *m*-xylylene **1**. (f) Difference IR spectrum obtained after irradiation of an oxygen doped matrix containing the FVP products of 1,3-*bis*-(iodomethyl)benzene **17**. Peaks showing downwards are decreasing, peaks showing upwards are increasing in intensity upon photolysis.

Increasing the amount of oxygen in the matrix leads to relative little change in the IR spectrum. Some new signals are appearing. The photochemistry of these new bands is very similar to that assigned to peroxy biradical **22**. It might be assumed, that a *bis*oxygen adduct **150** could be formed by oxygen addition to both methylene units of *m*-xylylene **1**. A comparison of the new signals, which are visible at oxygen concentration of more than 1 % is given in Figure 33 together with the calculated IR spectrum of a *bis*oxygen adduct **150**. The number of signals as well as the intensity of these do not allow an unambiguous assignment of these signals to any calculated species.

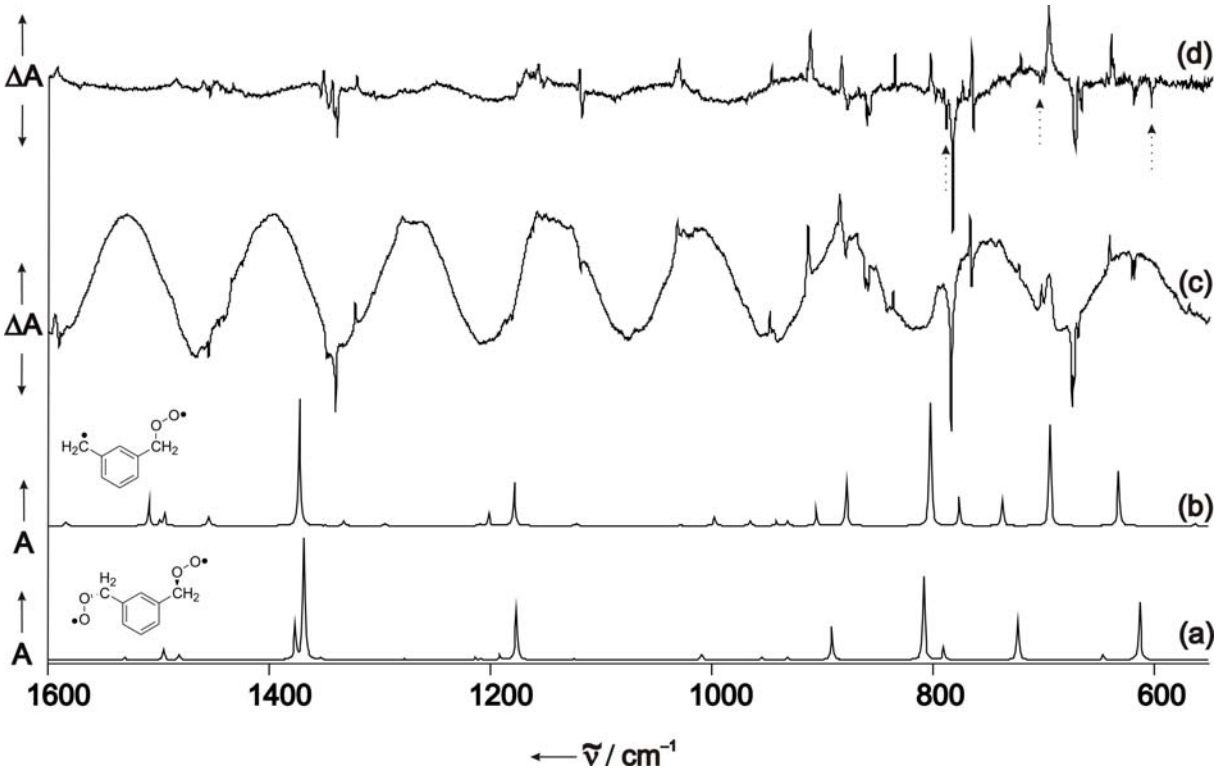

Figure 33. UB3LYP/cc-pVTZ calculated IR spectra of a *bis*oxygen adduct **150** of *m*-xylylene **1** (a) and the peroxy biradical **22** (b). (c) Difference IR spectrum obtained after irradiation of an oxygen doped (1 %) argon matrix containing the FVP products of 1,3-*bis*-(iodomethyl)benzene **17**. (d) Difference IR spectrum obtained after irradiation of an oxygen doped (2 %) argon matrix containing the FVP products of 1,3-*bis*-(iodomethyl)benzene **17**. Arrows indicate new signals at higher oxygen concentration which show similar photochemistry as peroxy biradical **22**.

In order to clarify if the peroxy biradical is indeed observed, the same experiments were performed with ^{18}O labelled oxygen. The IR spectrum of the resultant biradical should not be very different from the ^{16}O isomer. The observed difference spectrum is shown in the following Figure 34.

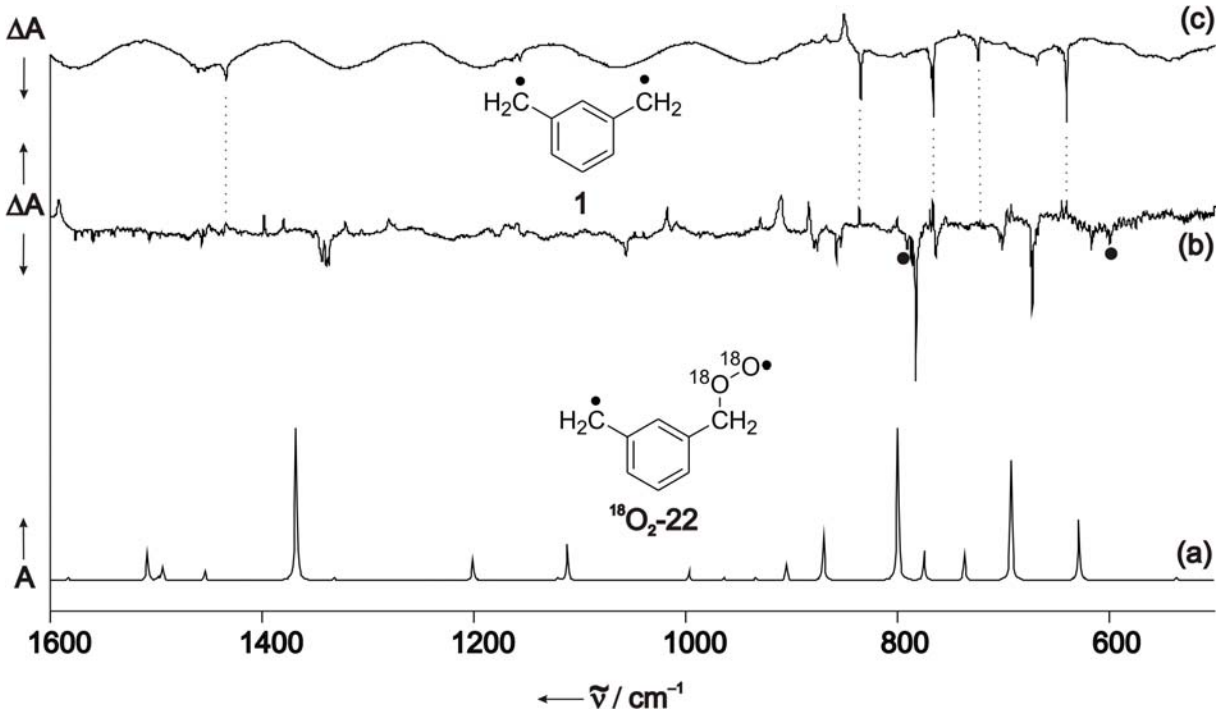

Figure 34. (a) UB3LYP calculated IR spectrum of labelled triplet peroxy biradical $^{18}O_2$-**22**. (b) Difference spectrum obtained after photolysis of an $^{18}O_2$ doped argon matrix containing the FVP products of 1,3-*bis*-(iodomethyl)benzene **17**. Peaks showing downwards are decreasing in intensity, peaks showing upwards are increasing in intensity upon irradiation. (c) Difference spectrum showing the photochemistry of triplet *m*-xylylene **1**, which is decreasing in intensity. Points denote a possible *bis*oxygen adduct **150**.

A comparison of all IR bands assigned to peroxy biradical **22** and the ^{18}O isotopic labelled peroxy biradical $^{18}O_2$-**22** are given in Figure 34 and Table 11.

Table 11. IR spectroscopic data of **22** and $^{18}O_2$-**22**.

Vib. #	Argon, 10 K **22**	B3LYP[a] **22**	Argon, 10 K $^{18}O_2$-**22**	B3LYP[a] $^{18}O_2$-**22**	Assignment
9	[b]	435.4 (15)	[b]	434.4 (14)	skeletal vib.
11	-	537.7 (4)	-	537.4 (4)	ring def.
13	618.1, 620.3 (20)	633.0 (43)	614.8, 617.3 (25)	629.7 (40)	ring def.
14	674.5 (70)	694.1 (80)	672.8, 674.2 (70)	693.8 (76)	$C_{2,4,6}$-H oop vib.
15	732.4 (5)	737.2 (20)	-	737.0 (18)	C_8-H_2 oop vib.

16	765.5 (20)	776.5 (23)	764.2 (20)	775.3 (21)	ring def.
17	784.0 (100)	802.5 (97)	782.9 (100)	800.9 (100)	$C_{2,4,5,6}$-H oop vib.
18	858.7, 859.9 sh, 861.7 (25)	878.9 (34)	853.6, 857.9 (20)	870.6 (29)	C-O stretching, C_2-H oop vib.
19	879.2 (15)	905.0 (13)	879.1 (15)	905.0 (12)	$C_{2,4,6}$-H oop vib.
20	-	931.4 (4)	-	929.2 (2)	complex rocking vib.
21	-	941.7 (4)	-	934.2 (3)	complex rocking vib.
22	-	965.4 (3)	-	964.1 (3)	complex rocking vib.
24	-	997.5 (7)	-	997.4 (7)	ring def.
26	-	1122.0 (2)	-	1122.0 (2)	$C_{4,6}$-H in plane bending
27	1118.4 (15)	1178.3 (34)	1056.3 (15)	1112.3 (25)	O-O stretching vib.
29	1180.8 (5)	1201.5 (10)	1180.5 (5)	1201.0 (13)	$C_{2,5}$-H in plane bending
30	-	1209.2 (2)	-	1208.0 (2)	C_7-H_2 twisting
31	-	1295.3 (2)	-	1295.3 (2)	ring def., C_8-H_2 scissoring
32	-	1332.1 (4)	-	1332.0 (4)	ring def.
34	1339.8, 1341.7 sh, 1343.7 sh, 1346.0, 1348.1 (65)	1372.1 (101)	1336.7, 1339.7, 1342.4, 1344.0 sh, 1345.7 (50)	1368.6 (99)	C_7-H_2 wagging
35	-	1454.9 (7)	-	1454.9 (7)	ring def.
36	-	1494.7 (10)	-	1494.6 (9)	C_7-H_2

					scissoring
37	-	1498.2 (4)	-	1498.2 (4)	C8-H2 scissoring
38	1454.8 (10)	1508.3 (19)	1454.2 (10)	1508.3 (18)	complex
39	-	1583.9 (3)	-	1583.9 (3)	C_4-C_5, C_6-C_1 stretching
41	2961.0 (10)	3066.2 (30)	2961.3 (10)	3066.2 (29)	sym. C_7-H_2 stretching
42	[c]	3120.9 (18)	[c]	3120.9 (17)	asym. C_7-H_2 stretching
43	[c]	3150.4 (10)	[c]	3150.4 (9)	sym. C_8-H_2 stretching
44	[c]	3164.9 (17)	[c]	3164.9 (16)	C_2-H stretching
45	[c]	3166.5 (10)	[c]	3166.5 (10)	$C_{4,5,6}$-H stretching
46	[c]	3177.2 (26)	[c]	3177.2 (25)	asym. $C_{4,6}$-H stretching
47	[c]	3190.3 (28)	[c]	3190.3 (27)	sym. $C_{4,5,6}$-H stretching
48	[c]	3246.1 (15)	[c]	3246.1 (14)	asym. C_8-H_2 stretching

[a] UB3LYP/cc-pVTZ. [b] Not observed due to low signal to noise ratio in this region. [c] Not observed due to broad signals in this region.

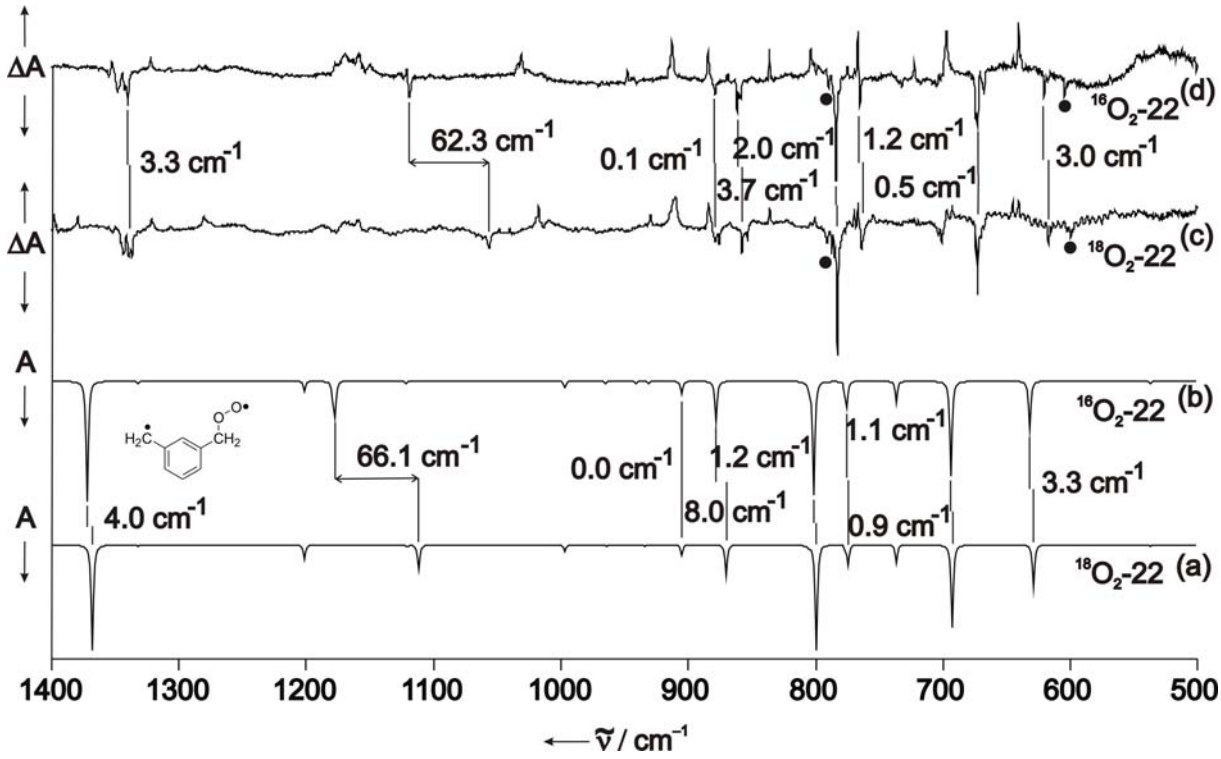

Figure 35. UB3LYP/cc-pVTZ calculated IR spectra of labelled peroxy biradical $^{18}O_2$-**22** (a) and **22** (b). (c) Difference spectrum obtained after photolysis of an $^{18}O_2$ doped argon matrix containing the FVP products of 1,3-*bis*-(iodomethyl)benzene **17**. (d) Difference spectrum obtained after photolysis of an oxygen doped argon matrix containing the FVP products of **17**. Peaks pointing downwards are decreasing in intensity, peaks pointing upwards are increasing upon irradiation.

As might be deduced from this comparison, larger changes are only expected and observed for vibrational modes, which are mainly or partly composed of oxygen stretching. An isotopic shift of 3.3 cm^{-1} is calculated for the wagging vibration of the CH_2 group connected to the oxygen center. This is found to be in good agreement with the observed shift of 3.1 cm^{-1}. A similar shift of 3.0 cm^{-1} was found for the skeletal vibration at 620.3 cm^{-1} in **22** (calc. 633.0 cm^{-1}), again in good accordance with a vibration at 617.3 cm^{-1} in $^{18}O_2$-**22** (calc. 629.7 cm^{-1}), thus the calculated isotopic shift amounts to 3.3 cm^{-1}. The transition energy of the C-O stretching vibration at 861.7 cm^{-1} is shifted by 3.8 cm^{-1} through ^{18}O labelling and therefore found at 857.9 cm^{-1} in $^{18}O_2$-**22**. An isotope effect of 8.3 cm^{-1} is predicted by the DFT calculations. The discrepancy in this special case might be due to the uncertainty in determination of the IR signal, because this vibration seems to be splitted due to matrix site effects, and therefore some vibrational excitations are found quite near to each other. A better agreement is found, if the lower energy transition is chosen for the comparison. The largest effect due to the oxygen labelling is found for the O-O stretching vibration at 1118.4 cm^{-1} for **22**, which for the higher isotope has a

corresponding signal at 1056.3 cm^{-1} (calc. 1178.3 cm^{-1} **22**; 1112.2 cm^{-1} $^{18}O_2$-**22**). The isotopic shift is found to be 62.1 cm^{-1}, nicely resembled by the UB3LYP/cc-pVTZ calculations which predict a shift of 66.1 cm^{-1}.

Further confirmation for peroxy biradical **22** can be obtained by deuteration of the exocyclic methylene units. FVP of 1,3-*bis*-(iodomethyl-d_2)-benzene **17**-d_4 and trapping of the products in an oxygen or ^{18}O labelled oxygen matrix yielded two similar IR spectra, which gave hints on the occurence of peroxy biradical **22**-d_4 and $^{18}O_2$-**22**-d_4. The comparison of IR bands is given below (Figure 36).

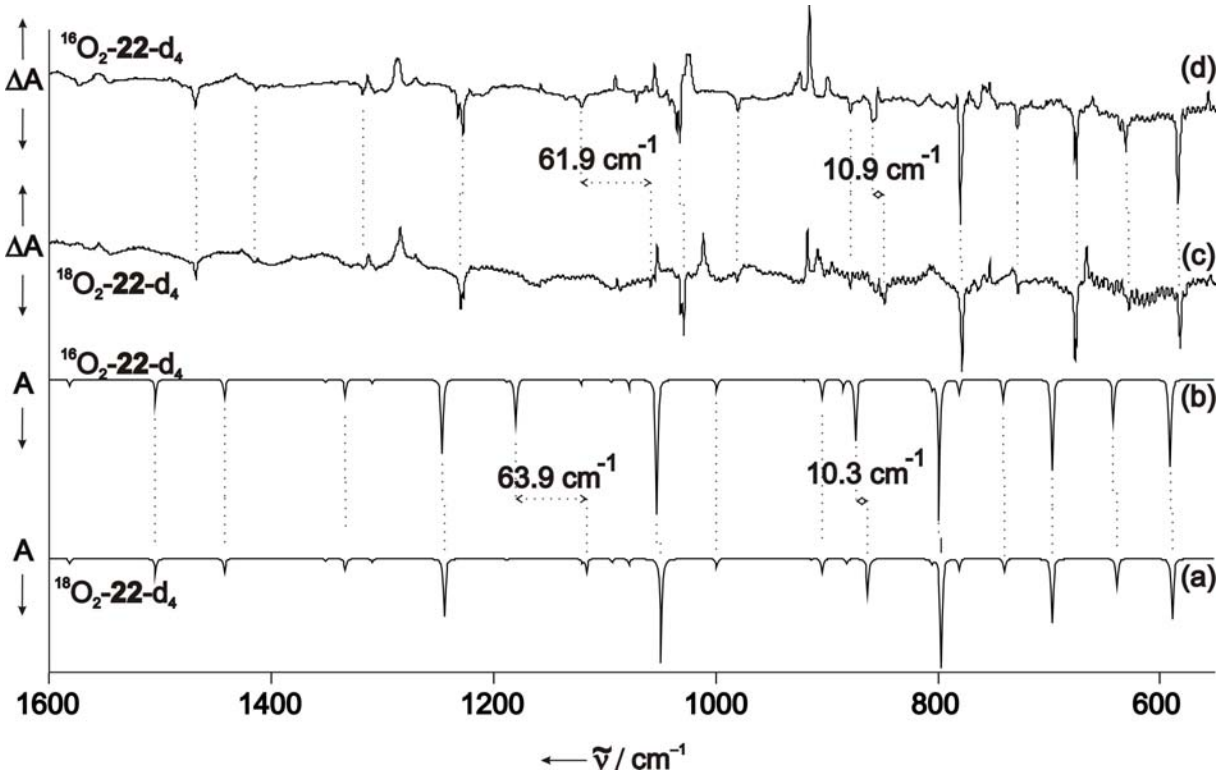

Figure 36. UB3LYP/cc-pVTZ calculated IR spectra of labelled peroxy biradical $^{18}O_2$-**22**-d_4 (a) and **22**-d_4 (b). (c) Difference spectrum obtained after photolysis of an $^{18}O_2$ doped argon matrix containing the FVP products of 1,3-*bis*-(iodomethyl-d_2)-benzene **17**-d_4. (d) Difference spectrum obtained after photolysis of an oxygen doped argon matrix containing the FVP products of 1,3-*bis*-(iodomethyl-d_2)-benzene **17**-d_4. Peaks pointing downwards are decreasing in intensity, peaks pointing upwards are increasing upon irradiation.

In analogy to *m*-xylylene **1**, the IR spectra of the deuterated peroxy biradical **22**-d_4 and $^{18}O_2$-**22**-d_4 are quite similar and most changes upon oxygen labelling are within 1 cm^{-1}. An exception is again found for the C-O stretching vibration at 859.2 cm^{-1} (calc. 874.3 cm^{-1} for **22**-d_4 and 864.0 cm^{-1} for $^{18}O_2$-**22**-d_4), which is shifted by 4.8 cm^{-1} to 854.4 cm^{-1} in $^{18}O_2$-**22**-d_4, thus half of the predicted shift of 10.3 cm^{-1}. The second remarkable change in the IR

spectra is found for the O-O stretching vibration. In **22**-d_4 this vibration is observed at 1120.3 cm^{-1}. However, the ^{18}O-^{18}O stretching vibration in $^{18}O_2$-**22**-d_4 is found at 1058.7 cm^{-1}, thus an isotope effect of 61.6 cm^{-1} on the wavenumber is experimentally observed. UB3LYP in combination with the cc-pVTZ basis set place the O-O stretching vibration of biradical **22**-d_4 at 1180.4 cm^{-1}, while the analogous vibration of ^{18}O labelled biradical is predicted to appear at 1116.5 cm^{-1}, so that the isotopic shift in this vibration amounts to 63.9 cm^{-1}. Again, the experimentally observed shift is nicely reproduced by the calculations. All vibrations and assignments are collected in Table 12.

Table 12. IR spectroscopic data of **22**-d_4 and $^{18}O_2$-**22**-d_4.

Vib. #	Argon, 10 K **22**-d_4	B3LYP[a] **22**-d_4	Argon, 10 K $^{18}O_2$-**22**-d_4	B3LYP[a] $^{18}O_2$-**22**-d_4	Assignment
10	433.7 (15)	446.1 (23)	[b]	445.9 (20)	skeletal vib.
11	510.4 (5)	520.6 (5)	-	519.7 (6)	ring def.
12	520.6 (5)	527.5 (7)	-	526.2 (6)	ring def.
13	584.2 (70)	591.6 (62)	582.7 (40)	589.8 (55)	C_8-H oop vib.
14	630.7 (10)	642.1 (29)	629.2 (20)	639.4 (26)	$C_{4,5}$-H, C_8-H_2 oop vib.
15	675.2 (70)	697.1 (65)	675.3, 676.9 (80)	697.0 (59)	$C_{2,4,6}$-H oop vib.
16	729.3 (15)	741.2 (15)	728.0 (10)	740.2 (12)	ring def.
17	-	781.4 (10)	-	781.2 (10)	C_7-H_2, C_8-H_2 rocking
18	779.8 (100)	799.8 (100)	778.4 (100)	798.0 (100)	$C_{2,4,5,6}$-H oop vib.
19	-	805.4 (6)	-	805.3 (4)	complex rocking vib.
20	859.2 (35)	874.3 (44)	854.4 (40)	864.0 (33)	C-O stretching, C_2-H oop vib.
21	-	886.0 (7)	-	882.6 (5)	C_7-H_2 twisting
22	878.1 (10)	904.9 (13)	878.7 (10)	904.9 (13)	$C_{2,4,6}$-H oop def.

26	979.9 (5)	999.1 (9)	980.0 (10)	999.0 (9)	C-C-C in plane bending, ring def.
27	1031.9, 1034.8, 1041.2 (90)	1053.4 (96)	1028.5, 1031.6 (100)	1049.9 (95)	C_7-H_2 wagging
28	1071.5 (5)	1078.4 (7)	-	1078.3 (7)	C_8-H_2 scissoring
30	-	1121.1 (4)	-	1121.0 (4)	$C_{4,6}$-H in plane bending
31	1120.3 (10)	1180.4 (30)	1058.7 (5)	1116.5 (12)	O-O stretching
33	1227.1, 1231.6 (65)	1246.2 (52)	1226.8, 1229.3 (70)	1244.6 (53)	complex
34	-	1309.2 (3)	-	1309.1 (3)	C_7-H_2 wagging
35	1317.8 (5)	1333.4 (12)	1317.3 (5)	1333.3 (11)	ring def.
37	1413.2 (5)	1442.9 (14)	1415.2 (5)	1442.9 (12)	Complex ring def.
38	1468.0 (10)	1504.5 (17)	1467.3 (15)	1504.5 (15)	C_4-C_5, C_6-C_1 stretching
39	-	1581.2 (5)	-	1581.2 (5)	complex
41	2174.0 (10)	2227.6 (33)	2174.3 (10)	2227.6 (30)	sym. C_7-H_2 stretching
42	-	2286.9 (7)	-	2286.9 (6)	sym. C_8-H_2 stretching
43	2254.2 (10)	2320.8 (22)	2254.0 (10)	2320.8 (20)	asym. C_7-H_2 stretching
44	[c]	2419.9 (13)	[c]	2419.9 (12)	asym. C_8-H_2 stretching
45	[c]	3164.7 (23)	[c]	3164.7 (21)	C_2-H stretching
46	[c]	3166.2 (8)	[c]	3166.2 (7)	$C_{4,5,6}$-H stretching
47	[c]	3177.1 (34)	[c]	3177.1 (31)	asym. $C_{4,6}$-H stretching
48	[c]	3190.2 (40)	[c]	3190.2 (36)	sym. $C_{4,5,6}$-H stretching

[a] UB3LYP/cc-pVTZ. [b] Not observed due to low signal to noise ratio in this region. [c] Not observed due to broad signals in this region.

6.3 Photochemistry of the peroxy biradical

It was shown, that all IR data collected for the trapping products of triplet *m*-xylylene **1** with molecular oxygen are in relative good agreement with a peroxy biradical **22** which under irradiation with long wavelength gives rise to at least two but probably three photoproducts. One photoproduct definitely can be identified as triplet *m*-xylylene **1** (Figure 37).

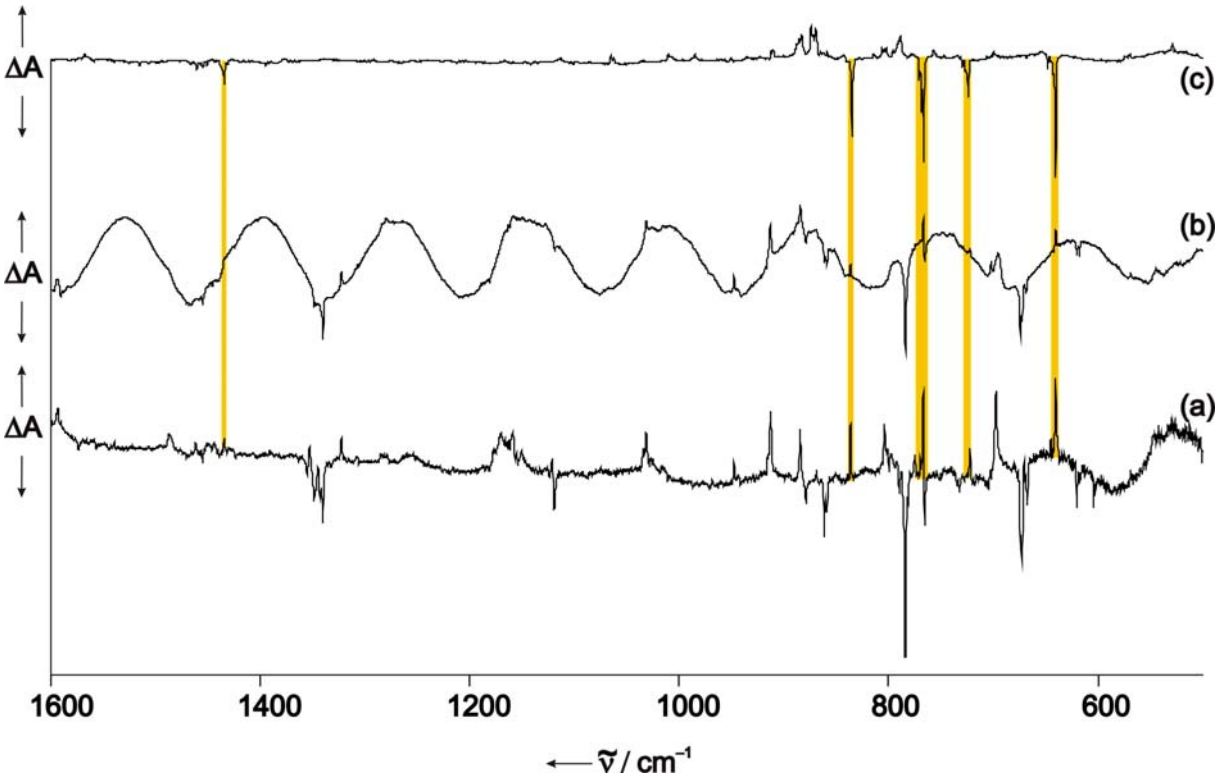

Figure 37. (a) and (b) IR difference spectra showing the photoproducts of peroxy biradical **22**. Peaks decreasing are mainly assigned to peroxy biradical **22**. Peaks increasing are partly due to complexed *m*-xylylene **1**. (c) IR difference spectrum showing the photochemistry of *m*-xylylene **1**. Peaks decreasing are assigned to **1**, peaks increasing are assigned to C_8H_8-isomers.

At low oxygen concentrations, there is always some free *m*-xylylene **1** formed under the trapping conditions. Upon irradiation with $\lambda > 475$ nm, some signals assignable to **1** are formed, while peaks belonging to **22** are decreasing. All four strong oop vibrations of the C-H bonds in *m*-xylylene **1** - which are well observable - are slightly shifted in comparison to the free **1**. Since free *m*-xylylene **1** was detected in argon and the trapping is as well conducted in argon, this effect is ascribed to an oxygen molecule which lies in close contact with the diradical in the matrix. The assignment of the most prominent signals of complexed **1**-O_2 and free **1** is shown below (Figure 38).

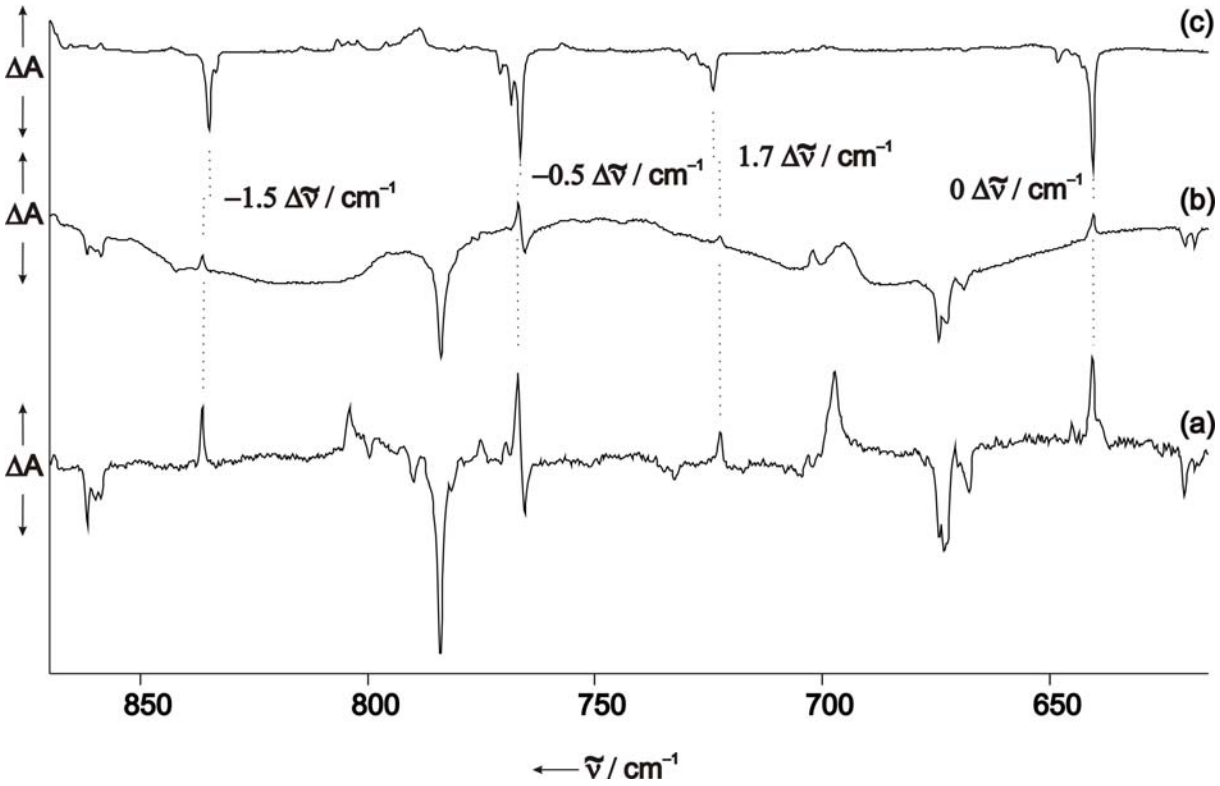

Figure 38. (a) and (b) IR difference spectra showing the photochemistry of peroxy biradical **22**. Peaks belonging to peroxy biradical **22** are decreasing, signals increasing are partly due to complexed *m*-xylylene **1**. (c) IR difference spectrum showing the photochemistry of *m*-xylylene **1**. Signals decreasing are due to uncomplexed **1**, signals increasing are due to C_8H_8-isomers.

Although complexed *m*-xylylene **1**-O_2 can be found as photoproduct, its way of formation from peroxy biradical **22** is unknown. In general, repulsive forces in an excited high-spin state could lead to extrusion of oxygen. Another important insight could come from further photoproducts. No photolytic conditions were found under which only a single photoproduct is formed from peroxy biradical **22**. The amount of peroxy biradical **22** is relatively low and thus branching in its photoproducts diminishes the chance to identify the products. In addition to the signals of *m*-xylylene **1**, some strong IR signals are observed which nevertheless could not be assigned yet. However, there are no strong C-O double bond stretching vibrations present in the experimental IR spectrum, thus some acylic and cylic ethers and peroxides are the most probable photoproducts.

6.4 Electronic structure of the peroxy biradical

In addition to different conformers of biradical **22**, it is important to distinguish the electronic isomers of **22**. Since it is a biradical, the ground state of peroxy biradical **22** can

be either a singlet or a triplet state. In some cases, as for example in *m*-xylylene **1** and TMM **49**, the molecule in its singlet state prefers a quite different bonding situation compared to its triplet state. In this instances, the IR spectra will unravel the electronic nature of the molecule. On the other side, in biradicals, which are composed of two very weakly interacting spin centers, the energy necessary to flip one spin and form the other electronic state, will be quite low. It can therefore be expected, that the singlet-triplet gap ΔE_{ST} will be very small. Furthermore, the geometries of both electronic levels could also be similar, as strong destabilizing interactions are missing. The IR spectrum in these cases could be almost indistinguishable for the singlet and the triplet state. Peroxy biradical **22** clearly belongs to the second class of molecules, as it is assembled from a benzyl radical **55** and a remote oxygen radical center. Its structure will not allow for substantial through-bond, through-space, or other effects, which could stabilize one of the electronic states over the other.

DFT methods are single-determinantal in nature and are expected to fail to describe electronic states which are linear combinations of several electronic configurations. Nevertheless, it was found by Sheridan et al. that the IR spectrum of singlet ground state *bis*carbene **151**, could be well described by DFT methods (Scheme 69).

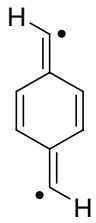

151

Scheme 69. Ground state singlet *bis*carbene **151** studied by Sheridan et al..

The authors noted that UB3LYP/6-31G** calculations on the corresponding triplet (excited) state of biradical **151** nicely reproduce the experimental IR spectrum. Furthermore, it was implemented that this approach is not unreasonable, as ΔE_{ST} is small. Their broken-symmetry UB3LYP calculations on the singlet biradical state of **151** gave nearly the same molecular geometry and IR predictions as for the triplet state ($<S^2>$ = 1.17), but 1.2 kcal/mol lower in energy.

Initial calculations on peroxy biradical **22** using UB3LYP in combination with the cc-pVTZ basis set, find an energy difference between the broken-symmetry singlet and the

triplet electronic state of 0.19 kcal/mol (ΔE_{ST} = 0.19 kcal/mol). The triplet state should be well described by a single-determinant and indeed, the spin expectation value is found to be 2.034, close to the expected value of a triplet molecule of $<S^2>$ = 2.000. The broken-symmetry singlet instead is highly spin-contaminated by higher spin states and the $<S^2>$ is found to be 1.031. Since a singlet state should have $<S^2>$ = 0 and the triplet an corresponding value of 2, the broken-symmetry structure is an approximate 50:50 mixture of a singlet and triplet state. The small difference between both electronic states is also resembled in the IR spectra – the broken symmetry singlet state and the triplet state predict nearly superimposable IR spectra.

In order to evaluate if the calculated structure is prone to simple rearrangments, the hypersurface for rotation of the C-O bond around its axis was scanned by UB3LYP/cc-pVTZ calculations for triplet peroxy biradical **22** (Figure 39).

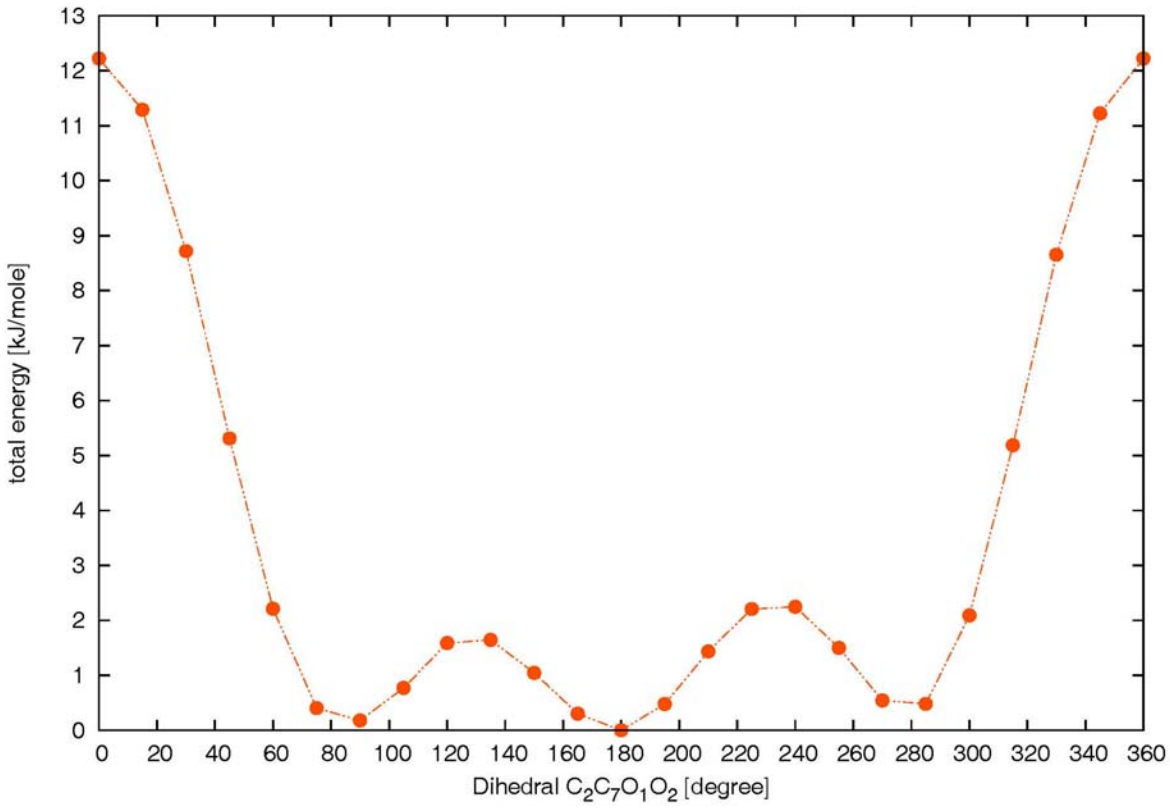

Figure 39. Potential energy surface for rotation around the C-O bond of peroxy biradical **22**.

It can be seen from Figure 39 that the rotation around the C-O bond is a relatively low-energy process with an activation energy of ca. 0.5 kcal/mol. Furthermore, both tilted peroxy biradical structures are only slightly higher in energy, with the *anti* conformer representing the global minima on this hypersurface (Scheme 70).

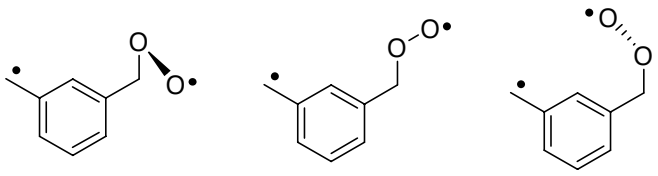

22

Scheme 70. Peroxy biradical **22** has different low-energy conformers.

Another important conclusion from the possible product studies regards the insight that possible closed-shell peroxy structures are lower in energy than the peroxy biradical **22**. Thus peroxy isomers **23**, **24**, and **25** have total energies that are 1.3, 9.2, and 9.5 kcal/mol lower in energy than **22** (Scheme 71).

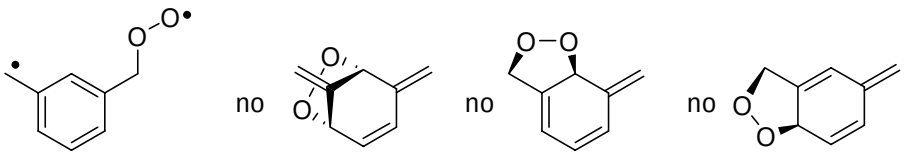

22 **23** **24** **25**

Scheme 71. Peroxy biradical **22** and several peroxides **23**, **24**, and **25**.

The trapped peroxy biradical **22** therefore represents a metastable biradical, only stable due to the rigid matrix surrounding and might convert into the isomeric structures **24** and **25** if the matrix is softened at higher temperature.

6.5 UV/Vis spectroscopy

Trapping of the FVP products of 1,3-*bis*-(iodomethyl)benzene **17** in an oxygen doped matrix results in new bands, which neither belong to **17** nor to triplet *m*-xylylene **1**. Furthermore, upon irradiation with $\lambda > 460$ nm, some of the new bands are disappearing, while only few new are evolving. The UV/Vis spectrum of triplet peroxy biradical **22** was calculated using the CC2 method in conjunction with the cc-pVTZ basis set. A low energy transition is calculated at 1085.7 nm with a negligible predicted oscillator strength of nearly 0. Stronger UV transitions are predicted to appear at 316.9 nm (0.00294) and 331.5

nm (f = 0.00080). An even stronger UV transition is calculated to be found at 267.9 (f = 0.05786). Moreover, two strong UV transitions are also predicted to be observed at 224.5 and 227.6 nm (f = 0.20215 and f = 0.26370, respectively). The experimentally observed UV/Vis spectrum tentatively assigned to peroxy biradical **22** is shown in Figure 40.

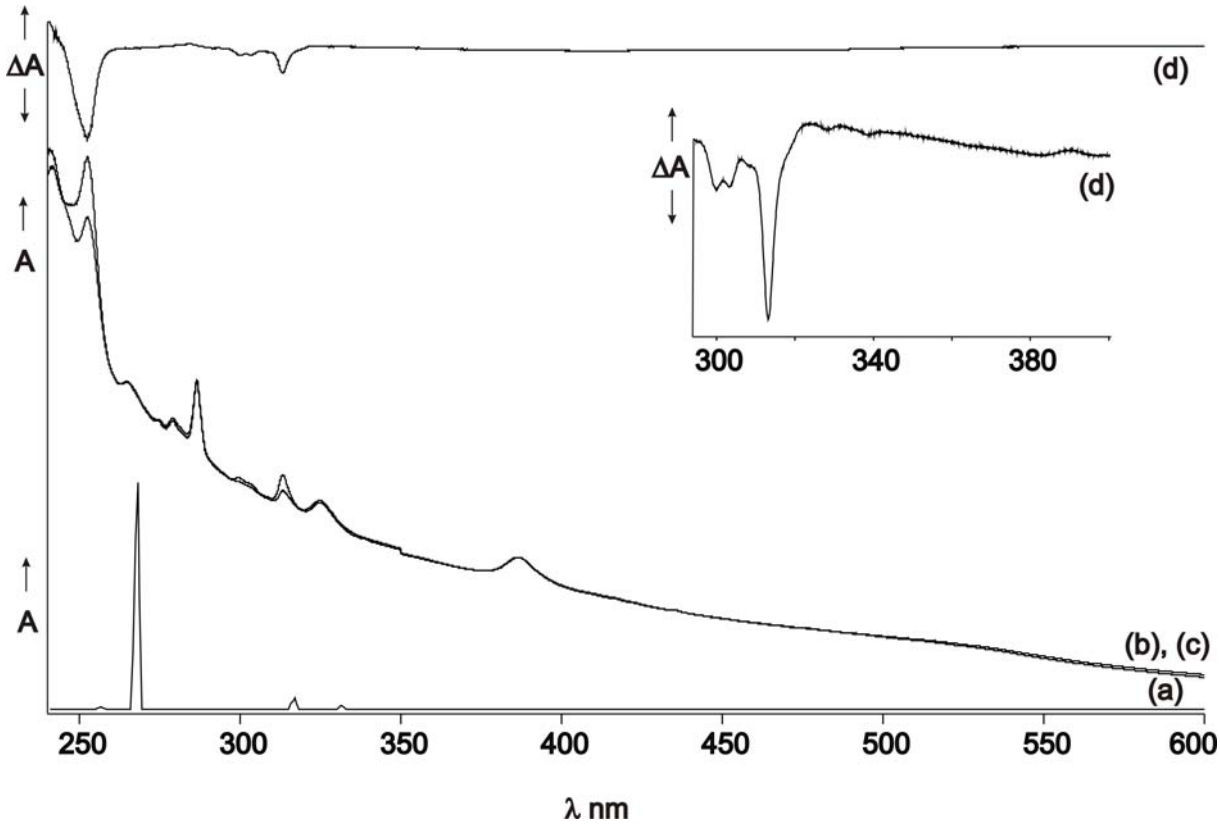

Figure 40. (a) CC2/cc-pVTZ calculated UV/Vis spectrum of triplet peroxy biradical **22**. (b) UV/Vis spectrum obtained after trapping of the FVP products of 1,3-*bis*-(iodomethyl)benzene **17** in an oxygen doped argon matrix at 27 K. (c) UV/Vis spectrum obtained after irradiation of an oxygen doped argon matrix containing the FVP products of 1,3-*bis*-(iodomethyl)benzene **17** with λ > 460 nm. (d) Difference UV/Vis spectrum (c) – (b). Bands showing downwards are decreasing, bands showing upwards are increasing in intensity upon irradiation.

Experimentally, some new bands can be distinguished which might belong to peroxy biradical **22**. The region below 240 nm is not shown since the bands in this region are quite large and the smaller but more indicative electronic transitions in the red part of the UV/Vis spectrum would be invisible. The strongest electronic transition in this part of the experimental UV/Vis spectrum is recorded at 252.4 nm. A second band system at 313.2 nm is also experimentally distinguished, presumably showing vibrational progression and thus giving rise to two bands at 303.4 and 299.8 nm. Moreover, a small redshifted transition is visible at 339.0 nm. In conclusion, the UV/Vis spectrum does not rule out a

triplet state of peroxy biradical T-**22**. The resemblance between the calculated UV/Vis spectrum and the experimental one is satisfying, but not convincing. Nevertheless no comparison to the UV/Vis spectrum of singlet peroxy biradical S-**22** is possible, as the UV/Vis spectrum is not calculated yet at this level of theory. Furthermore, no bands of iodine superoxide **146**, iodine dioxide **147** or iodine monoxide **148** are observed, neither before nor after photolysis.

7. 1,3,5-Trimethylenebenzene

7.1 Introduction

Construction of a molecule bearing three unpaired π electrons coupled through a benzene core in a ferromagnetic fashion is only possible if the radical centers are arranged in *meta* position to each other, leading to the triradical 1,3,5-trimethylenebenzene **2** (Scheme 72). Such a triradical, having all its unpaired electrons in p orbitals, is classified as π,π,π-triradical. Similar to its homologue diradical *m*-xylylene **1**, triradical **2** belongs to the class of non-Kekulé molecules, for which it is not possible to find a resonance form with all spins paired in π bonds.

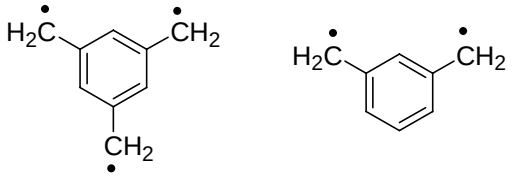

2 **1**

Scheme 72. High-spin coupled non-Kekulé polyradicals: Quartet 1,3,5-trimethylenebenzene **2** and *m*-xylylene **1**.

Instead, there will always remain at least three electrons unpaired in each resonance form. As there are no odd numbered rings contained in structure **2**, the π molecular framework can be subdivided into two different sets of carbons. One set consists of the positions where the unpaired electrons are located in the resonance forms, the starred set, while the second unpaired set containes the carbons, where only paired electrons are located in each resonance form (Scheme 73). Every starred carbon has only carbons of the unstarred set in its direct neighbourhood and vice versa, thus 1,3,5-trimethylenebenzene **2** and *m*-xylylene **1** belong to the class of alternant hydrocarbons.

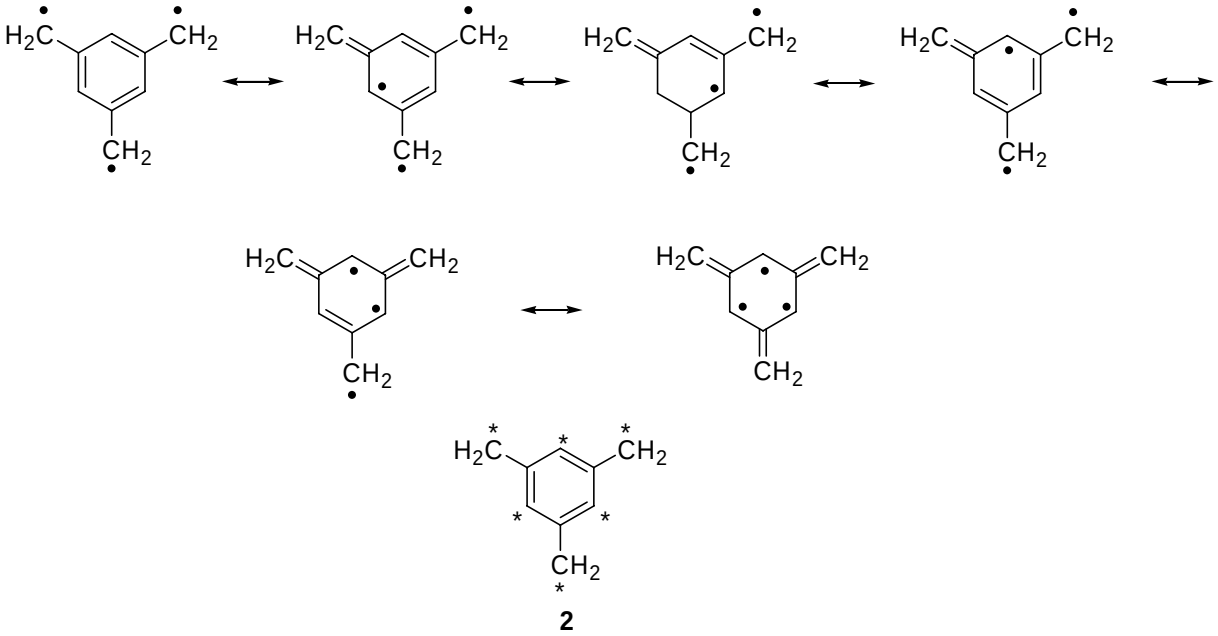

2

Scheme 73. Possible resonance forms for quartet triradical **2** and the two different carbon sets used by Ovchinnikov (starred/unstarred carbon atoms).

In its seminal paper Longuet-Higgins in 1950 predicted on the basis of molecular orbital theory that alternant non-Kekulé polyradicals should have a high-spin ground state.[12] The same prediction on another foundation was given later by Ovchinnikov using a valence bond formalism.[14] High-level *ab-initio* methods using multiconfigurational methods like CASSCF, CASPT2 or MR-CI confirmed this early predictions. The energy gap between the high-spin triradical $^4A_1$" state Q-**2** and the low-spin antiferromagnetic coupled $^2A_2$ D-**2** triradical state was calulated to be in the order of 14 +/- 1 kcal/mol or 12.4 +/- 2 kcal/mol, depending on the method of calculation.[120, 121] Having nearly no bonding effect for the molecule, the three highest MOs are called non-bonding molecular orbitals (NBMOs). Application of the zero-sum rule gives the coefficients of the three NBMOs and thus a qualitative picture while unrestricted density functional or *ab initio* methods have to be performed to obtain a more realistic appearance of the NBMOs (Scheme 74). As can be seen from this analysis, the orbital coefficients of the NBMOs span common atoms and are thus non-disjoint, leading to the prediction of a quartet high-spin state.[122] The reason for this is the coulomb repulsion, which for the doublet state is much higher due to unfavourable coulomb interaction on common atoms between the NBMOs, while it is prohibited in the quartet state.

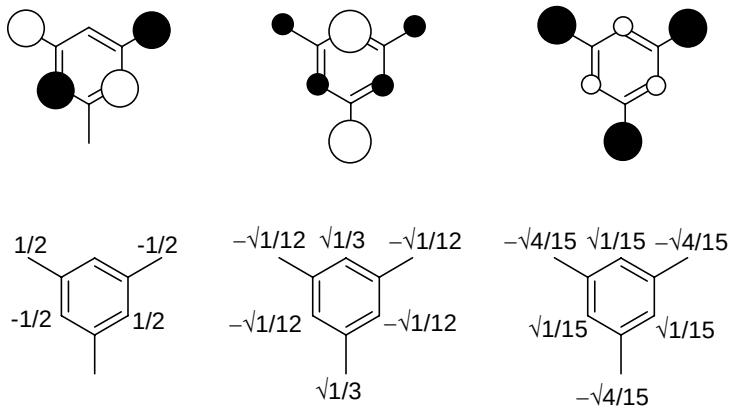

Scheme 74. The three nonbonding molecular orbitals of 1,3,5-trimethylenebenzene **2** predicted from the zero-sum rule. Schematic picture of all NBMOs.

In order to be high-spin coupled, each NBMO has to be occupied by one electron with all electrons showing in the same direction (and thus each electron must have the same spin-quantum number). Hund's rule will only be obeyed for molecules, where the energy difference between the NBMOs is relatively small. Baumgarten estimated that in diradicals the corresponding singlet state will be stabilized compared to the high-spin state, if the energy difference between the two NBMOs is as large as 1.5 eV.[123-125] No splitting between the NBMOs, i.e. degenerate NBMOs, is only found for molecules with high symmetry.

While most organic molecules have little symmetry, 1,3,5-trimethylenebenzene **2** belongs to the D_{3h} point group and thus has two degenerate NBMOs on the basis of this symmetry. The third NBMO of a_2"-symmetry is found by multiconfigurational methods to lie below these NBMOs by a small amount. Furthermore the e"-symmetry of the two NBMOs makes the lowest doublet states of 1,3,5-trimethylenebenzene **2** unstable in D_{3h} symmetry and leads via Jahn-Teller effect of first order to a symmetry lowering to C_{2v} in these doublet states.[126]

Some derivatives of **2** like the perchlorinated triradical **152** which is stable under ambient conditions and the sterically congested hexaphenyl derivative **153** were prepared (Scheme 75).[127, 128]

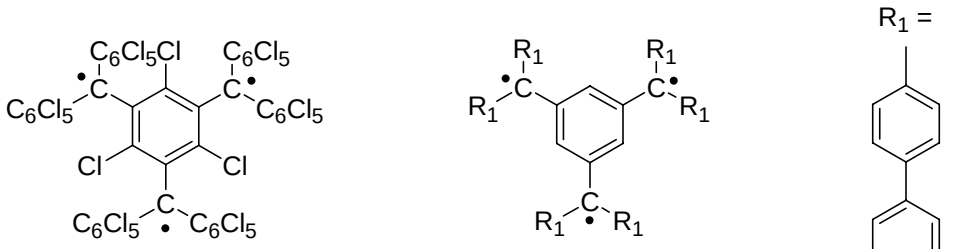

152 **153**

Scheme 75. Some experimentally observed high-spin quartet triradicals having a 1,3,5-trimethylenebenzene **2** core.

Substitution of each radical bearing CH_2 units by NH_2^+ was predicted to result in high-spin quartet amino radical cations, which was substantiated by the fact that the hexaphenyl-substituted quartet amino triradical **154** was prepared and found to be a high-spin ground state by linear Curie dependance of the EPR signal (Scheme 76).[121, 129]

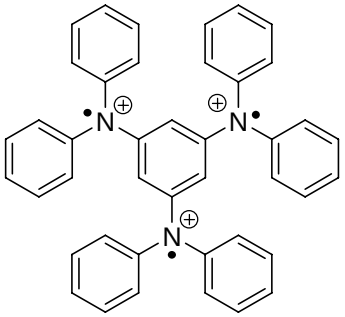

154

Scheme 76. Curie analysis of the EPR signal intensity of **154** showed the quartet state to be the ground state of the triradical trication.

Next to these experimental approaches on the stabilized triradicals, there is only one experimental study on the parent triradical **2**. Wenthold et al. measured the collision induced dissociation energy (CID) of biradical anion 5-chloromethyl-*m*-xylylene **155** to determine the heat of formation of quartet 1,3,5-trimethylenebenzene **2** (Scheme 73).[130] The heat of formation of quartet triradical **2** was found to be 111.0 +/- 4.1 kcal/mol and thus leads to a third bond dissociation energy of mesitylene **103** of 88.2 +/- 5.0 kcal/mol, almost indistinguishable from the "first" BDE in toluene **156** (89.8 +/- 0.6 kcal/mol) and the first and second BDEs in *m*-xylene **101** (90.1 +/- 1.7 kcal/mol and 90.7 +/- 2.9 kcal/mol), indicating that there is negligible interaction between the unpaired electrons in the NBMOs of triradical **2** and its ground state is the "$^4A_1$" state (Scheme 77).[130] If the doublet state would be the ground state, there would be some stabilizing interaction

between the low-spin coupled electrons in the triradical which would lower its energy. This effect would show up in a smaller heat of formation of 1,3,5-trimethylenebenzene **2** (and thus the third BDE of mesitylene **103**) than the one derived from bond additivity values (or the first and second BDE in mesitylene **103**).

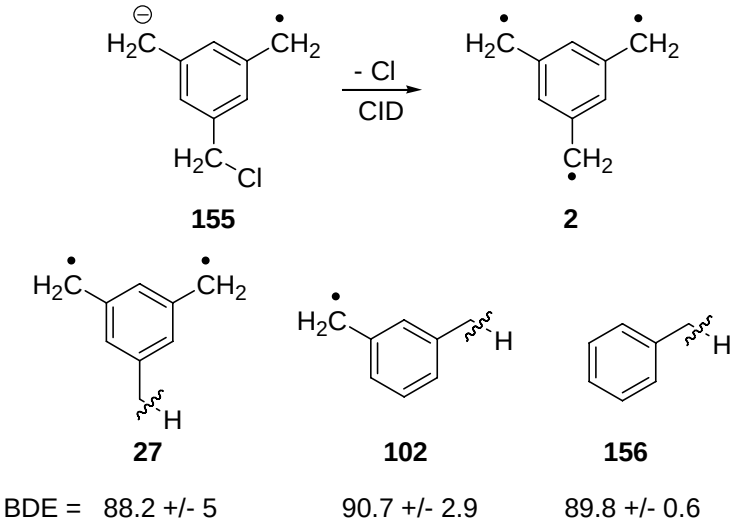

Scheme 77. Determination of the collision induced dissociation energy of 5-chloromethyl-*m*-xylylene anion **155** gives the heat of formation of 1,3,5-trimethylenebenzene **2** and its bond dissociation energy, which can be compared with the corresponding bond dissociation energies of 3-methylbenzyl radical **102** and toluene **156** [kcal/mol].[130]

Nguyen et al. studied the effect of protonation on the electronic structure of 1,3,5-trimethylenebenzene **2** and found that exocyclic protonation is favoured over ring-protonation while both processes lead to low-spin doublet ground states.[120] The exocyclic protonated doublet cation **157** is best described as distonic radical because the cationic charge and the unpaired electron are well separated into two distinct parts of the molecule: a pentadiene cation and a 2-methyl-allylradical as shown in Scheme 78.

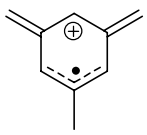

157

Scheme 78. Protonation of 1,3,5-trimethylenebenzene **2** takes favourably place at the exocyclic positions and leads to the distonic doublet ground state radical cation **157**.[120]

Moreover, it was shown by the use of mass spectrometry that the second protonation of 1,3,5-trimethylenebenzene **2** results in doublet ground states of the C_9H_{11}-dications **158** as well.[131] B3LYP calculations with 6-311G** basis set showed that the

second protonation can either take place at another methylene unit or in *ortho* or *para* position with respect to the methyl group, as the corresponding dicationic doublet isomers have nearly the same energy.[131]

1,3,5-trimethylenebenzene **2** is a planar system and Kemnitz et al. calculated the energy of **2** with one methylene unit perpendicular to the planar benzene ring to be 15.5 kcal/mol higher for the corresponding quartet state. It was found that this twisted geometry as well as the molecular orbitals closely resemble those of *m*-xylylene **1** with one electron of the same spin in an isolated p orbital at the perpendicular methylene group.[126] Furthermore, it was shown that reversing the spin of the electron in the isolated p orbital and therefore forming the corresponding doublet state has almost no influence on the energy at the CASSCF level of theory (6-31G* basis set), as the orbitals from *m*-xylylene **1** and the p orbital are disjoint from each other.[126]

The analogous change in energy on twisting *m*-xylyene **1** or the benzyl radical **55** were calculated at the same level of theory ((8/8)CASSCF/6-31G* for **1** and (7/7)CASSCF/6-31G* for **55**) to be 14.2 and 11.9 kcal/mol respectively, showing the cooperative effect of parallel spins in quartet **2** and triplet **1** to withstand rotation.[126]

Hu and Squires were able to generate the diradical anion $\mathbf{2}^-$ of 1,3,5-trimethylenebenzene **2** in a flowing afterglow apparatus through sequential desilylation of 1,3,5-*tris*-(trimethylsilymethyl)-benzene **159** and studied this species by its reactivity (Scheme 79).[132] The observed reactivity was interpreted in favour of a triplet ground state of diradical $\mathbf{2}^-$ as, for example, the reaction with oxygen leads to the oxidation of two methylene units to aldehyde groups instead of three. The benzyl anion is known not to react with oxygen any further. No photoelectron spectrum which could clarify the ground state of diradical anion $\mathbf{2}^-$ was ever reported. Furthermore, this would presumably permit the determination of some vibrational bands as well as the doublet-quartet splitting of π,π,π-triradical **2** in a similar way as it was done by Wenthold et al. for *m*-xylylene **1**.[65, 66]

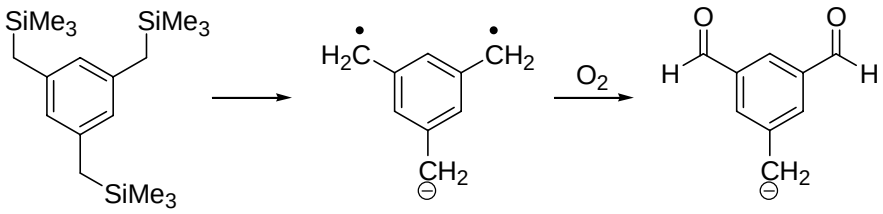

159 **2**$^{-}$ **160**

Scheme 79. Precursor used by Hu and Squires to produce the diradical anion of 1,3,5-trimethylenebenzene **2**$^{-}$ and reactivity with oxygen leading to benzyl anion dialdehyde **160**.[132]

Prerequisite for the study of triradical **2** was the observation that high yields of **1** are formed via flash vacuum pyrolysis of 1,3-*bis*-(iodomethyl)benzene **17** at 450°C and subsequent trapping of the products in argon at 10 K.[24] It was shown in this study, that the benzylic C-I bond can effectively be cleaved at higher temperatures to yield the corresponding radicals. It thus was anticipated that 1,3,5-*tris*-(iodomethyl)benzene **26** would be a good precursor for the 1,3,5-trimethylenebenzene triradical **2** (Scheme 80).

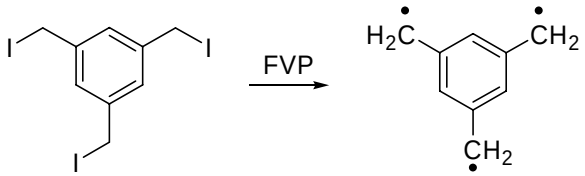

26 **2**

Scheme 80. Possible precursor for quartet triradical **2** via flash vacuum pyrolysis is 1,3,5-*tris*-(iodomethyl)benzene **26**.

7.2 Mass spectrometric study

In order to explore and determine the flash vacuum pyrolysis products of the parent 1,3,5-*tris*-(iodomethyl)benzene **26**, the mass spectra after flash vacuum pyrolysis of 1,3,5-*tris*-(iodomethyl)benzene **26** were studied. Using 70 eV for the electron beam in the quadrupole mass spectrometer at 160°C flash vacuum pyrolysis temperature (in order to prevent resublimation of **26** on the walls of the FVP tube) leads to the radical, diradical, and triradical cations of 1,3,5-*tris*-(iodomethyl)benzene **26** due to loss of one, two, or three iodine atoms. Reducing the energy of the electron beam to 15 eV allows the detection of a very small molecular peak at 498 m/z, assuring that the parent 1,3,5-*tris*-(iodomethyl)benzene **26** does not decompose before electron impact (Figure 41). The main peaks appearing in the mass spectra after decomposition due to electron impact belong to the monoradical cation at 371 m/z (middle intensity), the diradical cation at 244 m/z (very strong) and the triradical cation at 117 m/z (middle intensity). As the temperature of the FVP tube is increased up to 390°C, a slight change in the intensities of the three main products can be observed. While the monoradical cation and the diradical cation slightly decrease in their relative intensity, the triradical cation slightly increases suggesting that the thermal decomposition of the parent 1,3,5-*tris*-(iodomethyl)benzene **26** is starting at this temperature. At 450°C the decomposition of **26** into smaller fragments is more evident, while it can not unambiguously be clarified if the decomposition gives 3,5-*bis*-(iodomethyl)benzyl radical $\mathbf{161}^+$ (which decomposes mainly into the di and/or triradical cation upon electron impact), 5-(iodomethyl)-*m*-xylylene diradical cation $\mathbf{162}^+$ (which fragments to the triradical cation upon electron impact) or trimethylenebenzene triradical cation $\mathbf{2}^+$ (which gives its molecular peak at 117 m/z and is relatively stable towards fragmentation upon electron impact at 15 eV).

Furthermore, some hydrogen abstraction products are visible at a mass of 118 and 119 m/z, probably belonging to the cations of triplet 5-methyl-1,3-*bis*-methylenebenzene **27** and doublet 3,5-*bis*-methylbenzyl radical **28**, respectively.

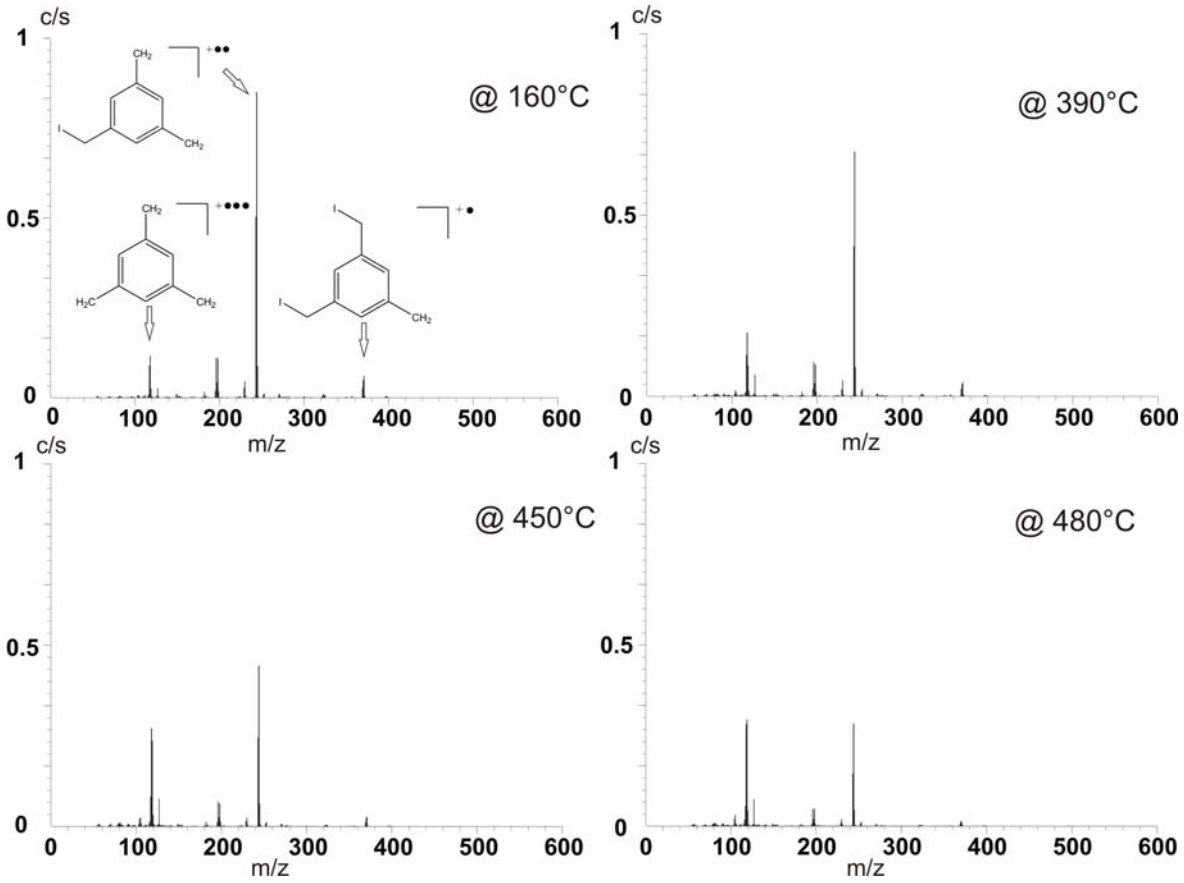

Figure 41. Mass spectra showing the successive thermal abstraction of iodine atoms from 1,3,5-*tris*-(iodomethyl)benzene **26** dependent on the temperature of the flash vaccum pyrolysis tube.

Increasing the temperature to 480°C shows equal absolute intensities for the two- and threefold iodine abstraction products, while the most intense peak at 550°C pyrolysis temperature belongs to the triradical cation and hydrogen abstraction products (Figure 42).

The iodine atom cation peak at 127 m/z can be seen in all spectra and increases slightly when the temperature of the pyrolysis is increased. Up to 600°C the peak resembling threefold iodine abstraction remains the highest absolute peak while some ring opening products seem to appear at lower m/z ratio. Decreasing the temperature of the pyrolysis tube to the starting value of 160°C shows the same relative heights of the above mentioned peaks, while the absolute intensities of all peaks are not as high as at the beginning of the experiment.

While the decomposition of 1,3,5-*tris*-(iodomethyl)benzene **26** can be investigated by the mass spectrometric experiment, it seems not to be possible to unravel the origin of the detected cations, i.e. if they are fragmentation products or not. Nevertheless, it can be

seen that **26** looses its iodine atoms upon FVP since the peak intensities of the lower molecular weigth cations increase upon higher pyrolysis temperatures. As the diradical cation is not increasing in intensity at any temperature compared to the triradical, it is rather improbable that 1,3,5-*tris*-(iodomethyl)benzene **26** cleaves only one iodine atom by FVP (because the “thermally born” monoradical cation should abstract an iodine atom upon electron impact, manifesting itself in this experiment as an increase in the relative amount of diradical cation). The molecular source of the increased triradical cation peak can either be a fragmentation of the diradical cation or the triradical itself. Furthermore, it is evident that hydrogen abstraction is taking place yielding hydrogen abstraction products with mass values of [M+1] and [M+2]. The pathway leading to this species seems to become more and more important as the temperature of the FVP is increased.

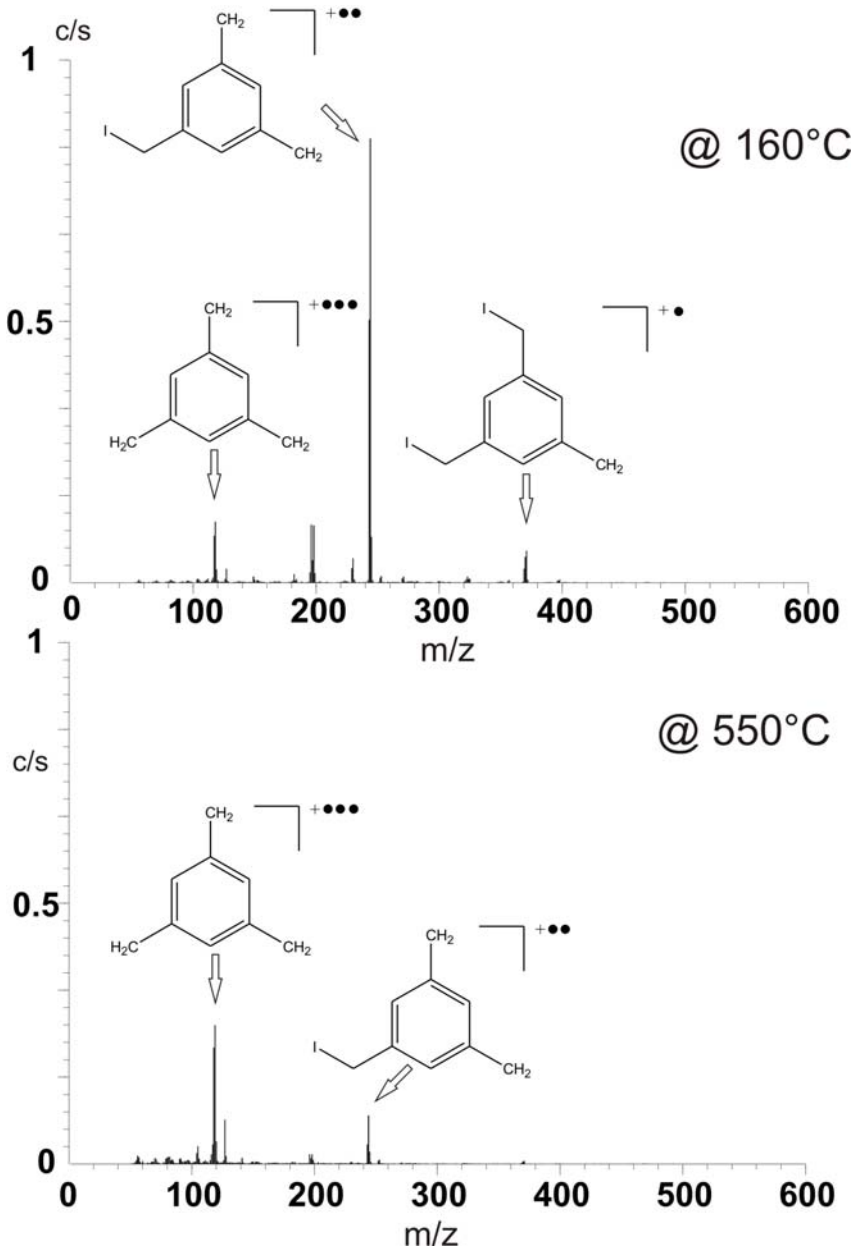

Figure 42. Mass spectrum obtained for 1,3,5-*tris*-(iodomethyl)benzene **26** and the mass spectrum obtained upon thermal decomposition of **26** at higher temperature.

After the appropriate conditions for flash vaccum pyrolysis were identified from the mass spectra, a FVP temperature of 450°C to 550 °C was chosen for the corresponding infrared experiments.

7.3 FVP of 1,3,5-*tris*-(iodomethyl)benzene – Infrared experiments

In all experiments there is only a relatively little amount of triradical 1,3,5-trimethylenebenzene **2** formed in the argon matrix at 10 K, even though under optimal conditions it represents the signals with the highest intensity. It was inferred from the mass spectra and also obvious in the infrared spectra, that hydrogen abstraction from the reactive triradical **2**, or some intermediate diradical and monoradical species could take place under the conditions used for the matrix IR experiments.

In most IR experiments a signal at 1156 cm^{-1} was observed, which normally belongs to the C-I stretching vibration of iodinated compounds left after FVP of 1,3,5-*tris*-(iodomethyl)benzene **26**. Nevertheless, the intensity is quite low and the corresponding species could not be identified due to its low abundancy in the argon matrix.

Hydrogen abstraction of triradical **2** will lead to 5-methyl-*m*-xylylene **27**, while double hydrogen abstraction of **2** via **27** produce 3,5-*bis*-methylbenzyl radical **28** (Scheme 81).

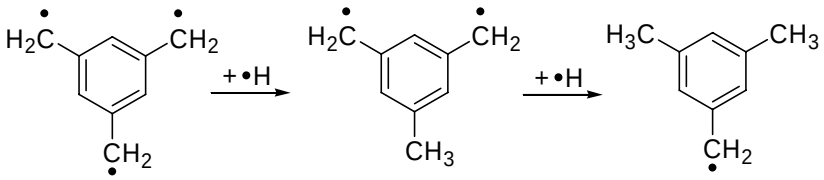

2 **27** **28**

Scheme 81. Hydrogen abstraction of 1,3,5-trimethylenebenzene **2** results in the diradical 5-methyl-*m*-xylylene **27** and the 3,5-*bis*-methylbenzyl radical **28**.

The UB3LYP/6-311+G** calculated absolute intensities of quartet triradical **2**, triplet diradical **27**, and benzyl radical **28** are shown in Table 13. It can be seen, that the out of plane vibration around 650 cm^{-1} is best suited to directly compare the amounts of radical species observed. The oop vibration of 3,5-*bis*-methylbenzyl radical **28** is calculated to be found at 679.9 cm^{-1} and to have an intensity of 39.9 km/mol. The corresponding oop vibration of 5-methyl-*m*-xylylene **27** is shifted 25.6 cm^{-1} to the red (654.3 cm^{-1} and 43.1 km/mol), while the triradical **2** oop vibration is further redshifted about 30.2 cm^{-1} to 624.1 cm^{-1} (44.6 km/mol).

Table 13. UB3LYP/6-311+G** calculated absolute intensities of the strongest vibrations of quartet triradical **2**, triplet diradical **27**, and doublet monoradical **28**.

Compound	Vibration[a]/cm^{-1}	Abs. int.[a]/ km/mol
Monoradical **28**	679.7	39.9
	729	16.3
	843	29.8
Diradical **27**	654.3	43.1
	731.8	49.2
	827.6	15.9
	837.2	35.8
Triradical **2**	624.1	44.6
	727.4	73.9
	827.9	76.6

[a] Calculated with the B3LYP method and a 6-311++G** Pople basis set.

It was found that in contrast to *m*-xylylene **1** the corresponding 1,3,5-trimethylenebenzene triradical **2** did not show fast photochemistry, which might be due to the fact, that all following photochemical products have to be doublet radicals itself, lying higher in energy by at least 10 kcal/mol as it is shown in Table 14 (see also Scheme 82 for "expected" photoisomers).

Table 14. Calculated energy differences between quartet 1,3,5-trimethylenebenzene triradical **2** and some doublet C_9H_9-isomers **163**, **164**, and **165** (in kcal/mol).

Molecule	(E + ZPC)[a] /hartrees	ZPC /hartree per particle	S^2	$E_{rel.}$, kcal/mol
Quartet **2** (D_{3h}) [b]	-348.204518	0.142578	3.8298	0
Doublet **2** (C_{2v}) [b]	-348.188683	0.141583	1.7785	9.94
Doublet **163** (C_1)[b]	-348.171077	0.145238	0.7995	20.98
Doublet **164** [b]	-348.185664	0.144574	0.7915	11.83
Doublet **165** [b]	-348.116407	0.142936	0.7577	55.29

[a] All energies including zero-point vibrational energy correction (ZPC) without spin-projection. [b] UB3LYP/6-311+G**

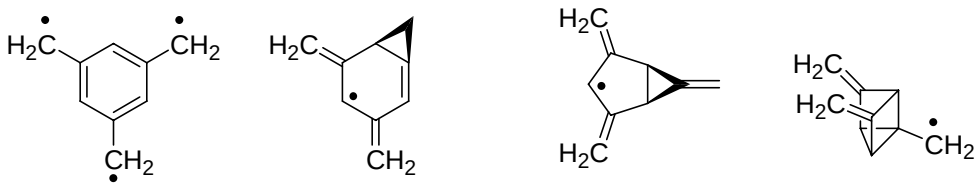

2 **163** **164** **165**

Scheme 82. Possible doublet C_9H_9-isomers which could be formed form triradical **2** upon irradiation.

Upon 680 to 420 nm irradiation with a high-pressure mercury lamp several signals are decreasing (also the triradical and at least one additional compound). Using 450 – 360 nm light of the same light source results in almost exclusive decrease of the triradical **2** peaks, so that an assignment of the infrared vibrations for quartet **2** is possible in comparison with the UB3LYP/6-311+G** calculated infrared spectrum of the triradical (Figure 43).

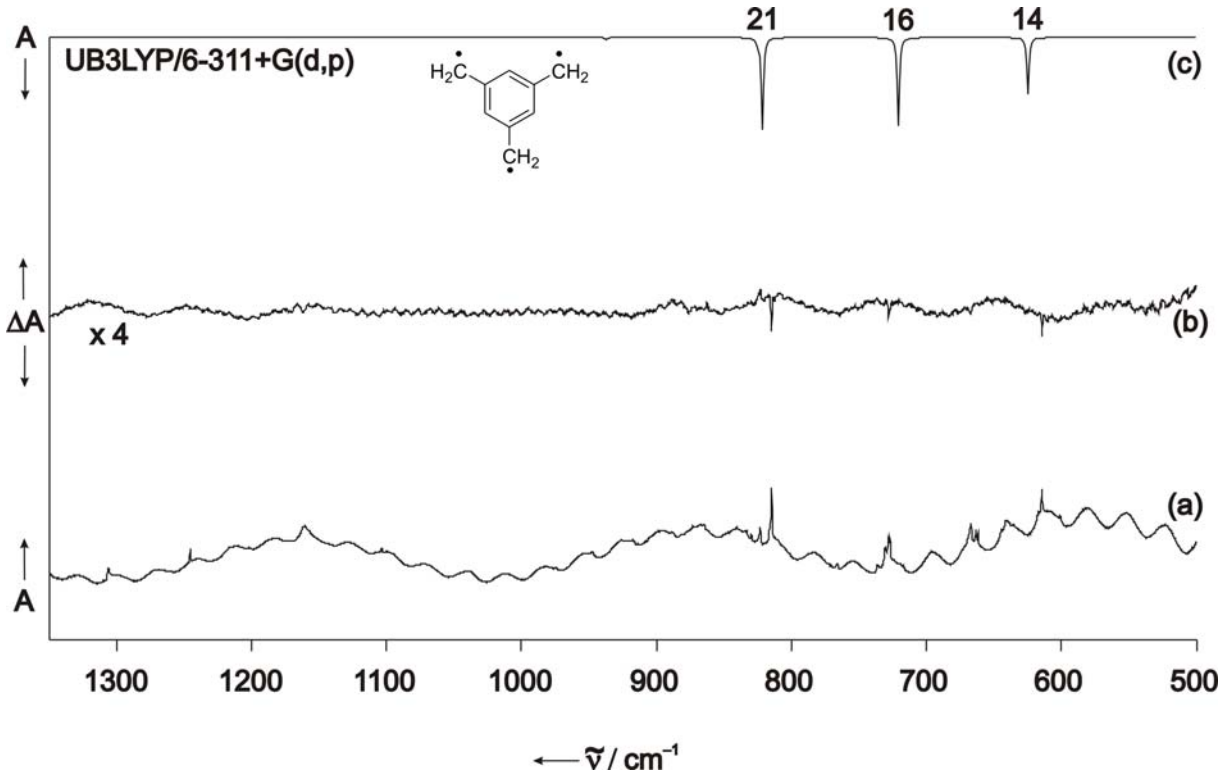

Figure 43. (a) Infrared spectrum obtained after FVP at 480°C of 1,3,5-*tris*-(iodomethyl)benzene **26**. (b) Difference spectrum of the same matrix after photolysis with λ = 450 – 360 nm of a high-pressure mercury lamp. (c) UB3LYP/6-311+G** calculated infrared spectrum of quartet triradical 1,3,5-trimethylenebenzene **2**.

The use of other density functional methods or larger basis sets results in systematic changes in the infrared spectrum while the pattern of the infrared signals remains constant. Using *ab initio* methods to optimize the geometry and calculate the IR spectrum of quartet triradical **2** is found to be highly dependent on the basis set. UMP2 calculations with different Pople basis sets results in most cases in a similar geometry but very different IR spectra compared to the DFT methods – UMP2/6-311+G(d) predicts an imaginary frequency for the quartet state of **2** (Table 15). Similar behaviour of some popular *ab initio* methods for the description of planar systems were obtained by Schleyer et al..[133] CCSD calculations with moderate basis sets as well did not give the same spectral pattern of IR signals. It can be concluded that as far as UMP2 is regarded, Dunning´s basis sets seem to be appropriate for a balanced description of the molecule. The IR spectrum predicted by UMP2/cc-pVTZ is very close to the one obtained by DFT methods.

Table 15. Geometrical parameters, symmetry, spin contamination, and some A_2'' oop vibrational modes for the quartet state of 1,3,5-trimethylenebenzene **2** using different theoretical methods.

Method	R_1	R_2	A_1	A_2	Sym.[a]	S^2	A_2"-frequencies
UMP2/cc-pVDZ	1.404	1.423	121.8	118.2		4.3432	771 (79); 731 (63.6); 610 (13.9)
UMP2/cc-pVTZ	1.391	1.410	121.8	118.2		4.3087	842 (73.7); 760 (65.7), 661 (41.5)
UMP2/6-31G(d)	1.396	1.415	121.8	118.2		4.3432	710 (211.4); 699 (0.5), 496 (0.7)
UMP2/6-31+G(d)					C_s		C_s symmetry
UMP2/6-31G(d,p)	1.396	1.415	121.8	118.2		4.340	710 (114.3); 702 (69.4); 466 (1.4)
UMP2/6-311+G(d)	1.399	1.417	121.8	118.2		4.4345	696 (141.7); 664 (108.4);

							176 (6.6) (1 imaginary freq.)
UCCSD/6-31G(d)	1.404	1.426	121.9	118.1		4.3698	694 (189.9); 673 (5.9); 510 (0.0)
UCCSD/6-311G(d)	1.405	1.428	121.8	118.2		4.3660	670 (192.1); 651 (16.6); 466 (0.8)
USVWN/ 6-311++G(d,p)	1.390	1.413	121.9	118.1	C_{2v}	3.7652	833 (95.3); 707 (69.3); 609 (55.3)
UBLYP/ 6-311++G(d,p)	1.410	1.433	122.1	117.9		3.7862	808 (75.4); 702 (68.4); 608 (45.3)
UBPW91/ 6-311++G(d,p)	1.407	1.428	122.0	118.0		3.7953	811 (81.6); 700 (67.1); 611 (50.1)
UBHandHLYP/ 6-311++G(d,p)	1.393	1.415	121.9	118.1	C_{2v}	3.9354	858 (88); 753 (68.9); 646 (51.6)
UPBEPBE/ 6-311++G(d,p)	1.407	1.428	122.0	118.0		3.7908	808 (79.9); 698 (67.3); 608 (50.6)
UBP86/ 6-311++G(d,p)	1.408	1.430	122.0	118.0		3.7909	806 (83.6); 699 (66.9); 607 (48.3)
UM062X/ 6-311++G(d,p)	1.400	1.419	121.9	118.2		3.8493	840 (87.2); 725 (67.7); 628 (56.7)

UPW91PW91/ 6-311++G(d,p)	1.405	1.426	122.0	118.0	3.7919	812 (82.5); 701 (66.8); 610 (51.6)
UHCTH/ 6-311++G(d,p)	1.401	1.421	122.2	117.8	3.8046	813 (56.6); 696 (68.0); 614 (53.2)
UB3P86/ 6-311++G(d,p)	1.398	1.419	122.0	118.0	3.8366	835 (89.8); 726 (67.1); 628 (51.4)
UTPSSh/ 6-311++G(d,p)	1.404	1.424	121.9	118.1	3.8391	824 (84.6); 719 (66.6); 626 (51.4)
UVSXC/ 6-311++G(d,p)	1.404	1.426	121.7	118.3	3.8151	791 (87.1); 709 (63.8); 606 (36.6)
UB3LYP/ cc-pVDZ	1.404	1.427	122.0	118.0	3.8338	840 (45.5); 726 (52.3);634 (29.5)
UB3LYP/ cc-pVTZ	1.397	1.419	122.0	118.0	3.8292	840 (61.6); 733 (64.9); 631 (38.9)
UBLYP/ cc-pVDZ	1.413	1.436	122.1	117.9	3.7885	823 (39.0); 706 (48.6); 618 (24.6)
UBLYP/ cc-pVTZ	1.405	1.429	122.1	117.9	3.7865	812 (56.3); 708 (62.6); 612 (34.9)
UB3LYP/ 6-31G(d)	1.402	1.425	122.1	117.9	3.8375	829 (84.0); 714 (65.1); 631 (28.2)
UB3LYP/	1.402	1.425	122.0	118.0	3.8366	825 (77.9); 717

6-31G(d,p)							(59.7); 630 (26.1)
UB3LYP/ 6-311G(d,p)	1.400	1.423	122.0	118.0		3.8316	823 (68.8); 721 (66.0); 626 (42.1)
UB3LYP/ 6-31+G(d)	1.404	1.426	122.0	118.0		3.8333	829 (93.7); 723 (80.6); 623 (42.0)
UB3LYP/ 6-311+G(d,p)	1.401	1.423	122.0	118.0		3.8298	828 (76.6); 727 (73.9); 624 (44.6)
UB3LYP/ 6-311++G(d,p)	1.401	1.423	122.0	118.0		3.8298	834 (82.8); 727 (69.1); 627 (48.6)
UB3LYP/ 6-311++G(2df,2pd)	1.397	1.420	122.0	118.0	C_{2v}	3.8283	844 (59.1); 738 (67.7); 629 (43.7)
UB3LYP/ 6-311++G(3df,2p)	1.397	1.420	122.0	118.0	C_{2v}	3.8285	840 (62.3); 738 (63.2); 628 (42.3)
UHF/4-31G//UHF/STO-3G	-	1.425	-	-		4.4 – 4.5	Mol. Cryst. Liq. Cryst., 1993, 232, 323
UHF/6-31G	1.411	1.425	120	120		3.93	J. Chem. Phys., 100, 6, 1994, 4454
CAS(7/8)/6-31G(d)	1.408	1.414	118.2	121.8		-	Bull. Chem. Soc. Jpn., 71, 337, 1998
CASPT2/X//CAS(9/9)/X; MS-	1.405	1.424	120	120		-	J. Chem. Phys., 122, 154308,

CASPT2/X//CAS(9/9)/X; X = 6-31G(d,p) or (ANO-I)						2005
CASPT2/ANO-L//CAS(9/9)/ANO-L; MS-CASPT2/ANO-L//CAS(9/9)/ANO-L	1.400	1.421	118.1	120.9	-	Chem. Phys. Lett., 411, 2005, 450
CASPT2N/6-31G(d)//CAS(9/9)/6-31G(d) MR-CI(π-SD,σ-S)+Q/6-31G(d)//CASSCF(9/9)/6-31G(d)	1.403	1.424	118.1	120.9	-	J. Am. Chem. Soc. 119,1997, 28

[a] No specified symmetry means D_{3h} symmetry.

The observed photochemistry of 1,3,5-trimethylenebenzene **2** was confirmed by isotopic labelling of 1,3,5-*tris*-(iodomethyl)benzene **26**. FVP at 480°C of the hexadeuterated 1,3,5-*tris*-(iodomethyl)benzene isotopomer **26**-d_6 in which all exocyclic hydrogens were replaced by deuterium atoms while the ring hydrogens remain unsubstituted, results in the infrared spectrum shown in Figure 44. From a first view, it is obvious that the infrared spectrum has changed remarkably upon exocyclic deuteration.

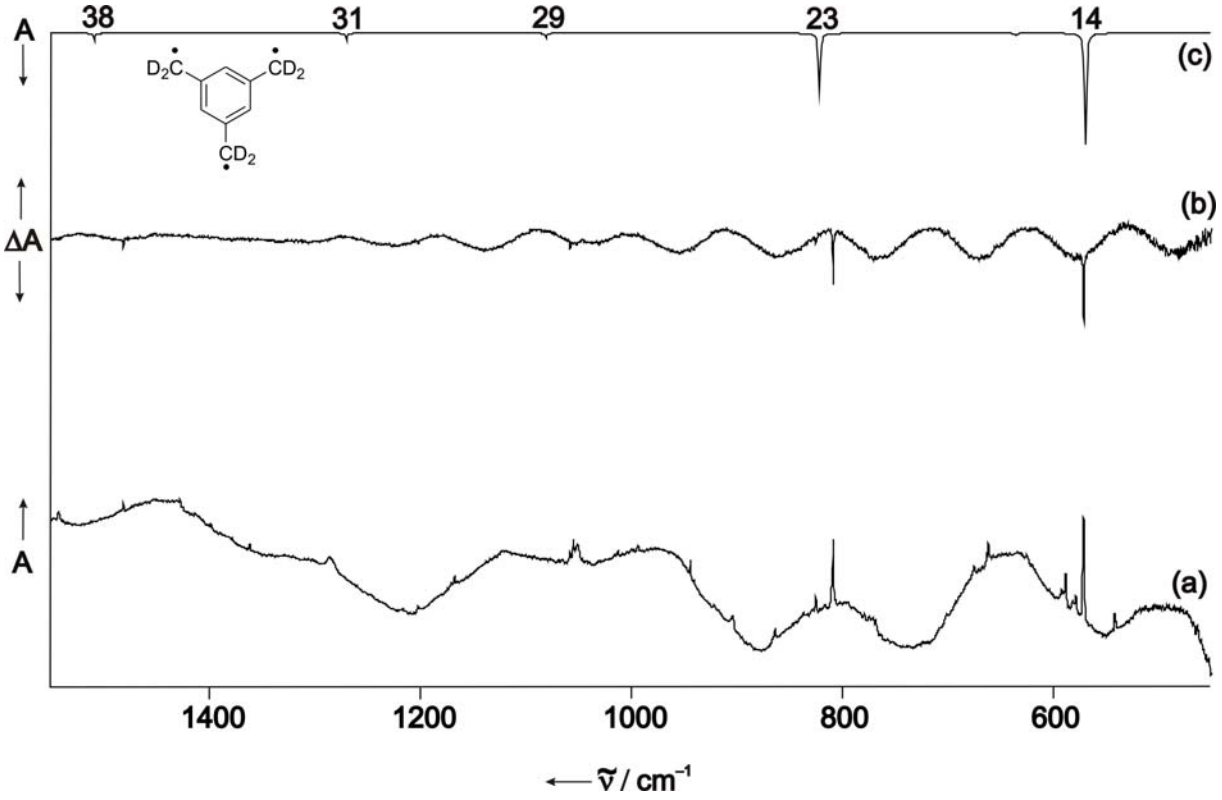

Figure 44. (a) Infrared spectrum obtained after FVP at 480°C of 1,3,5-*tris*-(iodomethyl)benzene-d_6 **26**-d_6. (b) Difference spectrum of the same matrix after photolysis with λ = 450 – 360 nm of a high-pressure mercury lamp. (c) UB3LYP/6-311+G** calculated infrared spectrum of quartet triradical 1,3,5-trimethylenebenzene-d_6 **26**-d_6.

The changes can be followed with the help of calculations which are able to predict the change in intensity and signal position not only from the hydrogenated and the deuterated quartet triradical **2** and **2**-d_6, respectively, but also for hypothetical nuclear masses of 1.1, 1.2, etc.. The variation in the infrared spectrum upon successive increase of the nuclear mass of all exocyclic hydrogen atoms from 1.0 (hydrogen) to 2.0 (deuterium) is shown in Figure 45.

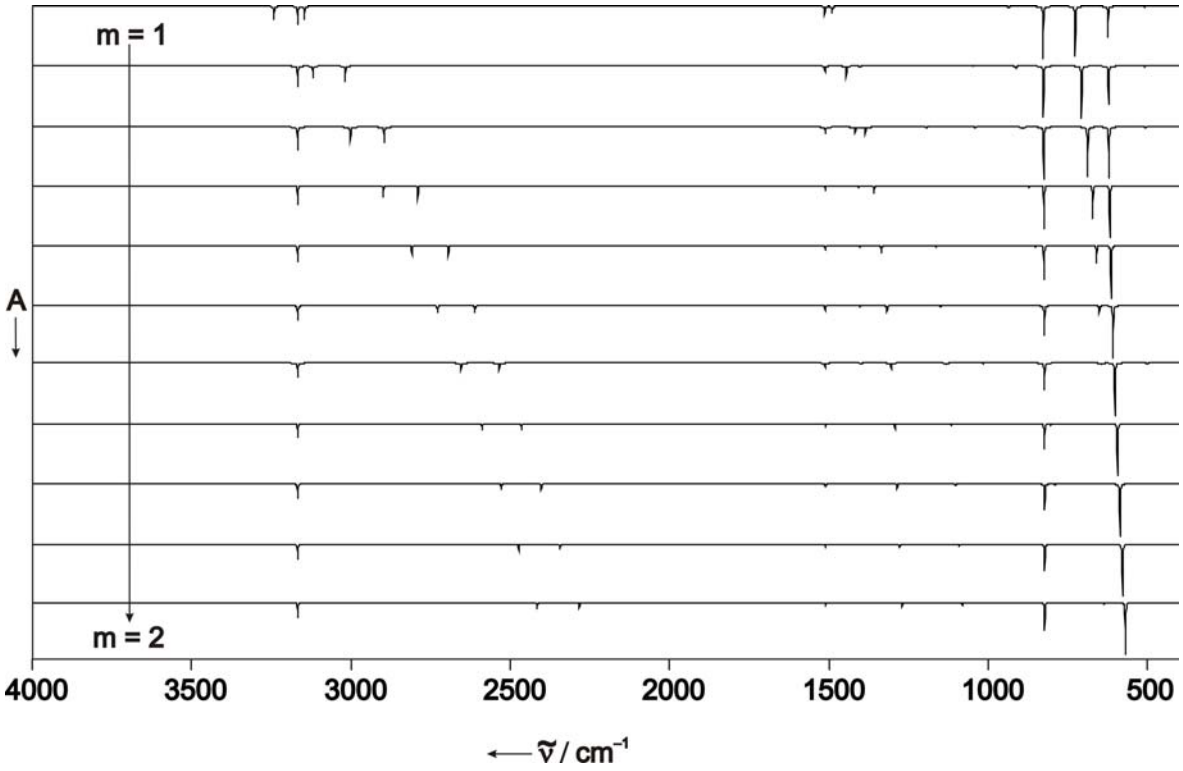

Figure 45. (a) UB3LYP/6-311+G** calculated infrared spectrum for quartet triradical **2**. (b) UB3LYP/6-311+G** calculated infrared spectrum for hexadeuterated quartet triradical **2**-d_6. In between is shown the effect on the infrared spectrum by successively increasing the nuclear mass in steps of 0.1 atomic mass unit.

The most obvious change in the infrared spectrum is observed for the vibrations between 600 cm^{-1} and 800 cm^{-1} which can be assigned to oop C-H deformation vibrations of the methylene and ring hydrogen atoms, respectively. The three intense oop vibrations in the nondeuterated triradical **2** correlate with only two intense oop vibrations in the deuterated triradical **2**-d_6. Apparently, one oop vibration is remarkably decreasing in intensity upon exocyclic deuteration.

As expected, the experimentally observed phenyl C-H oop vibration at 814.7 cm^{-1} shows only a small isotopic shift of 5.7 cm^{-1} in excellent accord with the calculated isotopic shift of 5.1 cm^{-1} (Figure 46).

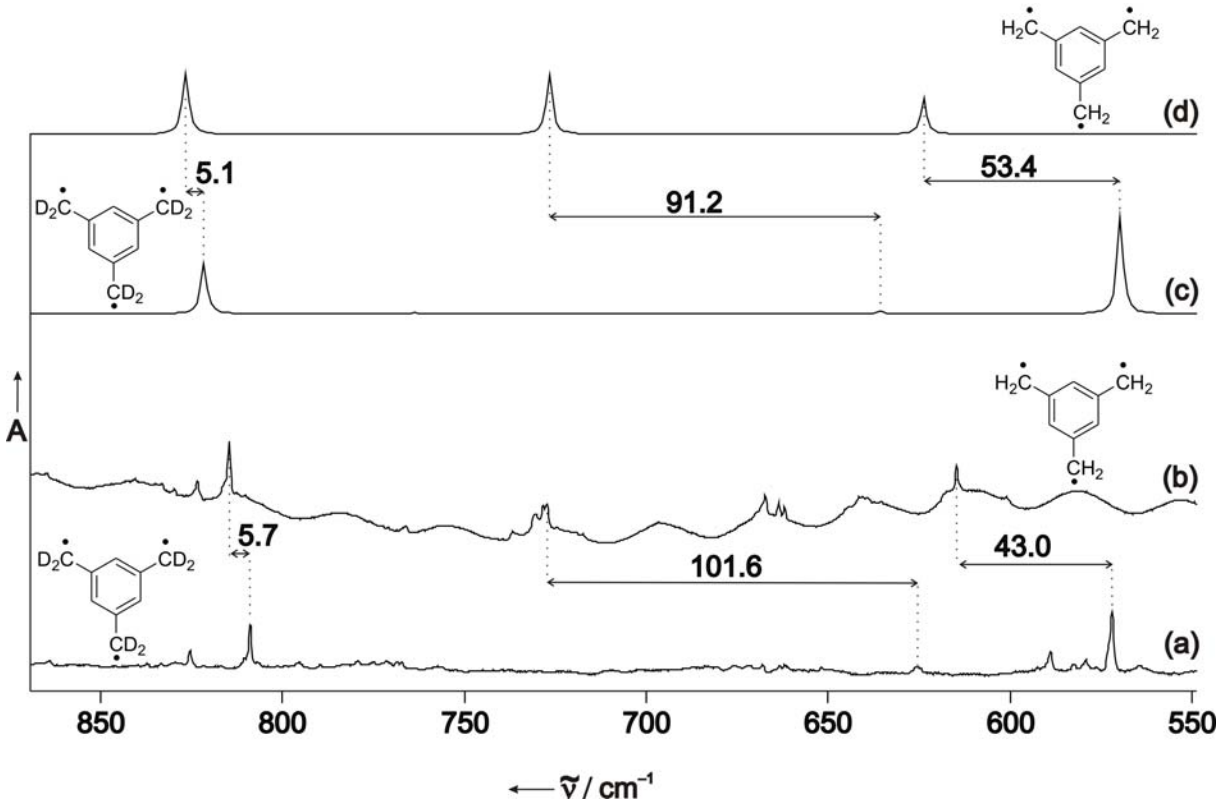

Figure 46. (a) Infrared spectrum obtained after FVP at 480°C of 1,3,5-*tris*-(iodomethyl)benzene-d_6 **26**-d_6. (b) Infrared spectrum obtained after FVP at 480°C of 1,3,5-*tris*-(iodomethyl)benzene **26**. (c) Calculated infrared spectrum of deuterated quartet 1,3,5-trimethylenebenzene triradical **2**-d_6. (d) Calculated infrared spectrum of quartet 1,3,5-trimethylenebenzene **2**.

The largest isotopic shift of 101.6 cm^{-1} is found for the exocyclic C-H oop vibration at 727.3 cm^{-1}, which drastically diminishes in intensity (calculated rel. intensity C_9H_9 : $C_9H_3D_6$; 96: 3). A closer look at this vibration reveals that the reason for this is the anticyclic relative phase of the methylene hydrogens compared to the ring hydrogen atoms (Figure 47).

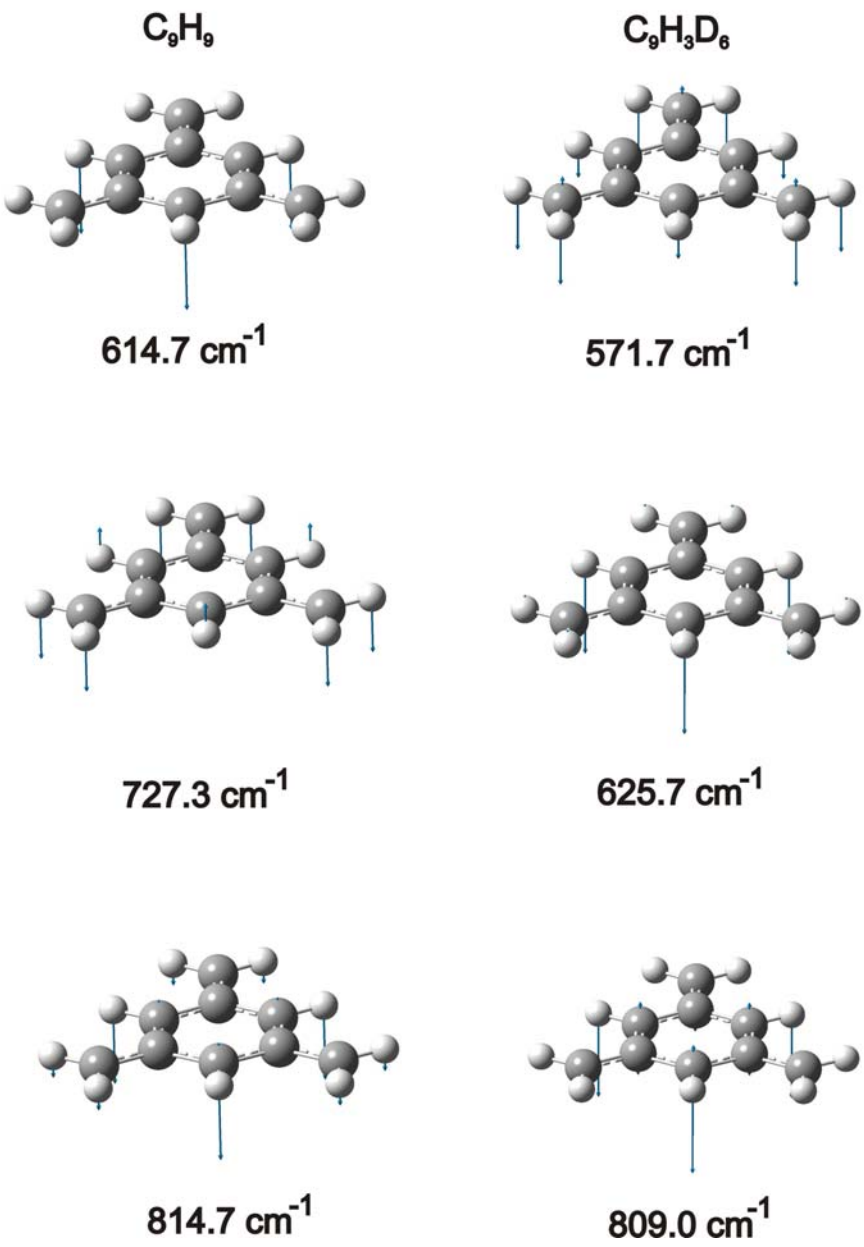

Figure 47. The three most intense A_2'' oop vibrations of 1,3,5-trimethylenebenzene **2** and the corresponding vibrations of deuterated triradical **2**-d_6.

This isotopic effect results in a fortuitous cancellation of the change in dipole moment for the hexadeuterated triradical **2**-d_6 compared to triradical **2** due to the strong impact of the exocyclic methylene groups for this vibration (a hypothetical hexatritium derivative would have an higher intensity for this vibration again). The predicted shift is 91.2 cm^{-1}. The third strong vibration at 614.7 cm^{-1} shows a medium shift of 43.0 cm^{-1} upon isotopic labelling, in good accordance with the calculated value of 53.4 cm^{-1}. While this vibration is mainly composed of C-H ring hydrogen oop movement in triradical **2**, the methylene hydrogens show the largest vibrational displacement in its isotopomer **2**-d_6. All

assigned infrared signals observed in the argon matrix for quartet triradical **2** are summarized in Table 16.

Table 16. Infrared spectroscopic data for the quartet state of 1,3,5-trimethylenebenzene **2** and **2**-d_6.

Mode #	Sym.	Argon [b]	B3LYP [a]	Argon [b] **d_6**	B3LYP [a] **d_6**	Assignment	$\Delta\nu_{exp}$ ($\Delta\nu_{calc}$)
14	A_2"	614.7 (75)	624.1 (58)	571.7 (100)	570.7 (100)	C_3-H out-of-plane deformation	43.0 (53.4)
16	A_2"	727.3 (65)	727.4 (96)	625.7 (1)	636.2 (3)	C_1-H_2 out-of-plane deformation	101.6 (91.2)
21	A_2"	814.7 (100)	827.9 (99)	809.0 (60)	822.8 (53)	C_3-H out-of-plane deformation	5.7 (5.1)
22	E'	926.3 (2)	936.3 (2)	- [c]	764.8 (1)	C_1-H_2 rocking	(171.5)
28	E'	-	1214.9 (0)	1058.0 (5)	1081.1 (3)	C_1-H_2 scissoring, C_3-H in-plane deformation	(133.8)
35	E'	1462.6 (5)	1490.2 (7)	1246.3 (1)	1270.1 (4)	C_1-H_2 scissoring, C_1=C_2 stretching, C_3-H in-plane deformation	216.3 (220.1)
38	E'	1478.3 (5)	1512.5 (8)	1481.3 (5)	1509.4 (4)	C_1=C_2 stretching, C_1-H_2 scissoring, C_3-H in-plane deformation	- 3.0 (3.1)
41	E'	3018.9 (10)	3145.3 (12)	2214.9 (5)	2284.0 (5)	symmetric C_1-H_2 stretching	804.0 (861.3)
43	E'	3038.0 (10)	3167.8 (18)	3039.4 (5)	3167.7 (15)	C_3-H stretching	- 1.4 (0.1)
47	E'	3111.6 (10)	3241.7 (13)	- [c]	2416.5 (6)	asymmetric C_1-H_2 stretching	(825.2)

[a] UB3LYP/6-311+G**. [b] Argon, 10 K. [c] not assigned due to the overlap with a more intense signal in the vicinity.

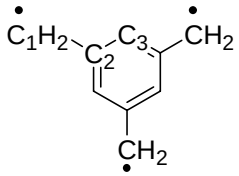

Scheme 83. Numbering of 1,3,5-trimethylenebenzene triradical **2**.

Further support for the assignment of the observed bands to the triradical **2** is given by the finding, that photolysis of the products obtained after FVP of 1,3,5-*tris*-(iodomethyl)benzene **26** in an argon matrix at 10 K with 308 nm monochromatic light of a XeCl excimer laser, produces small amounts of quartet triradical **2** from an unknown pyrolysis product. This finding is in accord with the behaviour of 1,3,5-*tris*-(iodomethyl)benzene **26** under photolysis with 308 nm of the same light source, as quartet signals are increasing upon irradiation as monitored by the sensitive electron paramagnetic resonance spectroscopy (no new signals are appearing in the infrared spectrum after photolysis with 308 nm of a XeCl laser, while 1,3,5-*tris*-(iodomethyl)benzene **26** is photolabile under these conditions).

In order to clarify if hydrogen abstraction is taking place during the FVP of 1,3,5-*tris*-(iodomethyl)benzene **26** at 500°C, additional infrared experiments with possible precursors of the corresponding mono- and diradical were performed. As C-I bonds in benzyl position are quite weak and can be easily cleaved in a homolytic fashion at higher temperatures, 3,5-*bis*-methylbenzyl iodide **30** and 5-methyl-1,3-*bis*-(iodomethyl)benzene **29** were chosen as precursors for 3,5-*bis*-methylbenzyl radical **28** and 5-methyl-*m*-xylylene **27**, respectively. The infrared spectrum obtained after FVP of 1,3,5-*tris*-(iodomethyl)benzene **26** at 550°C is shown in Figure 48.

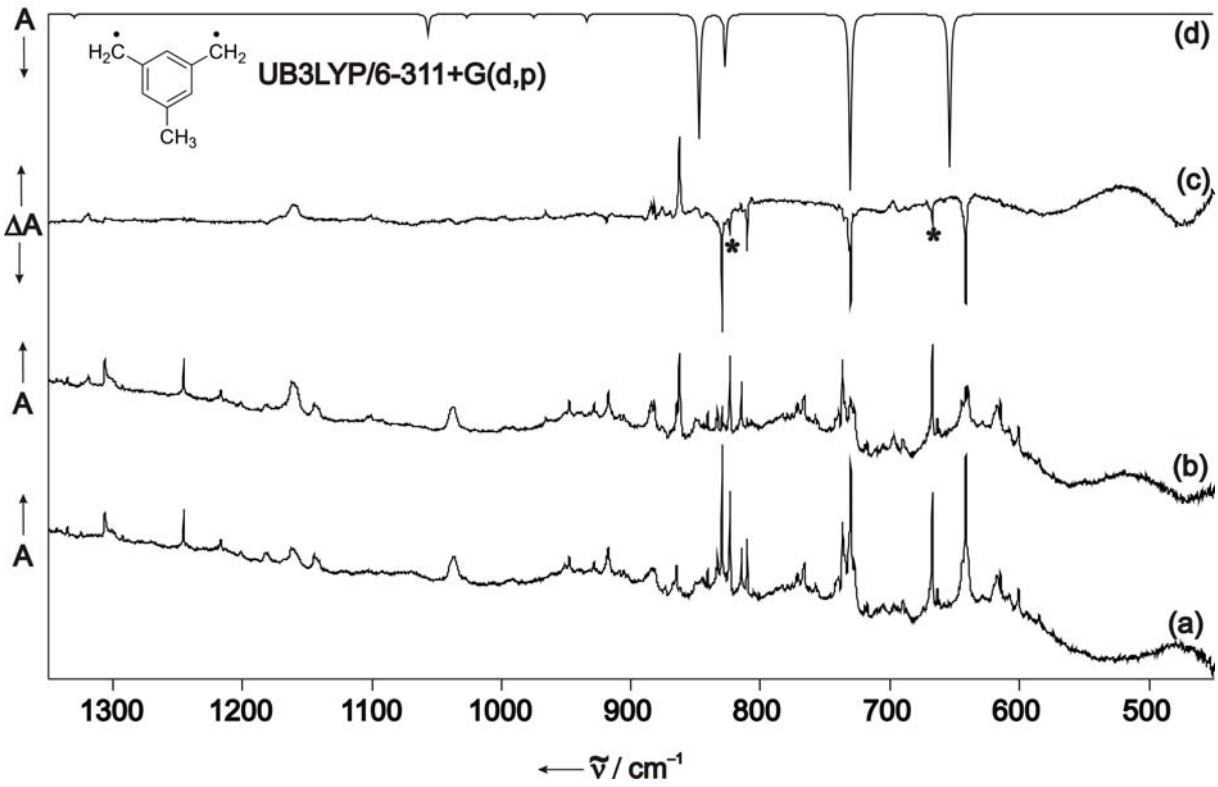

Figure 48. (a) IR spectrum obtained after FVP of 1,3,5-*tris*-(iodomethyl)benzene **26** at 550°C. (b) The same matrix after photolysis with a high-pressure mercury lamp and λ = 450-400 nm. (c) The resulting difference spectrum (a) - (b), peaks showing upwards are increasing in intensity upon irradiation with λ = 450-400 nm and peaks showing downwards are decreasing in intensity upon irradiation. (d) UB3LYP/6-311+G(d,p) calculated IR spectrum for triplet 5-methyl-*m*-xylylene **27**. Peaks denoted with a star belong to 3,5-*bis*-methylbenzyl radical **28**.

Apparently, at higher FVP temperature some additional products are formed and trapped in the matrix at low temperature. The main substance formed during this experiment is triplet 5-methyl-*m*-xylylene **27**. As was discussed above, the most intense signals belong to the oop vibrations of the methylene and ring hydrogens, respectively. The triplet 5-methyl-*m*-xylylene **27** diradical could be distinguished from the other products due to relative selective photobleaching of the argon matrix. After irradiation with 450 – 400 nm of a high-pressure mercury lamp, mostly the signals of triplet 5-methyl-*m*-xylylene diradical **27** were decreasing together with a small amount of 3,5-*bis*-methylbenzyl radical **28**. In an independent experiment, the starred signals were found after trapping the products of the FVP of 5-methyl-1,3-*bis*-(iodomethyl)benzene **29** at 10 K. It can be seen in this spectrum, the pyrolysis of **29** furnishes a mixture of triplet 5-methyl-*m*-xylylene diradical **27** together with the same product formed from 1,3,5-*tris*-(iodomethyl)benzene **26** at high temperature, namely 3,5-*bis*-methylbenzyl radical **28** (Figure 49).

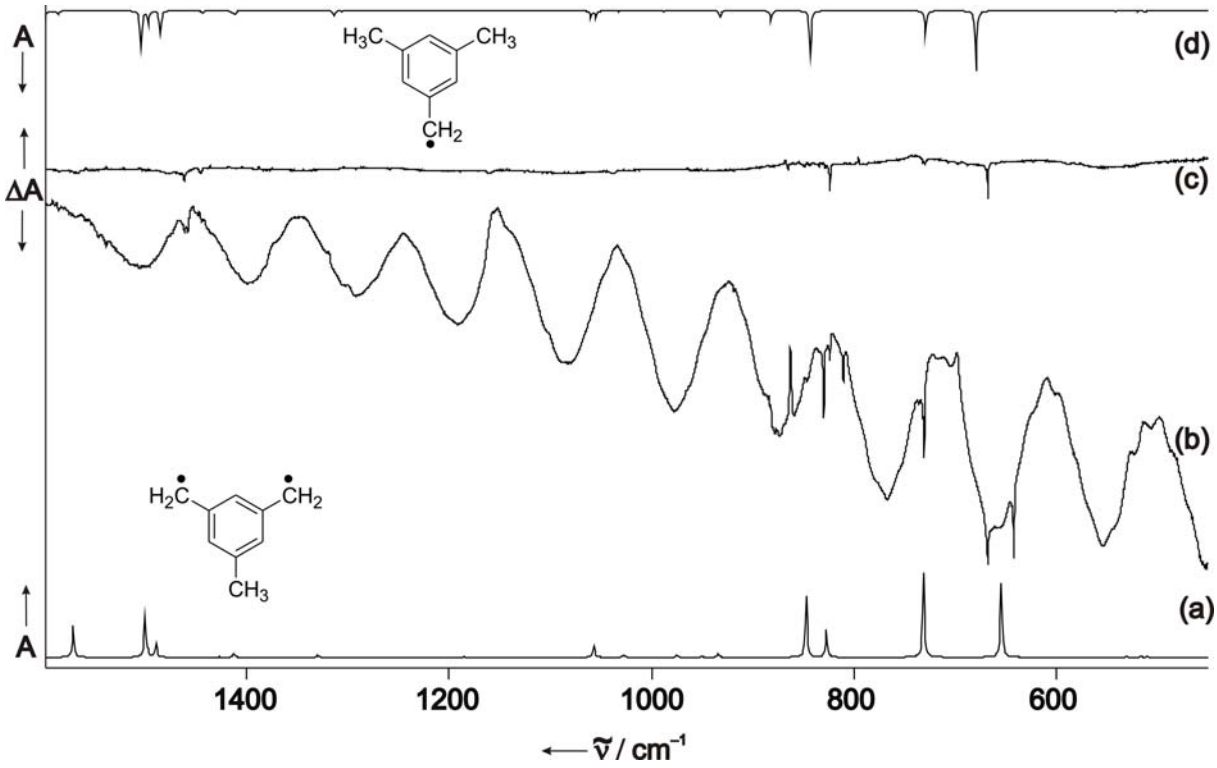

Figure 49. (a) UB3LYP/6-311+G(d,p) calculated IR spectrum for triplet 5-methyl-*m*-xylylene **27**. (b) Infrared difference spectrum obtained after FVP of 5-methyl-1,3-*bis*-(iodomethyl)benzene **29** at 450°C and photolysis with a high-pressure mercury arc lamp with λ = 450-400 nm. Peaks showing upwards are increasing in intensity and peaks showing downwards are decreasing in intensity upon irradiation. (c) Infrared difference spectrum obtained after FVP of 3,5-*bis*-methylbenzyl iodide **30** at 580°C and photolysis with λ = 308 nm and 10 Hz of a XeCl-excimer laser. Peaks showing upwards are increasing in intensity and peaks showing downwards are decreasing in intensity upon irradiation. (d) UB3LYP/6-311+G(d,p) calculated infrared spectrum for doublet 3,5-*bis*-methylbenzyl radical **28**.

An expansion of the spectrum showing only the most intense signals is given in Figure 50 to help to identify the observed reactive species (Figure 50).

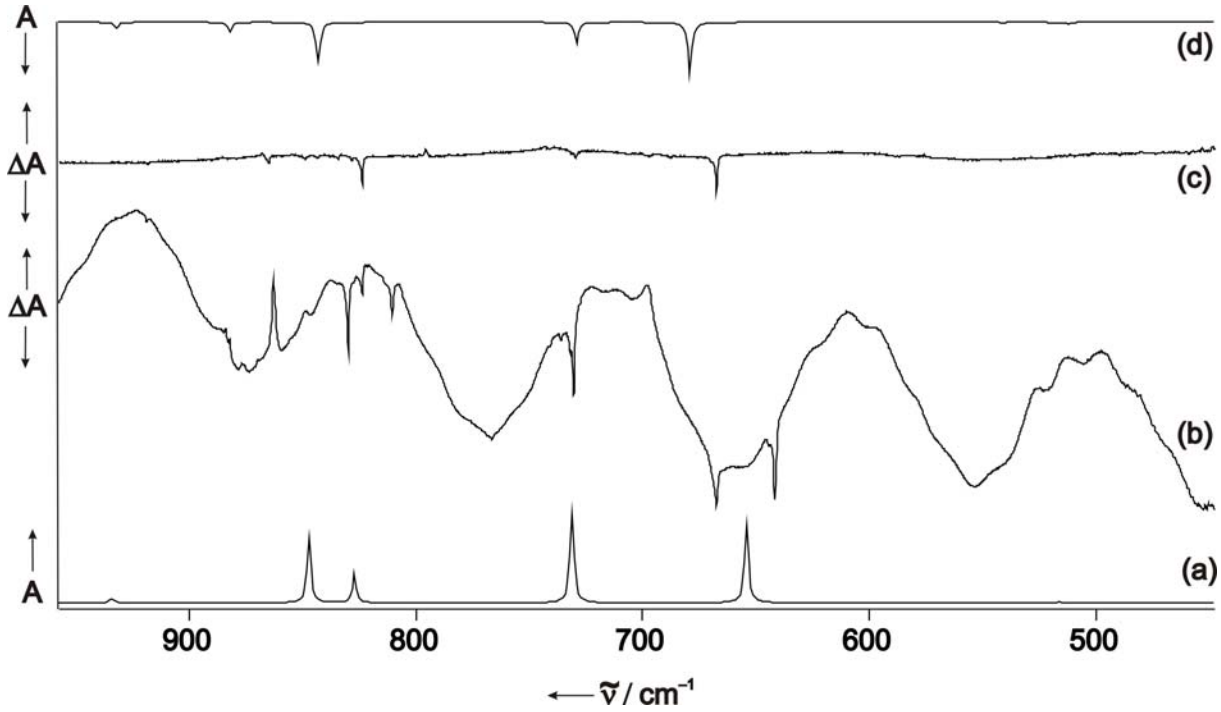

Figure 50. (a) UB3LYP/6-311+G(d,p) calculated IR spectrum for triplet 5-methyl-*m*-xylylene **27**. (b) Infrared difference spectrum obtained after FVP of 5-methyl-1,3-*bis*-(iodomethyl)benzene **29** at 450°C and photolysis with a high-pressure mercury arc lamp with λ = 450-400 nm. Peaks showing upwards are increasing in intensity and peaks showing downwards are decreasing in intensity upon irradiation. (c) Infrared difference spectrum obtained after FVP of 3,5-*bis*-methylbenzyl iodide **30** at 580°C and photolysis with λ = 308 nm and 10 Hz of a XeCl-excimer laser. Peaks showing upwards are increasing in intensity and peaks showing downwards are decreasing in intensity upon irradiation. (d) UB3LYP/6-311+G(d,p) calculated infrared spectrum for doublet 3,5-*bis*-methylbenzyl radical **28**.

The photochemistry of 5-methyl-*m*-xylylene **27** seems to be similar to the photochemistry of *m*-xylylene **1** as it is shown in Figure 51.

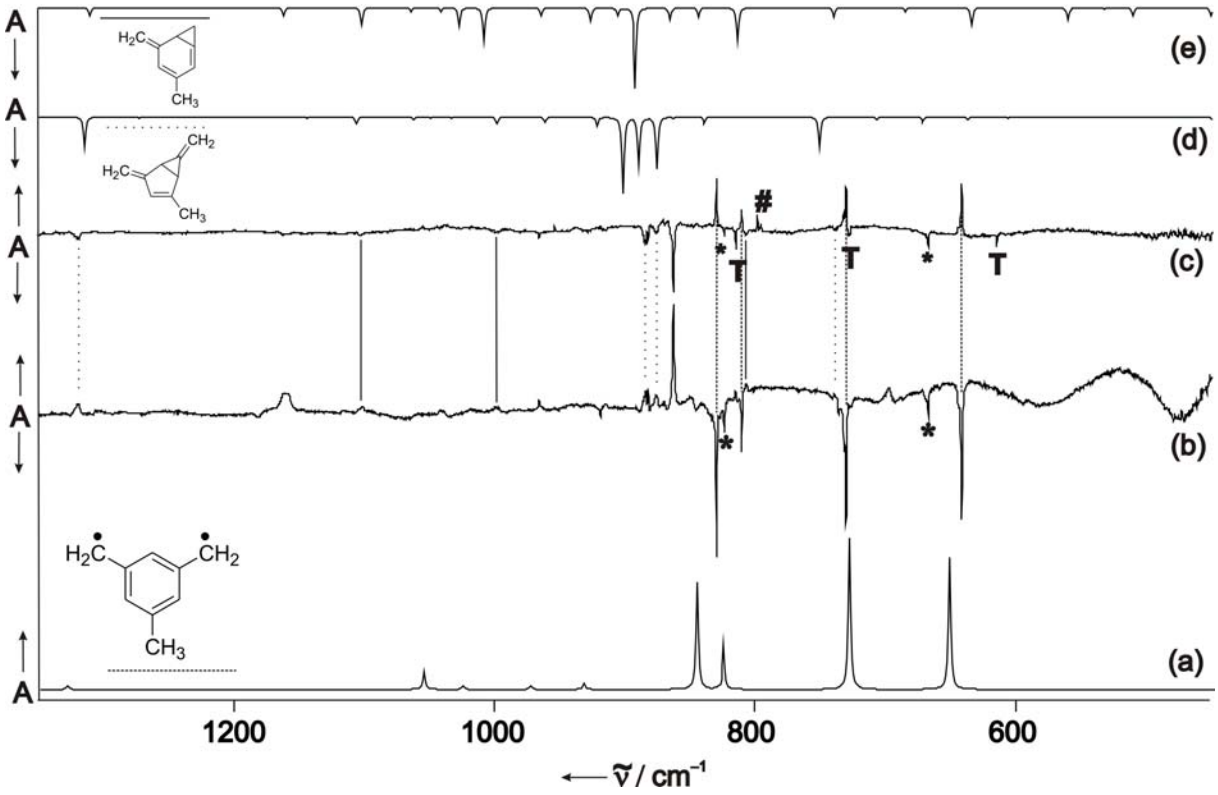

Figure 51. (a) UB3LYP/6-311+G(d,p) calculated infrared spectrum for triplet 5-methyl-*m*-xylylene **27**. (b) Infrared difference spectrum obtained after FVP of **29** with peaks showing upwards are increasing in intensity and peaks showing downwards are decreasing in intensity upon irradiation and are assigned to the triplet diradical **27**. Stars denote peaks which belong to the benzyl radical **28**. (c) Infrared difference spectrum obtained after photolysis of the same matrix as before with λ = 254 nm of a mercury low-pressure lamp. Peaks showing upwards are increasing in intensity upon irradiation and are assigned to the diradical **27** and peaks showing downwards are decreasing in intensity upon irradiation. Stars denote peaks belonging to the benzyl radical **28** while peaks assigned with a T belong to the quartet triradical **2** and the peak denoted with a route is a "ghost peak" not belonging to the substance but appearing due to the long irradiation times. (d) and e) UB3LYP/6-311+G(d,p) calculated infrared spectra for two possible isomers of the parent diradical.

The products trapped after FVP of 3,5-*bis*-methylbenzyl iodide **30** at 580°C is mostly the corresponding doublet 3,5-*bis*-methylbenzyl radical **28**. It was found to show selective photochemistry, as a matrix containing the FVP products of 3,5-*bis*-methylbenzyl iodide **30** was irradiated with 254 nm of a low-pressure mercury lamp and all signals belonging to 3,5-*bis*-methylbenzyl radical **28** are decreasing in intensity (Figure 52).

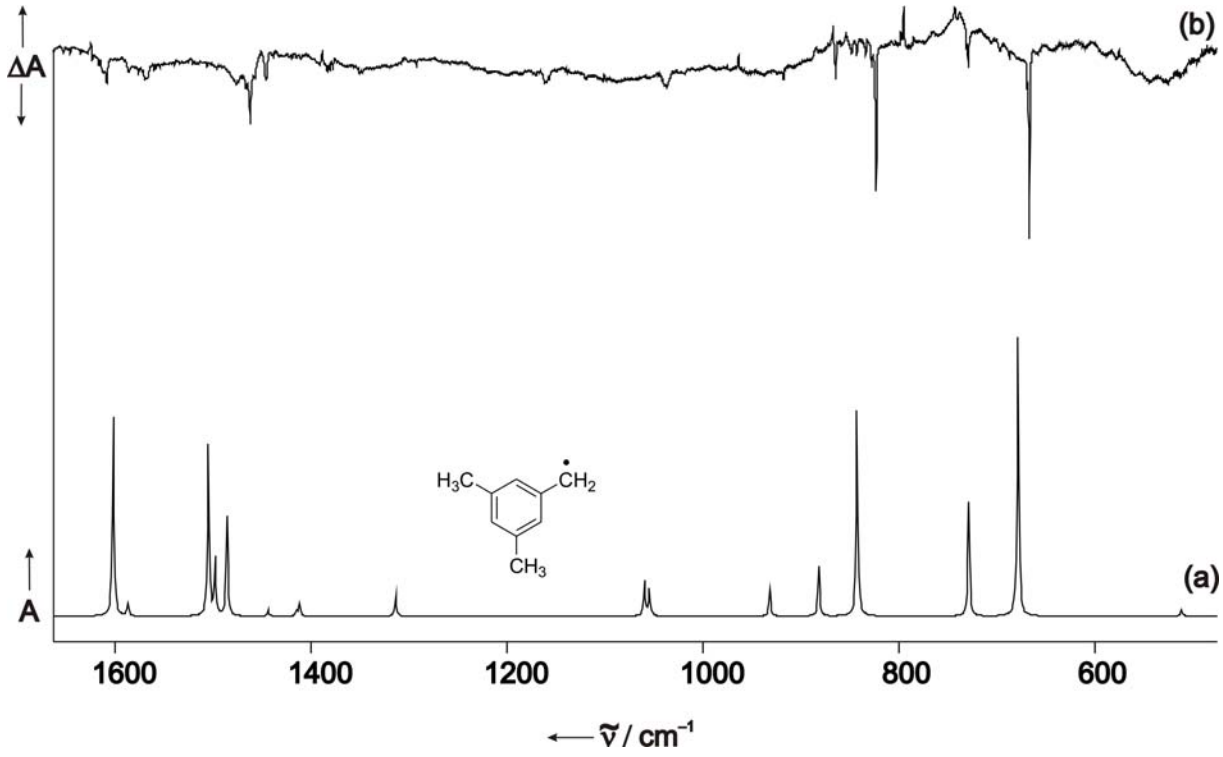

Figure 52. (a) UB3LYP/cc-pVTZ calculated infrared spectrum for doublet 3,5-*bis*-methylbenzyl radical **28**. (b) Infrared difference spectrum obtained after photolysis of an argon matrix containing the FVP products of 3,5-*bis*-methylbenzyl iodide **30** (580°C FVP temperature), Ar, 10K. Peaks showing upwards are increasing in intensity and peaks showing downwards are decreasing in intensity upon irradiation.

The corresponding infrared signals for triplet 5-methyl-*m*-xylylene **27** and doublet 3,5-*bis*-methylbenzyl radical **28** are summarized in Table 17.

Table 17. Observed and calculated infrared signals for triplet 5-methyl-*m*-xylylene **27** and doublet 3,5,-*bis*-methylbenzyl radical **28**.

Mode #	Sym.	Argon [b] **27**	B3LYP [a] **27**	Argon [b] **28**	B3LYP [a] **28**
10	A'	-(-)	510.2 (1)	-(-)	513.0 (3)
11	A"	-(-)	516.3 (1)	-(-)	519.4 (1)
13	A'	-(-)	530.2 (1)	-(-)	541.0 (1)
15	A'	641.6 (90)	654.3 (88)	667.3 (100)	679.7 (97)
16	A'	730.3 (100)	731.8 (100)	729.3 (30)	729.9 (40)
17	A'	810.2 (30)	827.6 (32)	823.5 (90)	843.4 (73)
19	A'	829.7 (90)	847.2 (73)	864.8 (15)	882.4 (17)
20	A'	-(-)	934.5 (5)	918.2 (5)	932.3 (11)

22	A"	-(-)	950.9 (1)	-(-)	988.8 (1)
24	A'	-(-)	975.1 (3)	-(-)	1032.4 (1)
25	A'	-(-)	1027.1 (2)	1036.8 (5)	1055.3 (11)
27	A"	-(-)	1028.5 (1)	1039.9 (5)	1060.3 (12)
30	A'	1043.4 (5)	1057.7 (13)	-(-)	1306.5 (1)
31	A'	-(-)	1330.7 (3)	1292.4 (5)	1314.1 (9)
33	A'	-(-)	1413.8 (5)	1377.9 (2)	1412.6 (6)
34	A'	1448.5 (10)	1490.8 (15)	1381.1 (2)	1415.3 (5)
35	A'	-(-)	1498.9 (5)	-(-)	1443.1 (1)
36	A"	1458.7 (25)	1501.8 (47)	1414.7 (2)	1444.2 (4)
37	A'	1547.1 (10)	1572.0 (38)	1445.2 (15)	1486.2 (36)
40	A'	2933.2 (20)	3024.2 (60)	1458.3 (5)	1498.7 (21)
41	A'	2964.0 (20)	3078.7 (38)	1462.1 (30)	1505.1 (60)
42		2981.2 (15)	3102.8 (29)	- (-)	1587.9 (7)
43	A'	c	3143.9 (7)	1569.9 (25)	1602.8 (70)
44	A"	3019.7 (15)	3144.3 (20)	2934.5 (20)	3023.1 (99)
45	A"	3035.8 (20)	3159.9 (35)	c	3023.8 (60)
47	A'	3037.8 (10)	3161.7 (28)	2965.2 (30)	3072.1 (83)
48	A'	3043.9 (5)	3166.3 (10)	2980.3 (15)	3102.2 (45)
49	A"	c	3240.2 (8)	c	3102.5 (35)
50	A'	3111.3 (15)	3240.4 (24)	c	3143.0 (18)
51				3019.7 (20)	3147.8 (38)
52				3030.0 (15)	3156.6 (56)
53				c	3159.3 (12)
54				3110.5 (5)	3239.3 (23)

[a] UB3LYP/6-311+G(d,p). [b] Argon, 10 K. [c] Not assigned due to a stronger signal in the vicinity of this signal.

7.4 EPR spectroscopy of quartet 1,3,5-trimethylenebenzene

High-spin states like quartet 1,3,5-trimethylenebenzene **2** can conveniently be studied also by EPR spectroscopy, as this method is quite sensitive and selective towards open-shell molecules. Photolysis of 1,3,5-*tris*-(iodomethyl)benzene **26**, matrix isolated in

argon at 4 K, with 308 nm of a XeCl excimer laser furnishes a centrosymmetric five-line EPR spectrum, which is centered at 3427 G (Figure 53).

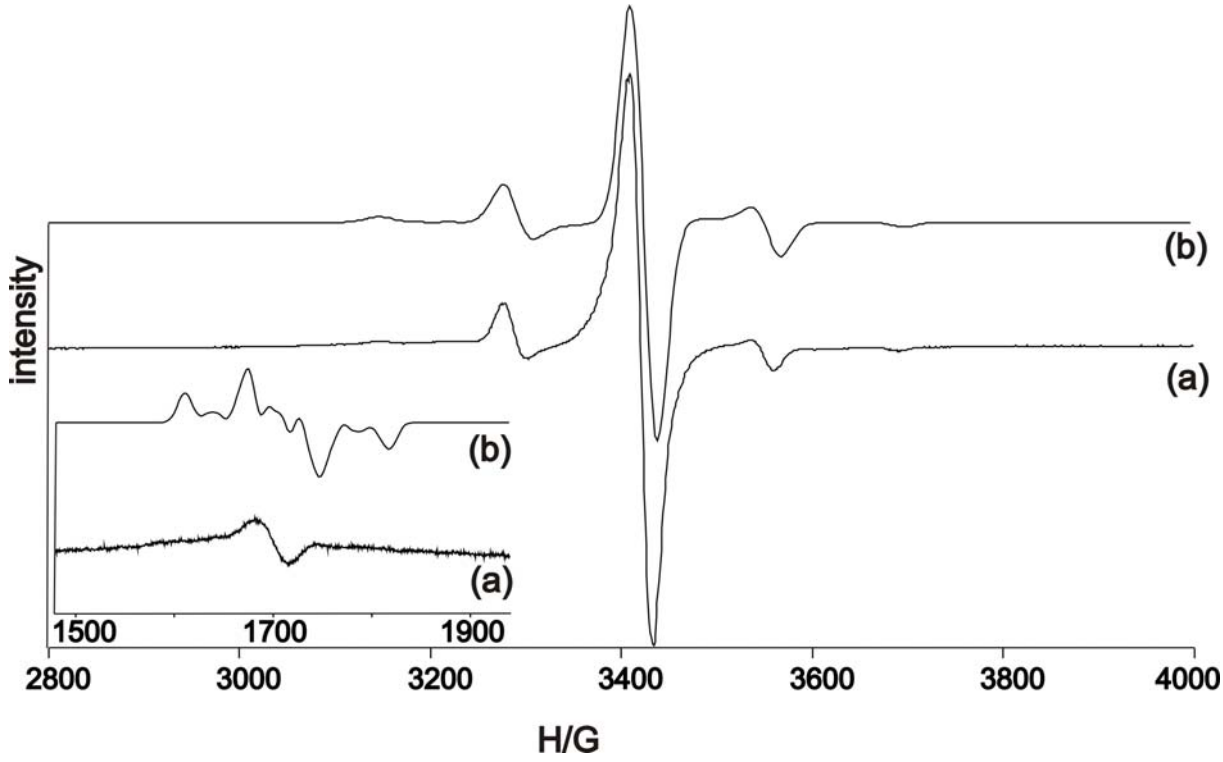

Figure 53. (a) EPR spectrum obtained after photolysis of 1,3,5-*tris*-(iodomethyl)benzene **26** with 308 nm of a XeCl excimer laser (1 Hz). (b) Simulated quartet EPR spectrum with $|D/hc|= 0.0128\ cm^{-1}$, $|E/hc|= 0\ cm^{-1}$, S = 3/2, ν = 9.58682 GHz.

The spectrum is persistent for days without a change at this temperature. A half field signal at 1702 G is also observable after irradiation of the matrix, a precondition for species with more than one ferromagnetically coupled electron. The simple five line spectrum can be assigned to the z and xy signals of a randomly oriented quartet molecule having a threefold or higher symmetry axis ($E = 0\ cm^{-1}$) in close resemblance to other quartet molecules with high symmetry as well as theory (Figure 54).[128, 134-140]

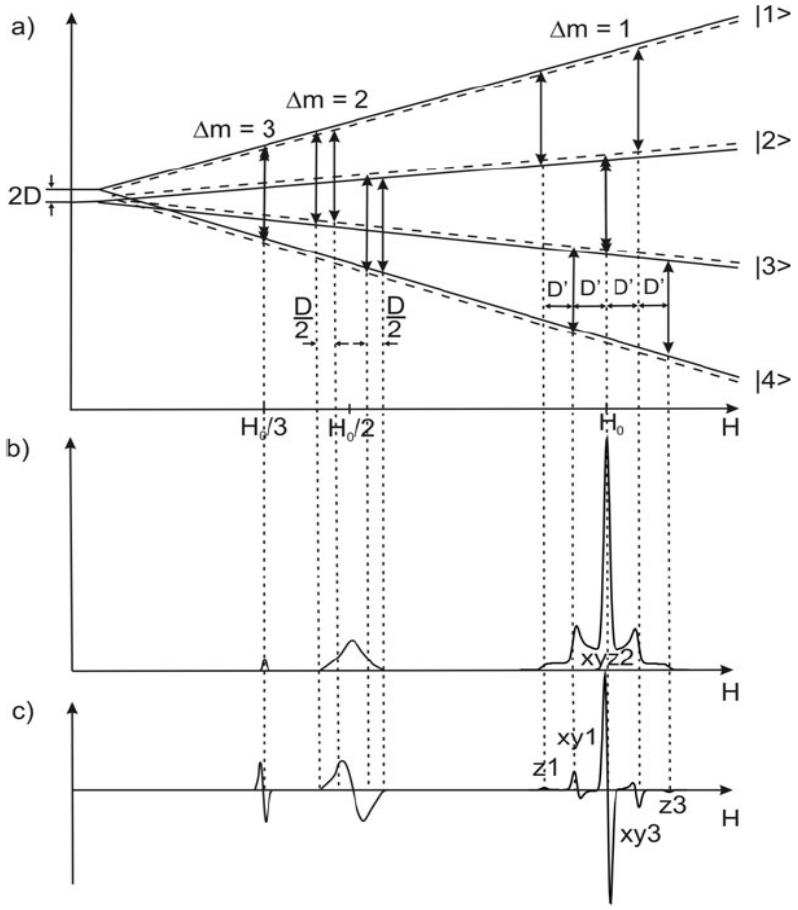

Figure 54. Theoretical calculated EPR spectrum by Brickmann et al. for quartet triradicals with an axis of threefold symmetry and a small D value.[134] a) Energy level splitting. b) absorption spectrum. c) First derivative spectrum.

Simulation, using the XSophe software, with the zero-field parameters |D/hc| = 0.0128 cm^{-1} and |E/hc| = 0 cm^{-1} gives the best accordance to the experimental low temperature X-band EPR spectrum. Exactly the same spectrum, superimposed with some amounts of other paramagnetic species, is obtained after trapping of the FVP products of **26** at 4 K in argon (Figure 55).

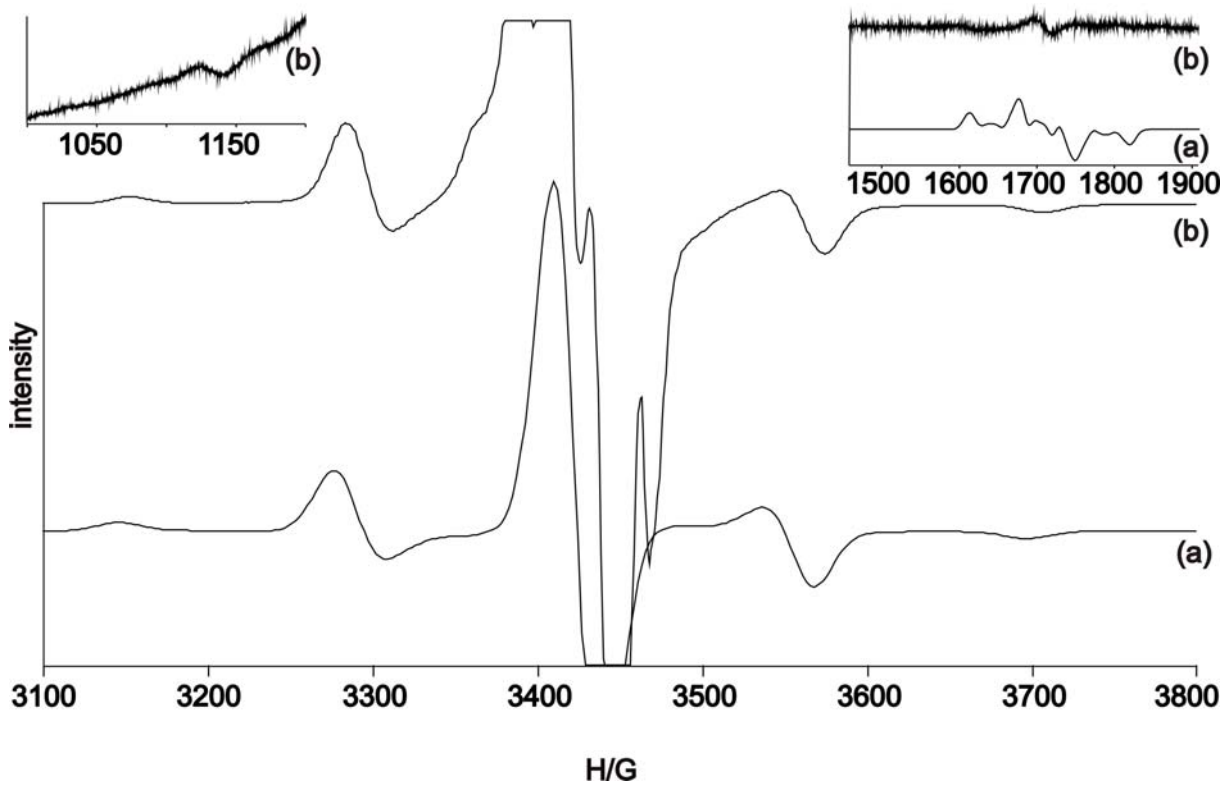

Figure 55. Experimental (a) and calculated (b) EPR spectra for quartet triradical **2** obtained after FVP of 1,3,5-*tris*-(iodomethyl)benzene **26**. The insets show the half-field signal at 1700 G and the Δm_s = +/-3 transition at 1130 G.

One advantage of the FVP with 1,3,5-*tris*-(iodomethyl)benzene **26** to produce quartet 1,3,5-trimethylenebenzene **2** in contrast to the irradiation of 1,3,5-*tris*-(iodomethyl)benzene **26** is the possibility to get much higher yields of the reactive triradical **2**, as filtering effects of the matrix limit the amount of quartet triradical **2** photochemically produced**.** On the other hand, photochemical cleavage of the weak C-I bonds clearly has the advantage that no hydrogen abstraction products can be formed. Other radical species like doublet 3,5-*bis*-(iodomethyl)benzene **161** or triplet 5-(iodomethyl)-*m*-xylylene **162** are normally not detected in high amounts in the low-temperature matrix EPR measurements, as the heavy atom disturbs the EPR signal.[141] For the iodinated diphenylcarbenes, the *meta* and *para* isomer give nice detectable triplet carbene signals, while the signals for the *ortho* isomer are very weak. While the interaction with the iodine in the diphenylcarbene isomers is a sigma interaction (as long as through space interaction is neglected), this is not necessarily true for the 5-(iodomethyl)-*m*-xylylene **162**.

A half field signal at 1702 G and a very weak third field signal at 1130 G concomitantly appears together with the main signals at g = 2, if the FVP of 1,3,5-*tris*-

(iodomethyl)benzene **26** is performed for long times. The D value is only slightly different in a nitrogen compared to an argon matrix. When nitrogen is used as matrix gas, no hydrogen atom absorptions are appearing in the EPR spectrum after FVP of 1,3,5-*tris*-(iodomethyl)benzene **26**. No change in the quartet EPR spectrum was obtained, if the hexadeuterated triiodide **26**-d_6 was used instead of the nondeuterated compound.

It was not possible to simulate the z_1, z_3, xy_1, and xy_3 signals appearing in the experimental spectrum for a triplet species, ruling out the possibility that the half-field signal stems from a triplet impurity. Nonetheless, 5-methyl-*m*-xylylene **27** was investigated by FVP of 5-methyl-1,3-*bis*-(iodomethyl)benzene **29** and subsequent trapping of the products in an argon matrix at 4 K (Figure 56).

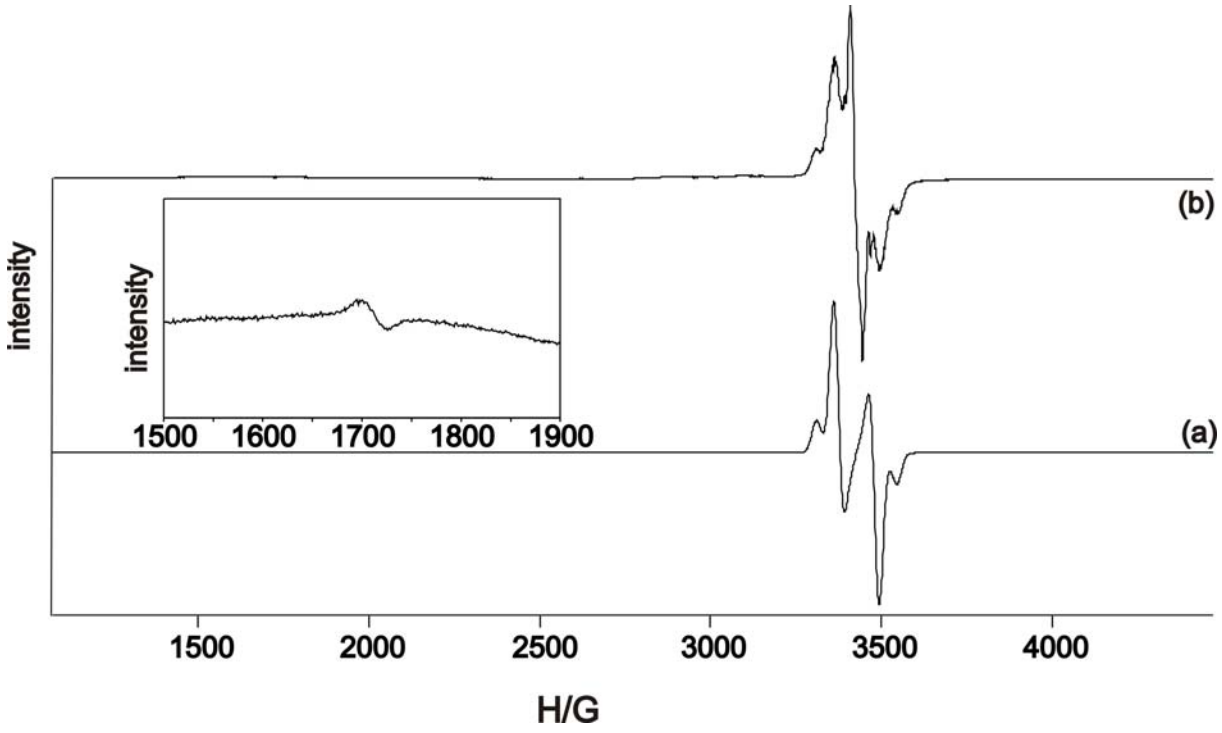

Figure 56. (a) Calculated EPR spectrum for a triplet species with D = 0.0111 cm^{-1} and E < 0.0009 cm^{-1}, ν = 9.608386 GHz. .(b) EPR spectra of triplet diradical **27** obtained after FVP of 5-methyl-1,3-*bis*-(iodomethyl)benzene **29**.

As can be expected, the substituent effect of one methyl group in relation to *m*-xylylene **1** has nearly no effect on the measured EPR spectrum as well as the ground state. The corresponding triplet EPR spectrum is shown in Figure 57 in comparison to the quartet triradical EPR spectrum of **2** and the doublet radical spectrum of 3,5-*bis*-methylbenzyl radical **28**. As expected, it can be observed that for higher spin multiplicities result in EPR spectra, which are extended over a larger magnetic field width (Figure 57).

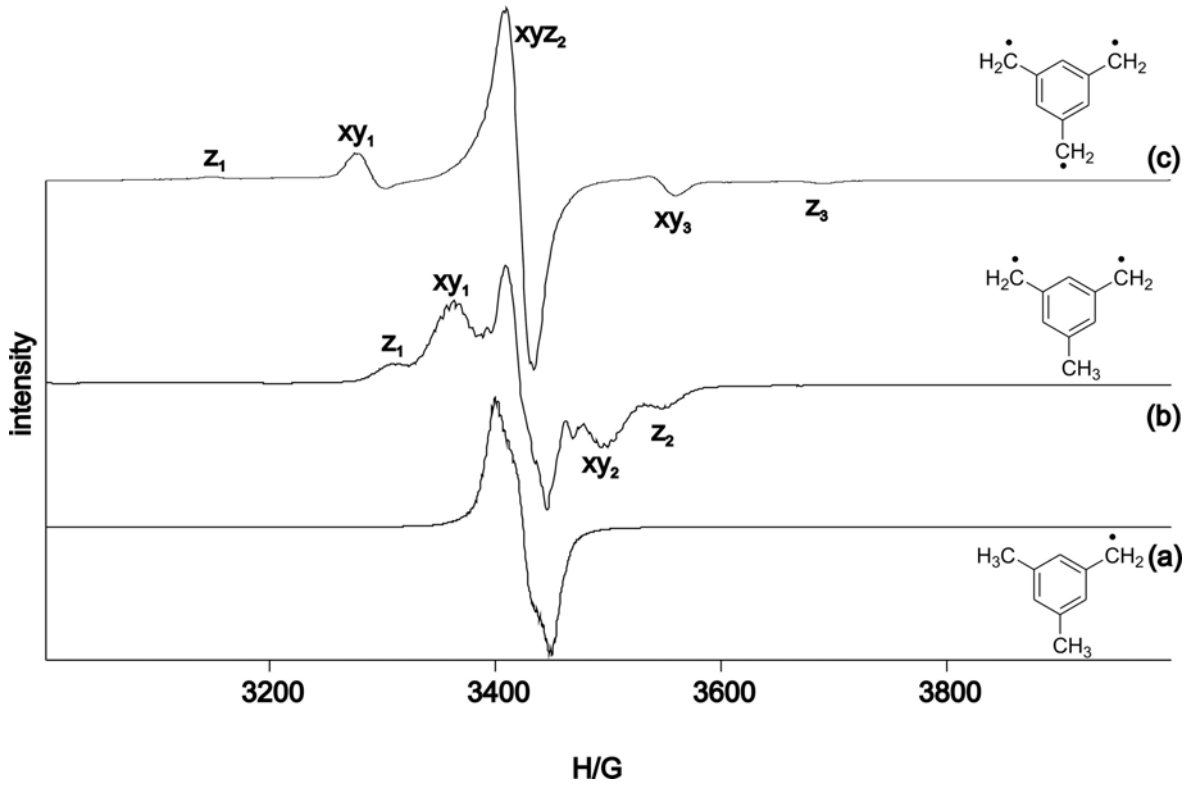

Figure 57. EPR spectra of quartet triradical **2** (c), triplet diradical **27** (b)**,** and doublet monoradical **28** (a).

Furthermore, it was not possible to detect a hyperfine splitting in the EPR spectrum of doublet 3,5-*bis*-methylbenzyl radical **28**, as in the low temperature powder spectrum the orientations of the atoms is not restricted to one specific direction and therefore it is often not possible to obtain hfs parameters, even so in other cases it is possible.[19, 30] The Curie analysis of the EPR signals is shown in Figure 58.

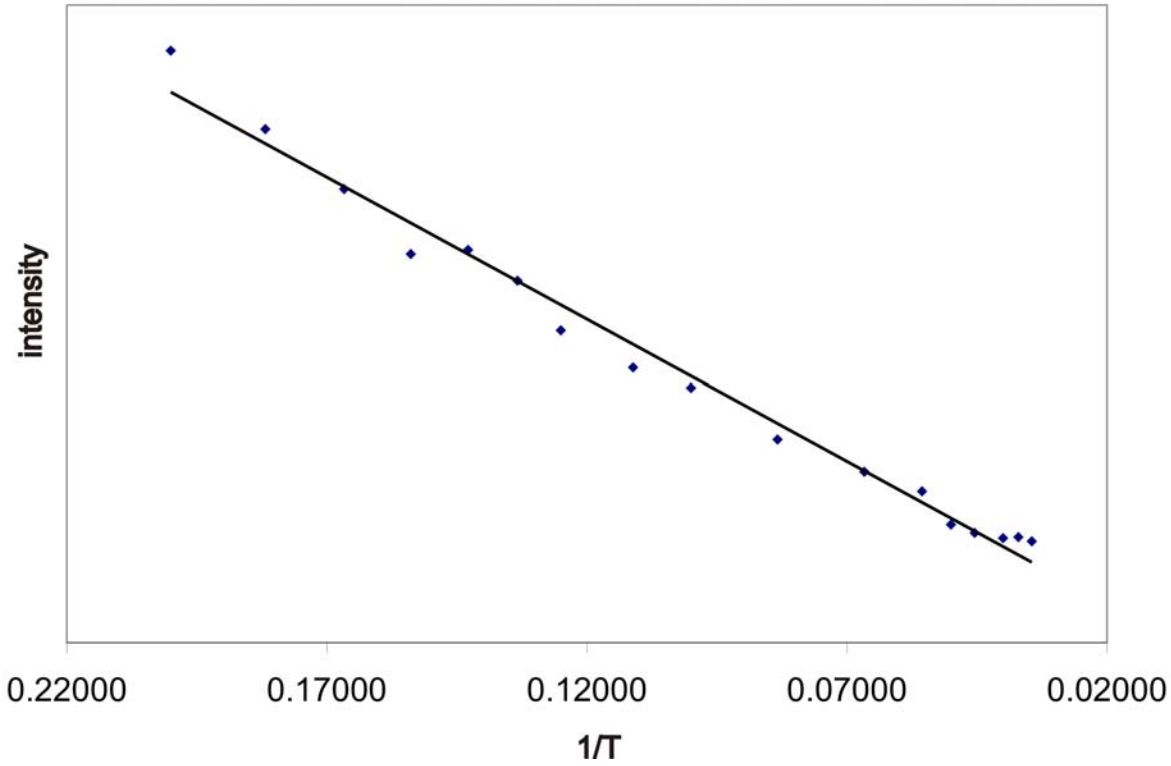

Figure 58. Curie-analysis of quartet triradical **2**.

The intensity of the EPR transition is found to be antiproportional to the temperature thus allowing to deduce that the quartet is the ground state or nearly degenerate with a doublet ground state. Since high-level *ab initio* multiconfigurational methods have found the quartet to be well below the doublet state by 12 – 14 kcal/mol, it is most probable that the quartet is the ground state of the parent triradical.[120, 121, 126]

7.5 UV/Vis spectrum

The UV/Vis spectrum of an argon matrix after FVP at 500°C of 1,3,5-*tris*-(iodomethyl)benzene **26** is very similar to the UV/Vis spectrum obtained after FVP of 1,3-*bis*-(iodomethyl)benzene **17** at 450°C (Figure 59). The strongest absorption is found at 230 nm (broad, 231 nm for *m*-xylylene **1**) while other transitions occur at 287 (weak), 293 (strong, sharp), 320 (weak), 389 (weak), and 451 nm (weak).

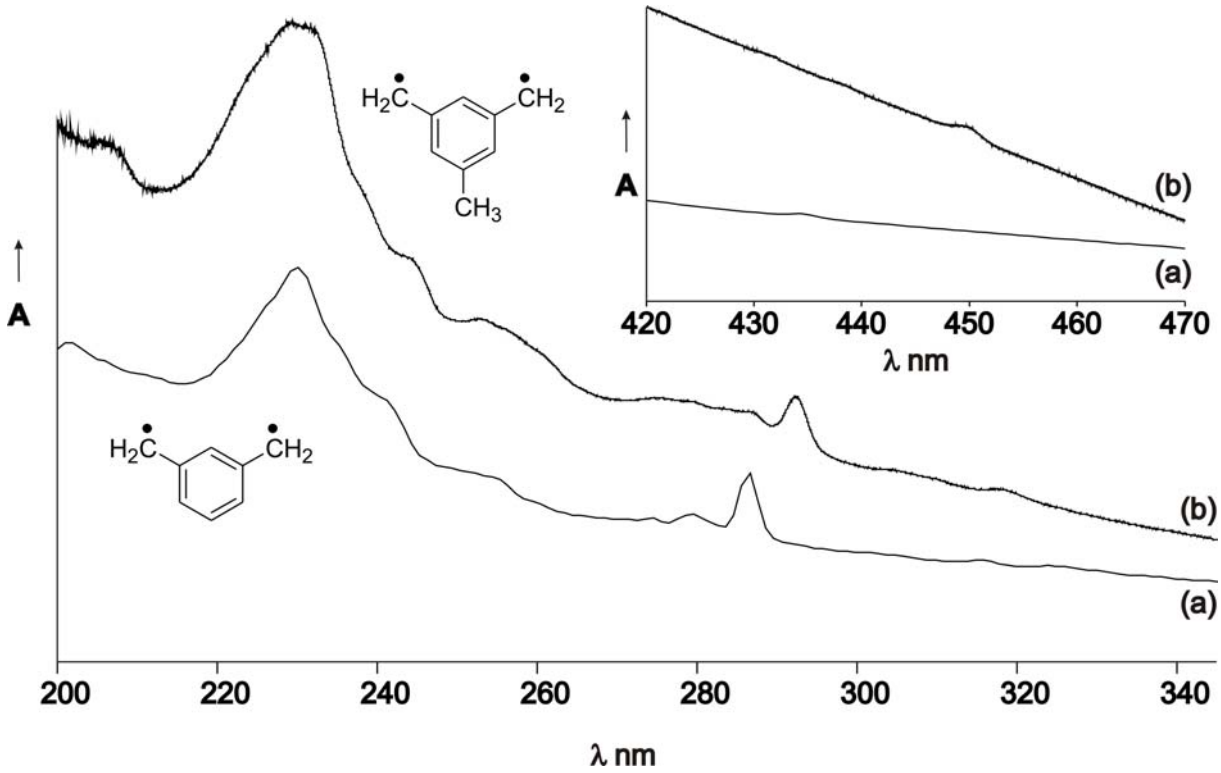

Figure 59. UV/Vis spectra obtained after FVP of 1,3,5-*tris*-(iodomethyl)benzene **26** at 500°C compared to *m*-xylylene **1**.

From a first view it was not clear whether the recorded spectra from the FVP of 1,3,5-*tris*-(iodomethyl)benzene **26** is the one from the triradical or if the absorptions origin from 5-methyl-*m*-xylylene **27**.

As was inferred from the IR spectra H abstraction in the FVP tube can take place, giving the possibility to add one hydrogen atom to the triradical to give 5-methyl-*m*-xylylene **27**, an derivative of *m*-xylylene **1**. In order to distinguish the UV/Vis spectra of this compound from the triradical it was synthesized independently by FVP of 5–methyl-1,3-*bis*-(iodomethyl)benzene **29**. All prominent UV/Vis absorptions of *m*-xylylene **1** are just shifted to the red in its methylated derivative **27** and indeed it is found that the main compound which could be detected in the above experiment is the diradical **27**, as can be seen from Figure 60 below.

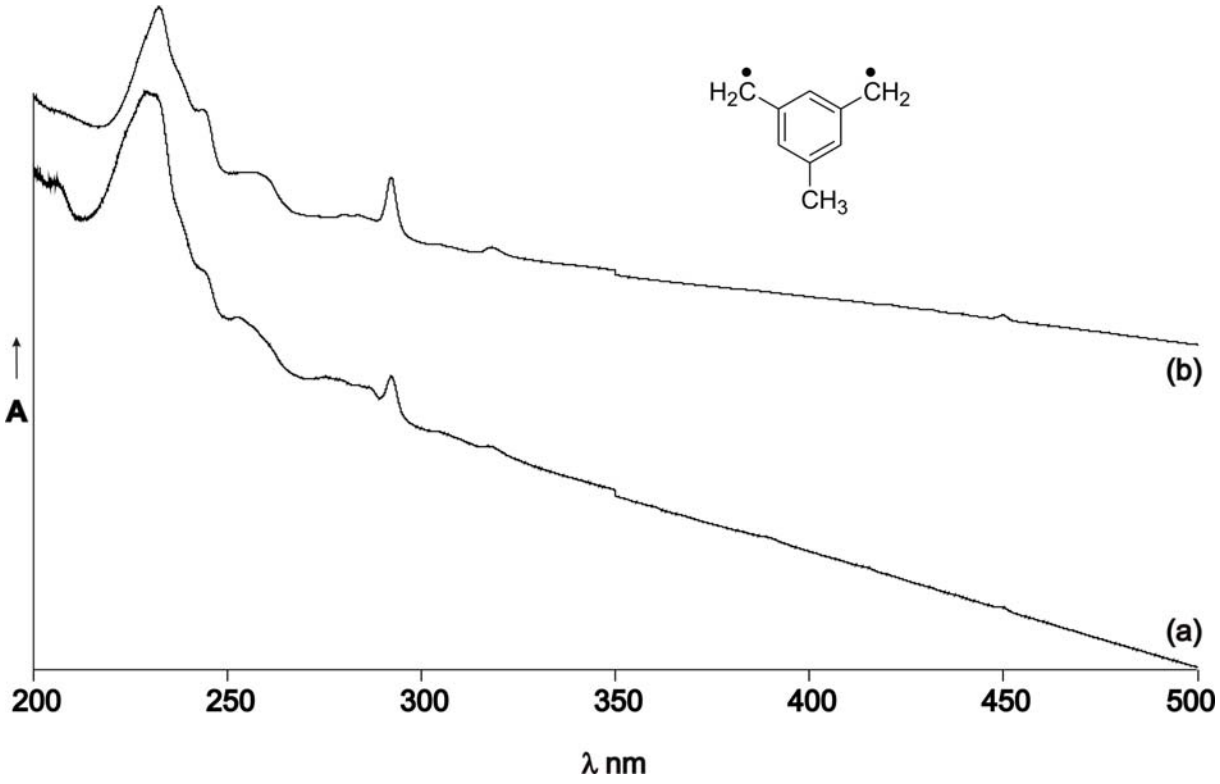

Figure 60. UV/Vis spectra obtained after FVP of 1,3,5-*tris*-(iodomethyl)benzene **26** at 500°C (a) compared to the FVP products of 5-methyl-1,3-*bis*-(iodomethyl)benzene **29** (b).

The signals at 287 and 293 nm probably belong to one electronic transition with vibrational progression as it was the case for *m*-xylylene **1** (279 and 287 nm). The transition at 389 nm can also be found at the same wavelength in the pyrolysis of 1,3-*bis*-(iodomethyl)benzene **17** and might be due to some common pyrolysis species. A transition at 451 nm is assigned to **27** as it is redshifted in comparision to *m*-xylylene **1**, where this transition was found at 433 nm.

The remarkable redshift of the fluorescent band at 451 nm was also found by Lejeune et al. in a *n*-hexane matrix after photolysis of mesitylene when studying the effect of substituents on the UV/Vis spectrum of *m*-xylylene derivatives.[142] Their CIS calculations indicate that the 5-methyl-*m*-xylylene diradical **27** should have a transition at 450 nm.[142] As was shown in the above spectra, one compound that definitely can be formed under the FVP conditions is the hydrogen abstraction product of triradical **2** diradical **27** (Scheme 84). In order to exclude further hydrogen abstraction products as for example the 3,5-*bis*-methylbenzyl radical **28**, **28** was independently synthesized by FVP of 3,5-*bis*-methylbenzyl iodide **30** at 580°C.

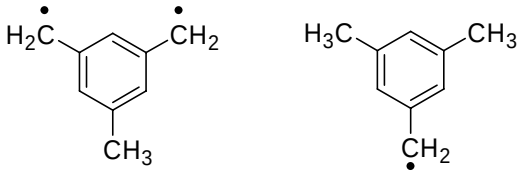

27 **28**

Scheme 84. UV/Vis transitions of 5-methyl-*m*-xylylene **27** and 3,5-*bis*-methylbenzyl radical **28** are observed if 1,3,5-*tris*-(iodomethyl)benzene **26** is pyrolysed.

The observed UV/Vis spectrum is shown below and can be compared to the UV/Vis spectrum observed by Albrecht et al. for the benzyl radical **55** in 3-methylpentane (Figure 61).[143, 144] Their main absorption signals were detected at ca. 430, 320, and 260 nm. The UV/Vis spectrum recorded after FVP of 3,5-*bis*-methylbenzyl iodide **30** is shown below a) together with the photochemical conversion of this compound b). The main signals are detected at 476.4 (weak), 328.4 (medium), and 257.6 nm (strong). The intensities as well as the signal positions and the vibrational progressions of the signals is quite similar to the published values of Albrecht et al..[143] Yoshida et al. have seen the "slight shift to the longer wavelength" for the 0,0 fluorescence transition of methylated benzyl radicals by methylation.[145] The published value for the 0,0 fluorescene transition of the benzyl radical **55** is at 462 nm in ethanol. For 3,5-*bis*-methylbenzyl radical **28** a value of 490.0 nm in ethanol and 482.0 nm in the less polar methylcyclohexane was found dependent on the solvent.[145]

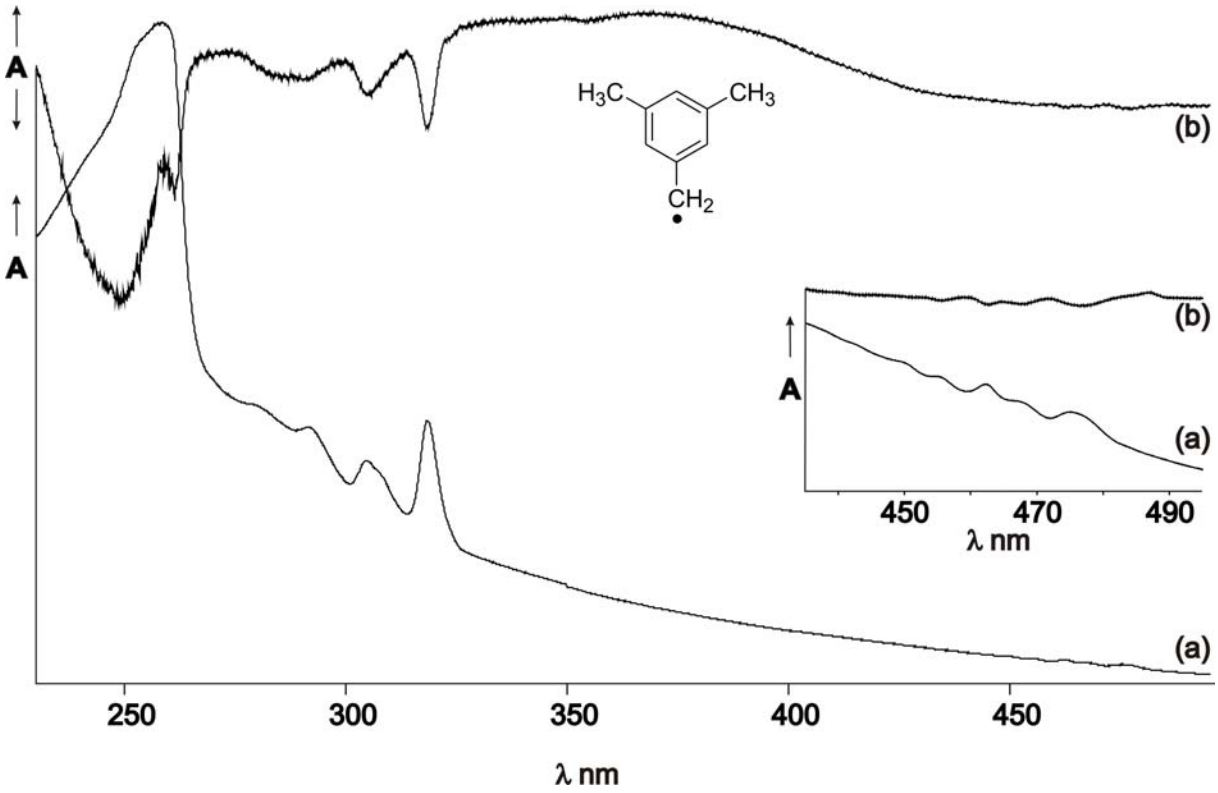

Figure 61. (a) UV/Vis spectrum obtained after FVP at 580°C of 3,5-*bis*-(iodomethyl)benzyl iodide **29**. (b) Difference spectrum after irradiation of the FVP products of 3,5-*bis*-(iodomethyl)benzyl iodide **29** with 254 nm of a mercury low pressure lamp.

Changing the conditions for the FVP results in the UV/Vis spectrum shown in Figure 62 below. As can be seen the first electronic transition is found at 415 nm and does not belong to **27** or **28**. Furthermore, little amounts of diradical **27** are obtained under these conditions.

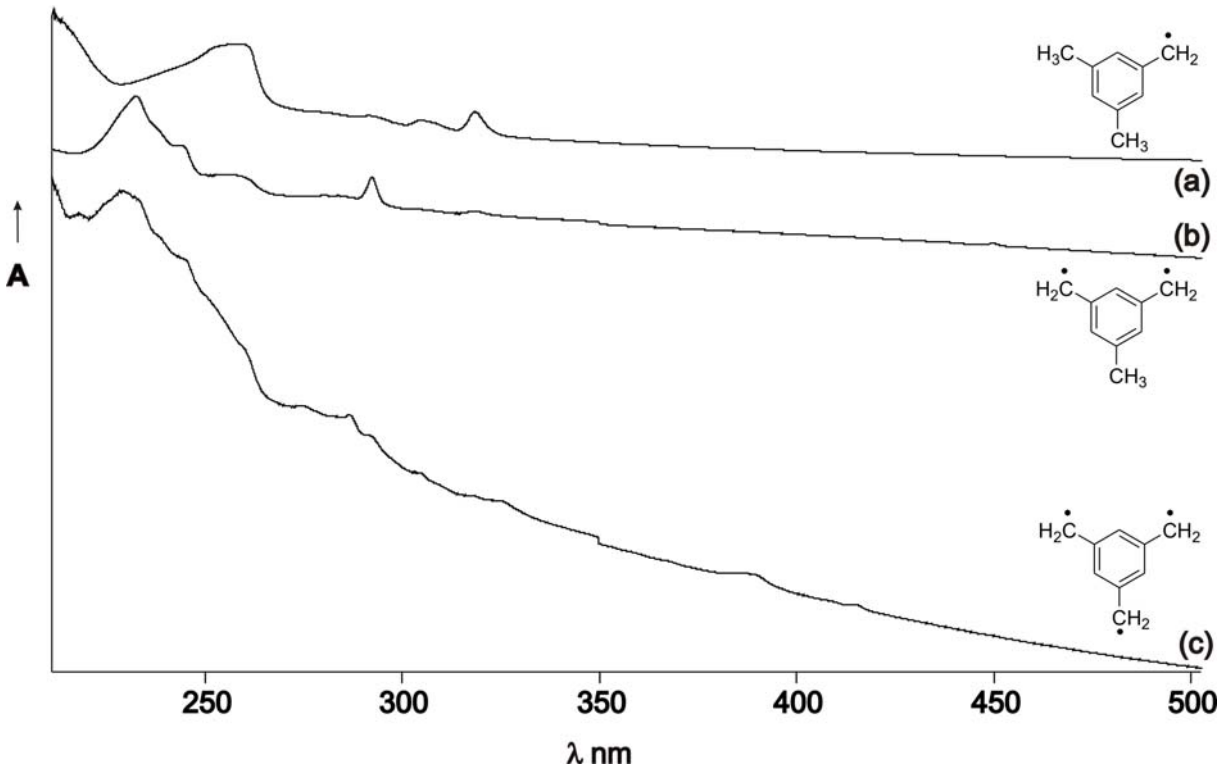

Figure 62. UV/Vis spectra obtained after FVP of 1,3,5-*tris*-(iodomethyl)benzene **26** (550°C, (c)), 5-methyl-1,3-*bis*-(iodomethyl)benzene **29** (450°C, (b)) and 3,5-*bis*-methylbenzyl iodide **30** (580°C, (a)).

This spectrum is remarkably different from the one observed before and might therefore belong to the triradical **2**. The remaining weak transition at 367 and 254.9 nm might be assigned to 1,3,5-trimethylenebenzene **2**, however, it can not be excluded that they are due to an unknown impurity. Nguyen calculated the first electronic transition of quartet **2** to be found at 354 nm by MS-CASPT2 theory, which would be in good agreement with the 367 nm band.[120]

8. 2-Dehydrophenylnitrene

8.1 Introduction

The simplest nitrene, imidogene **57**, has a very robust triplet ground state with a singlet-triplet splitting ΔE_{ST} of 36 kcal/mol, determined by fluorescence and laser photoelectron spectrometry, respectively.[146, 147] Like all other nitrenes, imidogen **57** is a neutral univalent species with two possible electronic states. The singlet state has four spin-paired electrons which could occupy two or three orbitals, while the triplet state has two spin-paired electrons occupying one orbital and two further electrons in two more orbitals with parallel spins. A general way to organic high-spin systems with multiplicities higher than a triplet state is the combination of (different) reactive motifs in a ferromagnetic coupling fashion. As imidogen **57** has only one more H atom next to the nitrogen atom, a combination with other reactive motifs is not possible and most work in the field of organic magnetism has focused on aromatic nitrenes. The parent phenylnitrene **56** is a well known triplet ground state molecule, with a diminished ΔE_{ST} of approximately 16 kcal/mol in comparison to imidogen **57** (Scheme 85).

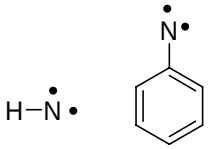

57 **56**

Scheme 85. Triplet ground state nitrenes, imidogen **57** and phenylnitrene **56**.

Ellison et al. found a value of 18 +/- 2 kcal/mol, while Wenthold et al. recently determined a value of 14.8 +/- 0.5 kcal/mol for ΔE_{ST} of phenylnitrene through negative ion photoelectron spectroscopy.[148, 149] The singlet-triplet splitting of phenylnitrene **56** was determined computaionally to be approximately 18 kcal/mol by Borden et al. using a MCSCF or CI methodology and to 17.7 kcal/mol by Schaefer et al. using the CISD method.[150, 151] It was found in these studies that the reduced ΔE_{ST} of phenylnitrene **56** compared to imidogen **57** is due to selective stabilization of the open-shell singlet state of **56** through delocalization of the π electron. Resonance structures of **56**, like **56o** and **56p** place the electron in *ortho* or *para* position to the *ipso* nitrogen atom and therefore diminish the electron-electron coulomb repulsion on the nitrogen, thus allowing the

singlet-coupled electrons to occupy different regions of space within the molecule (Scheme 86).[150]

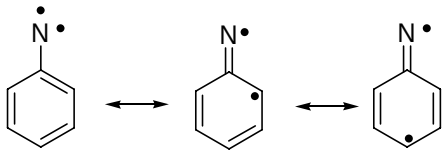

56

Scheme 86. Resonance structures of phenylnitrene **56**.

While one of the electrons in the triplet ground state of phenylnitrene **56** is in a p orbital which is parallel to the aromatic π system, the second electron resides in a p orbital which is perpendicular to the aromatic system and can therefore not be delocalized.

Addition of a second nitrene unit to phenylnitrene could be accomplished in three positions, leading to singlet[28, 152, 153] quinoidal diradicals **166** and **66**, for addition in *ortho* and *para* position, respectively, while attachment in *meta* position yields a quintet[57] ground state dinitrene **94** (Scheme 87).

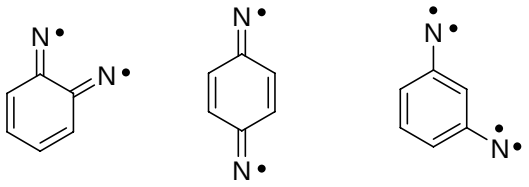

166 **66** **94**

Scheme 87. Studied dinitrenes with low-spin singlet ground state for **166** and **66** and high-spin quintet ground state for **94**.

The singlet state in **166** is calculated to lie approximately 3 kcal/mol lower in energy than the triplet state and 25 kcal/mol lower than the quintet state by CASPT2/6-31G(d)//CASSCF/6-31G(d) – with UB3LYP/6-31G(d) calculations within only 0.5 kcal/mol from the CASPT2 results.[152] The energy difference between the singlet ground state of **66** and its excited triplet state was found to be 0.58 kcal/mol by Curie law analysis of the EPR signal by Lahti et al.[28] Tomioka et al. profounded this result by an IR analysis and calculated the energy difference between the singlet and triplet state and between the singlet and quintet state to be 1.9 and 32.3 kcal/mol by CASPT2/6-31G(d), respectively – again the UB3LYP/6-31G(d) results vary only by a maximum of 0.7 kcal/mol.[154] A quintet ground state for dinitrene **94** was first found by Wasserman et al. using EPR

spectroscopy and was confirmed by Lahti et al. whose MRSDCI calculations found the triplet state to be higher in energy by 3.7 – 5.9 kcal/mol and the singlet state by 5.5 – 10.7 kcal/mol - depending on the used starting geometry.[55, 57, 155]

An explanation for the ground state ordering of **166**, **66**, and **94** could be given in terms of a spin polarization model, as was depicted by Lahti et al. for the localized diradical **66** and can as well be applied for **166** and **94** (Scheme 88).[28]

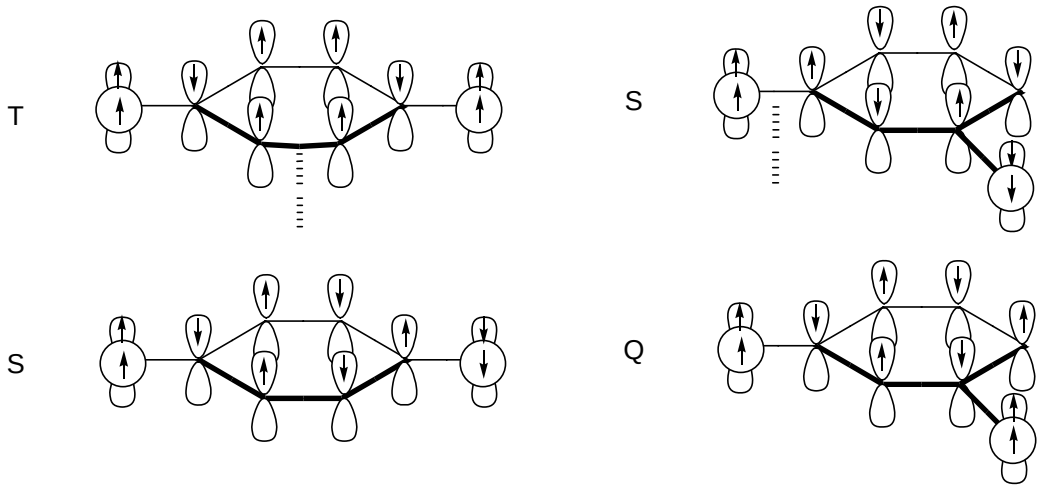

Scheme 88. Predicted preference for the low-spin singlet state of **66** and the high-spin quintet state of **94** by the spin polarization model. Mismatching is indicated by dashed lines.

As said above, one p orbital of each nitrene unit is perpendicular to the aromatic ring. For *para* dinitrene **66** in the triplet state, these perpendicular p orbitals are each occupied by one electron with parallel spin. These spins polarize the π-spins of the nitrogen atoms by one-center interactions to be parallel. As in the π space each α spin orbital prefers to be surrounded by a β spin orbital, it can be seen from Scheme 88 that the triplet state (as would be the quintet) is destabilized due to a mismatch in the π-space. The singlet state instead has no such mismatch in its π-space and represents the ground state for this reason. A reverse state ordering is found for dinitrene **94** and could be analysed in a similar manner – while also other models are suitable in this case.

Lahti et al. also studied the effect of addition of conjugated nitroxids on the ground state with respect to the position of attachment. In order to understand these results it is important to have a closer look at the SOMOs of the employed nitronyl nitroxides **167** and imino nitroxids **168** (Scheme 89).[156-159]

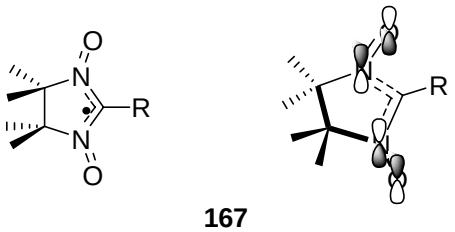

167

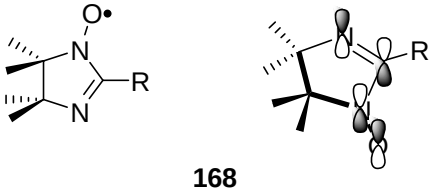

168

Scheme 89. Structures and SOMOs of nitronyl nitroxides **167** and imino nitroxides **168** studied by Lahti et al..

The symmetrical nitronyl nitroxide **167** is a 7 π electron system, with the SOMO having a node at the point of attachment. However, imino nitroxide **168** is an asymmetric system with 5 π electrons and thus has a nonvanishing orbital coefficent in its SOMO at the point of attachment. As the unpaired electron is delocalized above 5 atoms in **167**, it could be anticipated that the central carbon has a negative spin population at this atom, similar to the central carbon in the allyl radical system **54**. In **168** there is no *a priori* reason to assume that the nonnodal carbon has a negative spin population, which is nevertheless observed experimentally.[159] Furthermore, it was noted that the negative spin population in **167** is more pronounced than in **168**.[160]

An important conclusion drawn by Lahti et al. was the change in connectivity behaviour with the nitronyl nitroxide **169** and **171** and imino nitroxide **170** and **172**.[16, 161, 162] Since large π-spin bearing units like nitrenes give high-spin states if they are directly attached to the *meta* position relative to the parent phenylnitrene **56**, and low-spin states in other positions, it might be assumed that this "rule" would also be followed by the π systems **169** - **172**. Instead, a reversal of this "rule" was found experimentally with the *meta* connected molecules **171** and **172** resulting in a low-spin doublet state, while the *para* connectivity in **169** and **170** gives rise to a high-spin quartet ground state (Scheme 90).

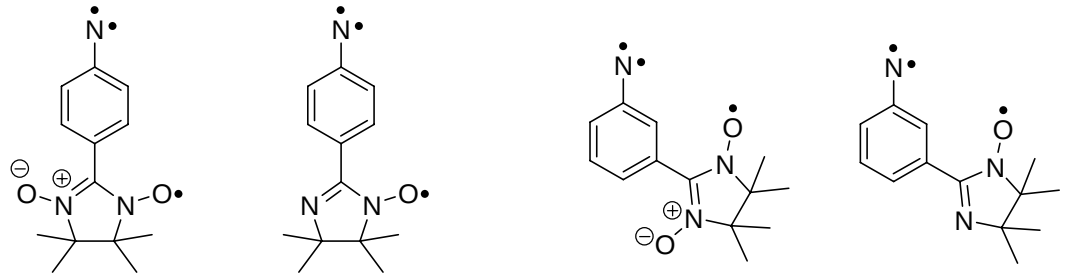

169 **170** **171** **172**

high-spin coupled low-spin coupled

Scheme 90. Systems studied by Lahti et al. with spin coupling preference reversed in comparison to dinitrenes **66**, **166**, and **94**.[16, 161]

An explanation is given by the spin density distribution in **167** and **168**. The main positive spin density is located on the N and O atoms, while the carbon atom has a negative spin density in both groups – in contrast to directly attached atoms which necessarily have their main positive spin distribution at the atoms itself. Since spin alternation about the p system is generally applicable in spin polarization mechanisms, the predictions are qualitatively correct for directly attached nitrene units as well as "indirectly" attached nitroxide based radicals (Scheme 89 and 91).

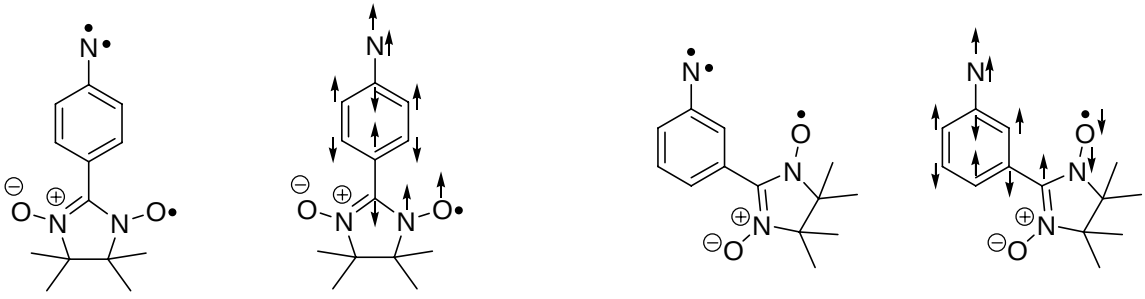

169 **169** **170** **170**

Scheme 91. Qualitative ground state spin multiplicity prediction by the spin polarization model for **169** and **170**.[16]

The π system plays an important role in these predictions and extremely distorted conformations in other nitroxide radicals could lead to discrepancies of these predictions.[163-166]

Formal detachment of a hydrogen from phenylnitrene **56** produces an additional phenyl radical. As three electrons are unpaired, triradicals with quartet or doublet ground state evolve from this. In contrast to the dinitrenes **66**, **166**, and **94** and the nitroxide based

triradicals **169** - **172**, the additional radical center is in a sp^2 orbital perpendicular to the π system of the aromatic ring. Since detachment could take place in three different positions, three isomeric dehydrophenylnitrenes **31**, **173**, and **174** can be distinguished (Scheme 92).

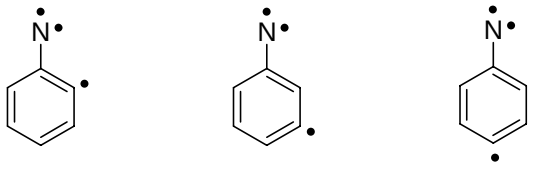

31 **173** **174**

Scheme 92. Three possible dehydrophenylnitrene isomers **31**, **173**, and **174**.

In general, possible quartet states of dehydrophenylnitrenes **31**, **173**, and **174** might be observed by the quite sensitive EPR technique, while an IR investigation has to take into account all singlet rearrangement products of phenylnitrene **56**, too. Photolysis or thermolysis of phenyl azide **175** yields phenylnitrene **56** as main product. Spin-conservation leads to the production of phenylnitrene in its excited singlet state S-**56** which at lower temperature through intersystem crossing falls down to the triplet ground state T-**56**. However, at higher temperatures it tends to rearrange to the corresponding ketenimine **176**, which could be trapped in solution chemistry. In the gasphase where no deactivation processes are available for the nitrene, the cyanocyclopentadienyl radical **177** is formed. Azirine **178**, the first product on the route to rearrangement to **176** was observed for different substituted phenylnitrenes, but not for the parent phenylnitrene **56** (Scheme 93).[167]

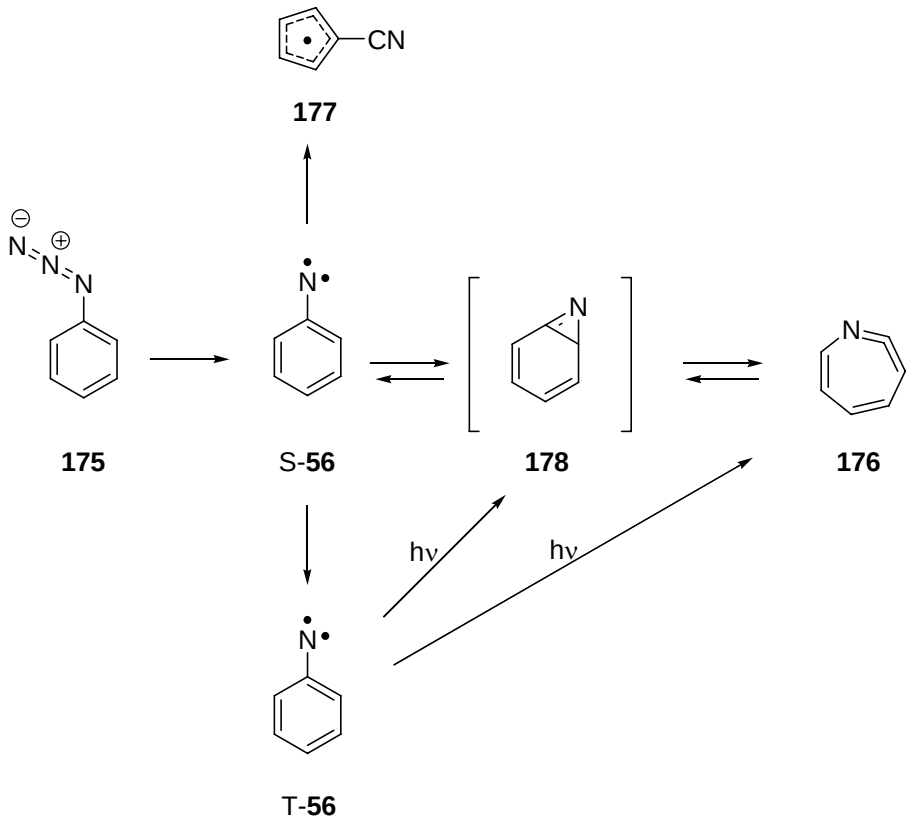

Scheme 93. Possible interconversion of phenylnitrene **56** with cyclopentadienyl radical **177**, ketenimine **176**, and azirine **178**.[167]

The first direct observation of a 4-dehydrophenylnitrene derivative was reported by Wenk and Sander.[168] Irradiation of the azidotetrafluoro derivate **79** in a matrix at low temperature gives the triplet nitrene **179**, the quartet 4-dehydrophenylnitrene **77**, and ketenimine **180** (Scheme 94). All compounds were identified by their IR spectra, with **179** and **77** also leading to characteristic EPR spectra.

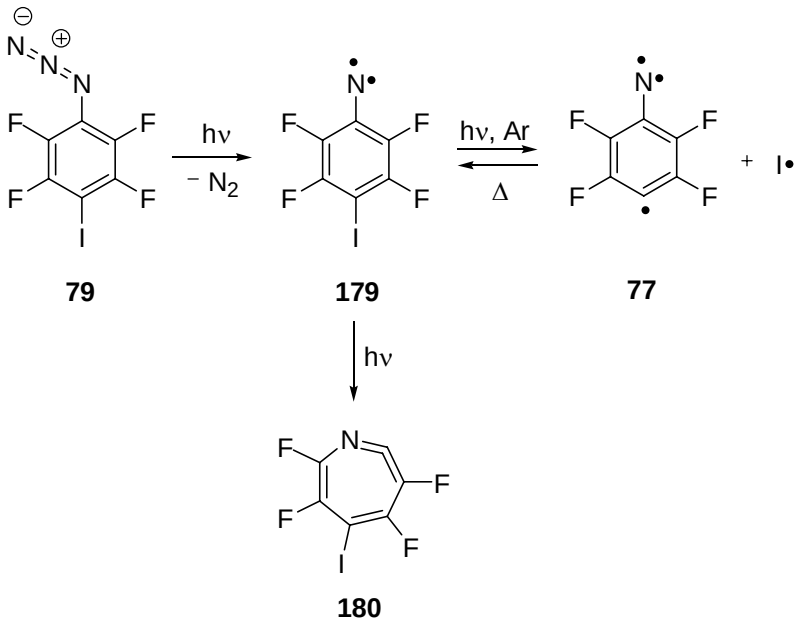

79 **179** **77** **180**

Scheme 94. Photochemistry of 79 studied first by Wenk and Sander by IR and EPR spectroscopy.[168]

Grote and Sander furthermore studied some 4-dehydrophenylnitrene derivatives with different fluorine substitution pattern by IR and EPR spectroscopy.[60] Besides an EPR detection of the quartet states of these molecules, one flourine atom in *ortho* position to the nitrene center should suppress rearrangement and was found a necessary condition for IR identification of these elusive triradicals. The same authors also reported on the EPR spectra of the corresponding quartet state of tetrafluoro-2-dehydrophenylnitrene **76**.[1] An IR detection was not possible in this case, but their IR analysis gave support for two isomeric ketenimines **181** and **182**, two isomeric azirines **183** and **184** and a previously unknown azirinyl radical **185** besides the triplet state of nitrene **186** (Scheme 95).

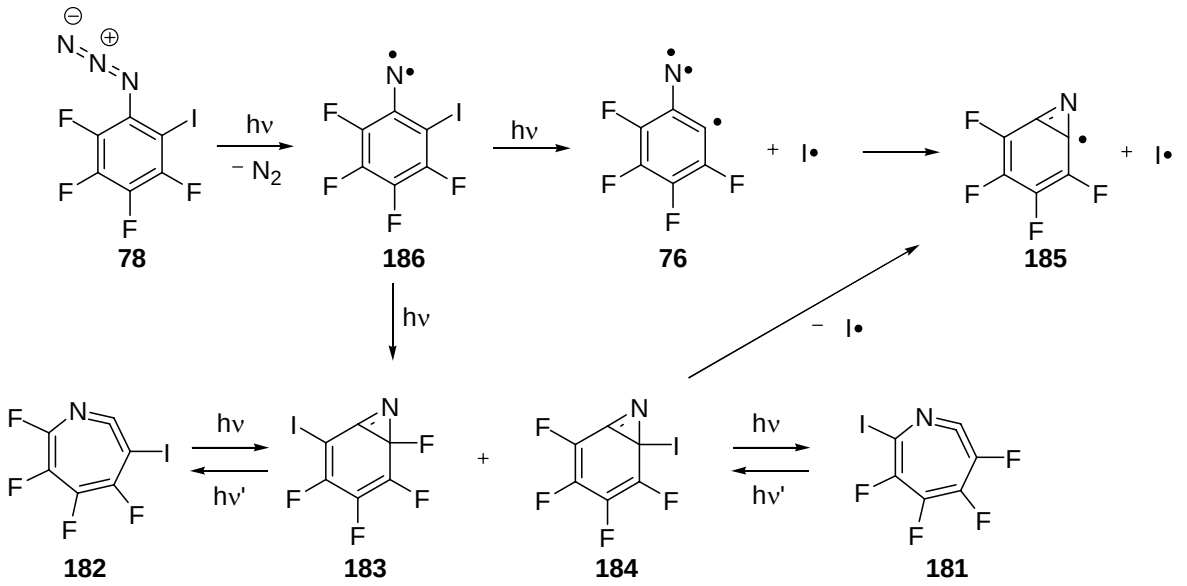

Scheme 95. Photochemical conversion of 2-iodo-3,4,5,6-tetrafluorophenyl azide **78**.[1]

Sander et al. also reported on the photochemistry of the corresponding 3-iodo-2,4,5,6-tetrafluorophenyl azide **187**.[169] The corresponding triradical could neither be identified by EPR nor IR spectroscopy, instead ring opening was the major pathway upon short wavelength photolysis. Regarding the unsubstituted dehydrophenylnitrenes **31**, **173**, and **174** no experimental studies are reported so far. Bettinger and Sander performed *ab initio* calculations on the parent systems and found the 4-dehydrophenylnitrene **174** and the 2-dehydrophenylnitrene **31** to be ground state quartets while the 3-dehydrophenylnitrene **173** was shown to have a doublet ground state by CASSCF and MRMP2 calculations (cc-pVTZ basis set).[170] The doublet-quartet splitting was calculated at the MRMP2/cc-pVTZ//(9,9)CASSCF/cc-pVTZ level and predicts an energy gap of 5.3 kcal/mol for **31**, -6.3 kcal/mol for **173**, and 7.3 kcal/mol for **174** with the doublet state of 3-dehydrophenylnitrene **173** being the most stable isomer. Quartet 2-dehydrophenylnitrene **31** is 3.5 kcal/mol less stable than D-**173** and 0.6 kcal/mol more stable than the quartet state of 4-dehydrophenylnitrene Q-**174**. In a qualitative sense, these findings are supported by the simple spin-polarization model (Scheme 96).

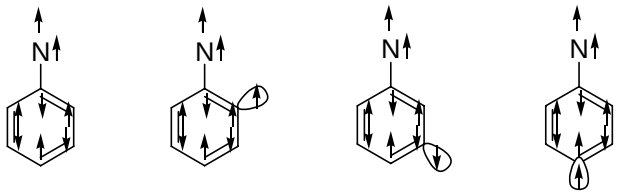

Scheme 96. Spin-polarization model for phenylnitrene **56** and the dehydrophenylnitrenes **31**, **173**, and **174**. The most stable configuration is shown for each isomer.

Since the π spin density of the nitrene unit is delocalized throughout the molecule with appreciable positive spin density at the *ortho* and *para* position, a favoured configuration on the same atoms can only be found with the phenyl radical spins in a parallel direction to the nitrene spins. In the *meta* position, the π system of phenylnitrene **56** has negative spin density, so a favourable configuration could only be obtained with the phenyl radical spin in an antiparallel orientation to the nitrene spins (or in other words with a parallel orientation with the excess β spin density on this atom – the nitrene unit is arbitrarily assumed to have α spin).

8.2 Computations on the C_6H_4NI-hypersurface

In order to get an idea of the energetics of possible rearrangements of 2-iodophenylnitrene **33** towards the isomeric ketenimines **34** and **35** and benzazirines **36** and **37**, the potential energy surface was calculated to locate all transition states and minima for the interconversion of the respective species. Borden et al. predicted that the rearrangement of singlet phenylnitrene S-**56** towards ketenimine **176** takes place by intermediate benzazirine **178**.[171] The open-shell nature of singlet phenylnitrene makes the ring-closure process to **178** much easier accessible for **56** than for the corresponding phenylcarbene – with a corresponding closed-shell singlet state.[167, 172] The ring-closure reaction to **178** was calculated at the CASPT2N/6-311G(2d,p) level to be the rate determining step on the conversion of S-**56** to ketenimine **176**. *Ortho* fluorine substituents were found to retard the ring-opening reaction of phenylnitrenes **56** towards ketenimines due to their enormous electronegativity which destabilizes the evolution of positive charge in the transition state to azirines.[173] With an asymmetric substitution pattern around the nitrene like in 2-iodophenylnitrene **33**, formation of two isomeric benzazirines **36** and **37** and their corresponding isomeric ketenimines **34** and **35** is possible (Scheme 97).

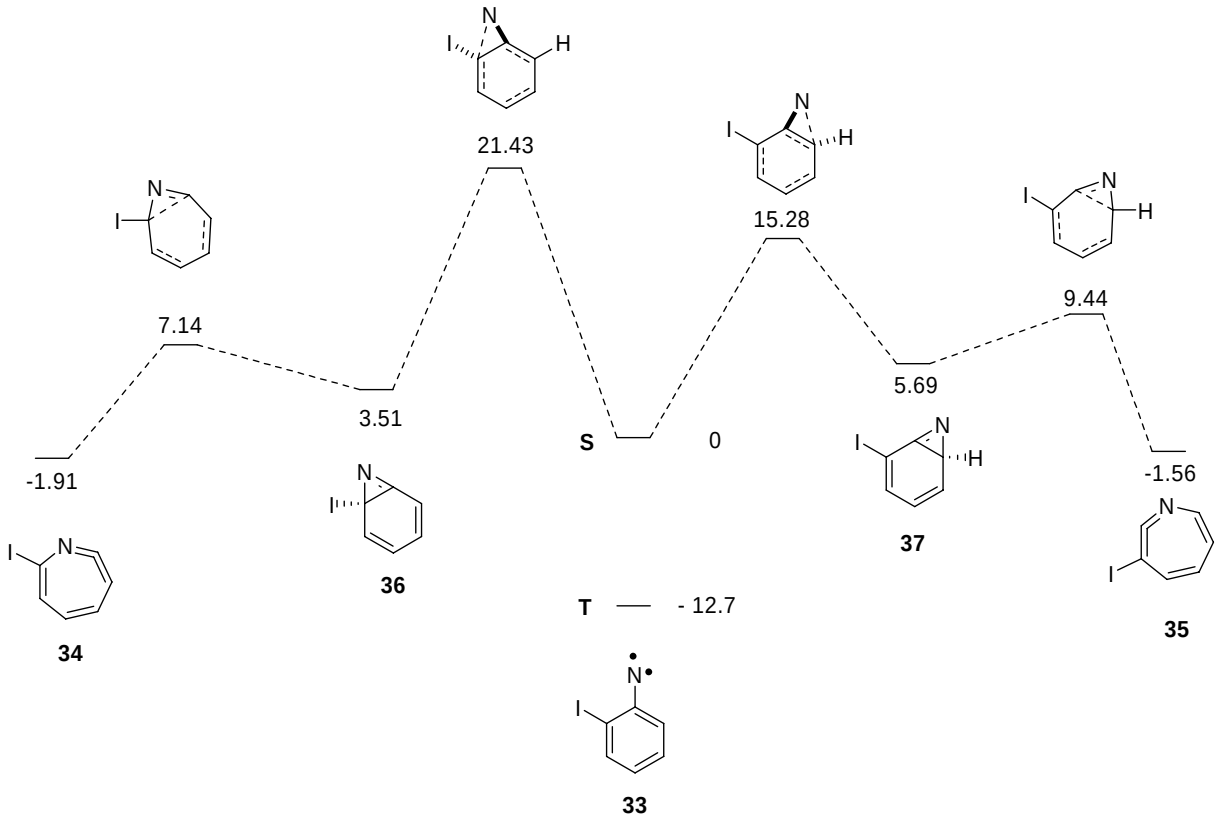

Scheme 97. Energetics of the rearrangement of 2-iodophenylnitrene **33** to benzazirines **37** and **36** as well as to ketenimines **35** and **34** calculated at the (U)B3LYP/6-311G(d,p) level of theory.

As is seen from Scheme 97, on the singlet surface both ketenimines **34** and **35** could be formed in exothermic processes as calculated at the (U)B3LYP/6-311G(d,p) level of theory. Ketenimine **34** is the more stable ketenimine isomer (by ca. 0.4 kcal/mol) and is formed from the more favourable benzazirine **36** through an absolutely smaller barrier of $\Delta E = 7.14 - 9.44 = -2.3$ kcal/mol, while the activation energies from **36** to **34** and **37** to **35** differ by only 0.1 kcal/mol – as benzazirine **37** is 2.2 kcal/mol less stable than benzazirine **36**. However, the most striking difference are the activation energies for conversion of **33** to benzazirines **36** and **37**. The transition state for conversion of singlet 2-iodophenylnitrene S-**33** to the less stable benzazirine **37** is calculated to have a relative energy of 15.28 kcal/mol and therefore is 6.15 kcal/mol lower in energy than the transition state for conversion of singlet **33** to benzazirine **36** (the corresponding TS has an energy of 21.43 kcal/mol).

In most cases, formation of one azirine is favoured to a great extent, as was experimentally found for the conversion of 2-fluorophenylnitrene **188** to **189** and 1-naphthylnitrene **190** to **191** as well as in several other cases (Scheme 98).[174-176]

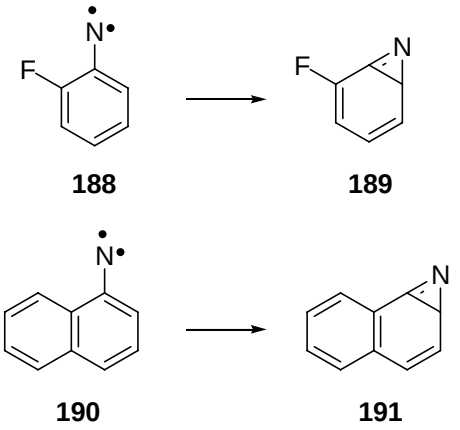

Scheme 98. Formation of only one of two possible isomeric azirines is preferred for 2-fluorophenylnitrene **188** and 1-naphthylnitrene **190**.[175, 176]

Furthermore, Sander and Grote reported that B3LYP calculations for the nitrenes and its rearranged products can be used to estimate the yield of the corresponding benzazirines and ketenimines.[177] Since the activation barrier is predicted to be the essential factor determining the yield of the isomeric benzazirines, it can be stated that **37** should greatly be favoured over **36** for the parent 2-iodophenylnitrene **33**. However, in the case of ketenimines **34** and **35** a different dependance is reported: the more stable isomer is expected to be found in higher concentration. The energy difference between **34** and **35**, which is calculated to be 0.4 kcal/mol therefore is expected to result in appearance of both isomers in the IR spectrum.

8.3 EPR analysis

It is known from the EPR studies of Grote and Sander that iodophenyl azides might serve as precursors of the respective dehydrophenylnitrenes.[1, 46, 60, 174] Nevertheless, most reported experimental studies of dehydrophenylnitrenes make use of fluorine substituents to destabilize ring enlargement reactions. Release of this constrained gives rise to the elusive parent dehydrophenylnitrenes. It is found that low-temperature (below 10 K) matrix isolation is a necessary condition for detection of the high-spin signals of 2-dehydrophenylnitrene **31** (Figure 63).

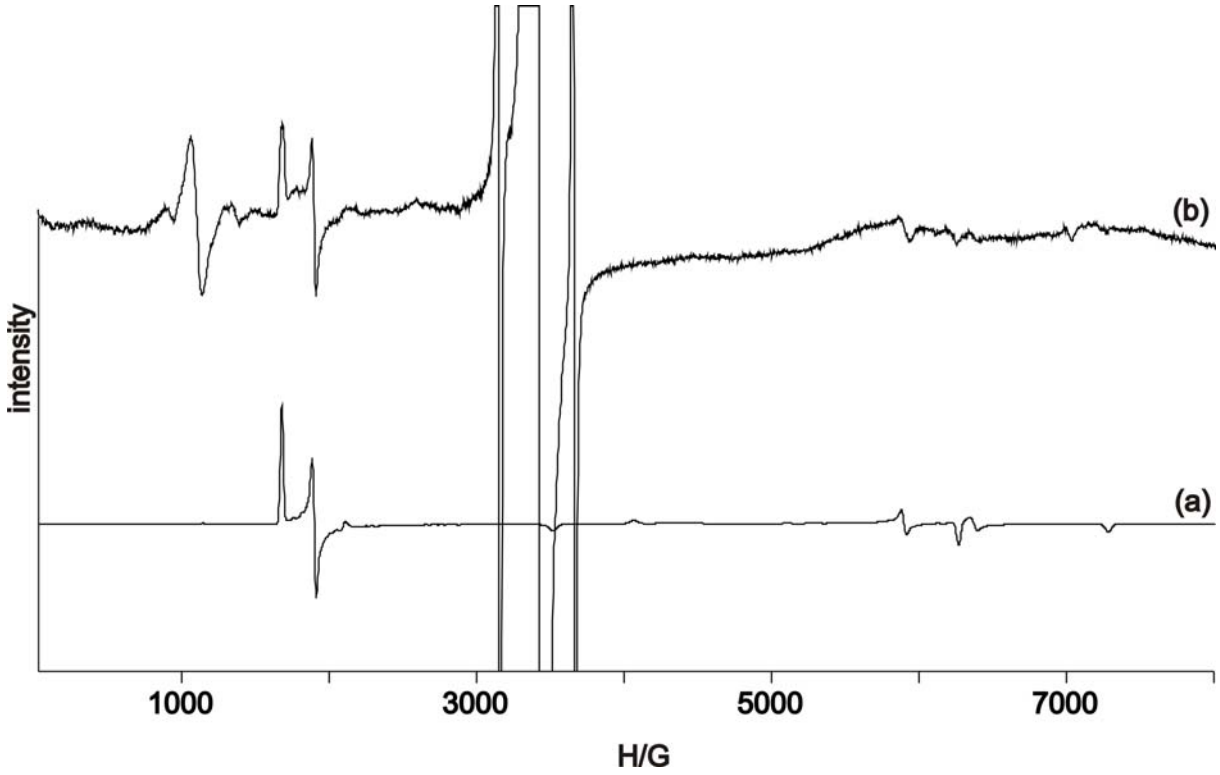

Figure 63. (a) Calculated EPR spectrum of a quartet triradical species with zfs parameters: |D/hc| = 0.355 cm^{-1} and |E/hc| = 0.014 cm^{-1}; g = 2.0023, ν = 9.60857 GHz. (b) Experimental EPR spectrum obtained after irradiation of an argon matrix at 4.2 K containing 2-iodophenyl azide **32** for 25 minutes with 254 nm of a mercury low-pressure lamp. The signal at 1200 G has not been assigned.

The EPR spectrum obtained after 254 nm photolysis of a matrix containing 2-iodophenyl azide **32** is shown in Figure 63. Obviously, in addition to a hugh radical signal at 3400 G, some EPR transitions of a high-spin molecule are developing in course of the irradiation. Another striking fact is the close resemblance of the high-spin part of the EPR spectrum with the published value of perfluorinated 2-dehydrophenylnitrene **76**.[1] The reported zfs parameters for 2-dehydro-3,4,5,6-tetrafluorophenylnitrene **76** are |D/hc| = 0.357 cm^{-1} and |E/hc| = 0.0136 cm^{-1} (g = 2.003; ν = 9.5904 GHz), showing that fluorine substitution has only a minor effect on the zfs parameters in this case. The difference in D and E amount to only 0.002 and 0.0004 cm^{-1}, respectively (|D/hc| = 0.355 cm^{-1} and |E/hc| = 0.014 cm^{-1} for the parent system). A clear effect of the carbenic resonance structure on the ground state properties of 2-dehydrophenylnitrene **31** can be infered and the assignments of all transitions is completely analogous to the one described for the perfluorinated derivative.[1] An apparent dissimilarity regards the amount of phenylnitrene **33** in the EPR spectrum. While nearly no EPR intensity is visible for the xy_2 transition of triplet nitrenes in the parent system, a transition due to the fluorinated triplet nitrene was also obtained as

well resolved signal. This might be explained due to the larger stability of the fluorinated nitrene derivative and the heavy atom effect of iodine in direct neighbourhood to a high-spin center.[141] However, triplet nitrene **33** was readily observable in IR studies.

8.4 Photolysis of 2-iodophenyl azide – Infrared experiments

The EPR analysis of 2-iodophenyl azide **32** revealed that short wavelength photolysis leads not only to signals that could be assigned to triplet 2-iodophenylnitrene T-**33**, but also to new - quite characteristic - transitions attributable to a quartet EPR spectrum. All signals could be assigned to the up to this point unknown 2-dehydrophenylnitrene Q-**31**. Even though, it was possible to identify Q-**31** by its EPR spectrum, it would also be highly desirable to characterize this elusive species by its infrared spectrum. However, it was already found in other related studies, that an IR analysis might be much more complicated – due to other products formed in equilibria with the parent nitrene – and difficult – as the sensitivity of IR spectroscopy is much lower than that of EPR spectroscopy.

Short wavelength photolysis (with 254 nm of a low-pressure mercury lamp) of an argon matrix at 4 K containing 2-iodophenyl azide **32** results in continous reduction of all infrared signals assigned to **32** and concomitant appearance of new signals. The newly formed species can be assigned to triplet 2-iodophenylnitrene T-**33** through comparison of the UB3LYP/6-311G(d,p) calculated infrared spectrum with the experimentally observed one (Figure 64).

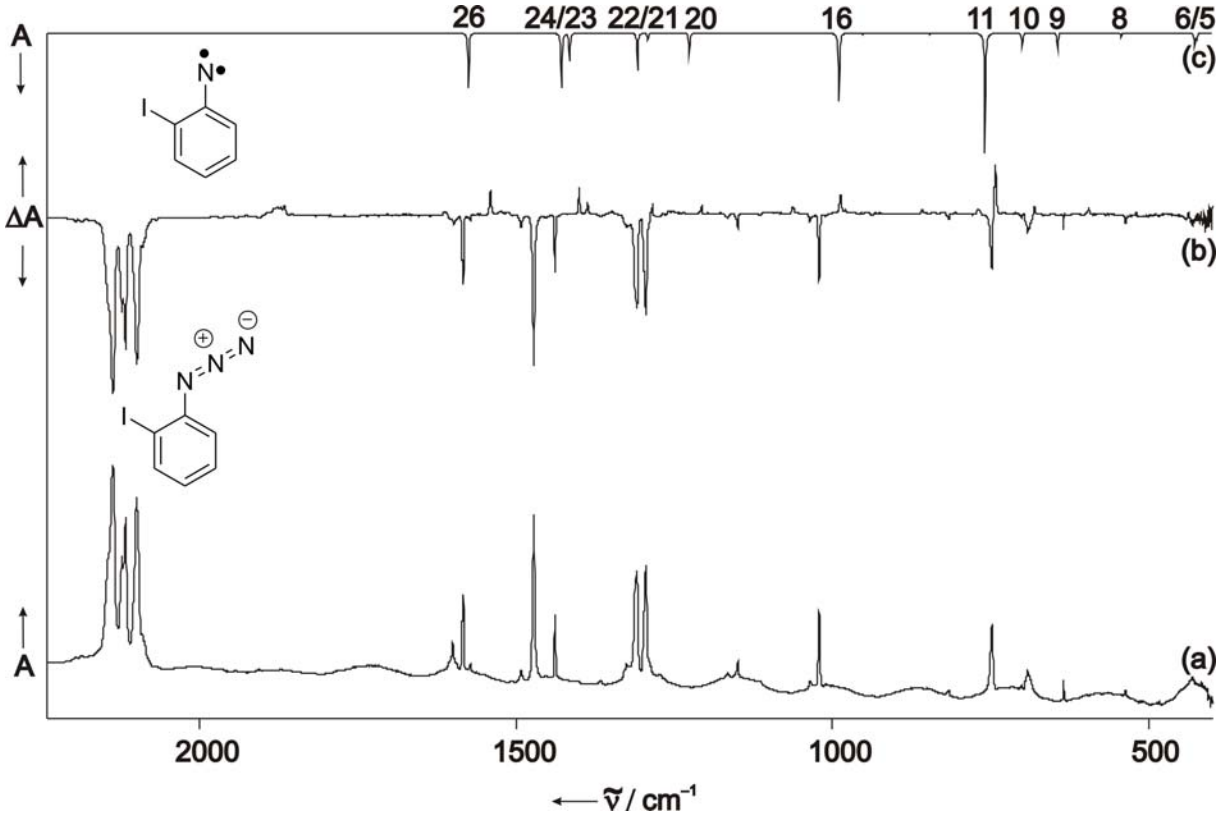

Figure 64. (a) IR spectrum of an argon matrix at 4 K containing 2-iodophenyl azide **32**. (b) The same matrix after 254 nm photolysis. Peaks pointing downwards are decreasing in intensity, peaks pointing upwards are increasing in intensity upon irradiation with 254 nm. (c) UB3LYP/6-311G(d,p) calculated infrared spectrum for triplet 2-iodophenylnitrene T-**33**.

Upon short wavelength excitation of 2-iodophenyl azide **32**, molecular nitrogen is excluded from the parent compound and the singlet state of 2-iodophenylnitrene S-**33** is formed. Since intersystem crossing is known to be fast for phenylnitrene at low temperature and the attached iodine atom is expected to increase the ISC rate constant, the singlet state of S-**33** crosses to the triplet surface fast and effectively – thus clearly no singlet state can be observed in these experiments.[167] Indirect evidence that the singlet state is formed first, could be found in rearrangements of the singlet nitrene to its isomers, which even at low temperature in a rigid noble gas matrix could not be suppressed. Next to the nitrene signals, some ring enlargement products are already detected under the experimental conditions while the main photoproduct is triplet nitrene T-**33** (Figure 65).

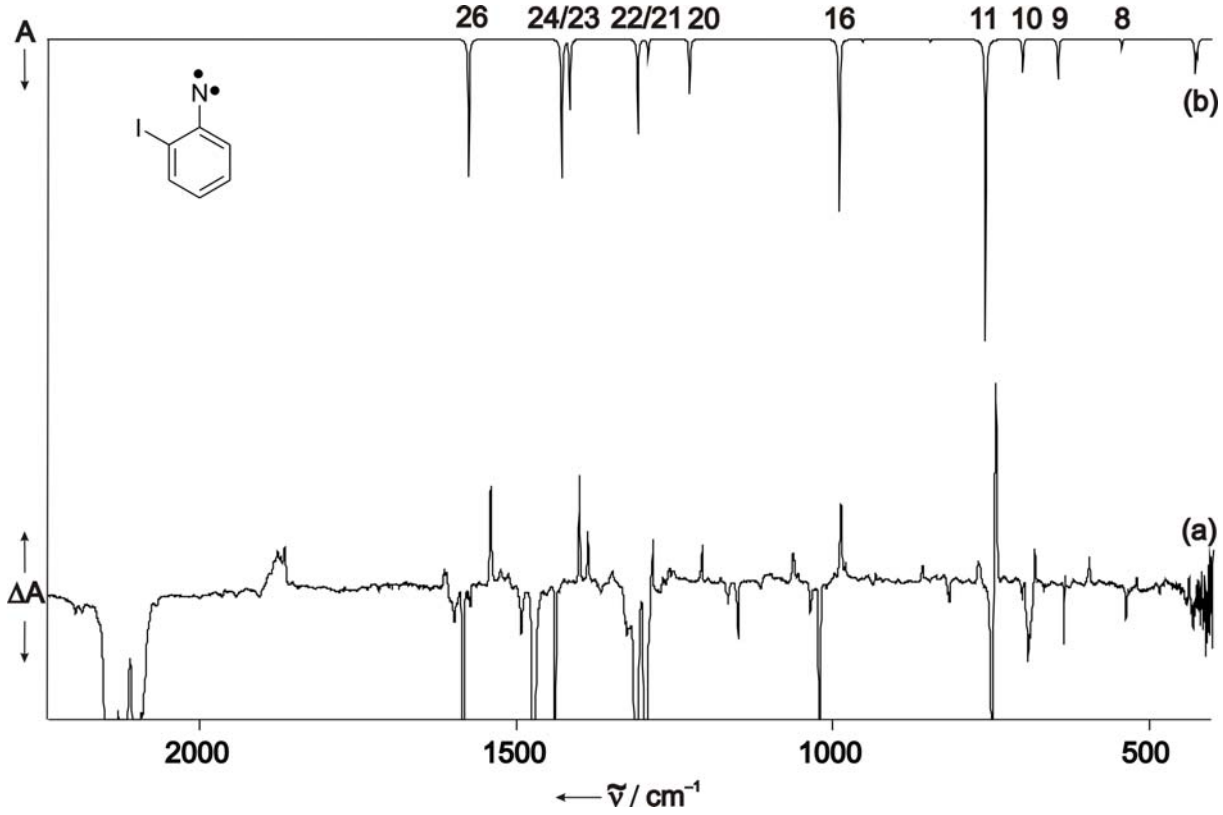

Figure 65. (a) Expansion of the IR difference spectrum showing the appearance of triplet 2-iodophenylnitrene T-**33**. (b) UB3LYP/6-311G(d,p) calculated IR spectrum of T-**33**. Some ring enlargement products around 1800 cm^{-1} are obvious.

All infrared signals belonging to T-**33** are collected in Table 18.

Table 18. IR spectroscopic data of triplet 2-iodophenylnitrene T-**33**.

Mode #	Sym.	Argon [b]	B3LYP [a]	Assignment
5	A"	e	425.8 (5)	Skeletal vib.
6	A'	e	428.2 (11)	CCN bending,
7	A"	-	507.9 (0)	Skeletal vib.
8	A'	520.6 (5)	544.5 (3)	In-plane ring deformation vib.
9	A'	595.7 (10)	645.7 (13)	In-plane ring deformation vib.
10	A"	681.4 (10)	701.7 (11)	oop vib. $C_{4,5,6}$-H
11	A"	742.6 (100)	759.4 (98)	Sym. oop vib. $C_{3,4,5,6}$-H
12	A'	-	846.4 (1)	Ring deformation
14	A"	-	953.6 (1)	Antisymmetric oop vib. $C_{3,4,5,6}$-H

16	A'	986.9 (40)	990.6 (56)	C-I stretch , in-plane ring-def.
20	A'	1206.2 (20)	1226.2 (18)	$C_{3,6}$-H in-plane bending
21	A'	1268.8 (5)	1292.5 (6)	$C_{3,4,6}$-H in-plane bending, C_2C_3; C_4C_5, C_6C_1 stretch
22	A'	1284.5 (25)	1308.7 (31)	CN stretch., $C_{3,5,6}$-H in-plane bending
23	A'	1386.8 (25)	1415.6 (23)	$C_{3,6}$-H in-plane bending, C=C stretching
24	A'	1399.8 (50)	1428.3 (45)	$C_{3,4,5,6}$-H in-plane bending, C=C stretching
26	A'	1539.9 (45)	1575.2 (45)	C_2C_3,C_5C_6 stretching
27	A'	c	3175.0 (1)	$C_{4,5}$-H asym. stretching
28	A'	c	3186.7 (5)	$C_{3,6}$-H, $C_{4,5}$-H asym. stretching
29	A'	c	3196.8 (5)	$C_{3,6}$-H asym. stretching
30	A'	c	3202.1 (13)	$C_{3,4,5,6}$-H sym. stretching

[a] UB3LYP/6-311G(d,p). [b] Argon, 4 K. [c] not assigned due to the broad peaks in this region.

The most intense signal in the experimental infrared spectrum is found at 742.6 cm^{-1} and belongs to the out of plane vibration of the phenylene hydrogens (calc. 759.4 cm^{-1}). The signal at 986.9 cm^{-1} can be assigned to the C-I stretching in combination with in plane deformation vibration of the hydrogen atoms and is in very good agreement with the calculated value of 990.6 cm^{-1}. A higher excitation energy is needed for the C-N stretching at 1284.5 cm^{-1} (calc. 1308.7 cm^{-1}), as well as the C=C stretching vibrations at 1399.8 and 1539.9 cm^{-1} which are calculated by the UB3LYP/6-311G(d,p) level of theory to appear at 1428.3 and 1575.2 cm^{-1}, respectively. Summing up, the experimental infrared spectrum for 2-iodophenylnitrene T-**33** is very well reproduced by the UB3LYP (6-311G(d,p)) method and therefore allows a clear assignment of this species.

Further irradiation of a matrix containing 2-iodophenylnitrene T-**33** with visible light in the range of 450 – 395 nm of a mercury high-pressure arc lamp causes a disappearance of all signals belonging to triplet nitrene T-**33** and simultaneous development of a series of new signals. However, the photochemistry does not lead to only one product instead at least two photoproducts are obtained. The same wavelength range also initializes rearrangement of the corresponding ketenimines **34** and **35**, as is discussed

later. Characteristic infrared absorptions are found at 1750 and 1727 cm^{-1}, an indication of a C=N double bond vibration in benzazirines. Since two isomeric benzazirines are possible photoproducts of **33**, assignment of the observed IR signals with the B3LYP/6-311G(d,p) calculated signals of benzazirines **37** and **36** is possible (Figure 66).

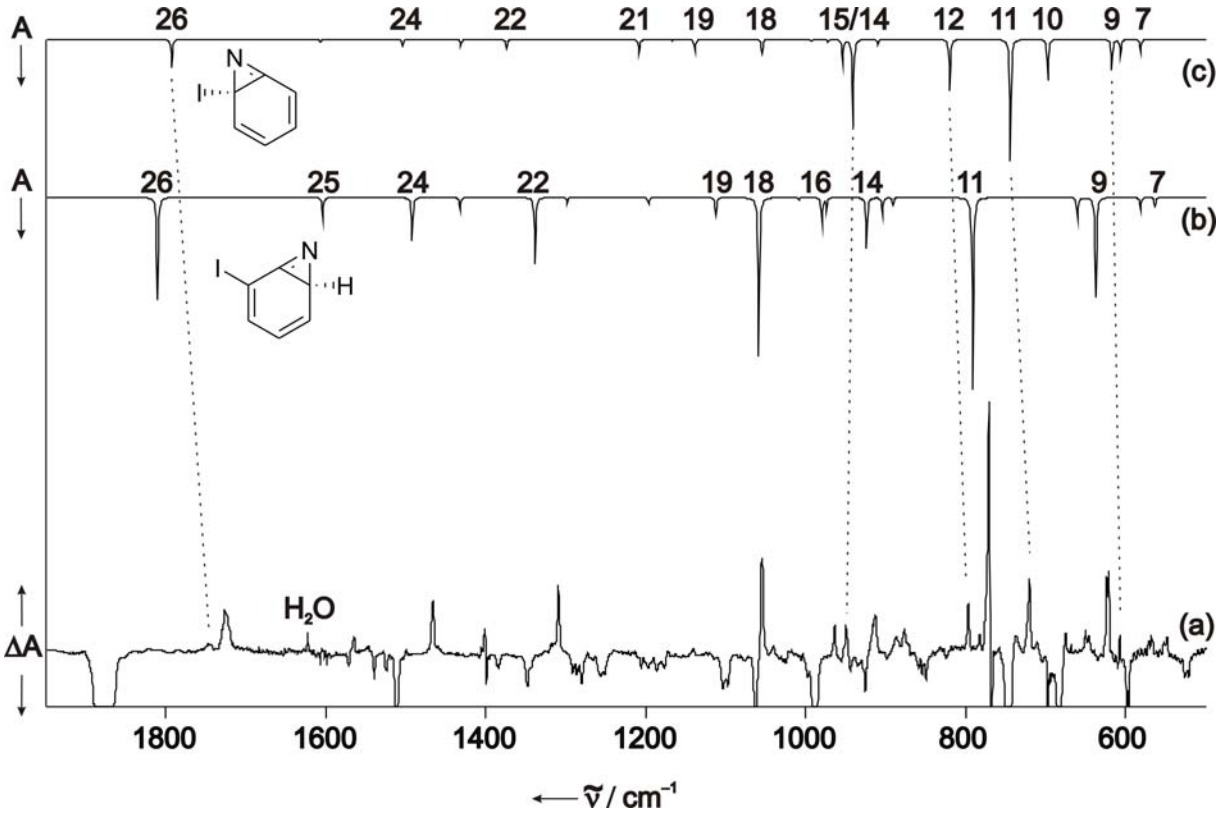

Figure 66. (a) Difference IR spectrum obtained of an argon matrix containing the photoproducts of 2-iodophenyl azide **32** with 450 – 395 nm. Peaks pointing downwards are decreasing upon irradiation, while signals pointing upwards are increasing in intensity upon irradiation. (b) IR spectrum calculated for benzazirine **37** at the B3LYP/6-311G(d,p) level of theory. (c) IR spectrum calculated for benzazirine **36** at the B3LYP/6-311G(d,p) level of theory.

The main species formed under photolysis with 450 – 395 nm apparently is benzazirine **37**, formed by ringclosure of nitrene **33** towards the nonsubstituted site or by ringclosure of ketenimine **35**. This finding is in good accordance with the proposed route from computational work and the conclusions of Grote and Sander, since benzazirine **37** is the isomeric benzazirine which is formed by the lower barrier from nitrene **33**.[177] IR signals due to benzazirine **36** make only a smaller contribution to the observed IR spectrum. A good comparison of the concentrations of these two species results from relation of the intensities of the C=N vibrations, which are found to have only a small difference in calculated absolute intensities (abs. Int. $\nu_{C=N}$ **37** : abs. Int. $\nu_{C=N}$ **36** = 29.8 :

23.4). All experimentally visible IR absorptions of benzazirines **37** are collected in Table 19.

Table 19. IR spectroscopic data of benzazirines **37**.

Mode #	Argon [b]	B3LYP [a]	Assignment
6	-	483.0 (1)	Ring deformation
7	547.6 (10)	563.5 (3)	Ring deformation
8	567.6 (10)	581.9 (5)	Ring puckering
9	620.8 (50)	637.1 (50)	Ring deformation
10	649.7 (10)	660.4 (10)	$C_{3,4,5}$-H oop deformation, C_6-N stretching
11	770.9 (100)	791.7 (98)	$C_{3,4,5}$-H oop deformation
12	-	891.7 (3)	$C_{3,6}$-H deformation
13	887.0 (5)	904.4 (8)	$C_{3,5,6}$-H deformation
14	913.2 (25)	924.1 (25)	C_6-H deformation
15	-	974.2 (5)	C_4-H deformation
16	963.9 (15)	980.7 (12)	$C_{4,5}$-H oop deformation
18	1054.9 (70)	1059.6 (82)	C-I stretching, $C_{3,6}$-H deformation
19	-	1114.0 (8)	C_6-H deformation, C_4-H in plane def., C_1-C_6 stretching
20	-	1197.5 (1)	$C_{4,5}$-H asym. bending
21	-	1299.6 (1)	$C_{3,6}$-H deformation
22	1309.9 (35)	1339.0 (33)	$C_{3,6}$-H bending
23	1402.0 (10)	1433.9 (5)	$C_{4,5}$-H sym. bending
24	1466.8 (25)	1494.0 (21)	C_2=C_3; C_4=C_5 sym vibration
25	1565.9 (10)	1605.6 (10)	C_2=C_3; C_4=C_5 asym vibration
26	1726.6 (45)	1812.9 (51)	C_1=N vibration
27	c	3153.2 (3)	$C_{5,6}$-H asym. stretching
28	c	3163.7 (32)	$C_{5,6}$-H sym. stretching
29	c	3176.9 (26)	$C_{3,4}$-H asym. stretching
30	c	3189.8 (7)	$C_{3,4}$-H sym. stretching

[a] B3LYP/6-311G(d,p). [b] Argon, 4 K. [c] not assigned due to the broad peaks in this region.

A strong and characteristic C=N vibration is experimentally observed at 1726.6 cm^{-1} and corresponds to the calculated vibration at 1812.9 cm^{-1} (B3LYP/6-311G(d,p)). The symmetric and asymmetric C=C double bond vibrations are expected to be found at 1494.0 and 1605.6 cm^{-1} by B3LYP/6-311G(d,p) calculations and are experimentally monitored at 1466.8 and 1565.9 cm^{-1}, respectively. A strong vibration is also found at 1054.9 cm^{-1} (calc. 1059.6 cm^{-1}) and can be assigned to a C-I stretching vibration coupled with C-H bending. The strongest IR absorption is found at 770.9 cm^{-1} (calc. 791.7 cm^{-1}) and corresponds to a out of plane deformation vibration of the HC=CH moieties. A quite strong ring deformation vibration is observed at 620.8 cm^{-1} and can be ascribed to be due to a ring deformation vibration, for which an infrared signal at 637.1 cm^{-1} is predicted by the DFT calculations. All IR signals assigned to the more stable but minor benzazirine **36** are given in Table 20.

Table 20. IR spectroscopic data of benzazirines **36**.

Mode #	Argon [b]	B3LYP [a]	Assignment
5	-	401.0 (4)	Ring deformation
6	-	435.8 (1)	Ring deformation
7	-	582.0 (9)	Ring deformation
8	-	606.7 (13)	Ring puckering
9	607.0 (10)	617.0 (24)	Ring deformation
10	674.9 (15)	697.6 (34)	$HC_3=C_4H$, $HC_5=C6_H$ sym. oop deformation
11	720.3 (100)	744.8 (100)	$HC_3=C_4H$; $HC_5=C_6H$ oop deformation
12	796.8 (50)	820.4 (42)	$HC_3=C_4H$; C_6H oop deformation
13	-	910.6 (3)	$C_2C_3C_4$ bending, $C_4C_5C_6$ bending, $C_{3,4,5,6}$-H oop deformation
14	950.0 (70)	941.2 (70)	C-I stretching, $C_{3,4,5,6}$-H deformation
15	952.0 sh	954.2 (19)	C-I stretching, $HC_3=C_4H$; $HC_5=C_6H$ asym. oop

			deformation
18	1040.4 (10)	1055.8 (11)	$C_{1,2}$-stretching. ring deformation
19	-	1139.3 (8)	C_2-C_3-stretching, $C_{4,5,6}$-H in plane bending
21	-	1209.2 (11)	$C_{3,4}$-H asym. bending
22	-	1375.0 (6)	$C_{4,5}$-H sym. bending
23	1406.1 (5)	1432.6 (4)	$C_{3,4,5,6}$-H in-plane bending
24	1473.3 (5)	1505.8 (4)	C_3=C_4; C_5=C_6 sym stretching
25	-	1608.2 (1)	C_3=C_4; C_5=C_6 asym stretching
26	1746.8 (10)	1794.1 (22)	C_1=N stretching
28	c	3177.5 (3)	$C_{3,5}$-H asym. stretching
29	c	3188.6 (9)	$C_{3,4,5}$-H sym. stretching
30	c	3214.6 (1)	C_6-H stretching

[a] B3LYP/6-311G(d,p). [b] Argon, 4 K. [c] not assigned due to the broad peaks in this region. sh = shoulder

The most diagnostic IR absorption signals of benzazirine **36** is ascribed to the C=N vibration which is experimentally observed at 1746.8 cm^{-1} and was calculated at the B3LYP/6-311G(d,p) level of theory to be found at 1794.1 cm^{-1}. The symmetric C=C vibration is found at 1473.3 cm^{-1} (calc. 1505.8 cm^{-1}), while all very intense vibrations are redshifted to the fingerprint region of the spectrum. The C-I stretching vibration is observed at 950.0 cm^{-1} while it was calculated to be obtained at 941.2 cm^{-1}. Strong out of plane deformation vibrations of the hydrogens attached to the double bonds have excitation energies of 796.8 (calc. 820.4 cm^{-1}) and 720.3 cm^{-1} (calc. 744.8 cm^{-1}). In conclusion, the overall appearance of all signals allows the identification of both possible isomeric benzazirines **36** and **37**.

Irradiation of a matrix with long wavelength in the range of 680 – 420 nm mainly results in formation of ketenimines. In analogy to the case of benzazirines, there are two isomeric ketenimines which could be produced from 2-iodophenylnitrene **33**. Ketenimine **34**, which has the iodine attached to a double bond is 0.4 kcal/mol more stable than ketenimine **35**, with the iodine attached to the end of the cumulene bond as was calculated at the B3LYP/6-311G(d,p) level of theory. It was reported in other cases that the main ketenimine formed under photolysis in a matrix corresponds to the more stable isomer.[177] Nevertheless, the small difference in energy between **34** and **35** affords that both isomers

might be visible under experimental conditions.[177] As expected, both ketenimine isomers **34** and **35** are formed and can be distinguished by photolysis as is shown in Figure 67.

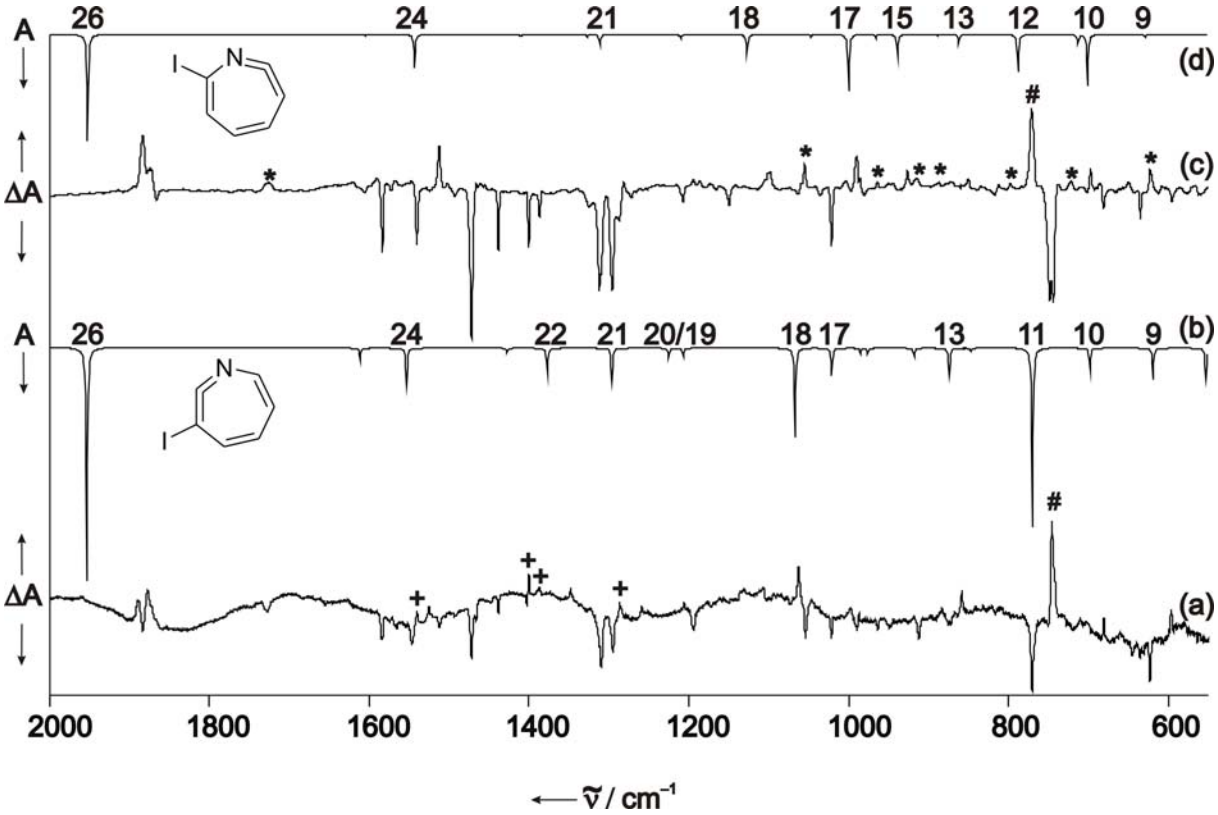

Figure 67. (a) IR difference spectrum obtained after short time irradiation with 254 nm of an argon matrix containing the photolysis products of 2-iodophenyl azide **32**. Peaks pointing downwards are decreasing in intensity upon irradiation (i.e. benzazirine **37**, benzazirine **36**, ketenimine **34**, and azide **32**). Peaks pointing upwards are increasing in intensity upon irradiation (i.e. nitrene **33** denoted with a plus sign and ketenimine **35**; the hash key is a superposition of signals of nitrene **33** and ketenimine **35**). (b) B3LYP/6-311G(d,p) calculated IR spectrum of **35**. (c) IR difference spectrum obtained after irradiation with 680 - 420 nm of an argon matrix containing the photolysis products of 2-iodophenyl azide **32**. Peaks pointing downwards are decreasing in intensity upon irradiation (i.e. ketenimine **35**, nitrene **33** and azide **32**). Peaks pointing upwards are increasing in intensity upon irradiation (i.e. ketenimine **35**, benzazirine **37**, and **36**, these signals are denoted with a star, the signal denoted with a hash key are partly from benzazirines **37** and **36** and partly from ketenimine **34**). (d) B3LYP/6-311G(d,p) calculated IR spectrum of ketenimine **34**.

Short wavelength photolysis of a matrix containing the photoproducts of 2-iodophenyl azide **32** with 254 nm for a short period of time leads partly to disappearance of ketenimine **34** and concomitantely appearance of signals which could be assigned to ketenimine **35** besides signals belonging to nitrene **33**. The most diagnostic signal which simultaneously is also the strongest vibration clearly belongs to the cumulene stretching at

1877.0 cm^{-1}. All assigned absorptions of ketenimine **35** are collected in the following Table 21.

Table 21. IR spectroscopic data of ketenimine **35**.

Mode #	Argon [b]	B3LYP [a]	Assignment
6	-	449.6 (12)	$C_1C_2C_3$ bending; ring deformation
8	521.0 (5)	553.2 (13)	N=C=C deformation, $C_{3,4,5,6}$-H oop deformation vib.
9	596.4 (10)	619.0 (13)	N=C=C bending; ring deformation
10	680.6 (10)	698.7 (8)	N=C=C bending; $C_{3,4,5,6}$-H deformation
11	745.1 (90)	770.2 (76)	$C_{3,4,5,6}$-H sym. oop deformation;
13	858.0 (10)	874.8 (11)	C_5-H oop deformation; $C_3C_4C_5$ bending
14	-	918.3 (2)	C_3-H deformation; C_4-C_5 stretching
15	-	976.8 (2)	$C_{5,6}$-H asym. oop deformation
16	-	985.4 (2)	$C_{3,4}$-H asym. oop deformation
17	997.6 (10)	1021.4 (11)	C_6-N stretching; $C_{5,6}$-H in plane deformation
18	1062.7 (30)	1067.5 (38)	C-I stretching, C_3-H deformation
19	-	1207.9 (2)	$C_{3,4}$-H asym. bending
20	1205.9 (5)	1225.9 (3)	$C_{5,6}$-H asym. bending
21	1259.4 (10)	1296.8 (14)	N=C=C sym. stretching, $C_{3,5}$-H bending
22	1348.0 (10)	1377.7 (10)	$C_{3,4,5,6}$-H sym. bending
23	-	1427.9 (1)	$C_{3,4}$-H; $C_{5,6}$-H asym. bending
24	1524.8 (15)	1553.5 (16)	C_3=C_4, C_5=C_6 sym. stretching
25	-	1611.5 (5)	C_3=C_4, C_5=C_6 asym. stretching
26	1877.0 (100)	1953.2 (99)	C=C=N asym. stretching
28	c	3152.6 (8)	C_3-H stretching
29	c	3160.8 (9)	$C_{3,4,5}$-H stretching
30	c	3186.3 (13)	C_6-H stretching

[a] B3LYP/6-311G(d,p). [b] Argon, 4 K. [c] not assigned due to the broad peaks in this region.

Moreover, an absorption at 1524.8 cm^{-1} is found in the experimental spectrum which could be assigned to the symmetric C=C double bond stretching with the help of the DFT calculations. The prediction for this vibration is at 1553.5 cm^{-1} and therefore in very good accordance. The intense C-I stretching vibration at 1062.7 cm^{-1} in combination with

the very intense out of plane deformation mode of the hydrogens of the double bonds helps to characterize this species. In good agreement with this findings are the calculated signals at 1067.5 and 770.2 cm^{-1}, respectively.

Fortunately, the second isomeric ketenimine **34** is the main product after irradiation of a matrix containing the photoproducts of 2-iodophenyl azide **32** with 680 – 420 nm light. Under these conditions, ketenimine **35** was found to be photolabile. Besides the main product ketenimine **34** also benzazirines **36** and **37** are found to be photoproducts under the chosen conditions. The most intense infrared signal in the fingerprint region is predicted by B3LYP/6-311G(d,p) calculations to be due to C-I stretching coupled with C-H deformation vibration and should appear at 1000.7 cm^{-1}, a value in very good accordance with the strong signal in the experimental IR spectrum at 989.7 cm^{-1} (Figure 67, Table 22).

Table 22. IR spectroscopic data of ketenimine **34**.

Mode #	Argon [b]	B3LYP [a]	Assignment
7	-	432.1 (3)	Ring deformation
8	474.7 (5)	495.0 (4)	N=C=C bending; $C_{2,3,4,5}$-H deformation
9	-	629.2 (2)	N=C=C bending; ring deformation; $C_{4,5}$-H deformation
10	-	702.0 (48)	$C_{2,3,4}$-H sym. oop deformation
11	697.1 (10)	713.2 (8)	N=C=C bending; C_2-H deformation
12	771.2 (50)	788.0 (34)	$C_{3,4,5}$-H oop deformation
13	850.0 (5)	862.7 (7)	$C_{3,5}$-H oop deformation
14	926.3 (15)	939.8 (20)	$C_{3,5}$-H bending; $C_3C_4C_5$ bending; C_5C_6N bending
15	-	967.0 (3)	C_4-H deformation
16	989.7 (25)	1000.7 (53)	C-I stretching, C_3-H deformation
18	-	1047.5 (2)	$C_{2,3}$-H; $C_{4,5}$-H bending
19	1099.5 (15)	1127.3 (18)	C_2-H bending
20	1194.3 (5)	1211.0 (3)	$C_{3,4}$-H in plane asym. bending
21	1281.5 (10)	1311.9 (9)	C_5-H in plane bending
22	-	1327.5 (2)	N=C=C sym. Stretching, C_2-H bending
23	-	1410.7 (1)	$C_{3,4}$-H in plane sym. bending
24	1512.2 (30)	1543.1 (31)	C_3=C_4; C_5=C_6 sym. stretching

25	-	1605.6 (1)	C_3=C_4; C_5=C_6 asym. stretching
26	1883.2 (100)	1952.1 (99)	N=C=C asym. stretching
27	c	3138.5 (1)	$C_{3,4}$-H asym. stretching
28	3025.1 (5)	3157.5 (13)	$C_{3,4}$-H sym. stretching

[a] B3LYP/6-311G(d,p). [b] Argon, 4 K. [c] not assigned due to the broad peaks in this region.

Furthermore, an intense absorption at 1099.5 cm^{-1} is experimentally observed and can be traced back to belong to the predicted absorption at 1127.3 cm^{-1}, mainly composed of C-H defromation with a small amount of CCN stretching. While a signal attributable to C-H deformation modes at 771.2 cm^{-1} (calc. 788.0 cm^{-1}) is well resolved, a similar strong signal is predicted at 702.0 cm^{-1} where appearently no signal evolves. However, this might be explained due to destructive superposition of several species which are photolabile at the irradiation conditions and which therefore destroy the absorption at this energy (Figure 65). Despite this, the symmetric double bond vibration at 1512.2 cm^{-1} is well resolved and found to be in nice agreement with the DFT prediction of 1543.1 cm^{-1}. However, the most characteristic vibration belongs to the cumulene stretching vibration at 1883.2 cm^{-1}, calculated to be at 1952.1 cm^{-1}, which similar to the finding for isomeric ketenimine **35** is the most intense absorption of ketenimine **34**.

Additional photochemical conversion takes place if 2-iodophenyl azide **32**, isolated in an argon matrix, is irradiated for a long time (24 hours) with λ = 400 – 385 nm. Some broad signal around 2258 cm^{-1} appears, which might be due to C-N triple bond stretching. Certainly, carbon carbon triple bonds could also show up at this energy, however, there is no corresponding C-H stretching around 3300 cm^{-1}. The possibility of an internal alkine could not be excluded. Since there is a high number of bands formed under these conditions, several isomeric species might be formed (Figure 68).

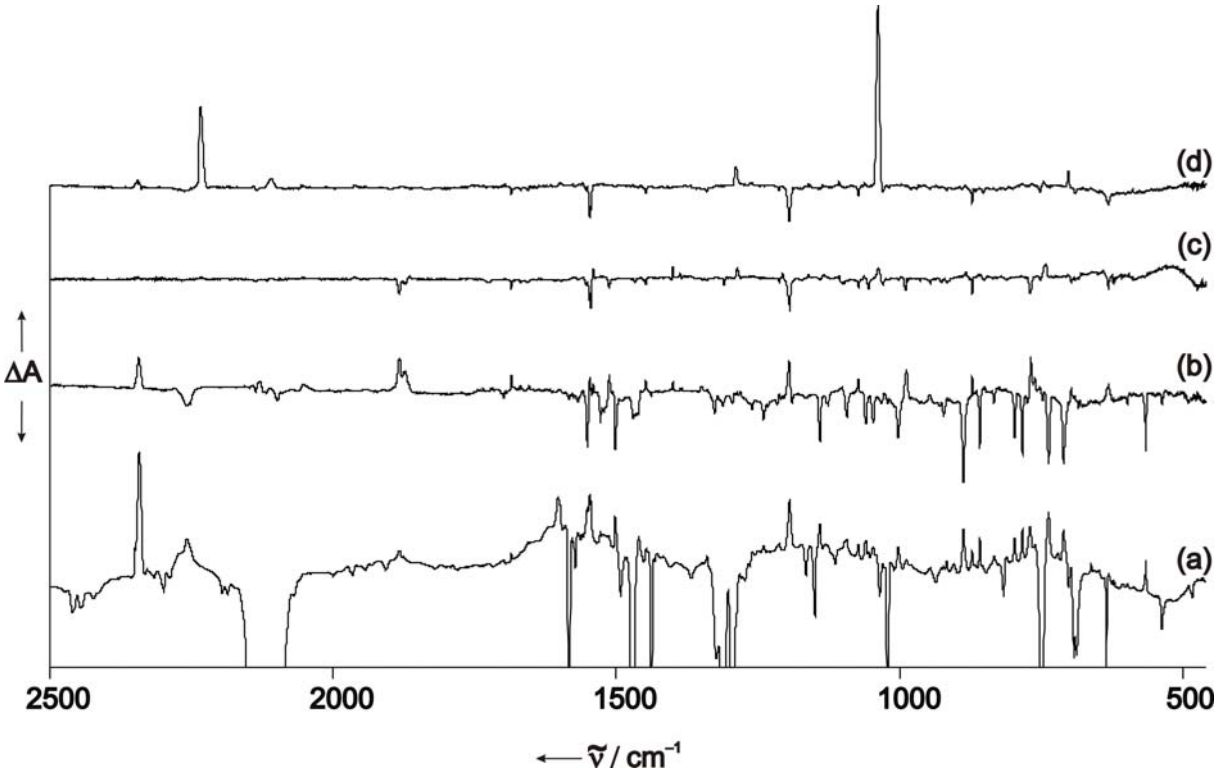

Figure 68. (a) IR difference spectrum obtained after irradiation of an argon matrix containing 2-iodophenyl azide **32** for 24 hours with λ = 400 – 385 nm light of a mercury high-pressure lamp. (b) IR difference spectrum obtained after irradiation of the same matrix with λ = 400 – 280 nm. (c) IR difference spectrum obtained after irradiation of a matrix containing photoproducts of 2-iodophenyl azide **32** with λ = 254 nm. (d) IR difference spectrum obtained after irradiation of matrix (b) with λ = 254 nm. Peaks pointing downwards are decreasing in intensity, peaks pointing upwards are increasing in intensity upon specified irradiation.

Further irradiation of this matrix results in diminuation of most formerly appearing signals and formation of ketenimines **34** and **35**, triplet 2-iodophenylnitrene **33** and one further not identified compound. Since no more 2-iodophenyl azide **33** is abundant in the matrix after prolonged 400 – 385 nm irradiation, it seems that the rearranged photoproducts are still C_6H_4IN-isomers, as otherwise evolution of signals belonging to **33**, **34**, and **35** could not be explained. Nevertheless, none of the signals could be identified to any of the numerous possible ring opening and ring contraction isomers. Moreover, different radical products were calculated, which could add a nearby iodine radical after rearrangement and come back to the C_6H_4IN-surface. However, none of the simulated IR spectra resembled the one obtained. A closer view of the region between 1800 and 500 cm^{-1}, shows that at least two unidentified photoproducts are formed by inital λ = 400 – 385 nm irradiation (Figure 69).

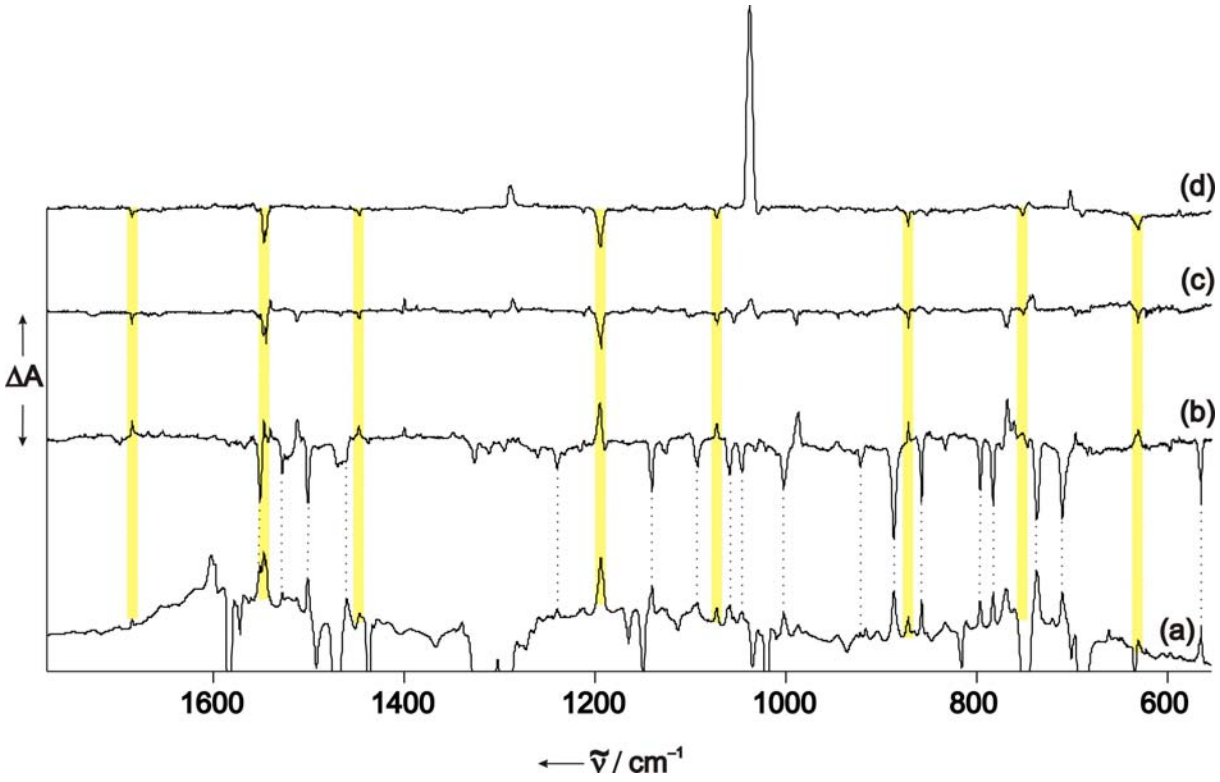

Figure 69. (a) IR difference spectrum obtained after irradiation of an argon matrix containing 2-iodophenyl azide **32** for 24 hours with λ = 400 – 385 nm light of a mercury high-pressure lamp. (b) IR difference spectrum obtained after irradiation of the same matrix with λ = 400 – 280 nm. (c) IR difference spectrum obtained after irradiation of a matrix containing photoproducts of 2-iodophenyl azide **32** with λ = 254 nm. (d) IR difference spectrum obtained after irradiation of matrix (b) with λ = 254 nm. Peaks pointing downwards are decreasing in intensity, peaks pointing upwards are increasing in intensity upon specified irradiation.

Yellow bars indicate signals belonging to a photoproduct which itself is photolabile towards irradiation with λ = 254 nm of a low-pressure mercury lamp. No signals attributable for ring-opening (2000 – 2400 cm^{-1}) are appearing which nevertheless might be too little in intensity to be differentiated. The second photolabile photoproduct (no yellow bars) is probably transformed back to a C_6H_4IN-isomers through irradiation with 400 – 280 nm. Signals at 2258 cm^{-1} and a small one at 1700 cm^{-1} are appearing for this species. However, as had been mentioned a hugh number of isomers are possible and none of these was in good resemblance with the obtained spectrum. Similar to the study of Maltsev et al. in which ring opening of 2-naphthylazide **192** was observed with proceeding irradiation, it can only be speculated on the formed species. A weak signal is obtained at 1960 cm^{-1} after irradiation with 254 nm, which might be due to an allene moiety in the molecule. Furthermore, growth of a weak signal at 2052 cm^{-1} in the difference spectrum is noted, which can possibly be traced back to an ketenimine, if it is not due to a combination

band or overtone. In conclusion, the nature of the species formed under long 400 – 385 nm photolysis is not known yet and under current further investigation.

In summary, in this study photochemical conversion of 2-iodophenyl azide **32** into different isomeric species was spectroscopically followed. The observed photoisomerization as well as conditions for interconversion of isomers are shown in Scheme 99.

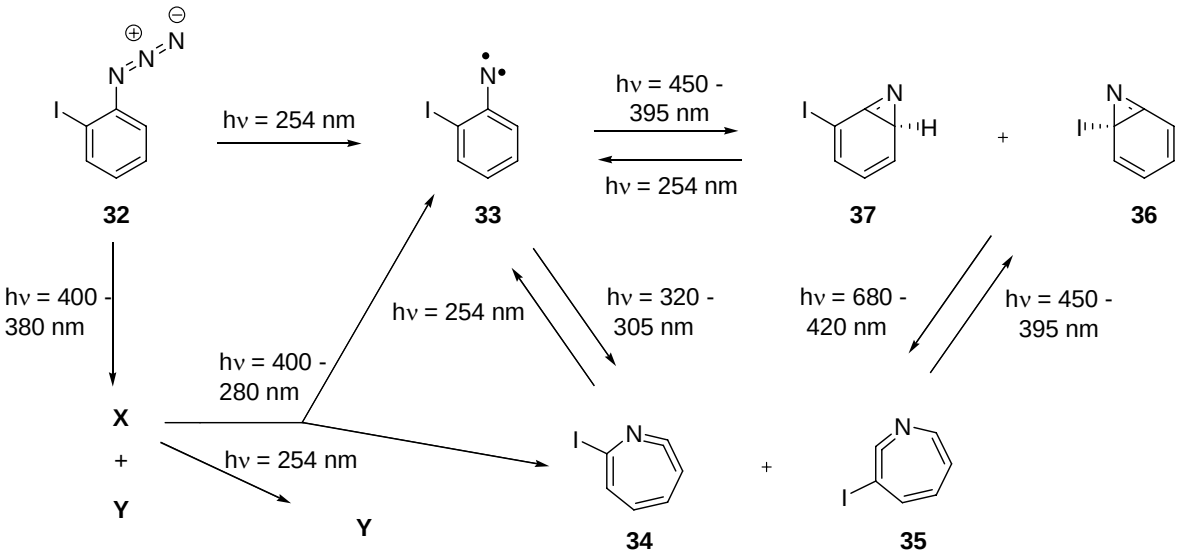

Scheme 99. Photochemical conversion of phenyl azide **32** into triplet 2-iodphenylnitrene **31**, benzazirines **36** and **37**, ketenimines **34** and **35**, and unknown ring-opening products **X** and **Y**.

9. Triazatrimethylenemethanes

9.1 Introduction

Trimethylenemethane (TMM) **49** has attracted chemists attention for a long time as possible intermediate in photochemical and thermal reaction processes. Dowd first prepared this *non-Kékule* diradical in 1966 by photolysis of the corresponding pyrazoline **193** (Scheme 100).[178]Due to its stability for months at low temperature and a linear Curie analysis, it was estimated that the observed electron paramagnetic resonance belongs to the triplet ground state, in accord with molecular orbital theoretical predictions.[12, 179, 180] Even simple Hückel theory predicts a triplet ground state and high level calculations supported this finding.[181] Some years later, it was again Dowd who observed a very clean triplet EPR spectrum of TMM **49** after photolysis of 3-methylene-cyclobutanone **194** with ultraviolet light (Scheme 100).[30] Since no suitable crystalline host was found for ketone **194**, a single crystal of the pure ketone was grown and studied by EPR spectroscopy. With the single crystal at hand and after photolysis at low temperature, the hyperfine splitting for the z_1-signal could be observed and was analyzed to belong to a D_{3h}-symmetric structure, due to a splitting into seven signals with nearly binomial distribution for six equivalent protons of 1:6:15:20:15:6:1.

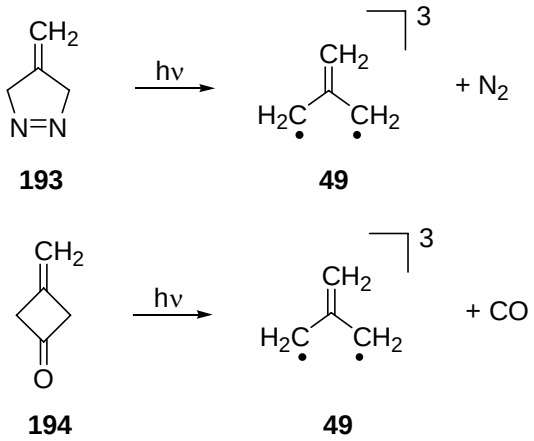

Scheme 100. Precursors of triplet TMM **49**.

After annealing a matrix containing TMM **49** to higher temperatures the triplet EPR signal diminished irreversely, as the parent diradical paired its electrons and formed a ring to give the corresponding singlet methylenecyclopropane **195** (Scheme 101).[178]

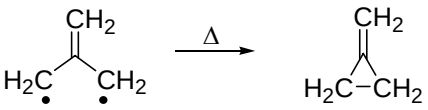

49 **195**

Scheme 101. Ring closure of TMM **49** at higher temperature to form methylenecyclopropane **195**.

With the aim to synthesize a more stable derivative of **49** without rigorously changing the electronic system, it was Bersons group at Yale university, who published their results on a cyclic TMM derivative **196**.[182] As both possible ring closure isomers **197** and **198**, respectively, should be highly strained, it was hoped to suppress this reaction channel (Scheme 102).[183] The parent TMM system **196** was shown to be a triplet ground state with a linear signal intensity versus reciprocal temperature dependance while the excited singlet state is calculated to be higher in energy by ca. 15.5 kcal/mol.[184, 185] The separation between the $^3B'_2$-ground state and the excited $^1A_1$-state was determined to be 16.1 +/- 0.1 kcal/mol in the gas phase.[186] Both ring-closure isomers **197** and **198** are calculated to be higher in energy on the C_6H_8 potential energy surface than the triplet diradical.[183, 185]

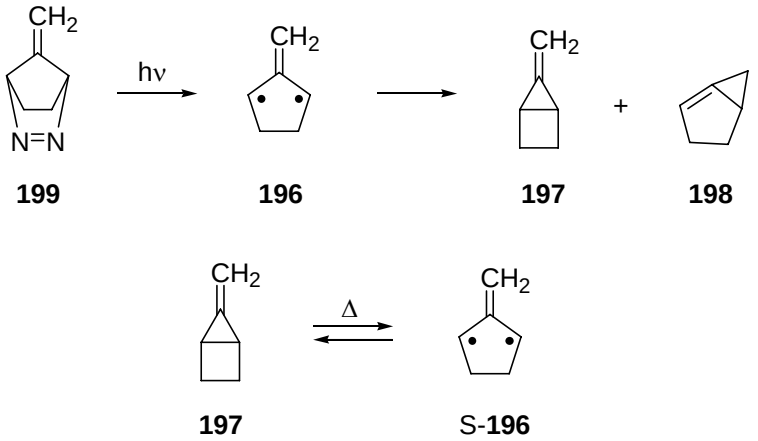

199 **196** **197** **198**

197 S-**196**

Scheme 102. Possible ring closure isomers of cyclic TMM derivative **196** and the equilibrium between singlet methylenecyclopropane **197** and singlet TMM S-**196**.

Nevertheless, compound **197** has a negative bond dissociation energy for the central cyclopropane bond, it was quantitatively "synthesized" to explore its (photo-) chemistry by irradiation of **199** in fluid media at -78 °C.[187] From different trapping experiments after pyrolysis of **199** to produce the parent cyclic TMM **196**, it was deduced that there has to be more than one species involved in the kinetics of this reaction. While **197** did not react

with olefins in the trapping studies, the singlet state of **196** which is in equilibria with **197** at higher temperature, reacts with olefins quite readily (Scheme 102).[188] Furthermore, it was shown through regioselective and stereoselective trapping of singlet **196** with butadiene, dimethylmaleate, and dimethylfumarate, that the excited singlet state is not of the bisected form with the exocyclic methylene p orbital perpendicular to the p orbitals of the ring, but is a planar singlet with conjugation between all four p orbitals.[189] Selectively stabilizing one of the two NBMOs through electron-releasing groups at the unique methylene unit, results in a change of the HOMO from asymmetric to symmetric with regard to the C_s-symmetry axis. Frontier molecular orbital theory predicts a change in reactivity as well as in regioselectivity and both predictions are verified by independent experiments.[190, 191]

1,3-diradicals like trimethylene **200**, which is formed by pyrolysis of the corresponding pyrazoline **201**, could be formed through diazenyl radicals as intermediate states in the first step, if one of the C-N bonds is broken before the other (Scheme 103). These diazenyl diradicals loose nitrogen to form the corresponding trimethylene **200**, reacting without a barrier to cyclopropane **202** as detectable species. Berson and co-workers were the first, who reported similar ideas for one of their TMM molecules.[192-194]

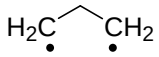

200

Scheme 103. Some derivatives of trimethylene **200** were discussed to be formed by stepwise nitrogen exclusion.

The bridged diazene **135** can rearrange to the fused diazene **203** upon thermal deazetation, which was explained by the authors through the possible formation of a diazenyl diradical **204** (Scheme 104). Support for their interpretation was found by the fact that photochemical conversion from **135** to **203** was not possible, while cyclic TMM **134** is formed by this way.[192] Recapture of molecular nitrogen from TMM **134** is therefore less probable than the two step mechanism through an intermediate diazenyl diradical **204**, which can rotate and form the fused diazene **203**.

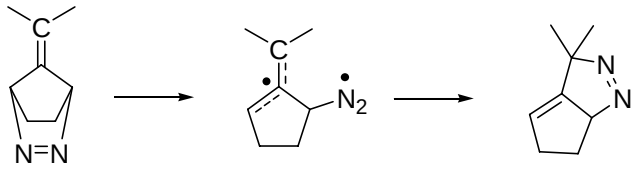

135 **204** **205**

Scheme 104. Rearrangement of diazene **135** to fused diazene **203** was explained by intermediate formation of diazenyl diradical **204**.

It is assumed that only those TMM derivatives for which the concerted two-bond cleavage to loose molecular nitrogen is orbitally symmetry forbidden, should give rise to a stepwise nitrogen extrusion via diazenyl diradicals.[183] A similar interpretation was given by Sheridan et al. for the isomerization of their azo compound **205** which under thermal and photochemical conditions can be transformed into its isomer **206** with a yield of 28 % (from **205** to **206**) or 13 % (from **206** to **205**) in the reverse direction (Scheme 105).[195] An intermediate diazenyl diradical **207** is formulated to explain this turnaround isomerization.[195]

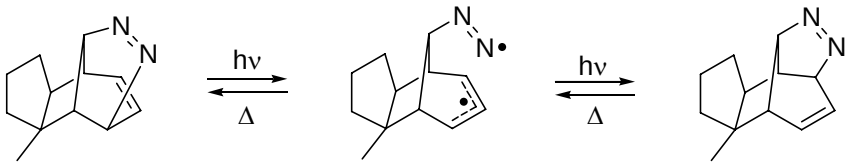

205 **207** **206**

Scheme 105. Isomerization of azo compound **205** to **206** through an intermediate diazenyl diradical **207**.

Adam et al. as well proposed a turnaround isomerization for their tetramethyl TMM precursor **208** because they were able to isolate 0.5 % of isomer **209** by GC analysis: a stable isomer of the highly hygroscopic diazene **210**, formed through possible diazenyl diradical **211** and its turnaround isomer **212**.[196] No thermal isomerization was observed in this case. In an independent study, Quast et al. were not able to reproduce the proposed photochemistry (as they did not observe isomer **210**) but found instead - highly dependent on the used solvent and only under strict exclusion of oxygen - reduction product **209** (Scheme 106).[197]

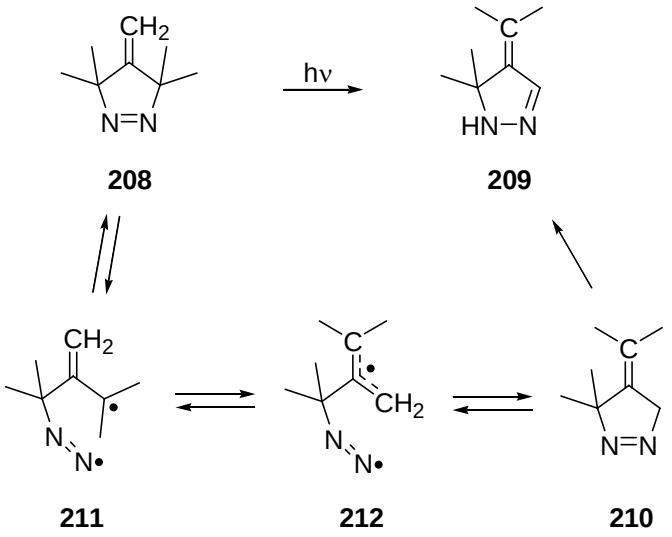

Scheme 106. Possible reaction path from diazene **208** to **209**. While **210** was observed in one study, an independent study did not find **210** but **209** as byproduct.

Compared with the rich exploration of TMM **49** and its derivatives, the chemistry of azaTMMs, is rather rare studied. It was mainly the group of Quast et al. who studied these elusive diradicals experimentally. Upon irradiation of an organic glass of iminotetrazoline **213** at low temperatures in a butyronitrile matrix, a clear centrosymmetric four-line triplet EPR spectrum was recorded, which was subscribed to belong to triplet diradical **214**, a *tris*(imino)methane (Scheme 107).[198]

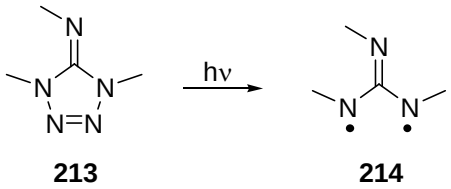

Scheme 107. Ultraviolet irradiation of iminotetrazoline **213** leads to triplet *tris*(imino)methane **214**.

The half-field signal assists the assignment to a triplet species and the zero-field parameters were determined to be $|D/hc| = 0.033$ cm^{-1} and $|E/hc| \sim 0$ cm^{-1}. An average distance between the unpaired electrons of 3.4 Å is calculated using a dipolar model. With a (single) crystal at hand, it was also possible to record the hyperfine splitting of the half-field transition, which showed at least nine equally spaced lines for the perhydro diradical, less signals for the diradical with only one [D_3]-methyl group, and no splitting for the perdeutero diradical.

It was the same group who observed the first EPR spectrum of a diazaTMM derivative, the diazaTMM diradical **215** (Scheme 108). After photolysis of tricyclic alkylidenedihydrotetrazole **216** in 2-MTHF or butyronitrile at 77 K a triplet EPR diradical spectrum with a half-field transition at 1669 G could be detected and it was concluded to belong to the diazaTMM diradical **215**.[199] The half-field signal showed hyperfine structure with at least 12 equidistant lines separated by 8.5 +/- 1 G. The zfs parameters for **215** were simulated to be |D/hc| = 0.031 cm^{-1} and |E/hc| = 0.0014 cm^{-1}. Assuming a dipolar model, the average distance between the radical centers is calculated to 3.5 Å, in good accordance with the calculations. Annealing of the organic glass or thermal decompositon of the parent compound **216** at higher temperatures gives rise to isomer **217** as only detectable species.

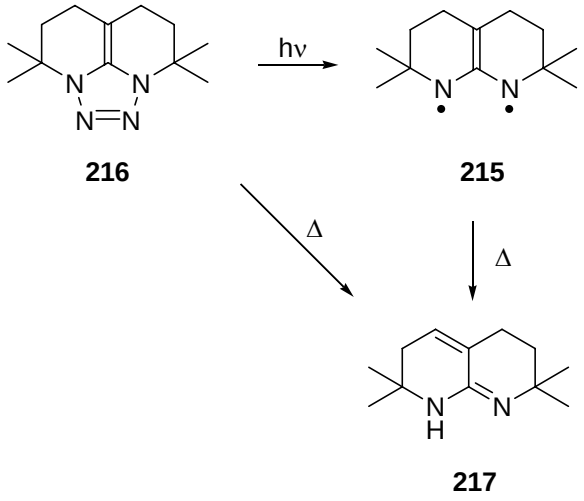

216 **215** **217**

Scheme 108. First triplet diazaTMM derivative **215** experimentally observed through irradiation of **216** and its isomerization to **217** upon annealing of the organic glass containing **215**.

As some shoulders were detected in the experimental spectrum, which could not be fitted in the calculation, a minor paramagnetic species was formed under the photolysis conditions besides some monoradical. Strain in the resulting diazaTMM derivatives was concluded to be decisive for the investigation of triplet diradicals of the azaTMM type as it was shown that most other studied diazaTMM precursors did not show any triplet EPR signals upon similar irradiation in organic glasses, but gave singlet iminoaziridines.[199] Relating diradical **215** with its hydrogen analog **218** which could not be detected, kinetic stabilization of the resulting diazaTMM is another possibility to increase the chance to detect the triplet EPR spectrum of these species (Scheme 109).

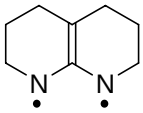

218

Scheme 109. Elusive diazaTMM diradical **218** which showed no triplet EPR spectrum, because of its high reactivity under the conditions studied.

Besides this direct observation of triplet azaTMMs, there are different studies which use the elusive triplet or singlet azaTMMs as intermediate to explain their product distribution. The high diastereoselectivity observed during photolysis of alkylidenedihydrotetrazole **219**, was rationalized by the assumption of singlet diazenyl-1-azaallyldiradical **220** or diazaTMM **221** which exhibits some configuration stability (Scheme 110). The main photoproduct observed is (*E*)-iminodiaziridine **222**, which upon shorter wavelength photolysis reacts under cycloreversion to produce methylisonitrile **223** and the corresponding imine **224**.[200]

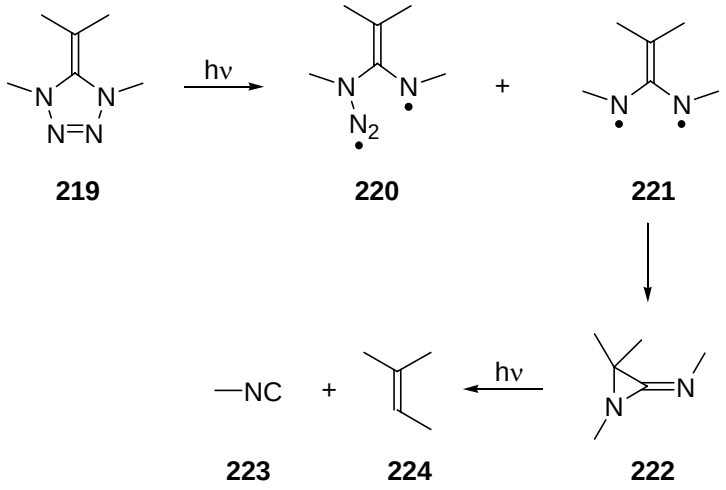

219 **220** **221** **222** **223** **224**

Scheme 110. Photoproducts of alkylidenedihydrotetrazole **219** and the proposed reaction pathway.

Similarly the cascade cyclization sequences induced by thermolysis of allenylazides and 2-(allenyl)phenyl azide were invoked to result from intermediate formation of azaTMMs and its turnaround isomerization.[201, 202] The same rationalization for their product distribution was given by Barker and Storr in the study on flash pyrolysis at 600°C of 1-vinylbenzotriazoles to give indoles.[203] Despite this indirect proofs, there is no direct spectroscopic observation of an azaTMM, so far, even though Cramer et al. have shown by CASSCF and CASPT2 calculations (cc-pVDZ and cc-pVTZ basis set) that the triplet state is expected to be the ground state of these diradicals.[204] Futhermore, it was shown that the

singlet-triplet gap of these azaTMM (iminoallyl) diradicals **225** is reduced in comparison to the parent TMM **49** by 7 kcal/mol to amount to ca. 9 kcal/mol in favour of the triplet. The ground state of these diradicals was found to be highly dependent on the substitution. A nice example is given by oxyallyl **226** and its dimethylderivative **227** (Scheme 111).[205, 206]

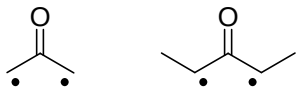

226 **227**

Scheme 111. While several calculations predict oxyallyl **226** to be a ground state triplet molecule, its dimethyl derivative **227** is shown computationally to have a singlet ground state. Recently, **226** was experimentally determined to be a singlet ground state.[207]

While oxyallyl diradical **226** is calculated to be a ground state triplet molecule, the computational prediction for its dimethylderivative **227** is a singlet ground state since the zwitterionic configuration takes over a higher part in the hamiltonian for this molecule. This resembles the ability of oxygen to stabilize a negative charge (because of its high electronegativity) combined with the capability of the C-H bonds to stabilize a positive charge by hyperconjugation. Recently, **226** was observed to be a singlet ground state molecule by photoelectron spectroscopy.[207, 208]

9.2 EPR analysis

As most TMMs as well as most azaTMMs studied up to date are triplet ground state molecules, an appropriate and very sensitive method to study them is EPR spectroscopy. Upon short 308 nm XeCl-Laser irradiation (15 sec, 1 Hz), the iminodihydrotetrazole **43** shows a relative strong half-field triplet EPR signal at 1630 gauss (Scheme 112, Figure 70).

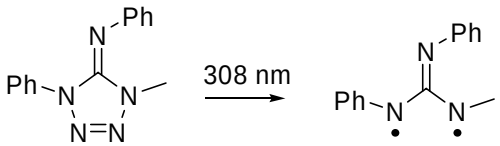

43 **41**

Scheme 112. Photochemistry of iminodihydrotetrazole **43** resulting in formation of triplet triazaTMM **41**.

Further irradiation with the same wavelength leads to the appearance of x- and y-signals at g = 2 and concomitant growth of the strong xy-signal of triplet phenylnitrene **56**. Besides this, the formation of a shoulder at the strong half-field signal is striking.

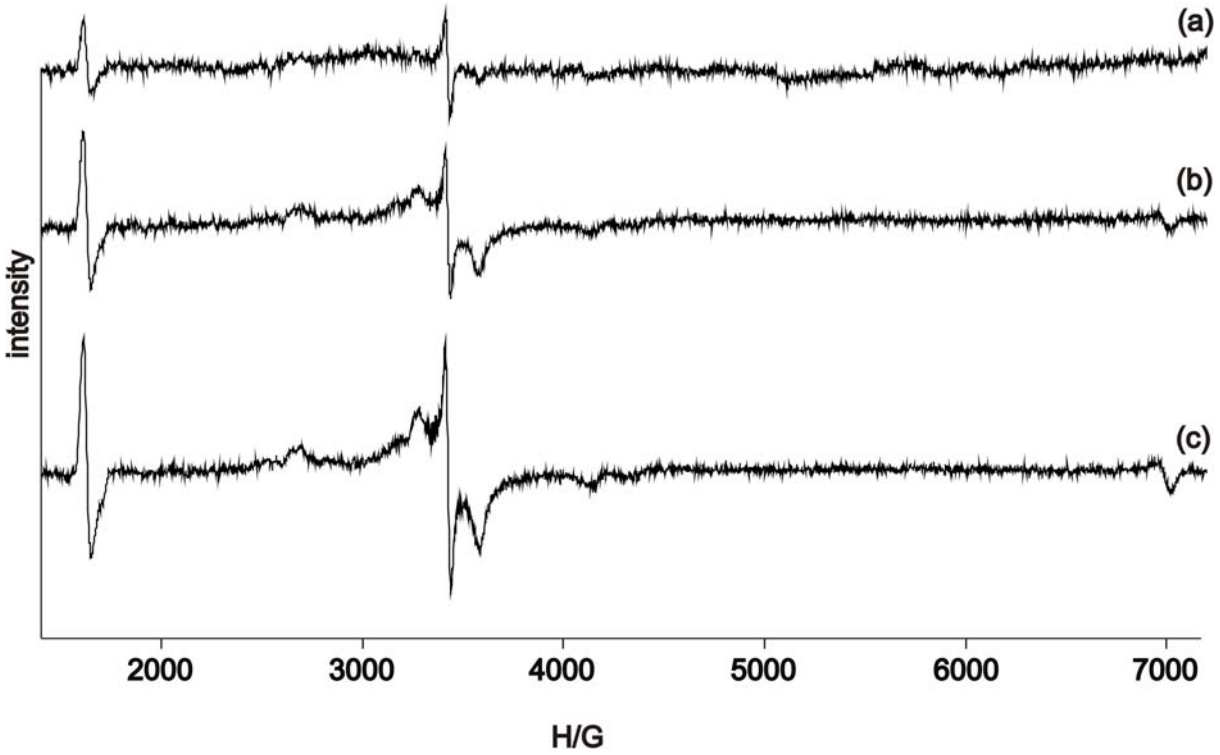

Figure 70. EPR spectrum obtained after photolysis of a matrix containing iminodihydrotetrazole **43** after different irradiation times with 308 nm of a XeCl excimer laser.

Longer irradiation leads to a clearer spectrum of this second triplet diradical as is shown in Figure 71 below.

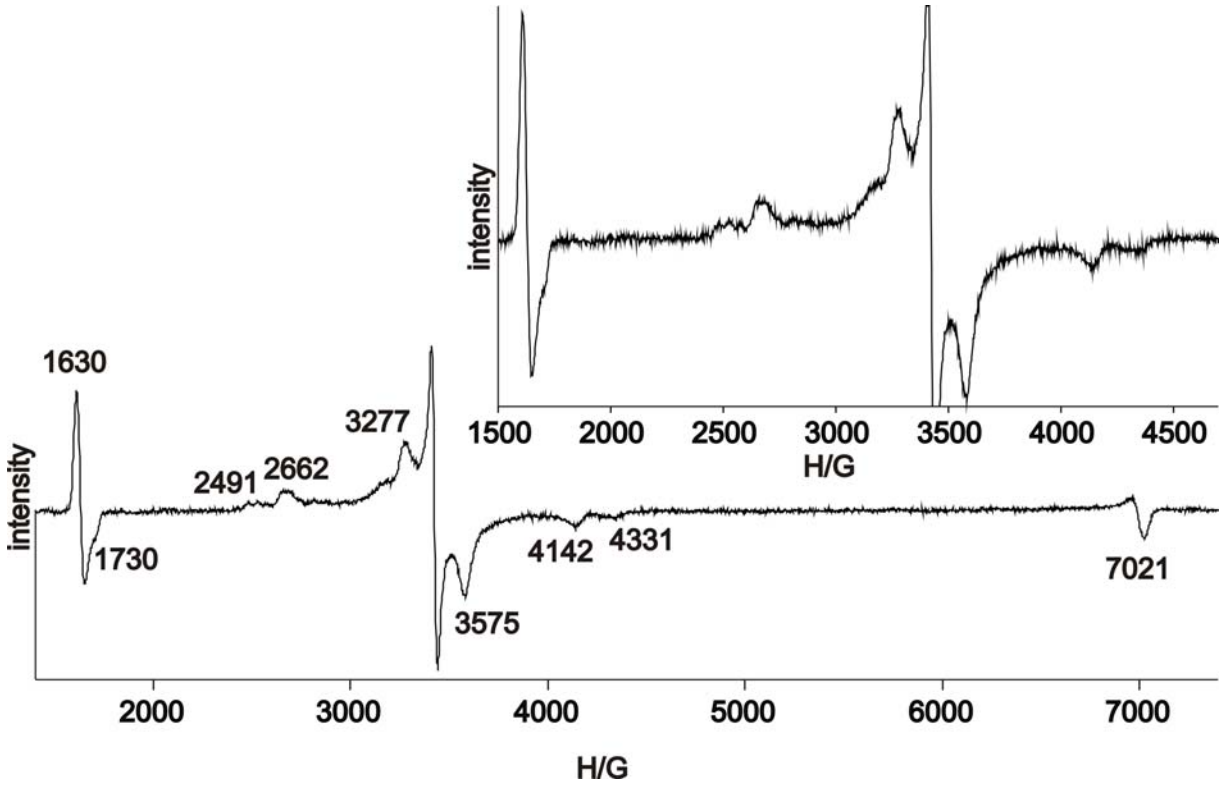

Figure 71. EPR spectrum obtained after prolonged photolysis of a matrix containg iminodihydrotetrazole **43** with 308 nm of a XeCl excimer laser. The inset shows an expansion of the triplet diradical region.

As the D and E value of these two diradicals are quite different, it is easy to assign the triplet diradical signals of the compound with |D/hc| = 0.0237 cm^{-1} and |E/hc| = 0.0017 cm^{-1} to the triazaTMM derivative **41**, as this is in very good accordance with former studies on azaTMMs in organic glasses. The second triplet photoproduct can be fitted to zero-field values of |D/hc| = 0.085 cm^{-1} and |E/hc| = 0.0174 cm^{-1}, however, it is not clear what compound it represents. No linear response of the signal intensity on reciprocal temperature in the temperature range of 4.6 to 12.4 K was detected for **41**, as the triplet signals are irreversely disappearing on annealing and no new signals are showing up. If the triplet is the ground state or just an excited state of a singlet ground state molecule could not be verified experimentally, but due to some related experimental studies on similar azaTMMs, it is highly improbable that the triplet should not be the ground state.

The monophenyl derivative of **43**, namely **42**, also photodenitrogenates to the corresponding triazaTMM derivative **40** upon 308 nm irradiation (Scheme 113).

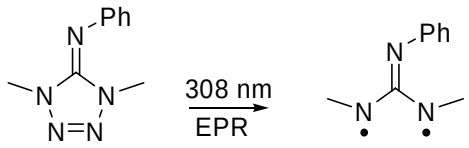

42 **40**

Scheme 113. Photochemistry of iminodihydrotetrazole **42** resulting in formation of triplet triazaTMM **40**.

Already after one minute irradiation at one hertz repetition rate of a XeCl excimer laser (λ = 308 nm), different signals are visible in the EPR spectrum (Figure 72).

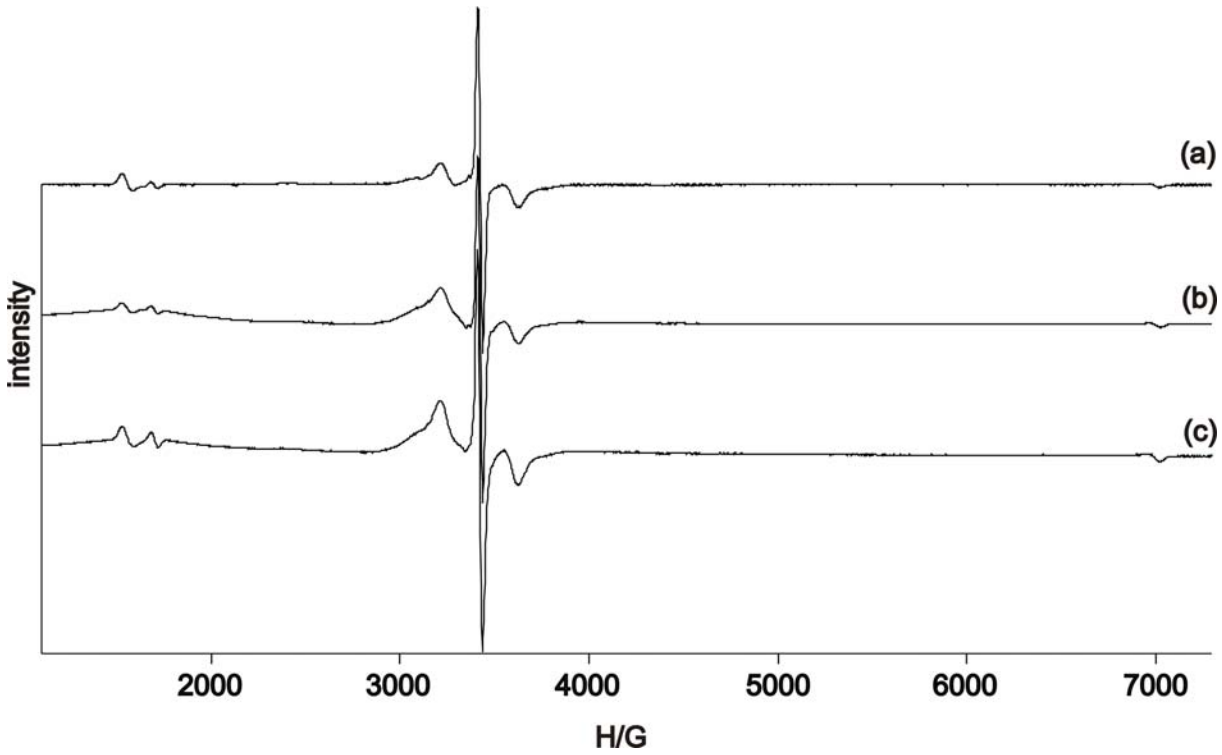

Figure 72. EPR spectrum obtained after photolysis of a matrix containing iminodihydrotetrazole **42** after different irradiation times with 308 nm of a XeCl excimer laser.

Especially striking are the two relatively strong half-field signals around 1700 gauss which belong to two different triplet diradicals, as can be seen from the further photochemistry (Figure 72) as well as in an direct comparison of the signal intensities of two independent experiments (Figure 73).

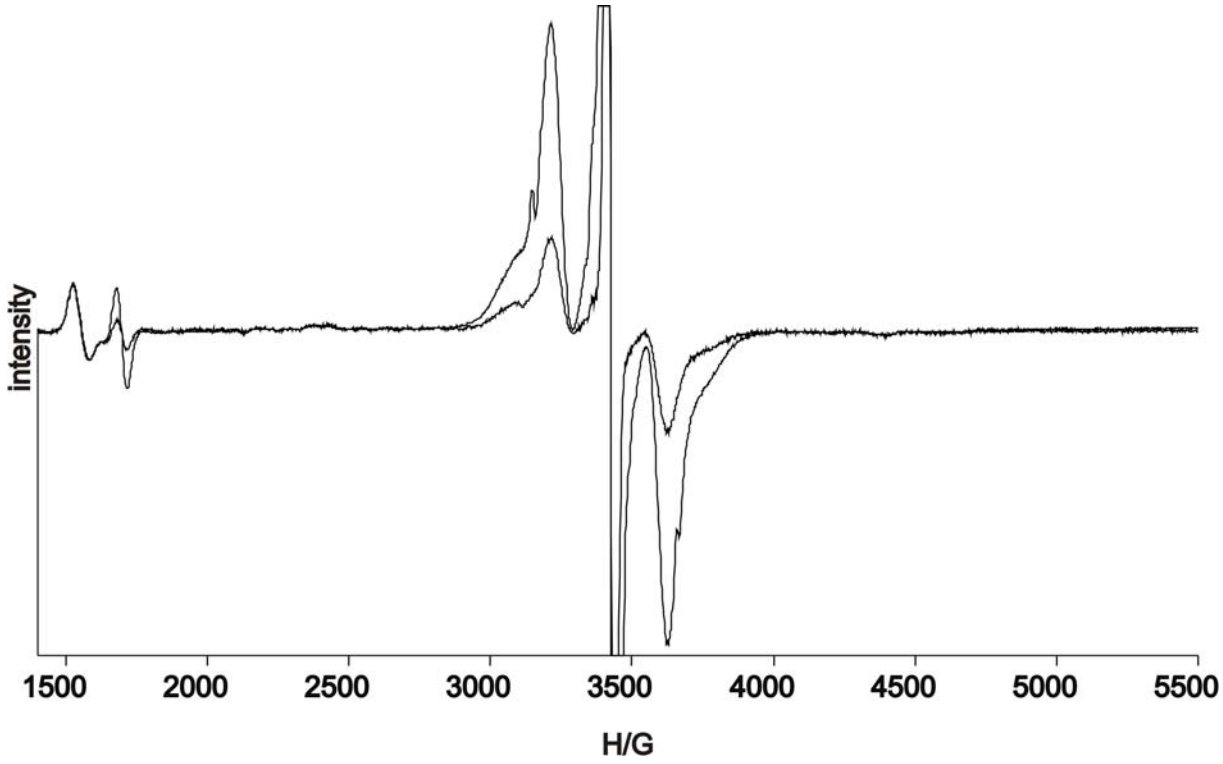

Figure 73. Direct comparison of the signal intensities of two independent experiments fitted to the half field signal at 1600 gauss.

One set of these signals with the smaller half-field triplet signal clearly belongs to the triazaTMM **40**. The calculated zero-field parameters are $|D/hc| = 0.032$ cm^{-1} and $|E/hc| = 0.002$ cm^{-1} and are in very good accordance with the experimental spectrum (Figure 74).

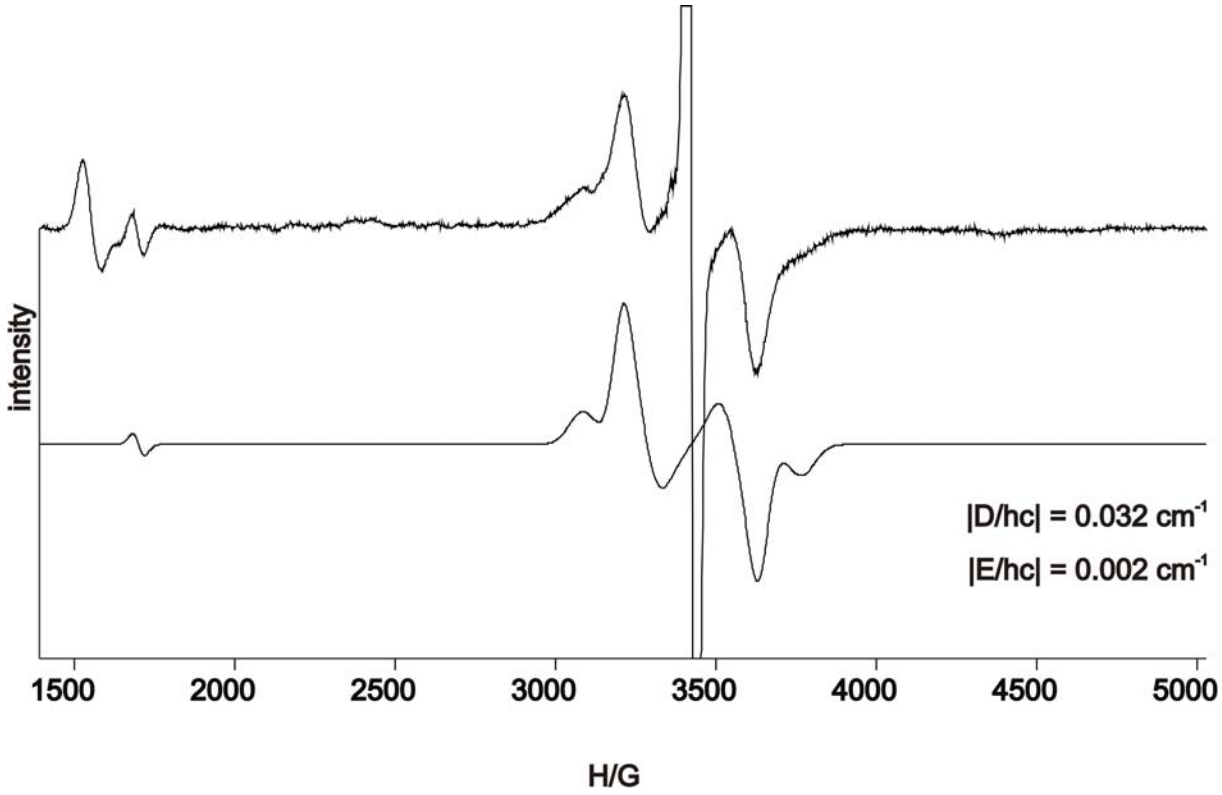

Figure 74. Experimental EPR spectrum obtained after photolysis of a matrix containing **42** and calculated EPR spectrum for a triplet diradical with the specified zero-field parameters.

For the second unknown compound a D value of 0.113 cm^{-1} and an E value of 0.024 cm^{-1} is found, also in good agreement with the experimental spectrum (Figure 75). The Curie plot for triplet triazaTMM **40** is linear and reversible in the range of 5 to 12.3 K, but becomes irreversible afterwards. While phenylnitrene **56** can also be seen after short irradiation times, some new EPR signals are appearing in the spectrum only after prolonged irradiation times. The origin of these signals is unknown.

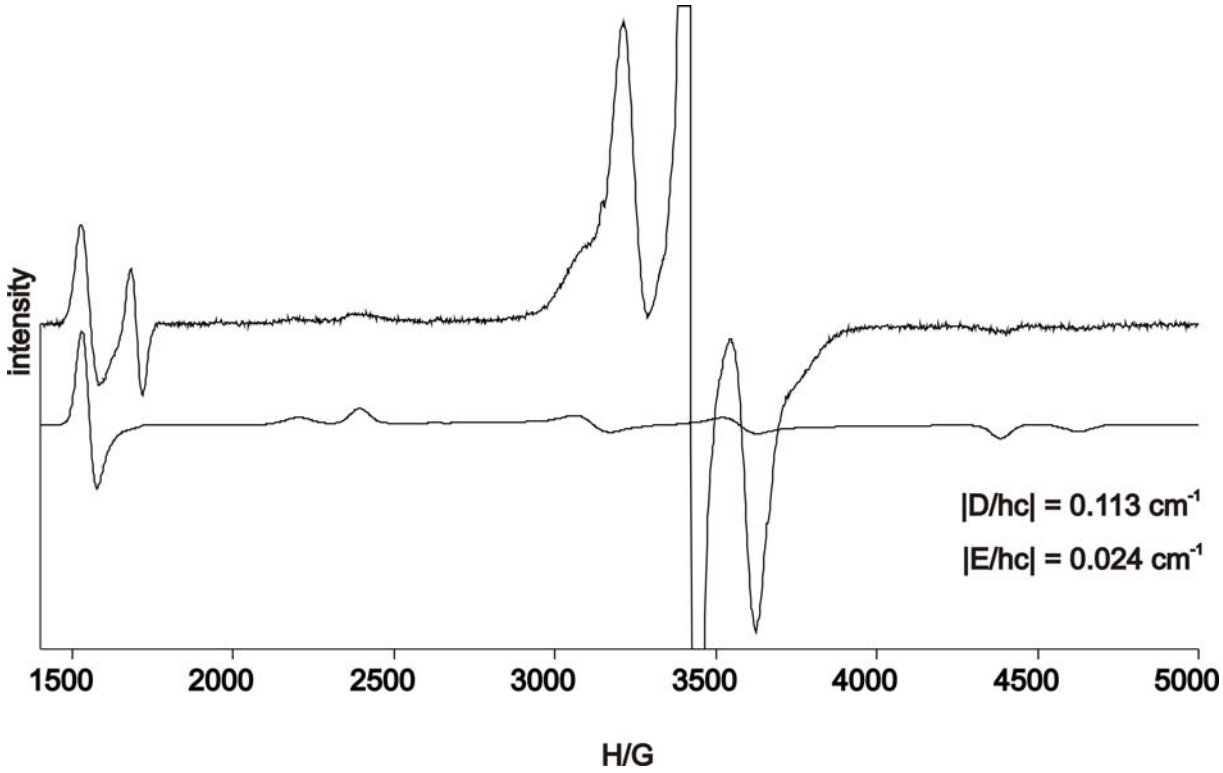

Figure 75. Experimental EPR spectrum obtained after photolysis of a matrix containing **40** and calculated EPR spectrum for a triplet diradical with the specified zero-field parameters.

It can not be differentiated from the observed photochemistry, if the unknown triplet diradicals with high D value are precursors of the triazaTMMs **40** and **41**, as the signals for all four triplet diradicals grow in intensity from the beginning on, without ever decreasing in intensity. The amount of triazaTMM **41** is increasing at longer irradiation times relative to the unknown triplet component, while both molecules are increasing on an absolute scale. It seems, that two independent pathways are responsible for the observed photochemistry. Nevertheless, it is rather hard to imagine that a diazenyl diradical would "survive" this harsh photolysis conditions, as it should effectively absorb 308 nm light, besides the fact, that the geometric structure as well as the ground spin state of such a species is not undoubtedly known. Wentrup et al. postulated diradical species **228** and **229**, accessible by photolysis of tetrazoles or azides **230** and **231**, respectively. Different rearrangement products were identified by IR spectroscopic investigation while hints on the proposed diradicals were obtained only from EPR spectroscopy. Transitions of nitrenes **232** and **233** are also visible. The zfs parameters of **228** and **229** are determined to |D/hc| = 0.0874 cm^{-1} (and |D/hc| = 0.0518 cm^{-1} isomer 2) and |E/hc| = 0.0037 cm^{-1} (|E/hc| = 0.0036 cm^{-1} isomer 2) for diradical **228**, and |D/hc| = 0.1187 cm^{-1} and |E/hc| = 0.0026 cm^{-1} for **229**, respectively (Scheme 114).

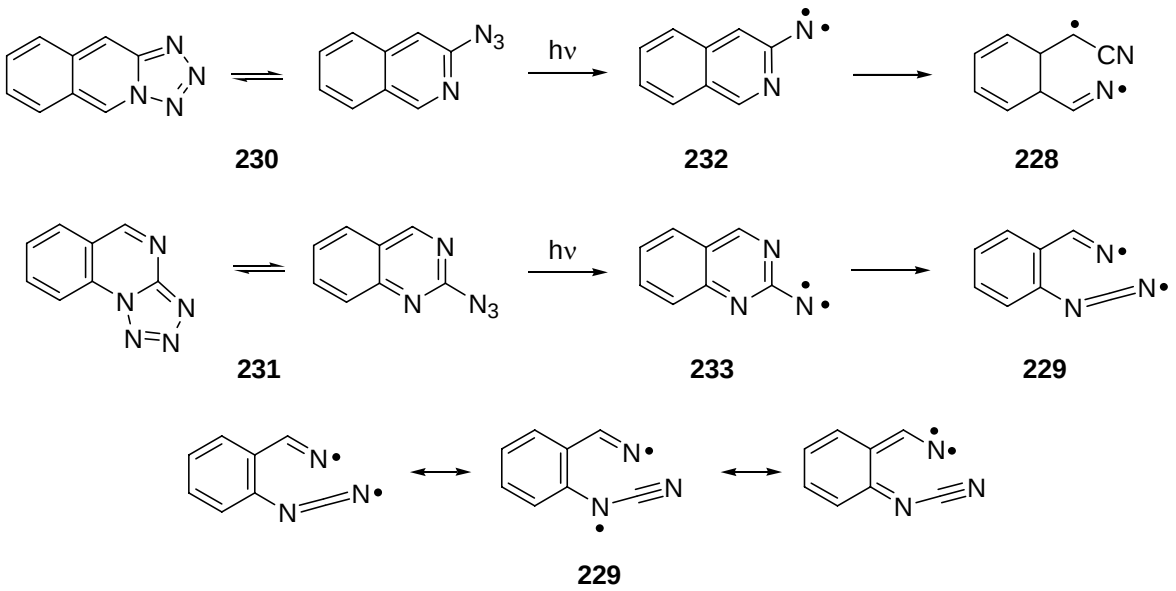

Scheme 114. Diradical species observed by Wentrup et al. via EPR spectroscopy.

The D value, recognizing its physical significance as a characteristic of the mean distance between the triplet coupled unpaired electrons, is quite similar to the experimental values obtained after photolysis of **42** and **43**, thus some similar diradical species might be formed in both processes. The E value is found nearly one order of magnitude higher in the experimental spectra of the unknown diradical species in comparison to the diradical species obtained by Wentrup et al..

A single EPR active triplet diradical species is obtained if tetrazoline **38** is irradiated with 345 nm of a mercury high-pressure lamp (Figure 76, Scheme 115).

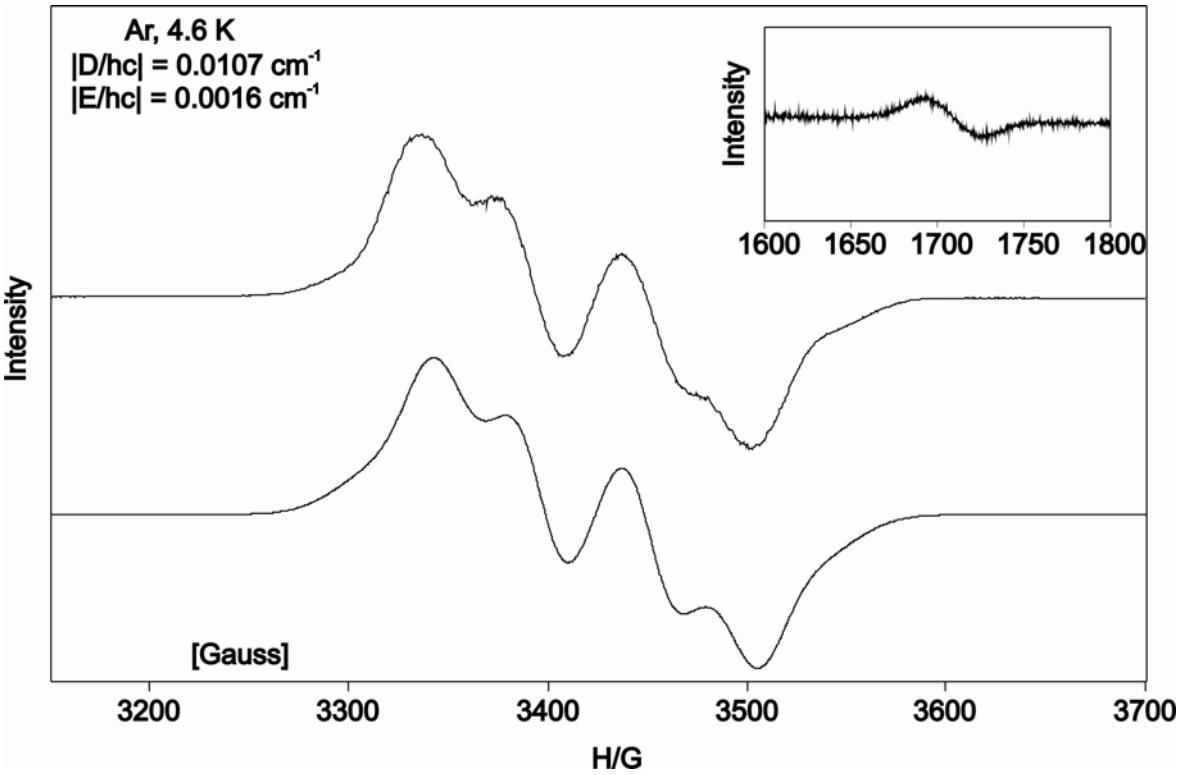

Figure 76. EPR spectrum obtained after photolysis with 345 nm of a mercury high-pressure lamp of a matrix containing tetrazoline **38** and the simulated triplet EPR spectrum for a species with the specified zero-field splitting parameters. The inset shows an expansion of the experimentally observed half-field signal.

As it can be seen in the Figure, the experimental spectrum is nicely reproduced from a calculation with |D/hc| = 0.0107 cm^{-1} and |E/hc| =0.0016 cm^{-1}. Assurance that the observed spectrum is indeed that of a triplet molecule comes from the half-field signal around g = 4. Comparison with literature for different TMMs leads to the assignment of the signals to the triazaTMM **39**.

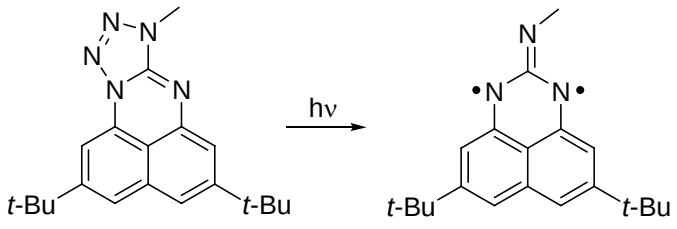

38 **39**

Scheme 115. Photochemistry of tetrazoline **38** results in formation of triplet triazaTMM **39**.

A linear Curie plot is obtained for **39** in argon between 4 and 24 K, as shown in Figure 77.

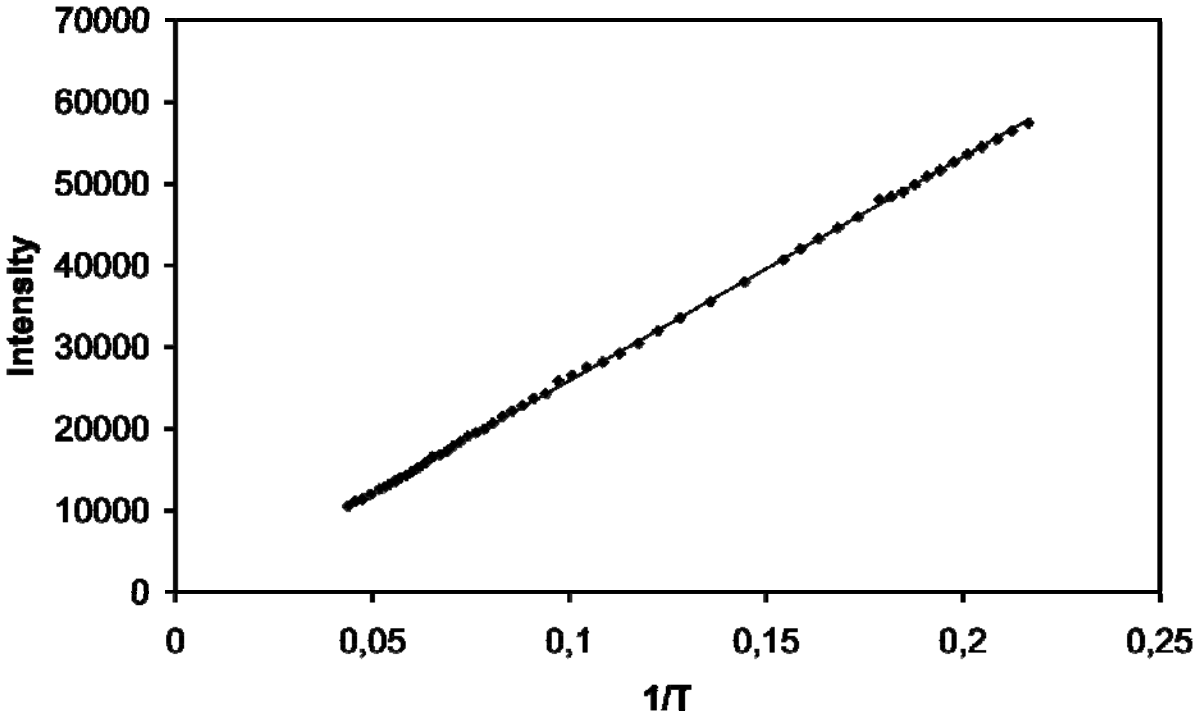

Figure 77. Curie analysis of triplet triazaTMM derivative **39** in the temperature range of 4 to 24 K.

While a linear Curie plot is obtained, if either the singlet and triplet state are degenerate or if the triplet state is the ground state, theory predicts the triplet to be the ground state.

9.3 IR analysis

Due to the promising detection of triplet diradical species by EPR spectroscopy, it was tried if it would be possible to detect such an elusive molecule in a rare gas matrix at low temperature by IR spectroscopy. The monophenyl iminodihydrotetrazole **42** was chosen for this study, as its IR spectrum should be easier to investigate than the corresponding diphenyl derivative **43**. Dunkin et al. have shown in a similar study on the 1,4-dimethyl-5-methylimino-1,4-dihydro-5H-tetrazole **213** that the corresponding tetrazole is photolabile under photolysis with $\lambda > 200$ nm of a mercury high-pressure lamp in a rare gas matrix.[209] The assigned photoproducts found in this study are the corresponding dimethylcarboddiimide **234** and the iminodiaziridine **235** while traces of methylazide **236** could also be detected. To be close to the EPR experiments in photolysis conditions, the photolysis of the precursor was accomplished with 308 nm of a XeCl excimer laser. The

deposition spectrum of tetrazole **42** is shown in Figure 78 and is compared to the calculated IR spectrum (B3LYP/6-311+G**), obvious in good accordance.

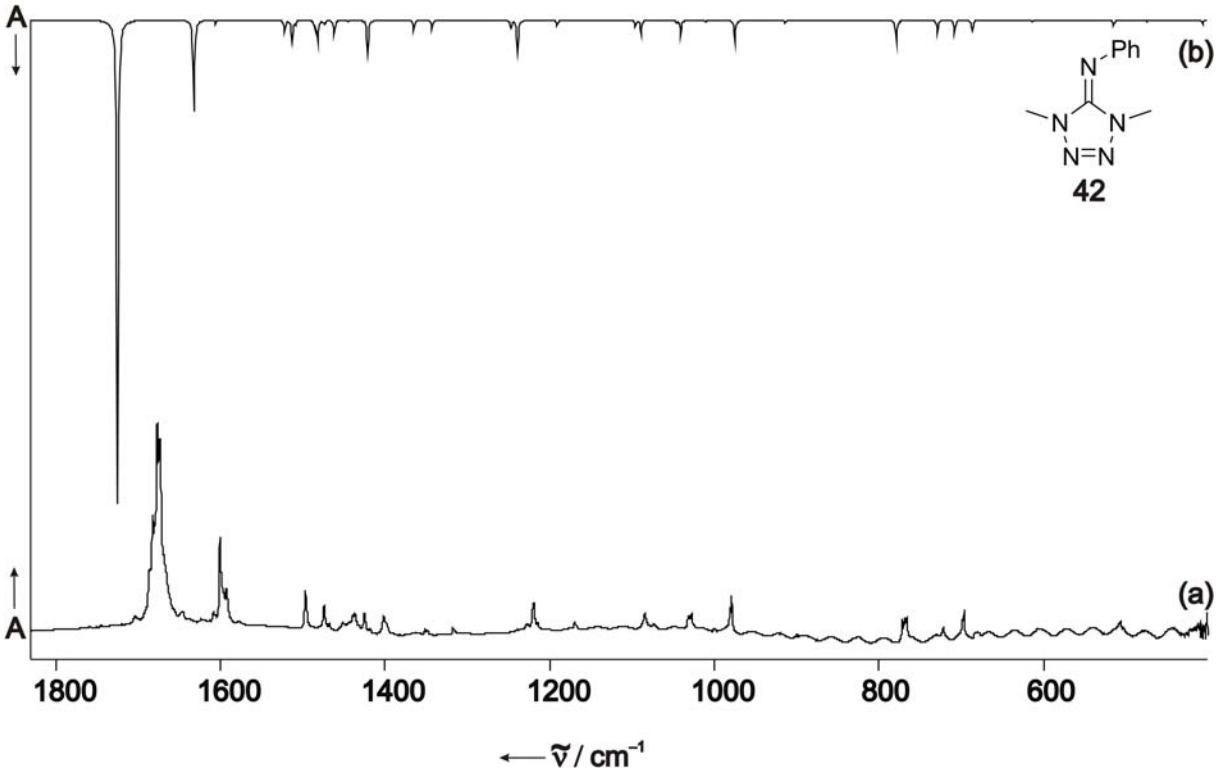

Figure 78. (a) IR deposition spectrum of iminodihydrotetrazole **42** in an argon matrix at 3.4 K. (b) B3LYP/6-311+G** calculated IR spectrum of **42**.

After short photolysis time with 308 nm, a new signal is appearing at 2151.9 cm^{-1} which is splitted and shows a shoulder at 2140.4 cm^{-1}, while all tetrazole signals are diminishing under these conditions. The signal can be assigned to the carbodiimide **44**, formed through [2+3]-cycloelimination, as a similar signal was observed at 2153 cm^{-1} by Dunkin et al. for the corresponding dimethylcarbodiimide **234** (Scheme 116).[209]

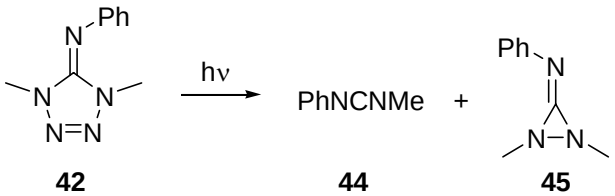

Scheme 116. Photochemistry of iminodihydrotetrazole **42**.

Further irradiation with the same wavelength forms more carbodiimide and this signal is the highest in intensity of the newly formed signals under all conditions. Calculations show, that the N=C=N vibration is the most intense signal for this molecule,

at least with a factor of 20 more intense than all other vibrations and that makes it rather difficult to unequivocally assign further peaks to this species. Another molecule, which is formed is the iminodiaziridine **45** which could be formed after photodenitrogenation by ring-closure of the corresponding triazaTMM diradical **40** (Scheme 116). Its strongest IR active signals belong to the C=N stretching and are found at 1811 and 1838.7 cm^{-1}, while especially the absorption at 1811 cm^{-1} is further splitted (Figure 79). No other signals could be identified for this species, whose assignment is supported by the fact, that related iminodiaziridines show similar intense signals in this wavenumber region.[209]

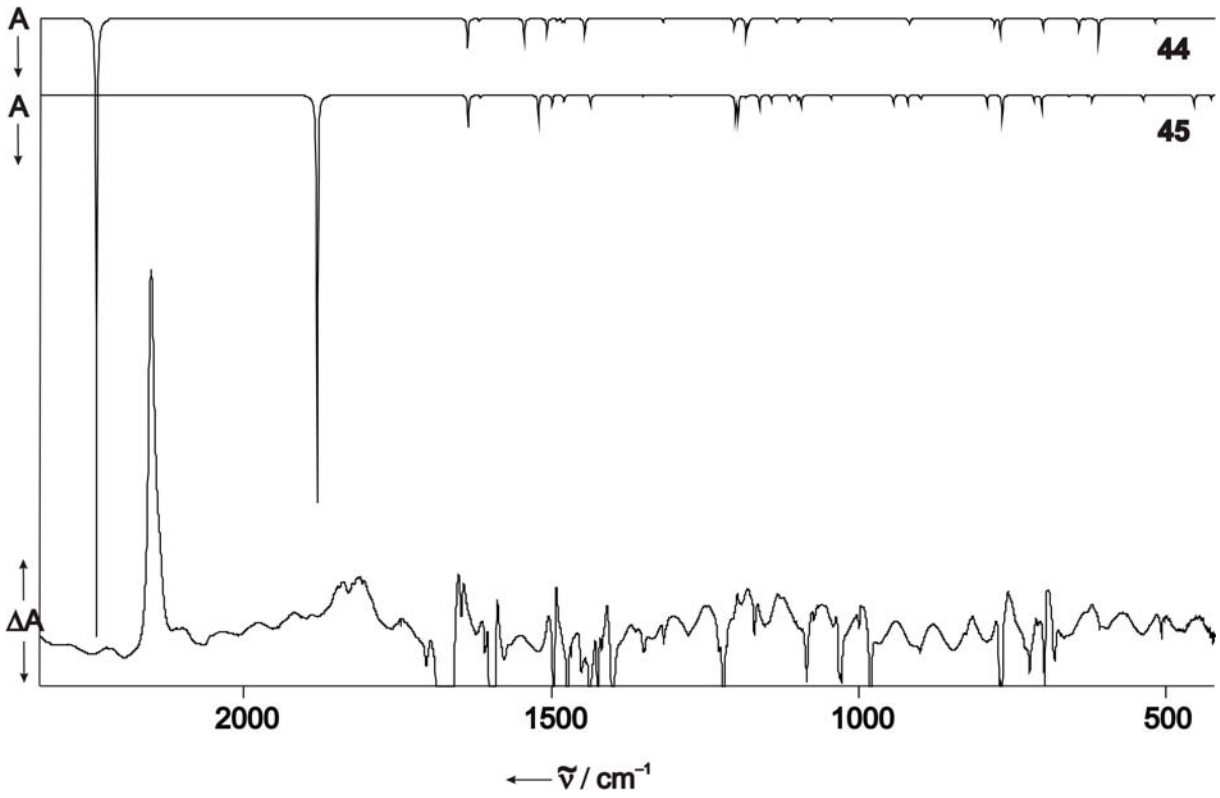

Figure 79. IR difference spectrum obtained after 308 nm irradiation of an argon matrix containing tetrazole **42** together with the calculated (B3LYP/6-311+G**) IR spectrum of iminodiaziridine **45** and carbodiimide **44**.

An expansion of the region between 2250 and 1700 cm^{-1} is shown in Figure 80.

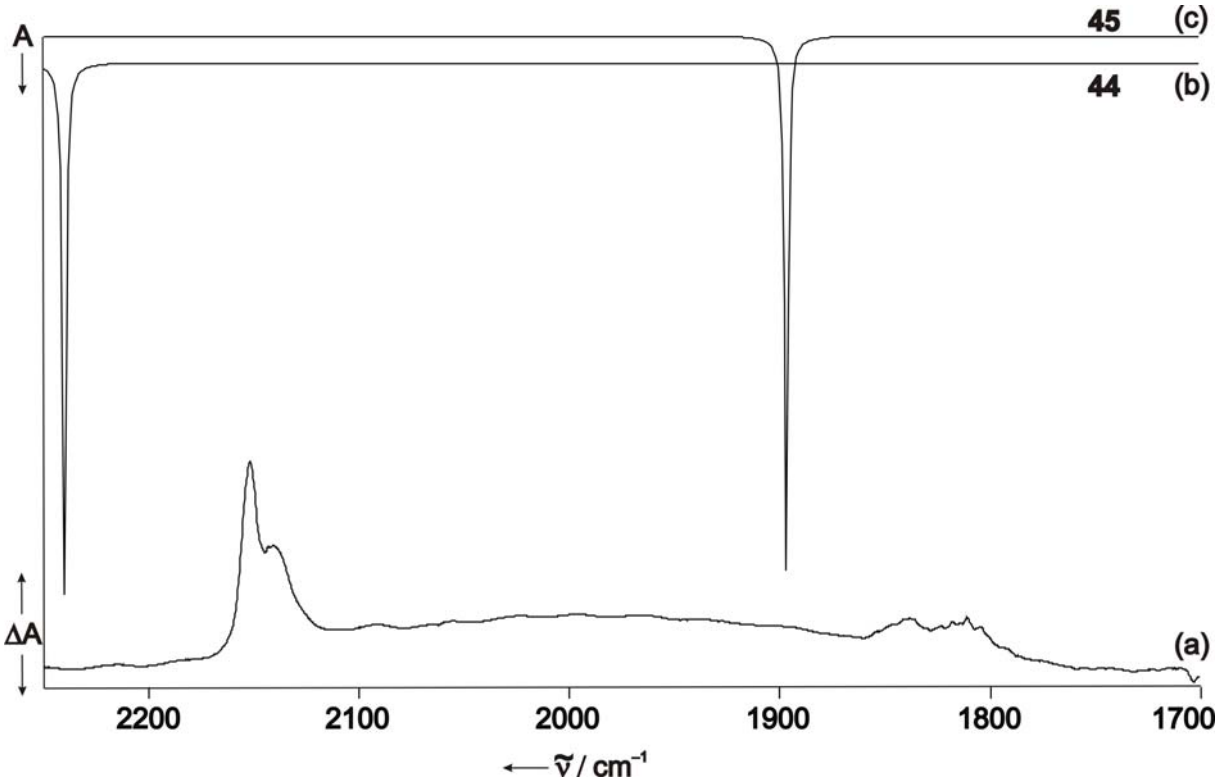

Figure 80. (a) Expansion of the IR difference spectrum obtained after 308 nm irradiation of an argon matrix containing tetrazole **42**. (b) Calculated (B3LYP/6-311+G**) IR spectrum of carbodiimide **44**. (c) Calculated (B3LYP/6-311+G**) IR spectrum of iminodiaziridine **45**.

It is expected that an intermediary formed triplet diradical is very reactive and should react upon annealing of the rare gas matrix under cyclization towards the iminodiaziridine. Furthermore, no linear Curie-Weiss analysis was obtained at higher temperatures, because of irreversible disappearance of the species responsible for the triplet EPR spectrum. Upon annealing of an argon matrix containing the photoproducts of tetrazoline **42** to 35 K, some changes are evident (Figure 81 and 82). The most prominent absorption at 2155.6 cm^{-1} is decreasing in intensity while in direct neighbourhood a new signal at 2148.0 cm^{-1} is showing up. A similar effect is seen for the signal at 1838.7 cm^{-1} of the iminodiaziridine absorption, which is decreasing while new signals are increasing at 1814.6 and 1824.9 cm^{-1}. It seems that both main photoproducts are formed in an unrelaxed geometry upon photolysis in the rare gas matrices and relaxe to their minimum geometries at elevated temperatures (Figure 81).

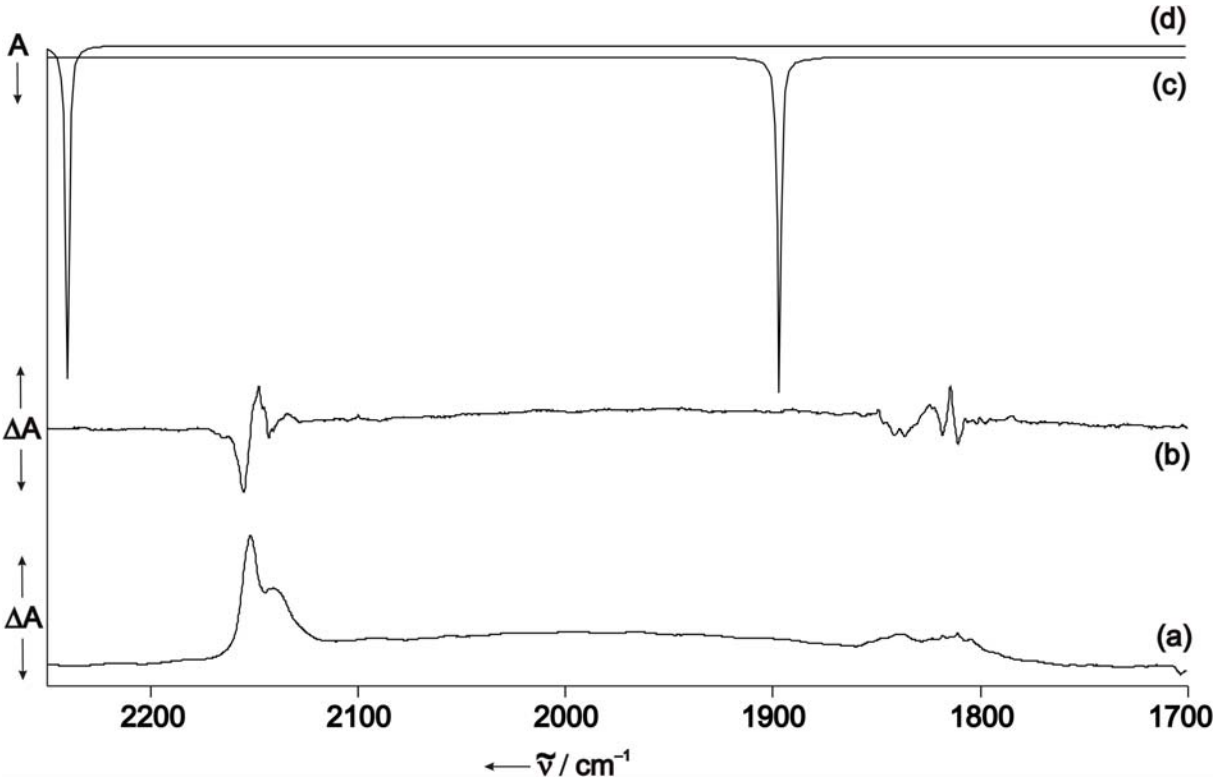

Figure 81. (a) Expansion of the IR difference spectrum obtained after 308 nm irradiation of an argon matrix containing tetrazole **42**. (b) Expansion of the IR difference spectrum obtained of the same matrix after annealing to 35 K. (c)/(d) Calculated (B3LYP/6-311+G**) IR spectrum of iminodiaziridine **45** and carbodiimide **44**, respectively.

Nevertheless, there are some more changes taking place at this temperature, as it is shown in Figure 82 by yellow bars.

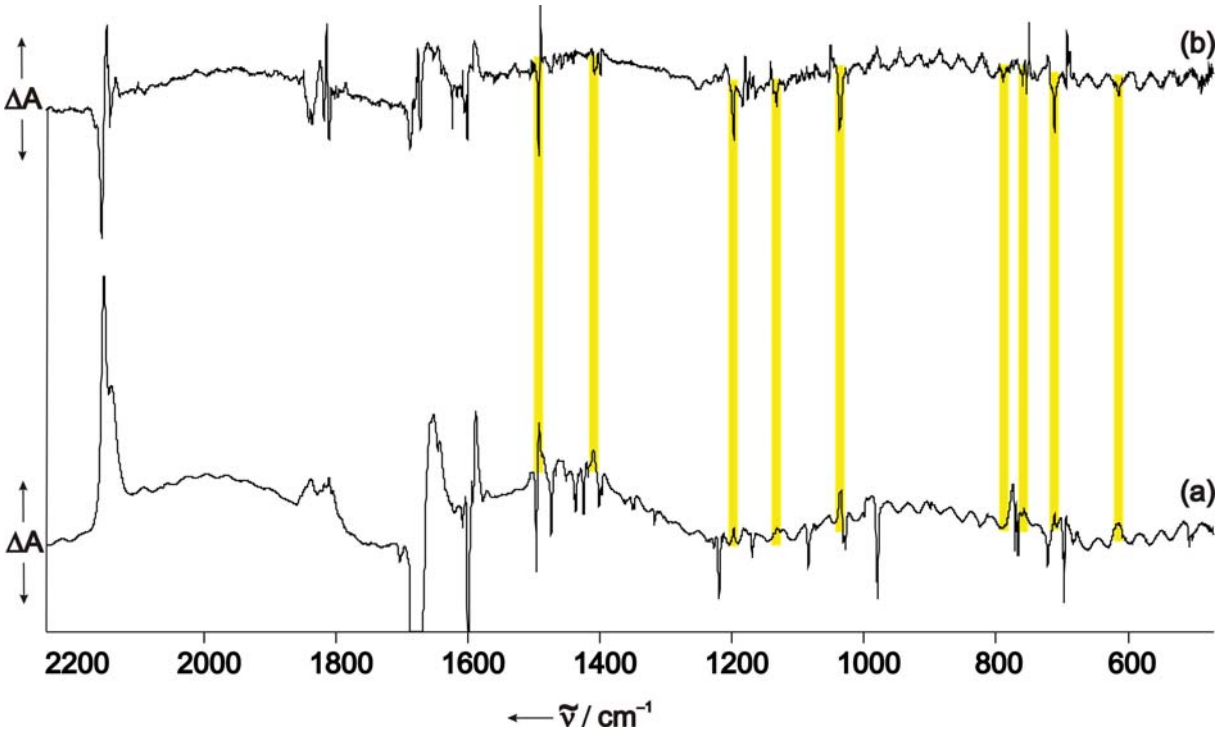

Figure 82. (a) Difference IR spectrum obtained after 308 nm photolysis of an argon matrix containing **42**. (b) Difference IR spectrum (5 times expanded) of the same matrix after annealing to 35 K. Signals decreasing upon annealing, which can not be assigned unequivocally to iminodiaziridine **45** or carbodiimide **44** are highlighted.

The highlighted signals do not belong to the carbodiimide **44** nor to the iminodiaziridine **45**, while they are formed by 308 nm photolysis and decrease in intensity, when the matrix is annealed to 35 K. The decreasing signals are found at 613.9 (w), 711.4 (vs), 759.6 (m), 789.1 (w), 1037.1 (s), 1131.7 (m), 1197.6 (s), 1408.5 (w) and 1493.1 (vs) cm^{-1}. Even though, there are a lot of different triazaTMMs which could be formed from the tetrazole, no one of these expected species shows the IR pattern found in the annealing experiments. Furthermore, the decreasing signals do not belong to phenylnitrene **56**, methylnitrene **237**, methylimine **238**, phenyl azirine **178**, or to the corresponding ketenimine **176**. Up to this point it is not clear, what the origin of these peaks is and it is also observed that the increasing signals do not belong to any species formed as primary photoproduct from tetrazole **42**, as its signal positions are different from all others found before.

10. Materials and methods

10.1 General

Synthesis

Most solvents were distilled and dried before use. TLC analysis were carried out using Polygram G/UV_{254} silica gel pre-coated plates and the spots were analyzed using a CAMAG UV lamp. Column chromatography was carried out using ICN silica 32-63 (60A). High-pressure liquid chromatography was carried out using a Knauer HPLC PUMP 64 system with a 20 x 2 cm LiChrospher Si 100 – 5 μ column and simultaneous detection of the spots using a Knauer UV photometer. Most of the substances were bougth from Acros Organics, with exceptions being 1,3,5-*tris*-(bromomethyl)benzene and 3,5-*bis*-(bromomethyl)toluene which were bought from Aldrich and ABCR, respectively.

Analytic equipment

NMR spectroscopy

NMR spectra were recorded on a Bruker DPX-200 (200.13 MHz: ^{1}H-NMR, and 50.3 MHz: ^{13}C-NMR) spectrometer. 1H NMR shifts are described as parts per million (ppm) downfield shift from TMS and consecutively reported as position (δH and δC), relative integral and multiplicity. Signals are distinguished as singlet (s), doublet (d), triplet (t), quartet (q), doublet of doublets (dd), doublet of triplets (dt), doublet of doublet of doublets (ddd), and multiplet (m) signal. Coupling constants are reported in hertz (Hz). ^{1}H-NMR and ^{13}C-NMR spectra were internally referenced to $CHCl_3$ (7.26 ppm and 77.16 ppm, respectively).

Mass spectrometry

Mass spectra were recorded on a Varian MAT-CH5 spectrometer at 70 eV with electron impact as ion source. Characteristic peaks were given with their relative intensities. HR-MS-EI spectra were recorded on a Jeol AccuTOF GCv JMS-T100GCV apparatus.

10.2 Matrix isolation

Apparatus

The basic set-up of matrix isolation spectroscopy and all standard techniques are given in the book of Dunkin. A Sumitomo Heavy industries RDK-408 D three-staged closed-cycle helium cryostats was used for temperatures around 4 K, while an Air products CSW-20 Displex two-staged helium cryostat was used for temperatures around 10 K. To obtain high vacuum an oil diffusion pump in combination with a rotary vacuum pump was used. A further rotary vacuum pump was used for evacuation of gas tanks and gas lines. A Penning vacuum gauge was used forhigh vacuum measurement. IR measurements are made with a CsI window connected to a copper framework of the cryostat and a thermal contact is made using an indium wire. UV/Vis measurements are made using a sapphire window. The temperature of the window was measured using a silicon diode at the copper mounting plate and an Oxford ITC4 temperature controller. Annealing was performed using a resistance heater.

Deposition conditions

Matrices were generated by co-deposition of the compound with a large excess of inert gases, based on slow-spray on techniques. All precursors were sublimed separately from a second arm using a furnace (Büchi GKR-51) and heating bands. The spectroscopic window was retained at 30 K for argon and 4 K for neon matrices, in order to obtain optical clear matrices, during deposition. Normal deposition times were between 30 minutes and 4.5 hours. The deposition time for UV/Vis spectroscopy was between 10 minutes and 1 hour. The flow of the inert gases were controlled using MKS Mass-Flow mass flow controller with a MKS type 247 four channel readout apparatus. The flow-rate

was kept constant between 0.7 and 2 sccm per minute. All inert gases were purchased from Messer Griesheim with purity of 99.9999 %.

Flash vaccum pyrolysis

For pyrolysis a pyrolysis oven was used, consisting of a quartz tube of diameter of 1 cm, which is coiled over a length of 9 cm with tantalum wire. The coil could be heated by electrical resistance using an external power supply. Outward heat radiation was minimized using a sheet of tantalum metal taped around the heating zone, which was slightly bigger in diameter than the quartz tube. The external part of the apparatus was cooled using water circulation. The sample is sublimed into the pyrolysis zone at high vacuum and trapped with an excess of codeposited inert gas on top of the spectroscopic window. The temperature of the pyrolysis is measured using a PT100-sensor, which is placed in such a way to avoid contact to the quartz surface. Pyrolysis was performed without additional heating of the spectroscopic window at temperatures between 12 and 18 K. Impurities in the oven are removed through pre-heating of the oven to temperatures around 100 °C higher than the final pyrolysis temperature. The FVP deposition time was between 1 and 4.5 hours.

10.3 EPR spectrometer

Matrix EPR spectra were recorded with a Bruker ELEXSYS500 X-band spectrometer, consisting of an ER077R magnet with 75 mm pole distance, an ER047 XG-T microwave bridge and an ER4102ST TE_{102} cavity. Data acquisition and controlling of the spectrometer were performed with the Bruker XEPR 2.0 software on a SGI 02 workstation. Simulation of all EPR spectra was done with the XSophe software of Fa. Bruker.

The constant microwave irradiation is produced in a microwave bridge from which it propagates through the waveguide to the cavity. The waveguide and the cavity have the dimension of the microwave wavelength and a standing wave is produced inside the cavity. The iris screw allows for changes of the microwave energy inside the resonator. In equilibrium no energy exchange is possible. Energy absorption of the sample inside the cavity in case of resonance results in disturbance of this equilibrium, the impedance becomes smaller and more microwave energy is reflexted back to the waveguide. A circulator avoids acquisition of incoming microwave energy from the microwave source as only reflected microwave energy from the cavity is passed through the circulator to the detector. Magnetic modulation coils next to the cavity modulate the magnetic field with a

specified frequency and improve the S/N ratio of the spectra. A phase sensitive diode detector is used for the detection of the modulated signal. In effect, the first derivate of the signal is recorded in usual EPR experiments. For further comments on the spectrometer see the Ph. D. thesis of Grote.[210]

X-band EPR spectra were recorded from a sample deposited on an oxygen-free high-conductivity copper rod (75 mm length, 2 mm diameter) cooled to 4 K with a Sumitomo Heavy industries RDK-408 D three-staged closed cycle cryostat. A nice description of the apparatus can also be found in the Ph. D. thesis of Wenk.[211]

10.4 IR and UV/Vis spectrometer

Matrix infrared spectra were recorded with Bruker IFS66 and IFS66s FTIR spectrometers with a standard resolution of 0.5 cm^{-1} using a liquid nitrogen cooled MCT detector in the range of 400 – 4000 cm^{-1}. For each spectrum, 500 -2000 scans were accumulated. The spectrometer and outer windows were purged with dry air in order to get rid of CO_2 and water from the atmosphere. UV/Vis spectra were recorded in the range of 200 – 800 nm (2000 in some experiments) using a Varian Cary 5000 UV-Vis-NIR spectrophotometer with a resolution of 0.2 nm.

10.5 Light sources

Broad band UV/Vis irradiation were carried out using a 500 W high-pressure mercury arc lamp (Ushio) having a quartz optics (L.O.T. Oriel). The housing of the lamp contains a collimator to get parallel beams, a 10 cm long water filter to avoid heat radiation and a slit to adjust the beam profile. The wavelength can be chosen by varying dichroic mirrors or by using cut-off filters (Schott). Irradiation at 254 nm was carried out with a Gräntzel low-pressure mercury arc lamp. A Compex 100 excimer laser (Lambda Physik LPX 105 SD) with a krypton and flourine gas mixture was used for λ = 248 nm and an argon and fluorine gas mixture for λ = 192 nm. 308 nm photolysis was accomplished with a Compex110 excimer laser (Lambda Physik) containing a xenon and chlorine gas mixture.

10.6 Quantum chemical calculations

Quantum chemical calculations were carried out using Gaussian 03 and Molpro 2001 on Linux PCs as well as on SGI power challenge and SGI Origin work stations. Geometry optimizations and frequency calculations were done with the Gaussian 03 and Gaussian 09 program packages. CASSCF, SA-CASSCF, CASPT2, CASPT3, and MRCI calculations were performed using the Molpro 2001 package. Visualization of the optimized structure, molecular orbitals, and normal modes was done with Gauss View and Molden.

Geometry optimizations of all molecules were fully optimized using different DFT functionals (mainly B3LYP) and analytic second derivatives were calculated to characterize stationary points as minima or transition states. Tight convergence criteria for gradients with maximum residual forces on nuclei below 0.000015 au were used throughout to obtain accurate geometries. For open-shell systems a spin-unrestricted formalism was used. All π electron orbitals were chosen as active spaces in multi-reference calculations. For molecules containing a σ radical, this orbital has also been taken in the active space.

For most computations a Pople type basis set of 6-311G(d,p) quality was chosen, as this basis set was also available for iodinated compounds. The basis set was taken from the Extensible Computational Chemistry Enviroment Basis Set Database. Molecules containing no iodine atom were often calculated with the 6-311++G(d,p) Pople basis set and the cc-pVTZ correlation consistent basis set of Dunning.

11. Synthesis

11.1 1,3-*Bis*-(iodomethyl)benzene 17.

Compound **17** was synthesized according to a literature procedure of Kida et al..[212]

11.2 1,3-*Bis*-(hydroxymethyl)benzene-d_4.

To a refluxing and stirred suspension of lithiumaluminiumdeuterid LAD (0.60 g, 14.3 mmol) in anhydrous THF (20 mL) under argon a solution of dimethyl benzene-1,3-dicarboxylate (1.29 g, 6.65 mmol) in 10 mL of anhydrous THF was added dropwise. The mixture was refluxed for 5 h and cooled with ice. The excess LAD was hydrolyzed by careful addition of water (2 mL), 15% aq. NaOH (2 mL), and again water (5 mL). After stirring overnight, the white solid was filtered off and washed with several portions of THF. All organic extracts were combined, and the solvent was removed in vacuum to give a colorless oil which solidified rapidly. The crude product was used without further purification in the next step. Yield: 85%. IR (KBr) 3214, 2213, 2090, 1432, 1266, 1187, 1107, 1082, 1059, 954, 723, 690 cm^{-1}; mass spectrum, *m*/*z* 142 (M^+).

11.3 1,3-*Bis*-(bromomethyl)benzene-d_4.

To a stirred solution of 0.90 g (6.33 mmol) 1,3-*bis*-(hydroxymethyl)benzene-d_4 in 30 mL of anhydrous THF a solution of 0.77 mL (2.23 g, 8.23 mmol) phosphorus tribromide in 15 mL of dry ether was added dropwise and stirred for 4 h at room temperature. 30 mL of water were added, and the organic layer was washed two times with 15 mL of water. After drying of the organic layer over $MgSO_4$ and evaporation of the solvent, a colorless oil was obtained which was purified by column chromatography (dichloromethane/hexane, 1:1). Yield: 75%. IR (KBr) 2274, 2179, 1483, 1427, 1186, 1064, 953, 867, 791, 694 cm^{-1}; mass spectrum, *m*/*z* 268 (M^+).

11.4 1,3-*Bis*-(iodomethyl)benzene-d_4 d_4-17.

0.106 g (0.40 mmol) of 1,3-*bis*-(bromomethyl)benzene-d_4 was dissolved in 10 mL of dry acetone, and 0.6 g of NaI (4.0 mmol) was added. After stirring under reflux for 12 h the solvent was removed, 150 mL of dichloromethane were added, and the precipitate was filtered off. Removal of the solvent under reduced pressure gave 1,3-*bis*-(iodomethyl)benzene-d_4 d_4-**17**, which was further purified by column chromatography using dichloromethane and hexane (1:2) as eluent. Yield: 80%. IR (KBr) 2174, 1581, 1480, 1426, 1183, 1058, 926, 851, 783, 690, 505 cm^{-1}; mass spectrum, *m*/*z* 362 (M^+).

11.5 1,3,5-*Tris*-(bromomethyl-d_2)benzene.

1,3,5-*tris*-(bromomethyl-d_2)benzene was synthesized according to a literature procedure starting from trimethyl-1,3,5-benzenetricarboxylate.[213]

11.6 1,3,5-*Tris*-(iodomethyl-d_2)benzene d_6-26.

0.363 g (1 mmol) 1,3,5-*tris*-(bromomethyl-d_2)benzene was dissolved in 10 mL of dry acetone. To this solution 2.248 g NaI (15 mmol) was added and the mixture stirred for 3 hours at room temperature. The suspension was filtered and after removal of the solvent a yellow-white solid remained. This was further purified by column chromatography using hexane as eluent. Yield: 85 %. IR (KBr) 2271, 2263, 1593, 1436, 1183, 1070, 951, 909, 852, 830, 694, 512, 499 cm^{-1}; HRMS(EI) $C_9H_3D_6I_3$ *m*/*z* = calc. 503.8215, found 503.8211.

11.7 1,3-*Bis*-(iodomethyl)-5-methylbenzene 29.

0.556 g (2 mmol) 1,3-*bis*-(bromomethyl)-5-methylbenzene was dissolved in 20 mL dry acetone. To this solution, 3.0 g (20 mmol) sodium iodide was added and the mixture stirred for 5 hours at room temperature. The solvent was removed in vacuo and the solid residue was washed three times with a total amount of 100 mL *n*-pentane. The organic solvent is removed in vacuo to yield a white solid which is further purified by column chromatography using *n*-pentane as eluent. Yield: 75 %. IR (KBr) 1600, 1453, 1156, 868, 810, 702, 605, 570, 526, 471 cm^{-1}; ^{1}H-NMR ($CDCl_3$): δ = 7.19 (s, 1H), 7.07 (s, 2H), 4.38 (s, 4H), 2.30 ppm (s, 3H); ^{13}C-NMR ($CDCl_3$): δ = 139.91, 139.33, 129.30, 126.27, 21.27,

5.14 ppm; *m/z* = 372.0 (2 %, M^+), 245.0 (100 %, M-I) , 118.1 (80 %, M-2I). HRMS-(EI) $C_9H_{10}I_2$ calc. 371.8783, found 371.8872.

11.8 3,5-Dimethylbenzyl iodide 30.

0.400 g (2 mmol) 3,5-dimethylbenzyl bromide was dissolved in 15 mL dry acetone. To this solution, 1.506 g (10 mmol) sodium iodide was added and the mixture stirred for 3 hours at room temperature. The solvent was removed in vacuo and the solid residue was washed three times with a total amount of 75 mL *n*-pentane. The organic solvent is removed in vacuo to yield a white solid which is further purified by column chromatography using *n*-pentane as eluent. Yield: 80 %. IR (KBr) 3015, 2908, 1603, 1431, 1373, 1298, 1149, 851, 697, 587, 522, 454 cm^{-1}; ^{1}H-NMR ($CDCl_3$): δ = 6.99 (s, 2H), 6.87 (s, 1H), 4.40 (s, 2H), 2.29 ppm (s, 6H); ^{13}C-NMR ($CDCl_3$): δ = 139.19, 138.52, 129.86, 126.67, 21.28, 6.31 ppm; *m/z* = 246.0 (4 %, M^+), 119.1 (100 %, M-I) , 91.1 (40 %, M-ICH_2-CH_2). HRMS-(EI) $C_9H_{11}I_1$ calc. 245. 99054 , found 245.98697.

11.9 2-Iodophenyl azide 32.

To a solution of 2.19 g (10 mmol) 2-iodoaniline in 20 mL trifluor-acetic acid held at 0°C, a solution of 0.759 g (11 mmol) sodium nitrite in 15 mL water is added slowly with rigorous stirring. The solution is maintained at 0°C for 15 minutes and a solution of 0.715 g (11 mmol) sodium azide in 15 mL water is added dropwise. The solution is stirred for a further hour after which 70 mL ether is added. The organic phase is extracted with water and diluted sodium hydroxide solution. The organic phase is dried with $NaSO_4$ and the solvent removed in vacuo. The yellow oil is further purified through column chromatography using *n*-pentane as eluent to give a pale yellow liquid.[214] Yield: 65 %. IR (3 K, Ar) 2136, 2122, 2117, 2099, 1600, 1583, 1472, 1438, 1310, 1295, 1022, 748, 692 cm^{-1}; ^{1}H-NMR ($CDCl_3$): δ = 7.79 (dd, 1H, *J* = 7.9, 1.43 Hz), 7.39 (dt, *J* = 1.43, 8.00 Hz, 1H), 7.14 (dd, 1H, ,*J* = 1.41, 8.0 Hz), 6.86 ppm (dt, *J* = 1.41, 7.9 Hz, 1H); ^{13}C-NMR ($CDCl_3$): δ = 141.84, 140.16, 129.64, 126.40, 118.56, 87.94 ppm; *m/z* = 245.0 (15 %, M^+), 217.0 (70 %, M-N_2) , 90.0 (100 %, M-I-N_2). HRMS-(EI) $C_6H_4I_1N_3$ calc. 244.9450 , found 244.9472.

11.10 General procedure for iodobenzyl iodides 8 - 10.

0.594 g (2 mmol) of the corresponding iodobenzyl bromide were dissolved in 25 mL dry acetone. To this solution, 1.506 g (10 mmol) sodium iodide was added and the mixture stirred for 3 hours at room temperature. The solvent was removed in vacuo and the solid residue was washed three times with a total amount of 75 mL *n*-pentane. The organic solvent is removed in vacuo to yield a white-yellow solid which is further purified by column chromatography using *n*-pentane as eluent to give a white solid.

11.11 2-Iodobenzyl iodide 8.

Yield: 80 %. IR (KBr) 1462, 1431, 1421, 1271, 1211, 1149, 1010, 758, 715, 643, 571, 552, 463 cm^{-1}; ^{1}H-NMR ($CDCl_3$): δ = 7.84 (dd, *J* = 1.1, 7.9, 1H), 7.50 (dd, *J* = 1.7, 7.7, 1H), 7.32 (td, *J* = 1.1, 7.9, 1 H), 6.95 (td, *J* = 7.7, 1.7, 1H), 4.58 ppm (s, 2H); ^{13}C-NMR ($CDCl_3$): δ = 141.6, 140.4, 129.9, 129.7, 129.1, 99.9, 12.3 ppm, *m/z* = 343.9 (7 %, M^+), 217.0 (100 %, M-I) , 90.1 (30 %, M-2I). HRMS-(EI) $C_7H_6I_2$ calc. 343.8559 , found 343.8375.

11.12 4-Iodobenzyl iodide 9.

Yield: 85 %. IR (KBr) 1498, 1397, 1148, 1055, 1006, 821, 793, 704, 555, 449 cm^{-1}; ^{1}H-NMR ($CDCl_3$): δ = 7.62 (d, *J* = 8.3, 2H), 7.12 (d, *J* = 8.3, 2H), 4.38 ppm (s, 2H); ^{13}C-NMR ($CDCl_3$): δ = 139.1, 138.1, 130.7, 93.5, 4.4 ppm, *m/z* = 343.9 (5 %, M^+), 217.0 (100 %, M-I) , 90.1 (30 %, M-2I). HRMS-(EI) $C_7H_6I_2$ calc. 343.8559 , found 343.8413.

11.13 3-Iodobenzyl iodide 10.

Yield: 85 %. IR (KBr) 3041, 1583, 1550, 1463, 1417, 1209, 1156, 1061, 991, 884, 844, 777, 652, 585, 539, 459 cm^{-1}; ^{1}H-NMR ($CDCl_3$): δ = 7.73 (s, 1H), 7.57 (d, *J* = 7.9, 1H), 7.34 (d, *J* = 7.8, 1H), 7.03 (t, *J* = 7.8, 1H), 4.35 ppm (s, 2H); ^{13}C-NMR ($CDCl_3$): δ = 141.7, 137.7, 137.1, 130.6, 128.2, 94.4, 3.6 ppm, *m/z* = 343.9 (7 %, M^+), 217.0 (100 %, M-I) , 90.1 (40 %, M-2I). HRMS-(EI) $C_7H_6I_2$ calc. 343.8559 , found 343.8452.

11.14 3-Methylazidobenzene.

To a solution of 5 g (46.7 mmol) 3-methylaniline in 35 mL trifluor-acetic acid at 0°C is added a solution of 3.54 g (51.4 mmol) sodium nitrite in 25 mL water is added slowly with rigorous stirring. The solution is maintained at 0°C for 15 minutes and a solution of 3.34 g (51.4 mmol) sodium azide in 25 mL water is added dropwise. The solution is stirred for a further hour after which 100 mL ether is added. The organic phase is extracted with water and diluted sodium hydroxide solution. The organic phase is dried with $NaSO_4$ and the solvent removed in vacuo. The yellow oil is further purified through column chromatography using *n*-pentane as eluent.

11.15 3-(Bromomethyl)azidobenzene.

0.532 g (4 mmol) 3-methylazidobenzene was added to a suspension of 0.783 g NBS and 0.01 g AIBN in 25 mL CCl_4. The mixture is heated to reflux for 12 hours after which the solvent is removed in vacuo. The residue is washed three times with each 25 mL *n*-pentane. The organic solvent is removed in vacuo and the residue purified by high-pressure liquid chromatography using cyclohexane as eluent to separate dibromide product from monobromide product. The product is obtained as pale yellow liquid. Yield: 25 %. IR (KBr) 2231, 2128, 1608, 1586, 1485, 1446, 1303, 1224, 1201, 885, 789, 691, 636, 560 cm^{-1}; ^{1}H-NMR ($CDCl_3$): δ = 7.33 (t, *J* = 7.8, 1H), 7.16 (dt, *J* = 7.8, 1.2, 1H), 7.05 (t, *J* = 2.0, 1H), 6.97 (ddd, *J* = 7.8, 2.0, 1.2, 1H), 4.45 ppm (s, 2H); ^{13}C-NMR ($CDCl_3$): δ = 140.5, 139.7, 130.1, 125.5, 119.6, 119.0, 32.5 ppm, *m/z* = 211.0 (10 %, M^+), 183.0 (30 %, M-N_2), 132.1 (30 %, M-Br), 104.1 (75 %, M-Br-N_2) 77.1 (100 %, M-CHBr-N_3).

11.16 3-(Iodomethyl)azidobenzene 90.

0.212 g (1 mmol) of 3-(bromomethyl)azidobenzene were dissolved in 20 mL dry acetone. To this solution, 0.749 g (5 mmol) sodium iodide was added and the mixture stirred for 5 hours at room temperature. The solvent was removed in vacuo and the solid residue was washed three times with a total amount of 50 mL *n*-pentane. The organic solvent is removed in vacuo to yield a white slightly yellow solid which is further purified by column chromatography using *n*-pentane as eluent to give a pale yellow liquid. Yield: 85 %. IR (KBr) 2225, 2108, 1606, 1586, 1480, 1443, 1300, 1284, 1157, 785, 687, 542 cm^{-1}; ^{1}H-NMR ($CDCl_3$): δ = 7.28 (t, *J* = 7.8, 1H), 7.15 (dt, *J* = 7.8, 1.2, 1H), 7.03 (t, *J* = 2.0,

1H,), 6.91 (ddd, *J* = 7.8, 2.0, 1.2, 1H), 4.41 ppm (s, 2H); ^{13}C-NMR ($CDCl_3$): δ = 141.3, 140.5, 130.3, 125.4, 119.3, 118.6, 4.3 ppm, *m/z* = 259.0 (15 %, M^+), 231.0 (25 %, M-N_2), 132.1 (30 %, M-I), 104.1 (80 %, M-I-N_2), 77.0 (100 %, M-CHI-N_3), HRMS-(EI) $C_7H_6IN_3$ calc. 258.99604 , found 258.9562.

11.17 3,5-Dimethylazidobenzene.

3,5-*Bis*-methyl-azidobenzene was synthesized in a similar fashion as 3-methylazidobenzene.

11.18 3,5-*Bis*-(bromomethyl)azidobenzene.

0.5 g (3.4 mmol) 3,5-dimethylazidobenzene were added to a suspension of 1.3 g (7.3 mmol) NBS and 0.025 g AIBN in 30 mL CCl_4. The mixture is heated to reflux for 12 hours after which the solvent is removed in vacuo. The residue is washed three times with each 35 mL *n*-pentane. The organic solvent is removed in vacuo and the residue purified by high-pressure liquid chromatography using cyclohexane as eluent to separate polybromide product from dibromide product. Yield: 33 %. IR (KBr) 2192, 2120, 1604, 1592, 1460, 1434, 1322, 1308, 1234, 1210, 955, 869, 695, 621, 601, 551 cm^{-1}; ^{1}H-NMR ($CDCl_3$): δ = 7.18 (t, *J* = 1.4, 1H), 6.98 (d, *J* = 1.4, 2H), 4.43 ppm (s, 4H); ^{13}C-NMR ($CDCl_3$): δ = 141.3, 140.4, 126.1, 119.7, 32.0 ppm, *m/z* = 304.9 (10 %, M^+), 276.9 (45 %, M-N_2), 224.0 (45 %, M-Br), 196.0 (50 %, M-Br-N_2), 116.1 (100 %, M-Br-HBr-N_2), 89.1 (60 %). HRMS-(EI) $C_8H_7Br_2N_3$ calc. 302.9007 , found 302.9105.

11.19 3,5-*Bis*-(iodomethyl)azidobenzene 16.

0.304 g (1 mmol) of 3,5-*bis*-(bromomethyl)-azidobenzene were dissolved in 20 mL dry acetone. To this solution, 0.749 g (5 mmol) sodium iodide was added and the mixture stirred for 5 hours at room temperature. The solvent was removed in vacuo and the solid residue was washed three times with a total amount of 50 mL *n*-pentane. The organic solvent is removed in vacuo to yield a white slightly yellow solid which is further purified by column chromatography using *n*-pentane as eluent to give a white solid. Yield: 90 %. IR (KBr) 2187, 2115, 2103, 1602, 1447, 1323, 1307, 1238, 1156, 859, 690, 580, 530 cm^{-1}; ^{1}H-NMR ($CDCl_3$): δ = 7.14 (t, *J* = 1.5, 1H), 6.90 (d, *J* = 1.5, 2H), 4.36 ppm (s, 4H); ^{13}C-NMR ($CDCl_3$): δ = 141.9, 141.1, 125.7, 118.9, 3.5 ppm, *m/z* = 398.9 (15 %, M^+), 370.9 (25

%, M-N_2), 272.0 (100 %, M-I), 244.0 (75 %, M-I-N_2), 116.1 (100 %, M-I-HI-N_2), 90.1 (75 %). HRMS-(EI) $C_8H_7I_2N_3$ calc. 398.8729 , found 398.8581.

11.20 2,4-Dimethyliodobenzene and 2,6-dimethyliodobenzene.

Both substances were synthesized from the corresponding aniline derivative. 5 g (41.3 mmol) aniline derivative were added to a 4.5 molar H_2SO_4 solution held at -10 °C. 3.13 g (45.4 mmol) of sodium nitrite solved in 10 mL water are added dropwise and after complete addition of the solution, the reaction mixture is stirred for further 15 minutes. The temperature is held below 0°C and a solution of 10.28 g (61.9 mmol) KI in 15 mL water is slowly added. The reaction mixture is stirred at 0°C, room temperature and 80°C each for 2 hours. The solution is extracted three times with 30 mL MTBE and the combined organic phases are extracted with 20 mL of water, 2 M NaOH, 2M Na_2SO_3, and brine. After removal of the solvent, the crude reaction mixture is further purified through column chromatography using pentane as eluent. A colourless liquid remains as pure product.

11.21 General procedure for the bromination of dimethyliodobenzenes.

2 g (8.62 mmol) of the corresponding dimethyliodobenzene were added to a suspension of 3.298 g (18.53 mmol) NBS and 0.03 g AIBN in 40 mL CCl_4. The mixture is heated to reflux for 16 hours after which the solvent is removed in vacuo. The residue is washed three times with each 35 mL *n*-pentane. The organic solvent is removed in vacuo and the residue purified by high-pressure liquid chromatography using cyclohexane as eluent to separate polybromide product from dibromide product.

11.22 3,5-*Bis*-(bromomethyl)iodobenzene.

Yield: 21 %. IR (KBr) 1596, 1564, 1433, 1256, 1210, 994, 970, 690, 596, 579, 535, 479 cm^{-1}; ^{1}H-NMR ($CDCl_3$): δ = 7.67 (d, *J* = 1.5, 2H), 7.37 (t, *J* = 1.5, 1H), 4.38 ppm (s, 4H); ^{13}C-NMR ($CDCl_3$): δ = 140.4, 138.0, 129.1, 94.4, 31.4 ppm; *m/z* = 389.8 (20 %, M^+), 308.9 (100 %, M-Br), 230.0 (60 %, M-2Br), 103.1 (40 %, M-2Br-I), HRMS-(EI) $C_8H_7Br_2I$ calc. 387.7959 , found 387.7723.

11.23 2,4-*Bis*-(bromomethyl)iodobenzene.

Yield: 31 %. IR (KBr) 3036, 1470, 1430, 1210, 1014, 953, 832, 742, 715, 600, 581, 562 cm^{-1}; ^{1}H-NMR ($CDCl_3$): δ = 7.83 (d, *J* = 8.1, 1H), 7.48 (s (t, *J* = 1.8), 1H), 7.02 (dd, J = 8.1, 1.8, 1H) 4.57 (s, 2H), 4.41 ppm (s, 2H); ^{13}C-NMR ($CDCl_3$): δ = 141.0, 140.7, 139.0, 131.0, 130.7, 99.9, 38.3, 31.9 ppm, *m/z* = 389.8 (15 %, M^+), 308.9 (100 %, M-Br), 262.9 (35 %, M-I), 230.0 (40 %, M-2Br), 184.0 (30 %, M-I-Br), 103.1 (50 %, M-2Br-I), HRMS-(EI) $C_8H_7Br_2I$ calc. 387.7939 , found 387.7927.

11.24 2,6-*Bis*-(bromomethyl)iodobenzene.

Yield: 42 %. IR (KBr) 3038, 1572, 1419, 1256, 1207, 1012, 866, 800, 722, 583, 542, 478 cm^{-1}; ^{1}H-NMR ($CDCl_3$): δ = 7.27-7.43 (m, AB_2-spinsystem, 3H), 4.68 ppm (s, 4H); ^{13}C-NMR ($CDCl_3$): δ = 142.1, 130.5, 129.1.7, 106.4, 40.0 ppm; *m/z* = 389.8 (15 %, M^+), 310.9 (98 %, M-Br), 308.9 (100 %, M-Br), 230.0 (5 %, M-2Br), 182.0 (40 %, M-I-Br), 103.1 (50 %, M-2Br-I), HRMS-(EI) $C_8H_7Br_2I$ calc. 387.7959 , found 387.7879.

11.25 Iodination of *bis*-(bromomethyl)iodobenzenes.

0.389 g (1 mmol) of 3,5-*bis*-(bromomethyl)-iodobenzene were dissolved in 20 mL dry acetone. To this solution, 1.5 g (10 mmol) sodium iodide was added and the mixture stirred for 12 hours at room temperature. The solvent was removed in vacuo and the solid residue was washed three times with a total amount of 50 mL *n*-pentane. The organic solvent is removed in vacuo to yield a white slightly yellow solid which is further purified by column chromatography using *n*-pentane as eluent to give a white solid.

11.26 3,5-*Bis*-(iodomethyl)iodobenzene 14.

Yield: 85 %. IR (KBr) 2922, 2851, 1563, 1428, 1254, 1151, 869, 833, 690, 561, 529 cm^{-1}; ^{1}H-NMR ($CDCl_3$): δ = 7.58 (s, 2H), 7.32 (s, 1H), 4.31 ppm (s, 4H); ^{13}C-NMR ($CDCl_3$): δ = 142.0, 137.2, 128.6, 94.4, 2.8 ppm, *m/z* = 483.8 (5 %, M^+), 356.9 (100 %, M-I), 230.0 (50 %, M-2I), 103.1 (20 %, M-3I); HRMS-(EI) $C_8H_7I_3$ calc. 483.7682 , found 483.7610.

11.27 2,4-*Bis*-(iodomethyl)iodobenzene 13.

Yield: 75 %. IR (KBr) 1466, 1423, 1148, 1014, 890, 817, 717, 537 cm^{-1}; ^{1}H-NMR ($CDCl_3$): δ = 7.72 (d, *J* = 8.1, 1H), 7.47 (d, *J* = 2.3, 1H), 6.94 (dd, *J* = 8.1, 2.3, 1H), 4.50 (s, 2H), 4.36 ppm (s, 2H); ^{13}C-NMR ($CDCl_3$): δ = 142.2, 140.9, 140.7, 130.0, 129.9, 98.8, 11.4, 3.5 ppm, *m/z* = 483.8 (5 %, M^+), 356.9 (100 %, M-I), 230.0 (30 %, M-2I), 103.1 (20 %, M-3I), HRMS-(EI) $C_8H_7I_3$ calc. 483.7682 , found 483.7623.

11.28 2,6-*Bis*-(iodomethyl)iodobenzene 12.

Yield: 70 %. IR (KBr) 2922, 2852, 1420, 1149, 1009, 793, 716, 543 cm^{-1}; ^{1}H-NMR ($CDCl_3$): δ = 7.16 – 7.38 (m, AB_2-spinsystem, 3H), 4.62 ppm (s, 4H); ^{13}C-NMR ($CDCl_3$): δ = 143.5, 129.14, 129.11, 105.7, 13.7 ppm, *m/z* = 483.8 (10 %, M^+), 356.9 (100 %, M-I), 230.0 (40 %, M-2I), 103.1 (30 %, M-3I), HRMS-(EI) $C_8H_7I_3$ calc. 483.7682 , found 483.7443.

12. Calculations

Triplet *m*-xylylene **1** ($^3B_2$) UB3LYP/6-311G(d,p)

6	0.000000	1.209478	1.094404	*E* =	-309.534386
6	0.000000	1.242354	-0.337428	*ZPVE* =	0.128326
6	0.000000	0.000000	-1.021205	$<S^2>$ =	2.0659
6	0.000000	-1.242354	-0.337428		
6	0.000000	-1.209478	1.094404		
6	0.000000	0.000000	1.777447		
1	0.000000	2.146132	1.640482		
1	0.000000	0.000000	-2.106461		
1	0.000000	-2.146132	1.640482		
1	0.000000	0.000000	2.862216		
6	0.000000	-2.456800	-1.034021		
6	0.000000	2.456800	-1.034021		
1	0.000000	-2.480846	-2.116584		
1	0.000000	-3.403333	-0.508227		
1	0.000000	2.480846	-2.116584		
1	0.000000	3.403333	-0.508227		

BS-*m*-xylylene **1** UB3LYP/6-311G(d,p)

6	0.000000	1.207668	1.088058	*E* =	-309.524472
6	0.000000	1.235060	-0.330940	*ZPVE* =	0.127835
6	0.000000	0.000000	-1.012318	$<S^2>$ =	1.0118
6	0.000000	-1.235060	-0.330940		
6	0.000000	-1.207668	1.088058		
6	0.000000	0.000000	1.774051		
1	0.000000	2.144532	1.634106		
1	0.000000	0.000000	-2.097648		
1	0.000000	-2.144532	1.634106		
1	0.000000	0.000000	2.858676		
6	0.000000	-2.467581	-1.036217		
6	0.000000	2.467581	-1.036217		
1	0.000000	-2.491123	-2.118425		
1	0.000000	-3.411644	-0.506804		
1	0.000000	2.491123	-2.118425		
1	0.000000	3.411644	-0.506804		

Singlet *m*-xylylene **1** ($^1A_1$) B3LYP/6-311G(d,p)

6	0.000000	1.192546	1.043931	*E* =	-309.486632
6	0.000000	1.230955	-0.384326	*ZPVE* =	0.128437
6	0.000000	0.000000	-1.076480		
6	0.000000	-1.230955	-0.384326		
6	0.000000	-1.192546	1.043931		
6	0.000000	0.000000	1.752843		
1	0.000000	2.134703	1.582884		

1	0.000000	0.000000	-2.159953	
1	0.000000	-2.134703	1.582884	
1	0.000000	0.000000	2.836303	
6	0.000000	-2.522387	-0.934712	
6	0.000000	2.522387	-0.934712	
1	0.000000	-2.684344	-2.004980	
1	0.000000	-3.393595	-0.294531	
1	0.000000	2.684344	-2.004980	
1	0.000000	3.393595	-0.294531	

4,6-dimethylene-bicyclo[3.1.0]hex-2-ene **19** (^{1}A) B3LYP/6-311G(d,p)

6	1.196602	-0.330547	0.029728	*E* =	-309.503791
6	1.174487	1.032136	-0.517784	*ZPVE* =	0.130256
1	1.952833	1.418077	-1.164294		
6	-0.836035	0.847577	0.692651		
6	0.069390	1.697119	-0.147182		
1	-0.184127	2.709686	-0.435530		
6	2.178728	-1.230378	-0.092041		
6	-0.098343	-0.519022	0.773224		
6	-1.360597	-0.356122	0.025352		
6	-2.326227	-0.927801	-0.664248		
1	-2.279538	-1.978729	-0.931629		
1	-3.195751	-0.367419	-0.992527		
1	2.112984	-2.210994	0.364570		
1	3.076184	-1.008297	-0.658384		
1	-0.108869	-1.115970	1.678971		
1	-1.361749	1.275874	1.540625		

3-methylene-bicyclo[4.1.0]hepta-1,4-diene **18** (^{1}A) B3LYP/6-311G(d,p)

6	1.437558	0.488527	0.420081	*E* =	-309.493361
6	0.939672	-0.862954	0.228211	*ZPVE* =	0.131123
6	-0.310631	-1.229255	-0.046029		
6	-1.336911	-0.167201	0.022084		
6	-0.807728	1.203049	-0.183160		
6	0.496592	1.520249	-0.094570		
1	1.890488	0.731248	1.381838		
1	-0.571504	-2.192833	-0.473691		
1	-1.533995	1.966706	-0.447055		
1	0.831731	2.538726	-0.267808		
6	-2.658237	-0.409512	0.083564		
6	2.281133	-0.621909	-0.307701		
1	-3.042951	-1.416708	0.194687		
1	-3.385091	0.392715	0.023431		
1	2.392715	-0.628999	-1.388227		
1	3.169915	-0.916819	0.241952		

Isomer **21** (^{1}A) B3LYP/6-311G(d,p)

6	-0.782828	1.342930	0.041467	*E* =	-309.491230

6	0.491931	1.799278	0.031291	*ZPVE* =	0.131049
6	1.602461	0.854885	-0.136744		
6	1.336849	-0.411096	0.182705		
6	0.021649	-0.959091	0.502778		
6	-1.118604	-0.094974	0.037740		
1	-1.608568	2.048116	0.032201		
1	0.684197	2.866897	0.009976		
1	2.506092	1.170070	-0.649311		
6	-2.356428	-0.543270	-0.216871		
6	1.103708	-1.770380	-0.297511		
1	1.479786	-2.628467	0.251882		
1	1.020189	-1.923704	-1.369456		
1	-2.587073	-1.602386	-0.216173		
1	-3.172659	0.140491	-0.426112		
1	-0.114387	-1.380709	1.497857		

3,5-dimethylene-tricyclo[2.2.0.0*2,6*]hexane **20** (^{1}A') B3LYP/6-311G(d,p)

6	0.729737	0.902913	0.779991	*E* =	-309.456873
6	-0.007055	-0.323245	1.199743	*ZPVE* =	0.130086
6	-0.937666	-0.150994	0.000000		
6	-0.007055	-0.323245	-1.199743		
6	0.729737	0.902913	-0.779991		
6	-0.475360	1.381292	0.000000		
1	1.453171	1.493986	1.325435		
1	-1.954272	-0.534036	0.000000		
1	1.453171	1.493986	-1.325435		
1	-1.018432	2.314608	0.000000		
6	-0.007055	-1.111072	-2.265309		
6	-0.007055	-1.111072	2.265309		
1	-0.749007	-1.892243	-2.385623		
1	0.727510	-0.994493	-3.054371		
1	-0.749007	-1.892243	2.385623		
1	0.727510	-0.994493	3.054371		

TS-1-21 (^{1}A) UB3LYP/6-311G(d,p)

6	1.105041	1.157277	0.127612	*E* =	-309.473762
6	1.201461	-0.292470	0.042432	*ZPVE* =	0.128667
6	-0.037073	-0.957704	-0.300576	*IMF* =	-225.8714
6	-1.272891	-0.247175	-0.270020		
6	-1.330981	1.117699	-0.136216		
6	-0.087554	1.809332	-0.004887		
1	2.021669	1.718110	0.272487		
1	-0.007798	-1.979519	-0.656615		
1	-2.272202	1.622930	0.038105		
1	-0.098322	2.892986	0.060728		
6	-2.048511	-1.291028	0.302601		
6	2.368117	-1.005791	0.082170		
1	-2.127958	-2.263662	-0.167714		
1	-2.597608	-1.132908	1.224119		

1	2.366535	-2.087235	0.027985	
1	3.330027	-0.511538	0.142204	

TS-1-18 (^{1}A) UB3LYP/6-311G(d,p)

6	1.020415	1.131931	0.173626	*E* =	-309.476594
6	1.299623	-0.283660	-0.028779	*ZPVE* =	0.128770
6	0.124053	-1.139981	-0.110035	*IMF* =	-255.5404
6	-1.103065	-0.569442	-0.257356		
6	-1.310959	0.843020	-0.290866		
6	-0.230403	1.678271	0.105476		
1	1.868616	1.779043	0.379266		
1	0.218948	-2.199402	0.098287		
1	-2.223076	1.260672	-0.695172		
1	-0.376843	2.743558	0.244837		
6	-2.385119	-0.895971	0.281402		
6	2.591009	-0.715458	-0.030313		
1	-2.473343	-1.454773	1.206207		
1	-3.298279	-0.634344	-0.238572		
1	2.836767	-1.762154	-0.161088		
1	3.413886	-0.024865	0.107306		

TS-1-19 (^{1}A) UB3LYP/6-311G(d,p)

6	1.258476	1.043982	-0.313195	*E* =	-309.473898
6	1.197960	-0.390856	-0.034192	*ZPVE* =	0.127782
6	-0.066546	-0.993903	0.260649	*IMF* =	-144.3848
6	-1.316684	-0.321784	-0.032489		
6	-1.058418	1.060518	0.351453		
6	0.132327	1.745228	0.005815		
1	2.181382	1.502257	-0.641676		
1	-0.078077	-1.966794	0.741058		
1	-1.830311	1.597012	0.897143		
1	0.142180	2.829844	0.053735		
6	-2.512420	-0.872761	-0.319915		
6	2.354771	-1.098386	0.030158		
1	-2.614106	-1.941358	-0.466948		
1	-3.409531	-0.268003	-0.376347		
1	2.367615	-2.138640	0.338022		
1	3.304050	-0.646542	-0.234690		

TS-1-20 (^{1}A) UB3LYP/6-311G(d,p)

6	-0.900579	1.018537	-0.253970	*E* =	-309.409224
6	-1.171593	-0.443879	-0.049242	*ZPVE* =	0.125923
6	-0.000001	-1.171102	0.240903	*IMF* =	-491.0369
6	1.171593	-0.443873	-0.049239		
6	0.900582	1.018543	-0.253967		
6	0.000000	1.677417	0.614928		
1	-1.573756	1.573053	-0.906851		
1	0.000021	-2.242804	0.385600		

1	1.573767	1.573058	-0.906841	
1	-0.000017	2.710270	0.938460	
6	2.480286	-0.811653	-0.066471	
6	-2.480289	-0.811651	-0.066470	
1	2.811090	-1.749966	0.363244	
1	3.240914	-0.153842	-0.467847	
1	-2.811099	-1.749957	0.363258	
1	-3.240912	-0.153841	-0.467855	

Triplet **TS-1-20-T** (^{3}A) UB3LYP/6-311G(d,p)

6	0.958142	1.081709	0.172516	*E* =	-309.421886
6	1.227180	-0.333492	-0.020527	*ZPVE* =	0.124925
6	0.056527	-1.103067	-0.270184	*IMF* =	-901.4519
6	-1.164006	-0.430944	0.010984	$<S^2>$ =	2.0731
6	-1.032670	1.037237	0.221261		
6	-0.126136	1.800984	-0.528942		
1	1.561609	1.642177	0.880173		
1	0.091264	-2.150450	-0.543440		
1	-1.773228	1.498631	0.878158		
1	-0.162299	2.883716	-0.486126		
6	-2.387643	-1.022019	0.093524		
6	2.482856	-0.883308	0.106858		
1	-2.515482	-2.076270	-0.121334		
1	-3.272868	-0.457975	0.361597		
1	2.637139	-1.948203	-0.018322		
1	3.348362	-0.274229	0.336351		

1,3,5-Trimethylenebenzene **2** ($^4A_2$'') UB3LYP/6-311+G(d,p)

6	1.244776	0.718672	0.000000	*E* =	-348.204518
6	0.000000	1.408507	0.000000	*ZPVE* =	0.142578
6	-1.244776	0.718672	0.000000	$<S^2>$ =	3.8298
6	-1.219803	-0.704254	0.000000		
6	0.000000	-1.437344	0.000000		
6	1.219803	-0.704254	0.000000		
1	0.000000	2.493235	0.000000		
1	-2.159205	-1.246618	0.000000		
1	2.159205	-1.246618	0.000000		
6	0.000000	-2.838254	0.000000		
1	0.927149	-3.397700	0.000000		
1	-0.927149	-3.397700	0.000000		
6	-2.458000	1.419127	0.000000		
1	-3.406069	0.895915	0.000000		
1	-2.478920	2.501785	0.000000		
6	2.458000	1.419127	0.000000		
1	3.406069	0.895915	0.000000		
1	2.478920	2.501785	0.000000		

1,3,5-Trimethylenebenzene **2** ($^4A_2$'') UB3LYP/cc-pVTZ

6	1.241728	0.716912	0.000000	*E* =	-348.236708
6	0.000000	1.404596	0.000000	*ZPVE* =	0.142984
6	-1.241728	0.716912	0.000000	$<S^2>$ =	3.8292
6	-1.216416	-0.702298	0.000000		
6	0.000000	-1.433824	0.000000		
6	1.216416	-0.702298	0.000000		
1	0.000000	2.487006	0.000000		
1	-2.153810	-1.243503	0.000000		
1	2.153810	-1.243503	0.000000		
6	0.000000	-2.830448	0.000000		
1	0.925076	-3.388598	0.000000		
1	-0.925076	-3.388598	0.000000		
6	-2.451240	1.415224	0.000000		
1	-3.397150	0.893160	0.000000		
1	-2.472074	2.495438	0.000000		
6	2.451240	1.415224	0.000000		
1	3.397150	0.893160	0.000000		
1	2.472074	2.495438	0.000000		

1,3,5-Trimethylenebenzene **2** ($^4A_2$'') UMP2/cc-pVTZ

6	1.232435	0.711547	0.000000	*E* =	-347.279111
6	0.000000	1.397486	0.000000	*ZPVE* =	0.145893
6	-1.232435	0.711547	0.000000	$<S^2>$ =	4.3087
6	-1.210258	-0.698743	0.000000		
6	0.000000	-1.423093	0.000000		
6	1.210258	-0.698743	0.000000		
1	0.000000	2.478659	0.000000		
1	-2.146581	-1.239329	0.000000		
1	2.146581	-1.239329	0.000000		
6	0.000000	-2.814161	0.000000		
1	0.925750	-3.366967	0.000000		
1	-0.925750	-3.366967	0.000000		
6	-2.437135	1.407080	0.000000		
1	-3.378754	0.881761	0.000000		
1	-2.453004	2.485206	0.000000		
6	2.437135	1.407080	0.000000		
1	3.378754	0.881761	0.000000		
1	2.453004	2.485206	0.000000		

Doublet 1,3,5-trimethylenebenzene **2** ($^2A_2$) UB3LYP/6-311+G(d,p)

6	0.000000	1.236911	-0.718910	*E* =	-348.188683
6	0.000000	0.000000	-1.404998	*ZPVE* =	0.141583
6	0.000000	-1.236911	-0.718910	$<S^2>$ =	1.7785
6	0.000000	-1.208458	0.703518		
6	0.000000	0.000000	1.421209		
6	0.000000	1.208458	0.703518		
1	0.000000	0.000000	-2.489978		
1	0.000000	-2.147937	1.245940		
1	0.000000	2.147937	1.245940		

6	0.000000	0.000000	2.859366	
1	0.000000	0.928879	3.414732	
1	0.000000	-0.928879	3.414732	
6	0.000000	-2.457942	-1.423853	
1	0.000000	-3.405778	-0.900636	
1	0.000000	-2.476604	-2.506315	
6	0.000000	2.457942	-1.423853	
1	0.000000	3.405778	-0.900636	
1	0.000000	2.476604	-2.506315	

Doublet **163** (^{2}A) UB3LYP/6-311+G(d,p)

6	-0.337205	-1.426262	0.166540	*E* =	-348.171077
6	0.948612	-1.298305	-0.143163	*ZPVE* =	0.145238
6	1.531088	0.056306	0.025046	$<S^2>$ =	0.7995
6	0.592814	1.148244	-0.015756		
6	-0.823604	0.993224	0.034300		
6	-1.274240	-0.364850	0.501216		
1	1.526270	-2.060851	-0.656459		
1	0.995884	2.150222	-0.132708		
1	-1.686094	-0.367179	1.509542		
6	-1.692345	2.027153	-0.183930		
1	-2.764053	1.884491	-0.117397		
1	-1.334769	3.021099	-0.429502		
6	2.879910	0.268393	0.040454		
1	3.293679	1.269716	0.068517		
1	3.579205	-0.558888	0.023094		
6	-1.712634	-1.644087	-0.286967		
1	-2.389572	-2.288683	0.265585		
1	-1.894927	-1.608822	-1.357116		

Doublet **164** (^{2}A) UB3LYP/6-311+G(d,p)

6	0.000001	1.505520	0.013071	*E* =	-348.185664
6	0.777159	0.513430	0.772188	*ZPVE* =	0.144574
6	1.182391	-0.735912	0.029643	$<S^2>$ =	0.7915
6	-0.000001	-1.395871	-0.405622		
6	-1.182392	-0.735911	0.029643		
6	-0.777159	0.513430	0.772188		
1	1.352377	0.828996	1.636525		
1	-0.000001	-2.296354	-1.007410		
1	-1.352376	0.828997	1.636525		
6	-2.466824	-1.143285	-0.165303		
1	-3.305947	-0.576990	0.219814		
1	-2.687719	-2.052840	-0.711634		
6	2.466823	-1.143287	-0.165303		
1	2.687718	-2.052842	-0.711634		
1	3.305947	-0.576993	0.219814		
6	0.000001	2.588398	-0.739644		
1	-0.927532	3.049478	-1.063583		
1	0.927536	3.049477	-1.063582		

Doublet **165** (^{2}A'') UB3LYP/6-311+G(d,p)

6	0.895455	0.592684	0.762782	*E* =	-348.116407
6	0.166836	-0.628105	1.200364	*ZPVE* =	0.142936
6	-0.765936	-0.507096	0.000000	$<S^2>$ =	0.7577
6	0.166836	-0.628105	-1.200364		
6	0.895455	0.592684	-0.762782		
6	-0.396447	1.044345	0.000000		
1	1.560652	1.231750	1.327973		
1	-1.764726	-0.933977	0.000000		
1	1.560652	1.231750	-1.327973		
6	0.166836	-1.372778	-2.299646		
6	0.166836	-1.372778	2.299646		
1	-0.563101	-2.161266	-2.442146		
1	0.890569	-1.211920	-3.090769		
1	-0.563101	-2.161266	2.442146		
1	0.890569	-1.211920	3.090769		
6	-1.150267	2.244346	0.000000		
1	-2.231163	2.219151	0.000000		
1	-0.653967	3.206517	0.000000		

Doublet 3,5-*bis*-methylbenzyl radical **28** (^{2}A) UB3LYP/6-311+G(d,p)

6	-1.227118	-0.639415	0.000001	*E* =	-349.474126
6	-1.217717	0.746789	0.000001	*ZPVE* =	0.168402
6	0.000000	1.485817	0.000000	$<S^2>$ =	0.7816
6	1.217717	0.746789	-0.000001		
6	1.227118	-0.639415	-0.000001		
6	0.000000	-1.324414	0.000000		
1	-2.156431	1.292032	0.000002		
1	2.156431	1.292032	-0.000002		
1	0.000000	-2.410943	0.000000		
6	2.524941	-1.412570	0.000001		
1	2.600458	-2.057400	-0.881072		
1	3.387009	-0.742724	-0.000021		
6	0.000000	2.889543	0.000000		
1	0.927111	3.449262	-0.000002		
1	-0.927111	3.449262	0.000002		
6	-2.524941	-1.412569	-0.000001		
1	-2.600459	-2.057399	0.881073		
1	-3.387009	-0.742724	0.000020		
1	2.600477	-2.057365	0.881098		
1	-2.600476	-2.057366	-0.881097		

Triplet 5-methyl-1,3-*bis*-methylenebenzene **27** (^{3}A'') UB3LYP/6-311+G(d,p)

6	-0.002183	0.779062	1.238204	*E* =	-348.838618
6	0.002220	1.468337	0.000000	*ZPVE* =	0.155463
6	-0.002183	0.779062	-1.238204	$<S^2>$ =	2.0647
6	-0.008922	-0.651947	-1.202274		

6	-0.008071	-1.358052	0.000000	
6	-0.008922	-0.651947	1.202274	
1	0.005232	2.553394	0.000000	
1	-0.016430	-1.193154	-2.143086	
1	-0.016430	-1.193154	2.143086	
6	0.020976	-2.869260	0.000000	
1	-0.473904	-3.276979	0.884389	
1	-0.473904	-3.276979	-0.884389	
6	-0.002183	1.471675	-2.456292	
1	-0.006613	0.942878	-3.401305	
1	0.002722	2.554232	-2.483782	
6	-0.002183	1.471675	2.456292	
1	-0.006613	0.942878	3.401305	
1	0.002722	2.554232	2.483782	
1	1.051923	-3.238985	0.000000	

2-iodophenyl azide **32** (^{1}A) B3LYP/6-311G(d,p)

6	-1.267384	2.792923	0.000016	*E* =	-7314.763440
6	-0.055220	2.107372	0.000018	*ZPVE* =	0.092743
6	-0.035026	0.715436	-0.000002		
6	-1.236793	-0.008851	-0.000020		
6	-2.450118	0.692773	-0.000023		
6	-2.464294	2.081238	-0.000004		
1	-1.270737	3.876222	0.000029		
1	0.878100	2.654958	0.000033		
1	-3.384468	0.142196	-0.000039		
1	-3.412930	2.604906	-0.000007		
7	-1.158806	-1.418305	-0.000017		
7	-2.204139	-2.070736	-0.000052		
7	-3.078394	-2.791066	0.000073		
53	1.836461	-0.294394	0.000001		

Triplet 2-iodophenylnitrene T-**33** (^{3}A'') UB3LYP/6-311G(d,p)

6	-0.526146	2.897849	0.000000	*E* =	-7205.216731
6	-0.938363	1.560523	0.000000	*ZPVE* =	0.080454
6	0.000000	0.544817	0.000000	$<S^2>$ =	2.0503
6	1.405242	0.840826	0.000000		
6	1.789495	2.225386	0.000000		
6	0.838030	3.221661	0.000000		
1	-1.272340	3.683331	0.000000		
1	-1.994062	1.320433	0.000000		
1	2.848677	2.450887	0.000000		
1	1.146893	4.260467	0.000000		
7	2.333652	-0.098527	0.000000		
53	-0.612722	-1.486260	0.000000		

7-iodoazepine **34** (^{1}A) B3LYP/6-311G(d,p)

6	-2.522626	1.331738	0.149472	*E* =	-7205.199492

6	-1.079200	1.178074	-0.003798	*ZPVE* =	0.080796
6	-0.350454	0.052812	0.212798		
6	-1.988151	-1.308067	0.084553		
6	-3.108869	-0.956363	-0.513300		
6	-3.480853	0.394780	-0.072774		
1	-2.848089	2.329817	0.428989		
1	-0.528860	2.081681	-0.238309		
1	-3.627375	-1.523893	-1.272260		
1	-4.527317	0.650425	0.071305		
7	-0.940652	-1.131802	0.734466		
53	1.760323	0.004278	-0.061749		

3-iodoazepine **35** (^{1}A) B3LYP/6-311G(d,p)

6	2.258637	1.468245	-0.011029	*E* =	-7205.198945
6	1.037423	1.365018	-0.598294	*ZPVE* =	0.081400
6	0.311297	0.095237	-0.512179		
6	2.999468	-0.909926	0.469145		
6	3.003098	0.429950	0.692819		
1	2.751762	2.435865	-0.056308		
1	0.607263	2.210387	-1.128296		
1	3.658230	-1.581005	1.008872		
1	3.736801	0.785520	1.409955		
6	1.135872	-0.916238	-0.619325		
7	2.239679	-1.490732	-0.583533		
53	-1.715218	-0.049233	0.119315		

5-iodo-7-azabicyclo[4.1.0]hepta-2,4,6-triene **37** (^{1}A) B3LYP/6-311G(d,p)

6	2.494923	1.427881	-0.150812	*E* =	-7205.187393
6	1.046885	1.364975	-0.199178	*ZPVE* =	0.081121
6	0.374827	0.185900	-0.079289		
6	1.277047	-0.918252	-0.038201		
6	2.663771	-0.910888	0.491646		
6	3.281806	0.380930	0.236559		
1	2.946006	2.397054	-0.331662		
1	0.496861	2.290207	-0.325365		
1	2.971199	-1.529931	1.326022		
1	4.327908	0.549632	0.472890		
7	1.996104	-1.710080	-0.692847		
53	-1.727363	-0.017352	0.040447		

1-iodo-7-azabicyclo[4.1.0]hepta-2,4,6-triene **36** (^{1}A) B3LYP/6-311G(d,p)

6	-2.434485	1.316845	0.098233	*E* =	-7205.190867
6	-1.184230	1.229190	0.638948	*ZPVE* =	0.081014
6	-0.487767	-0.049539	0.537177		
6	-1.407946	-1.115797	0.142329		
6	-2.545477	-1.016430	-0.709240		
6	-3.060827	0.245476	-0.650775		
1	-2.964866	2.261061	0.150362		

1	-0.680566	2.108937	1.023298	
1	-2.961803	-1.825887	-1.292341	
1	-3.984462	0.465483	-1.175015	
7	-0.928257	-1.281511	1.304087	
53	1.581394	0.043444	-0.154244	

TS-35-37 (^{1}A) B3LYP/6-311G(d,p)

6	2.430499	1.442829	-0.126366	*E* =	-7205.181413
6	1.056024	1.354300	-0.392867	*ZPVE* =	0.079666
6	0.359811	0.144557	-0.276829	*IMF* =	-475.7
6	1.212363	-0.920220	-0.304967		
6	2.759595	-0.926240	0.504640		
6	3.163978	0.406794	0.471870		
1	2.889852	2.421567	-0.200799		
1	0.505923	2.257963	-0.631927		
1	3.013744	-1.596470	1.318195		
1	4.007873	0.682239	1.099467		
7	2.164867	-1.606070	-0.700973		
53	-1.725756	-0.028961	0.076773		

TS-33-36 (^{1}A) B3LYP/6-311G(d,p)

6	2.493040	-1.408541	0.182058	*E* =	-7205.162298
6	1.147648	-1.308368	0.447815	*ZPVE* =	0.079832
6	0.493265	-0.093980	0.122907	*IMF* =	-164.0
6	1.331173	1.107042	0.018931		
6	2.714830	0.934745	-0.422628		
6	3.250466	-0.309185	-0.349520		
1	2.992416	-2.359068	0.333106		
1	0.585188	-2.174673	0.774054		
1	3.278538	1.794876	-0.764132		
1	4.280538	-0.479946	-0.640978		
7	0.733230	1.978741	0.713573		
53	-1.600978	-0.078541	-0.088574		

TS-36-34 (^{1}A) B3LYP/6-311G(d,p)

6	-2.533360	1.285810	0.120610	*E* =	-7205.185074
6	-1.160086	1.249016	0.402083	*ZPVE* =	0.079400
6	-0.431417	0.056717	0.485500	*IMF* =	-472.3
6	-1.572505	-1.193627	0.164310		
6	-2.651221	-1.040908	-0.663362		
6	-3.225519	0.224649	-0.479228		
1	-3.036868	2.242861	0.192502		
1	-0.609150	2.183615	0.400704		
1	-2.993359	-1.782073	-1.370963		
1	-4.219865	0.407052	-0.873469		
7	-0.912112	-1.129114	1.219909		
53	1.635635	0.025706	-0.133351		

TS-33-37 (^{1}A) B3LYP/6-311G(d,p)

6	2.544452	-1.447363	0.153099	*E* =	-7205.172109
6	1.118096	-1.412687	0.095180	*ZPVE* =	0.080070
6	0.460469	-0.221392	0.010667	*IMF* =	-86.8
6	1.245648	1.012149	-0.059037		
6	2.667251	0.887363	-0.362732		
6	3.312768	-0.315395	-0.051034		
1	3.025243	-2.405040	0.316888		
1	0.566191	-2.341923	0.163877		
1	3.186380	1.776164	-0.686219		
1	4.394348	-0.385874	-0.080412		
7	1.095708	2.170471	0.434284		
53	-1.640268	-0.053824	-0.027754		

N-(1,4-dihydro-1,4-dimethyl-5H-tetrazole-5-ylidene)-benzenamine **42** (^{1}A) B3LYP/6-311+G(d,p)

6	1.167626	-0.223924	-0.026212	*E* =	-623.242101
7	2.695997	1.444568	-0.161116	*ZPVE* =	0.199139
7	3.349020	0.378705	0.035708		
7	2.473743	-0.652437	0.136482		
7	1.359916	1.141614	-0.194574		
7	0.156988	-1.011507	-0.041307		
6	-1.173697	-0.576704	0.017478		
6	-2.078443	-0.992223	-0.972980		
6	-1.668895	0.172731	1.099346		
6	-3.421521	-0.635378	-0.903435		
1	-1.707165	-1.596652	-1.792582		
6	-3.015568	0.523424	1.164699		
1	-0.993788	0.454812	1.900709		
6	-3.899928	0.128532	0.162042		
1	-4.100614	-0.960297	-1.684455		
1	-3.376293	1.099662	2.010198		
1	-4.947680	0.400140	0.216417		
6	0.403745	2.170787	-0.567683		
1	-0.179751	1.848804	-1.431227		
1	-0.276060	2.393976	0.254958		
1	0.980722	3.057566	-0.824663		
6	2.904818	-2.021462	0.326250		
1	2.697972	-2.614489	-0.567327		
1	3.974657	-2.004919	0.524932		
1	2.369534	-2.459900	1.169651		

1-Methyl-3-phenyl-carbodiimide **44** (^{1}A) B3LYP/6-311+G(d,p)

6	-1.894055	-0.381212	-0.263884	*E* =	-419.112783
7	-3.001825	0.074169	-0.447715	*ZPVE* =	0.142514
7	-0.810894	-0.951846	-0.208312		
6	-4.061631	0.385337	0.497983		
1	-4.310649	1.445870	0.423137		

1	-4.953241	-0.186091	0.231763	
1	-3.784867	0.154115	1.530563	
6	0.477372	-0.397992	-0.091472	
6	0.723084	0.980429	-0.161835	
6	1.548836	-1.279002	0.087681	
6	2.023243	1.462661	-0.049283	
1	-0.103652	1.666829	-0.310350	
6	2.846175	-0.788028	0.201256	
1	1.346062	-2.342061	0.134538	
6	3.090559	0.583053	0.134065	
1	2.203091	2.530514	-0.106588	
1	3.669075	-1.480085	0.340822	
1	4.101721	0.963176	0.221226	

1,3-Dimethyl-carbodiimide **234** (^{1}A) B3LYP/6-311+G(d,p)

6	0.000000	0.315270	0.000000	*E* =	-227.375450
7	1.155214	0.397082	-0.380238	*ZPVE* =	0.089751
7	-1.155214	0.397082	0.380238		
6	-2.299830	-0.352412	-0.118635		
1	-3.047061	0.349402	-0.496217		
1	-2.037312	-1.053311	-0.917349		
1	-2.754137	-0.907001	0.705547		
6	2.299830	-0.352412	0.118635		
1	2.754136	-0.907003	-0.705547		
1	3.047063	0.349402	0.496214		
1	2.037312	-1.053309	0.917351		

N-[1,2-*bis*-(1,1-dimethyl)-3-diaziridinylidene]-benzenamine **45** (^{1}A) B3LYP/6-311+G(d,p)

6	1.389307	-0.380722	-0.125790	*E* =	-513.689477
7	2.754357	-0.446633	-0.250080	*ZPVE* =	0.186571
7	1.970818	0.866907	0.047643		
7	0.359166	-1.093281	-0.152475		
6	-0.930857	-0.529865	-0.010529		
6	-1.984350	-1.163041	-0.681582		
6	-1.208006	0.578657	0.803497		
6	-3.283417	-0.677390	-0.570223		
1	-1.762713	-2.033368	-1.287785		
6	-2.512911	1.051567	0.919568		
1	-0.405403	1.055029	1.354185		
6	-3.554837	0.432158	0.230432		
1	-4.087889	-1.172677	-1.102630		
1	-2.716069	1.905367	1.556823		
1	-4.568728	0.803683	0.324578		
6	3.548381	-0.921623	0.887579		
1	3.639948	-2.006002	0.790500		
1	4.542941	-0.477680	0.834810		
1	3.083138	-0.679283	1.848254		
6	1.989790	1.803519	-1.082880		
1	1.092348	2.423222	-1.014437		

1	2.867491	2.444533	-0.992179	
1	2.005944	1.288674	-2.048162	

Triplet **40** (^{3}A) B3LYP/6-311+G(d,p)

6	-1.574328	-0.011028	-0.076999	*E* =	-513.686629
7	-2.732595	-0.612055	0.253443	*ZPVE* =	0.183117
7	-1.541701	1.307749	-0.352518	$<S^2>$ =	2.0579
7	-0.439572	-0.776688	-0.200396		
6	0.830867	-0.319965	-0.080445		
6	1.848265	-1.234160	-0.482725		
6	1.241876	0.935924	0.456551		
6	3.187449	-0.904124	-0.389453		
1	1.529534	-2.193120	-0.873059		
6	2.587313	1.242106	0.562655		
1	0.491704	1.643238	0.776076		
6	3.566768	0.336717	0.135851		
1	3.943528	-1.610006	-0.713998		
1	2.885606	2.197074	0.980981		
1	4.616544	0.593767	0.220234		
6	-2.778767	2.051353	-0.362329		
1	-3.630849	1.527190	0.073811		
1	-2.606404	3.004739	0.148812		
1	-3.010427	2.309138	-1.404882		
6	-2.740639	-2.039837	0.451681		
1	-2.367271	-2.273460	1.459341		
1	-3.770648	-2.397010	0.393143		
1	-2.097059	-2.576503	-0.252877		

Triplet peroxy diradical **22** (^{3}A) B3LYP/cc-pVTZ

6	2.331243	0.765214	-0.233784	*E* =	-459.965387
6	1.968815	-0.595699	-0.044872	*ZPVE* =	0.138399
6	0.608512	-0.867425	0.262117	$<S^2>$ =	2.0337
6	-0.326362	0.144686	0.378368		
6	0.068262	1.475726	0.185427		
6	1.395513	1.772946	-0.120915		
1	3.360694	1.003519	-0.467735		
1	0.304698	-1.896711	0.408168		
1	-0.660466	2.270468	0.273275		
1	1.693611	2.802486	-0.267809		
6	-1.755916	-0.177263	0.681251		
6	2.909929	-1.626924	-0.156153		
1	-1.877230	-1.163505	1.125043		
1	-2.231312	0.569642	1.314769		
1	2.626380	-2.659366	-0.012650		
1	3.942732	-1.415569	-0.391821		
8	-2.509132	-0.186986	-0.585778		
8	-3.785753	-0.420331	-0.375457		

BS - Singlet peroxy diradical **22** (^{1}A) B3LYP/cc-pVTZ

6	2.330568	0.761383	-0.238192	*E* =	-459.965687
6	1.964176	-0.598253	-0.043594	*ZPVE* =	0.138433
6	0.603662	-0.864544	0.268265	$<S^2>$ =	1.0310
6	-0.327178	0.151410	0.383588		
6	0.070793	1.480234	0.184176		
6	1.398705	1.772273	-0.126557		
1	3.360237	0.995375	-0.475511		
1	0.296572	-1.892210	0.418602		
1	-0.655390	2.277396	0.270872		
1	1.699667	2.800325	-0.277940		
6	-1.757346	-0.164236	0.686072		
6	2.901377	-1.632185	-0.153741		
1	-1.881200	-1.138836	1.154551		
1	-2.238082	0.598643	1.295963		
1	2.615110	-2.663285	-0.005963		
1	3.934261	-1.424884	-0.392696		
8	-2.499021	-0.208053	-0.586814		
8	-3.780944	-0.415575	-0.381683		

23 (^{1}A) B3LYP/cc-pVTZ

6	1.280470	-0.669620	-0.305554	*E* =	-459.967484
6	0.920948	0.786656	-0.345031	*ZPVE* =	0.140958
6	-0.244694	0.770943	0.600962		
6	-1.436848	0.128644	-0.083969		
6	-1.091611	-1.073399	-0.841970		
6	0.180048	-1.471516	-0.967796		
1	2.276737	-0.906272	-0.672518		
1	-1.897189	-1.639432	-1.293224		
6	-2.675379	0.612550	0.028877		
6	1.480752	1.795473	-0.986734		
1	-2.883870	1.503571	0.605517		
1	-3.516952	0.127673	-0.448240		
1	1.103723	2.805172	-0.890680		
1	2.330138	1.648004	-1.640667		
1	-0.479197	1.733216	1.052297		
1	0.440957	-2.373385	-1.504382		
8	1.313653	-0.920757	1.110950		
8	0.204289	-0.101359	1.663950		

24 (^{1}A) B3LYP/cc-pVTZ

6	0.264951	1.895867	-0.108827	*E* =	-459.980096
6	-0.611611	0.904267	0.033100	*ZPVE* =	0.141569
6	-0.172826	-0.470750	0.459025		
6	1.235599	-0.811995	0.046178		
6	2.142851	0.334807	0.077663		
6	1.689371	1.601773	0.041074		
1	-0.037330	2.894761	-0.396401		
1	3.206270	0.133383	0.072850		

1	2.390279	2.425723	0.031974	
6	1.625259	-2.049775	-0.271027	
6	-2.077417	0.771298	-0.251174	
1	0.925453	-2.871189	-0.319576	
1	2.661180	-2.261150	-0.501570	
1	-2.295702	0.917902	-1.314530	
1	-2.716644	1.424197	0.345445	
1	-0.235973	-0.529513	1.558348	
8	-1.164987	-1.327634	-0.101762	
8	-2.394337	-0.570750	0.147685	

25 (^{1}A) B3LYP/cc-pVTZ

6	-1.592938	1.180519	-0.186010	*E* =	-459.980451
6	-1.933249	-0.238391	-0.035277	*ZPVE* =	0.141575
6	-0.799734	-1.159250	0.081207		
6	0.427713	-0.697002	0.303633		
6	0.720853	0.754566	0.528645		
6	-0.356706	1.649424	-0.000815		
1	-2.392043	1.849865	-0.479892		
1	-0.978247	-2.212155	-0.100087		
1	-0.120452	2.696693	-0.133677		
6	1.772318	-1.317498	0.123898		
6	-3.201543	-0.672188	-0.100462		
1	1.766668	-2.221105	-0.483479		
1	2.294709	-1.500648	1.071040		
1	-3.443835	-1.722791	-0.015456		
1	-4.025423	0.014463	-0.239183		
1	0.841446	0.949690	1.604955		
8	2.031933	0.963736	-0.045175		
8	2.447677	-0.320622	-0.643966		

Triplet *Bis*oxygen adduct **150** (^{3}A) B3LYP/cc-pVTZ

6	-1.148813	1.663392	-0.354563	*E* =	-610.366799
6	-1.158034	0.269076	-0.359965	*ZPVE* =	0.148242
6	0.000007	-0.415887	0.000002	$<S^2>$ =	2.0078
6	1.158041	0.269092	0.359965		
6	1.148803	1.663407	0.354554		
6	-0.000009	2.357976	-0.000007		
1	-2.045305	2.204987	-0.627485		
1	0.000014	-1.499030	0.000007		
1	-0.000015	3.439295	-0.000009		
6	2.403487	-0.481365	0.709760		
6	-2.403472	-0.481395	-0.709755		
1	2.198623	-1.468597	1.119564		
1	3.048973	0.070405	1.390501		
1	-3.048955	0.070355	-1.390516		
1	-2.198601	-1.468637	-1.119530		
1	2.045289	2.205015	0.627472		
8	3.177211	-0.690824	-0.527632		

8	4.289421	-1.347909	-0.284232	
8	-3.177211	-0.690825	0.527636	
8	-4.289432	-1.347889	0.284234	

13. References

[1] D. Grote, C. Finke, S. Kossmann, F. Neese, W. Sander, *Chem.--Eur. J.* **2010**, *16*, 4496.
[2] T. Bally, *React. Intermed. Chem.* Wiley-Interscience, **2004**, 797.
[3] J. C. Scaiano, *React. Intermed. Chem.* Wiley-Interscience, **2004**, 847.
[4] M. Gomberg, *J. Am. Chem. Soc.* **1900**, *22*, 757.
[5] K. J. Skinner, H. S. Hochster, J. M. McBride, *J. Am. Chem. Soc.* **1974**, *96*, 4301.
[6] H. Lankamp, W. T. Nauta, C. MacLean, *Tetrahedron Lett.* **1968**, 249.
[7] W. Schlenk, M. Brauns, *Ber. Dtsch. Chem. Ges.* **1915**, *48*, 661.
[8] M. Leo, *Ber. Dtsch. Chem. Ges. B* **1937**, *70B*, 1691.
[9] D. A. Dougherty, *Acc. Chem. Res.* **1991**, *24*, 88.
[10] A. D. McNaught, A. Wilkinson, *IUPAC. Compendium of chemical terminology, Vol. 2nd ed.*, Oxford, **1997**.
[11] A. Rajca, *Chem. Rev.* **1994**, *94*, 871.
[12] H. C. Longuet-Higgins, *J. Chem. Phys.* **1950**, *18*, 265.
[13] K. Itoh, *Pure Appl. Chem.* **1978**, *50*, 1251.
[14] A. A. Ovchinnikov, *Theor. Chim. Acta* **1978**, *47*, 297.
[15] T. P. Radhakrishnan, *Chem. Phys. Lett.* **1991**, *181*, 455.
[16] P. Taylor, P. R. Serwinski, P. M. Lahti, *Org. Lett.* **2005**, *7*, 3693.
[17] C. A. Hutchison, Jr., *Triplet State, Proc. Int. Symp., Beirut,* **1967**, 63.
[18] C. A. Hutchison, Jr., *Pure Appl. Chem.* **1971**, *27*, 327.
[19] W. Weltner, Jr., *Magnetic Atoms and Molecules*, **1989**.
[20] M. Kuzaj, H. Luerssen, C. Wentrup, *Angew. Chem.* **1986**, *98*, 476.
[21] K. Haider, N. Soundararajan, M. Shaffer, M. S. Platz, *Tetrahedron Lett.* **1989**, *30*, 1225.
[22] B. R. Bicknell, W. R. M. Graham, W. Weltner, Jr., *J. Chem. Phys.* **1976**, *64*, 3319.
[23] E. Wasserman, A. M. Trozzolo, W. A. Yager, R. W. Murray, *J. Chem. Phys.* **1964**, *40*, 2408.
[24] P. Neuhaus, D. Grote, W. Sander, *J. Am. Chem. Soc.* **2008**, *130*, 2993.
[25] R. W. Brandon, G. L. Closs, C. E. Davoust, C. A. Hutchison, Jr., B. E. Kohler, R. Silbey, *J. Chem. Phys.* **1965**, *43*, 2006.
[26] R. A. Bernheim, R. J. Kempf, E. F. Reichenbecher, *J. Magn. Resonance* **1970**, *3*, 5.
[27] E. Wasserman, L. Barash, W. A. Yager, *J. Am. Chem. Soc.* **1965**, *87*, 2075.
[28] M. Minato, P. M. Lahti, *J. Am. Chem. Soc.* **1997**, *119*, 2187.
[29] A. S. Ichimura, K. Sato, T. Kinoshita, T. Takui, K. Itoh, P. M. Lahti, *Mol. Cryst. Liq. Cryst.* **1995**, *272*, 279.
[30] P. Dowd, *Acc. Chem. Res.* **1972**, *5*, 242.
[31] G. J. Snyder, D. A. Dougherty, *J. Am. Chem. Soc.* **1989**, *111*, 3927.
[32] R. M. Pagni, M. N. Burnett, J. R. Dodd, *J. Am. Chem. Soc.* **1977**, *99*, 1972.
[33] M. Rule, A. R. Matlin, E. F. Hilinski, D. A. Dougherty, J. A. Berson, *J. Am. Chem. Soc.* **1979**, *101*, 5098.
[34] J. L. Goodman, J. A. Berson, *J. Am. Chem. Soc.* **1985**, *107*, 5409.
[35] G. L. Closs, L. R. Kaplan, V. I. Bendall, *J. Am. Chem. Soc.* **1967**, *89*, 3376.
[36] M. S. De Groot, I. A. M. Hesselmann, J. H. Van der Waals, *Mol. Phys.* **1969**, *16*, 45.
[37] C. A. Hutchison, Jr., B. W. Mangum, *J. Chem. Phys.* **1958**, *29*, 952.
[38] C. A. Hutchison, Jr., B. W. Mangum, *J. Chem. Phys.* **1961**, *34*, 908.

[39] M. C. Biewer, C. R. Biehn, M. S. Platz, A. Despres, E. Migirdicyan, *J. Am. Chem. Soc.* **1991**, *113*, 616.
[40] K. W. Haider, E. Migirdicyan, M. S. Platz, N. Soundararajan, A. Despres, *J. Am. Chem. Soc.* **1990**, *112*, 733.
[41] K. Haider, M. S. Platz, A. Despres, V. Lejeune, E. Migirdicyan, T. Bally, E. Haselbach, *J. Am. Chem. Soc.* **1988**, *110*, 2318.
[42] A. Mardyukov, W. Sander, *Chem.--Eur. J.* **2009**, *15*, 1462.
[43] A. V. Friderichsen, J. G. Radziszewski, M. R. Nimlos, P. R. Winter, D. C. Dayton, D. E. David, G. B. Ellison, *J. Am. Chem. Soc.* **2001**, *123*, 1977.
[44] W. Sander, M. Exner, M. Winkler, A. Balster, A. Hjerpe, E. Kraka, D. Cremer, *J. Am. Chem. Soc.* **2002**, *124*, 13072.
[45] R. Marquardt, A. Balster, W. Sander, E. Kraka, D. Cremer, J. G. Radziszewski, *Angew. Chem., Int. Ed. Engl.* **1998**, *37*, 955.
[46] W. Sander, D. Grote, S. Kossmann, F. Neese, *J. Am. Chem. Soc.* **2008**, *130*, 4396.
[47] P. G. Wenthold, S. G. Wierschke, J. J. Nash, R. R. Squires, *J. Am. Chem. Soc.* **1994**, *116*, 7378.
[48] H. Tukada, *J. Chem. Soc., Chem. Commun.* **1993**, 302.
[49] P. G. Wenthold, S. G. Wierschke, J. J. Nash, R. R. Squires, *J. Am. Chem. Soc.* **1993**, *115*, 12611.
[50] P. G. Wenthold, S. G. Wierschke, J. J. Nash, R. R. Squires, *J. Am. Chem. Soc.* **1994**, *116*, 4529.
[51] J. Cabrero, N. Ben-Amor, R. Caballol, *J. Phys. Chem. A* **1999**, *103*, 6220.
[52] T. Wang, A. I. Krylov, *Chem. Phys. Lett.* **2006**, *425*, 196.
[53] L. V. Slipchenko, T. E. Munsch, P. G. Wenthold, A. I. Krylov, *Angew. Chem., Int. Ed. Engl.* **2004**, *43*, 742.
[54] H. Tukada, *Org. Lett.* **2001**, *3*, 3261.
[55] T. Koto, K. Sato, D. Shiomi, K. Toyota, K. Itoh, E. Wasserman, T. Takui, *J. Phys. Chem. A* **2009**, *113*, 9521.
[56] H. Tukada, K. Mutai, H. Iwamura, *J. Chem. Soc., Chem. Commun.* **1987**, 1159.
[57] E. Wasserman, R. W. Murray, W. A. Yager, A. M. Trozzolo, G. Smolinsky, *J. Am. Chem. Soc.* **1967**, *89*, 5076.
[58] W. Adam, C. van Barneveld, S. E. Bottle, H. Engert, G. R. Hanson, H. M. Harrer, C. Heim, W. M. Nau, D. Wang, *J. Am. Chem. Soc.* **1996**, *118*, 3974.
[59] S. J. Jacobs, D. A. Shultz, R. Jain, J. Novak, D. A. Dougherty, *J. Am. Chem. Soc.* **1993**, *115*, 1744.
[60] D. Grote, W. Sander, *J. Org. Chem.* **2009**, *74*, 7370.
[61] A. Rajca, J. Wongsriratanakul, S. Rajca, *Science* **2001**, *294*, 1503.
[62] G. Kothe, K. H. Denkel, W. Suemmermann, *Angew. Chem., Int. Ed. Engl.* **1970**, *9*, 906.
[63] E. Migirdicyan, J. Baudet, *J. Am. Chem. Soc.* **1975**, *97*, 7400.
[64] B. B. Wright, M. S. Platz, *J. Am. Chem. Soc.* **1983**, *105*, 628.
[65] P. G. Wenthold, J. B. Kim, W. C. Lineberger, *J. Am. Chem. Soc.* **1997**, *119*, 1354.
[66] L. A. Hammad, P. G. Wenthold, *J. Am. Chem. Soc.* **2000**, *122*, 11203.
[67] D. Y. Zhang, W. T. Borden, *J. Org. Chem.* **2002**, *67*, 3989.
[68] J. L. Goodman, J. A. Berson, *J. Am. Chem. Soc.* **1984**, *106*, 1867.
[69] C. R. Flynn, J. Michl, *J. Am. Chem. Soc.* **1974**, *96*, 3280.
[70] S. Kato, K. Morokuma, D. Feller, E. R. Davidson, W. T. Borden, *J. Am. Chem. Soc.* **1983**, *105*, 1791.
[71] R. C. Fort, Jr., S. J. Getty, D. A. Hrovat, P. M. Lahti, W. T. Borden, *J. Am. Chem. Soc.* **1992**, *114*, 7549.

[72] D. A. Hrovat, M. A. Murcko, P. M. Lahti, W. Thatcher Borden, *J. Chem. Soc., Perkin Trans. 2* **1998**, 1037.
[73] S. Fang, M.-S. Lee, D. A. Hrovat, W. T. Borden, *J. Am. Chem. Soc.* **1995**, *117*, 6727.
[74] G. Zhang, S. Li, Y. Jiang, *J. Phys. Chem. A* **2003**, *107*, 5573.
[75] G. Zhang, S. Li, Y. Jiang, *Tetrahedron* **2003**, *59*, 3499.
[76] T. Wang, A. I. Krylov, *J. Chem. Phys.* **2005**, *123*, 104304/1.
[77] W. Sander, M. Exner, *J. Chem. Soc., Perkin Trans. 2* **1999**, 2285.
[78] W. Sander, M. Exner, M. Winkler, A. Balster, A. Hjerpe, E. Kraka, D. Cremer, *J Am. Chem. Soc.* **2002**, *124*, 13072.
[79] E. W. Thulstrup, J. Michl, *Elementary Polarization Spectroscopy*, **1989**.
[80] J. Michl, E. W. Thulstrup, *Spectroscopy with Polarized Light. Solute Alignment by Photoselection, in Liquid Crystals, Polymers, and Membranes*, **1986**.
[81] V. LeJeune, A. Despres, E. Migirdicyan, *J. Phys. Chem.* **1984**, *88*, 2719.
[82] P. Bilski, K. Reszka, M. Bilska, C. F. Chignell, *J. Am. Chem. Soc.* **1996**, *118*, 1330.
[83] D. Rehorek, E. G. Janzen, *J. Prakt. Chem.* **1985**, *327*, 968.
[84] T. Svensson, B. Nelander, *Chem. Phys.* **2000**, *262*, 445.
[85] H. E. Hunziker, H. R. Wendt, *J. Chem. Phys.* **1974**, *60*, 4622.
[86] D. W. Smith, L. Andrews, *J. Chem. Phys.* **1974**, *60*, 81.
[87] M. E. Jacox, D. E. Milligan, *J. Mol. Spectrosc.* **1972**, *42*, 495.
[88] S. Nandi, S. J. Blanksby, X. Zhang, M. R. Nimlos, D. C. Dayton, G. B. Ellison, *J. Phys. Chem. A* **2002**, *106*, 7547.
[89] S. J. Blanksby, T. M. Ramond, G. E. Davico, M. R. Nimlos, S. Kato, V. M. Bierbaum, W. C. Lineberger, G. B. Ellison, M. Okumura, *J. Am. Chem. Soc.* **2001**, *123*, 9585.
[90] P. Ase, W. Bock, A. Snelson, *J. Phys. Chem.* **1986**, *90*, 2099.
[91] G. Chettur, A. Snelson, *J. Phys. Chem.* **1987**, *91*, 3483.
[92] J. E. Bennett, R. Summers, *J. Chem. Soc., Faraday Trans. 2* **1973**, *69*, 1043.
[93] A. Fahr, A. H. Laufer, M. Krauss, R. Osman, *J. Phys. Chem. A* **1997**, *101*, 4879.
[94] G. I. Khaikin, P. Neta, *J. Phys. Chem.* **1995**, *99*, 4549.
[95] R. Yang, L. Yu, X. Jin, M. Zhou, B. K. Carpenter, *J. Chem. Phys.* **2005**, *122*, 014511/1.
[96] K. Tonokura, Y. Norikane, M. Koshi, Y. Nakano, S. Nakamichi, M. Goto, S. Hashimoto, M. Kawasaki, M. P. S. Andersen, M. D. Hurley, T. J. Wallington, *J. Phys. Chem. A* **2002**, *106*, 5908.
[97] Z. B. Alfassi, G. I. Khaikin, P. Neta, *J. Phys. Chem.* **1995**, *99*, 265.
[98] N. Sebbar, J. W. Bozzelli, H. Bockhorn, *J. Phys. Chem. A* **2004**, *108*, 8353.
[99] M. Krauss, R. Osman, *J. Phys. Chem.* **1995**, *99*, 11387.
[100] S. L. Boyd, R. J. Boyd, L. R. C. Barclay, *J. Am. Chem. Soc.* **1990**, *112*, 5724.
[101] G. O. Schenck, O. A. Neumuller, W. Eisfeld, *Angew. Chem.* **1958**, *70*, 595.
[102] W. F. Brill, *J. Chem. Soc., Perkin Trans. 2* **1984**, 621.
[103] S. Olivella, A. Sole, *J. Am. Chem. Soc.* **2003**, *125*, 10641.
[104] S. L. Boyd, R. J. Boyd, Z. Shi, L. R. C. Barclay, N. A. Porter, *J. Am. Chem. Soc.* **1993**, *115*, 687.
[105] E. G. Baskir, O. M. Nefedov, *Izv. Akad. Nauk, Ser. Khim.* **1996**, 109.
[106] G. El Dib, A. Chakir, E. Roth, J. Brion, D. Daumont, *J. Phys. Chem. A* **2006**, *110*, 7848.
[107] M. Michalczyk, W. Sander, *unpublished results*.
[108] J. S. Wright, H. Shadnia, L. L. Chepelev, *J. Comput. Chem.* **2009**, *30*, 1016.
[109] J. C. Scaiano, A. Martin, G. P. A. Yap, K. U. Ingold, *Org. Lett.* **2000**, *2*, 899.
[110] D. Griller, K. U. Ingold, *Acc. Chem. Res.* **1976**, *9*, 13.

[111] A. Rajca, S. Rajca, S. R. Desai, V. W. Day, *J. Org. Chem.* **1997**, *62*, 6524.
[112] O. L. J. Gijzeman, F. Kaufman, G. Porter, *J. Chem. Soc., Faraday Trans. 2* **1973**, *69*, 708.
[113] M. Abe, S. Kawanami, A. Masuyama, T. Hayashi, *J. Org. Chem.* **2006**, *71*, 6607.
[114] M. N. Burnett, R. Boothe, E. Clark, M. Gisin, H. M. Hassaneen, R. M. Pagni, G. Persy, R. J. Smith, J. Wirz, *J. Am. Chem. Soc.* **1988**, *110*, 2527.
[115] W. Adam, S. Grabowski, R. M. Wilson, K. Hannemann, J. Wirz, *J. Am. Chem. Soc.* **1987**, *109*, 7572.
[116] M. Bobrowski, A. Liwo, S. Oldziej, D. Jeziorek, T. Ossowski, *J. Am. Chem. Soc.* **2000**, *122*, 8112.
[117] A. Maranzana, G. Ghigo, G. Tonachini, *J. Am. Chem. Soc.* **2000**, *122*, 1414.
[118] A. G. Leach, K. N. Houk, *Chem. Commun.* **2002**, 1243.
[119] A. G. Leach, K. N. Houk, *J. Am. Chem. Soc.* **2002**, *124*, 14820.
[120] H. M. T. Nguyen, T. T. Hue, M. T. Nguyen, *Chem. Phys. Lett.* **2005**, *411*, 450.
[121] H. M. T. Nguyen, A. Dutta, K. Morokuma, M. T. Nguyen, *J. Chem. Phys.* **2005**, *122*, 154308/1.
[122] W. T. Borden, E. R. Davidson, *J. Am. Chem. Soc.* **1977**, *99*, 4587.
[123] Y. Zhang, P. M. Lahti, R. Wang, M. Baumgarten, *Heteroat. Chem.* **1998**, *9*, 161.
[124] J. Zhang, M. Baumgarten, *Chem. Phys.* **1997**, *214*, 291.
[125] M. Baumgarten, J. Zhang, K. Okada, N. Tyutyulkov, *Mol. Cryst. Liq. Cryst.* **1997**, *305*, 509.
[126] C. R. Kemnitz, R. R. Squires, W. T. Borden, *J. Am. Chem. Soc.* **1997**, *119*, 6564.
[127] J. Veciana, C. Rovira, N. Ventosa, M. I. Crespo, F. Palacio, *J. Am. Chem. Soc.* **1993**, *115*, 57.
[128] G. Kothe, E. Ohmes, J. Brickmann, H. Zimmermann, *Angew. Chem., Int. Ed. Engl.* **1971**, *10*, 938.
[129] K. Yoshizawa, M. Hatanaka, A. Ito, K. Tanaka, T. Yamabe, *Mol. Cryst. Liq. Cryst.* **1993**, *232*, 323.
[130] L. A. Hammad, P. G. Wenthold, *J. Am. Chem. Soc.* **2001**, *123*, 12311.
[131] P. Milko, J. Roithova, D. Schroeder, H. Schwarz, *Int. J. Mass Spectrom.* **2007**, *267*, 139.
[132] J. Hu, R. R. Squires, *J. Am. Chem. Soc.* **1996**, *118*, 5816.
[133] D. Moran, A. C. Simmonett, F. E. Leach, III, W. D. Allen, P. v. R. Schleyer, H. F. Schaefer, III, *J. Am. Chem. Soc.* **2006**, *128*, 9342.
[134] J. Brickmann, G. Kothe, *J. Chem. Phys.* **1973**, *59*, 2807.
[135] T. D. Selby, K. R. Stickley, S. C. Blackstock, *Org. Lett.* **2000**, *2*, 171.
[136] K. R. Stickley, T. D. Selby, S. C. Blackstock, *J. Org. Chem.* **1997**, *62*, 448.
[137] K. Yoshizawa, A. Chano, A. Ito, K. Tanaka, T. Yamabe, H. Fujita, J. Yamauchi, M. Shiro, *J. Am. Chem. Soc.* **1992**, *114*, 5994.
[138] K. Yoshizawa, A. Chano, A. Ito, K. Tanaka, T. Yamabe, H. Fujita, J. Yamauchi, *Chem. Lett.* **1992**, 369.
[139] S. I. Weissman, G. Kothe, *J. Am. Chem. Soc.* **1975**, *97*, 2537.
[140] A. Rajca, S. Utamapanya, *J. Am. Chem. Soc.* **1993**, *115*, 2396.
[141] K. Hirai, K. Bessho, T. Kitagawa, H. Tomioka, *J. Phys. Org. Chem.* ***2010***, *23*, 347.
[142] V. Lejeune, A. Despres, E. Migirdicyan, J. Baudet, G. Berthier, *J. Am. Chem. Soc.* **1986**, *108*, 1853.
[143] D. M. Friedrich, A. C. Albrecht, *Chem. Phys.* **1974**, *6*, 366.
[144] A. Bromberg, D. M. Friedrich, A. C. Albrecht, *Chem. Phys.* **1974**, *6*, 353.
[145] T. Izumida, T. Ichikawa, H. Yoshida, *J. Phys. Chem.* **1980**, *84*, 60.
[146] A. Gilles, J. Masanet, C. Vermeil, *Chem. Phys. Lett.* **1974**, *25*, 346.
[147] P. C. Engelking, W. C. Lineberger, *J. Chem. Phys.* **1976**, *65*, 4323.

[148] M. J. Travers, D. C. Cowles, E. P. Clifford, G. B. Ellison, *J. Am. Chem. Soc.* **1992**, *114*, 8699.
[149] N. R. Wijeratne, M. Da Fonte, A. Ronemus, P. J. Wyss, D. Tahmassebi, P. G. Wenthold, *J. Phys. Chem. A* **2009**, *113*, 9467.
[150] D. A. Hrovat, E. E. Waali, W. T. Borden, *J. Am. Chem. Soc.* **1992**, *114*, 8698.
[151] S. J. Kim, T. P. Hamilton, H. F. Schaefer, III, *J. Am. Chem. Soc.* **1992**, *114*, 5349.
[152] A. Nicolaides, T. Nakayama, K. Yamazaki, H. Tomioka, S. Koseki, L. L. Stracener, R. J. McMahon, *J. Am. Chem. Soc.* **1999**, *121*, 10563.
[153] S. Koseki, H. Tomioka, K. Yamazaki, A. Toyota, *J. Phys. Chem. A* **1997**, *101*, 3377.
[154] A. Nicolaides, H. Tomioka, S. Murata, *J. Am. Chem. Soc.* **1998**, *120*, 11530.
[155] A. S. Ichimura, P. M. Lahti, *Mol. Cryst. Liq. Cryst.* **1993**, *233*, 33.
[156] H. Heise, F. H. Koehler, F. Mota, J. J. Novoa, J. Veciana, *J. Am. Chem. Soc.* **1999**, *121*, 9659.
[157] T. Takui, Y. Miura, K. Inui, Y. Teki, M. Inoue, K. Itoh, *Mol. Cryst. Liq. Cryst.* **1995**, *271*, 55.
[158] J. W. Neely, G. F. Hatch, R. W. Kreilick, *J. Am. Chem. Soc.* **1974**, *96*, 652.
[159] A. Zheludev, M. Bonnet, D. Luneau, E. Ressouche, P. Rey, J. Schweizer, *Physica B* **1995**, *213&214*, 268.
[160] D. B. Amabilino, J. Veciana, *Magn.: Mol. Mater. II* **2001**, 1.
[161] P. M. Lahti, B. Esat, Y. Liao, P. Serwinski, J. Lan, R. Walton, *Polyhedron* **2001**, *20*, 1647.
[162] P. R. Serwinski, B. Esat, P. M. Lahti, Y. Liao, R. Walton, J. Lan, *J. Org. Chem.* **2004**, *69*, 5247.
[163] R. Chiarelli, S. Gambarelli, A. Rassat, *Mol. Cryst. Liq. Cryst.* **1997**, *305*, 455.
[164] M. Dvolaitzky, R. Chiarelli, A. Rassat, *Angew. Chem.* **1992**, *104*, 180.
[165] A. Calder, A. R. Forrester, P. G. James, G. R. Luckhurst, *J. Am. Chem. Soc.* **1969**, *91*, 3724.
[166] F. Kanno, K. Inoue, N. Koga, H. Iwamura, *J. Am. Chem. Soc.* **1993**, *115*, 847.
[167] M. S. Platz, *React. Intermed. Chem. Wiley-Interscience*, **2004**, 501.
[168] H. H. Wenk, W. Sander, *Angew. Chem., Int. Ed. Engl.* **2002**, *41*, 2742.
[169] W. Sander, M. Winkler, B. Cakir, D. Grote, H. F. Bettinger, *J. Org. Chem.* **2007**, *72*, 715.
[170] H. F. Bettinger, W. Sander, *J. Am. Chem. Soc.* **2003**, *125*, 9726.
[171] W. L. Karney, W. T. Borden, *J. Am. Chem. Soc.* **1997**, *119*, 1378.
[172] W. L. Karney, W. T. Borden, *Adv. Carbene Chem.* **2001**, *3*, 205.
[173] W. L. Karney, W. T. Borden, *J. Am. Chem. Soc.* **1997**, *119*, 3347.
[174] D. Grote, Ph. D. thesis, **2007**.
[175] E. Leyva, M. S. Platz, *Tetrahedron Lett.* **1987**, *28*, 11.
[176] E. Leyva, R. Sagredo, *Tetrahedron* **1998**, *54*, 7367.
[177] D. Grote, W. Sander, *Nitreno Radical*, **2010**.
[178] P. Dowd, *J. Am. Chem. Soc.* **1966**, *88*, 2587.
[179] C. Vroelant, *Compt. rend.* **1952**, *234*, 2072.
[180] R. J. Baseman, D. W. Pratt, M. Chow, P. Dowd, *J. Am. Chem. Soc.* **1976**, *98*, 5726.
[181] C. J. Cramer, B. A. Smith, *J. Phys. Chem.* **1996**, *100*, 9664.
[182] J. A. Berson, R. J. Bushby, J. M. McBride, M. Tremelling, *J. Am. Chem. Soc.* **1971**, *93*, 1544.
[183] J. A. Berson, *Diradicals*, Wiley-Interscience, New York, **1982**.
[184] M. S. Platz, J. M. McBride, R. D. Little, J. J. Harrison, A. Shaw, S. E. Potter, J. A. Berson, *J. Am. Chem. Soc.* **1976**, *98*, 5725.

[185] D. A. Dixon, T. H. Dunning, Jr., R. A. Eades, D. A. Kleier, *J. Am. Chem. Soc.* **1981**, *103*, 2878.
[186] P. G. Wenthold, J. Hu, R. R. Squires, W. C. Lineberger, *J. Am. Chem. Soc.* **1996**, *118*, 475.
[187] M. Rule, M. G. Lazzara, J. A. Berson, *J. Am. Chem. Soc.* **1979**, *101*, 7091.
[188] M. R. Mazur, J. A. Berson, *J. Am. Chem. Soc.* **1981**, *103*, 684.
[189] M. R. Mazur, J. A. Berson, *J. Am. Chem. Soc.* **1982**, *104*, 2217.
[190] B. K. Carpenter, R. D. Little, J. A. Berson, *J. Am. Chem. Soc.* **1976**, *98*, 5723.
[191] R. Siemionko, A. Shaw, G. O'Connell, R. D. Little, B. K. Carpenter, L. Shen, J. A. Berson, *Tetrahedron Lett.* **1978**, 3529.
[192] D. Cichra, M. S. Platz, J. A. Berson, *J. Am. Chem. Soc.* **1977**, *99*, 8507.
[193] W. R. Roth, M. Martin, *Tetrahedron Lett.* **1967**, 4695.
[194] W. R. Roth, M. Martin, *Justus Liebigs Ann. Chem.* **1967**, *702*, 1.
[195] D. E. Reedich, R. S. Sheridan, *J. Am. Chem. Soc.* **1988**, *110*, 3697.
[196] W. Adam, M. Doerr, *J. Am. Chem. Soc.* **1987**, *109*, 1240.
[197] H. Quast, H. Jakobi, *Chem. Ber.* **1991**, *124*, 1613.
[198] H. Quast, L. Bieber, W. C. Danen, *J. Am. Chem. Soc.* **1978**, *100*, 1306.
[199] H. Quast, A. Fuss, W. Nuedling, *Eur. J. Org. Chem.* **1998**, 317.
[200] H. Quast, L. Bieber, G. Meichsner, *Chem. Ber.* **1988**, *121*, 2117.
[201] K. S. Feldman, M. R. Iyer, *J. Am. Chem. Soc.* **2005**, *127*, 4590.
[202] S. Feldman Ken, R. Iyer Malliga, D. K. Hester, 2nd, *Org Lett.* **2006**, *8*, 3113.
[203] S. J. Barker, R. C. Storr, *J. Chem. Soc., Perkin Trans. 1* **1990**, 485.
[204] J. Li, S. E. Worthington, C. J. Cramer, *J. Chem. Soc., Perkin Trans. 2* **1998**, 1045.
[205] M. B. Coolidge, K. Yamashita, K. Morokuma, W. T. Borden, *J. Am. Chem. Soc.* **1990**, *112*, 1751.
[206] A. S. Ichimura, P. M. Lahti, A. R. Matlin, *J. Am. Chem. Soc.* **1990**, *112*, 2868.
[207] T. Ichino, S. M. Villano, A. J. Gianola, D. J. Goebbert, L. Velarde, A. Sanov, S. J. Blanksby, X. Zhou, D. A. Hrovat, W. T. Borden, W. C. Lineberger, *Angew. Chem., Int. Ed. Engl.* **2009**, *48*, 8509.
[208] H. F. Bettinger, *Angew. Chem., Int. Ed. Engl.* **2010**, *49*, 670.
[209] I. R. Dunkin, C. J. Shields, H. Quast, *Tetrahedron* **1989**, *45*, 259.
[210] D. Grote, *Ph. D. thesis* **2007**.
[211] H. H. Wenk, *Ph. D. thesis* **2002**.
[212] T. Kida, A. Kikuzawa, H. Higashimoto, Y. Nakatsuji, M. Akashi, *Tetrahedron* **2005**, *61*, 5763.
[213] M. Nakazaki, K. Yamamoto, T. Toya, *J. Org. Chem.* **1981**, *46*, 1611.
[214] C.-Y. Liu, P. Knochel, *J. Org. Chem.* **2007**, *72*, 7106.

Acknowledgments

I have to thank all the present and past members of the Sander group for the nice atmosphere and help with all kinds of problems. In this regard, I want to thank:

Y-am, Fee, Dirk, Stefan, Artur, Melanie, Christopher, Andre, Kosta, Sugumar, Matthias Böhm, Matthias Filthaus, MiWi, Rafael, Sandra, Christina, Alex, Marc, Tammy, Magdalena, Kavitha, Saonli, Elsa, Holger, Sunanda, Arunlibertsen, Tuhin, Bayram, Arndt, Joel and Laura.

I am very grateful to Dirk for showing me the secrets of the EPR spectrometer as well as his help in interpreting all kinds of spin systems at a glance and giving me the opportunity to drink coffee in the secretary at late afternoons.

I extent my appreciation to Sugumar and Matthias Böhm for introducing me to the experimental part of matrix isolation spectroscopy and the evening sessions in the matrix lab.

I thank MiWi, Prof. Dr. Staemmler, Marc, and Holger for their help with all kinds of *ab initio* calculations.

I also thank Klaus for his kind neighbourhood in the lab, his patience with me, and the help with the EPR setup.

I want to thank Ulrike for all her help with administrative work, innumerable morning coffees and nice talks together with Margit and Klaus.

I extent my appreciation to Torsten for his tireless help with the new PC at home and the old one in the EPR lab as well as his help with running different Molpro versions.

Thanks to Heidi for her assistance with the matrix equipment and her help in constructing new FVP ovens.

I want to thank Frau Schröder for her help in the lab.

I also thank Prof. Dr. Bettinger and Prof. Dr. Bucher for their advices in scientific questions and above.

I would like to express my special thanks to all members of the “Wechhauer” for the time outside the lab, for non-scientific contributions to my life, and the successful sportive history: Maasi, Schweiand, Schmocke, König Borst, Feger, Eiko, Schlauch, Peils, Pimp, and Matze.

Last but not least I thank my parents Ulrike and Gregor for giving me all opportunities and support in life. In this regard I also thank Jürgen and Brigitte as well as my sister Ines, my brother Till and my stepsister Julia for all their help in all kinds of situations.

I want to say “Thank you” to Kanthi for his support in chemistry, the common passion for football, his time for Badminton and the numberless small and helpful ideas.
I am very much indebted to Y-am for all her support, tolerance, patience, and encouragement in chemistry, life, and at home. Without you, this work would not have been possible.